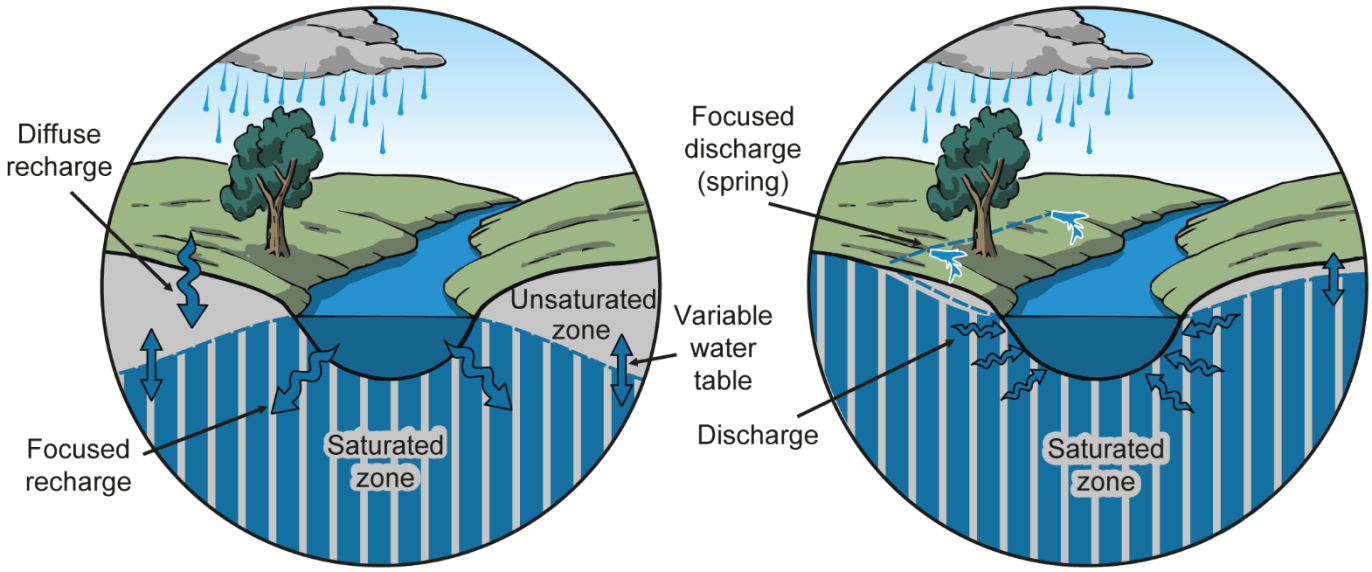

Groundwater Recharge to Discharge

Diana M. Allen

THE GROUNDWATER PROJECT

Groundwater Recharge to Discharge

The Groundwater Project

Diana M. Allen
Professor Emerita
Simon Fraser University
British Columbia, Canada

Groundwater Recharge to Discharge

The Groundwater Project
Guelph, Ontario, Canada

TDS

Technical Development Solutions

شركة حلول التقنية والتطوير

SUSTAINABLE INNOVATIVE RESOURCES MANAGEMENT

Smart solutions for using resources efficiently, protecting our planet, and securing a prosperous future.

SECTORS

WATER

ENVIRONMENT

MINING

INTEGRATED WATER SERVICES LIFECYCLE

GREEN ENERGY

DIGITIZATION AND AUTOMATION

COMPREHENSIVE MONITORING SOLUTIONS

DISASTER MANAGEMENT SYSTEMS CATEGORY

SERVICES

www.tds.com.sa

The Groundwater Project relies on private funding for book production and management of the Project.

Please consider donating to the Groundwater Project↗ so books will continue to be freely available.

Thank you.

Published by the Groundwater Project, Guelph, Ontario, Canada, 2026.

Groundwater Recharge to Discharge / Diana M. Allen - Guelph, Ontario, Canada, 2025.
195 pages

ISBN: 978-1-77470-142-3
DOI: https://doi.org/10.62592/GUTB8590↗.

Please consider signing up for the GW-Project mailing list to stay informed about new book releases, events, and ways to participate in the GW-Project. When you sign up for our email list, it helps us build a global groundwater community. Sign up↗.

APA (7th ed.) Citation

Allen, D. M. (2026). *Groundwater Recharge to Discharge*↗. The Groundwater Project. https://doi.org/10.62592/GUTB8590↗.

Table of Contents

The Groundwater Project Foreword

The 2022 United Nations (UN) World Water Day theme "*Groundwater – Making the Invisible Visible*" was pivotal in raising global awareness about groundwater as an invaluable resource, and the year concluded with the UN Water Summit on Groundwater at the UNESCO headquarters. One of the key outcomes of the Summit was a call for governments and other stakeholders to scale up their efforts to better manage groundwater.

Groundwater makes up 99% of all liquid fresh water on Earth, underpinning its importance in providing drinking water to the world, sustaining food production, and maintaining healthy ecosystems. Many important global organizations have concluded that there is a freshwater crisis and given that nearly all freshwater is groundwater, the freshwater crisis is a groundwater crisis. During drought in many locales, groundwater is the only freshwater available, putting even more pressure on groundwater resources.

According to the World Health Organization and UNICEF (WHO/UNICEF, 2025↗), 2.1 billion people (1 in 4) live without safely managed drinking water and 3.4 billion people (4 in 10) live without safely managed sanitation. With groundwater directly supporting 8 of the 17 UN Sustainable Development Goals, groundwater is an invaluable resource. Safe and reliable access to groundwater directly supports the 2026 UN World Water Day (March 22) Theme "*Water and Gender Equality*" focusing on ensuring that women and girls have equal rights and leadership in water management.

The Groundwater Project (GW-Project), a registered Canadian charity founded in 2018, pioneers in advancing the understanding of groundwater by providing groundwater education to everyone. Recognizing that the world needs more highly skilled groundwater scientists to solve the water crisis, the GW-Project plays a pivotal role in creating the knowledge base for building the much-needed human capacity for the development and management of groundwater.

The GW-Project gained global recognition with publication of 64 original books, 94 translated books (in 59 languages), 7 interactive groundwater educational tools/modules, and over 50 high-quality educational videos, all made possible by a dedicated international group of over 1000 volunteer professionals from a broad range of disciplines throughout 70 countries on six continents. Academics, practitioners, and retirees contribute by writing and/or reviewing books aimed at diverse levels of readers including children, youth, undergraduate and graduate students, groundwater professionals, and the general public.

The GW-Project operates with the philosophy that high-quality groundwater education should be freely accessible for everyone, and to that end our publications are available free-of-charge on our website↗. We thank our corporate sponsors and private donors for making this possible. Please consider sponsoring the GW-Project so we can continue to provide groundwater education free of charge.

The Groundwater Project *Board of Directors*, January 2026

Foreword

Knowledge of groundwater flow systems in which the flow results from gravity acting on water in natural hydrological settings is fundamental to understanding groundwater science. This concept is introduced in the first book published by the Groundwater Project, *Groundwater in Our Water Cycle*↗ (Poeter et al., 2020) and is also discussed in Chapter 6.1↗ of the book *Groundwater* by Freeze and Cherry (1979).

This book, *Groundwater Recharge to Discharge* by Diana Allen, elaborates on the introductory coverage of those books. It is the next step in learning about groundwater flow systems with emphasis on the water inputs and outputs. This book describes the many circumstances under which water known as recharge enters the system and later discharges from the system to become surface water, soil water, or atmospheric water vapor. The nature of recharge and discharge is described along with approaches for measuring their magnitude and estimating values of parameters that influence recharge and the discharge. In addition, it discusses the impact of recharge and discharge on the rise and decline of the water table and surface water flow in response to precipitation, especially as related to the changing seasons and climate.

The author of this book, Dr. Diana Allen, is recently retired from being the hydrogeology professor in the Department of Earth Sciences at Simon Fraser University, British Columbia, Canada, where for three decades she conducted field-focused and modeling studies of groundwater flow systems in a variety of settings. This book sets the stage for consideration of how climate change will impact groundwater, a topic of longstanding interest to Dr. Allen.

John Cherry, The Groundwater Project Leader

Guelph, Ontario, Canada, December 2025

Preface

This book is suitable for an upper-level undergraduate or graduate course on the broad topic of groundwater recharge and discharge. Select sections of the book—for example, Section 1 and Section 5—are appropriate to include in an introductory hydrogeology course. Because groundwater recharge and discharge occur at or near the land surface, and oftentimes in association with surface water bodies, it is important to explore the links to hydrometeorology, vadose zone hydrology, and surface water hydrology.

Section 1 introduces the concepts of recharge and discharge and recharge and discharge areas, and, importantly, how they relate to the groundwater flow system.

Section 2 is the most comprehensive, exploring diffuse recharge in detail, specifically the factors controlling diffuse recharge such as how precipitation partitions at the land surface, climate and weather, and the characteristics of precipitation. Next, evapotranspiration is discussed, including Earth's energy balance and the processes of evaporation and transpiration and how they are measured. Infiltration through the vadose zone follows, with details concerning capillarity and matric potential and soil moisture characteristic curves, ultimately ending with the infiltration process and how infiltration is quantified. The last two subsections of Section 2 discuss the redistribution of recharge and streamflow generation.

Section 3 focuses on groundwater discharge, beginning with exchanges between surface water and groundwater, a topic explored in Groundwater-Surface Water Exchange: Rivers, Lakes, and Wetlands↗ by Woessner (2020). Discharge to streams, lakes/wetlands, and saline water bodies is discussed, followed by discharge as springs/seeps. The last two subsections of Section 3 consider flowing wells and groundwater abstraction, both of which are due to human intervention.

Section 4 explores the dynamic nature of recharge and discharge, including an examination of groundwater-level hydrographs, the concept of groundwater storage, and methods used to estimate recharge and discharge. The seasonal variations in the timing and distribution are discussed, with examples from regions with cold, temperate, and semi-arid/arid climates. Variability is also explored at the sub-daily/daily timescales due to processes such as precipitation events, atmospheric pressure variations, air entrapment, and vegetation demand, as well as over longer periods due to climate cycles and climate change. The section ends with a discussion of the dynamic interactions between groundwater and surface water.

Section 5 focuses on a few topics related to the alteration of recharge and discharge, beginning with groundwater abstraction, irrigation, and managed aquifer recharge, the latter covered in Managed Aquifer Recharge: Southern Africa↗ by Braune and Israel (2022). The final two subsections of Section 5 skim the surface of two important topics:

groundwater and ecological systems, notably groundwater dependent ecosystems, and climate change impacts on recharge and discharge.

Acknowledgments

I deeply appreciate the thorough and useful reviews of this book by the following individuals:

- Masaki Hayashi, University of Calgary, Calgary, Alberta, Canada;
- Jana Levison, University of Guelph, Guelph, Ontario, Canada.

I am grateful to the authors who generously contributed boxes to this book:

- John Molson, Jean-Michel Lemieux, Rene Therrien, Nathan Young, Université Laval, Canada
- Vincent Post, Edinsi Groundwater, The Netherlands;
- David Bethune, University of Calgary, Canada; M. Cathryn Ryan, University of Calgary, Canada; Fluquer Peña Laureano, Pontificía Universidad Católica de Perú, Lima, Peru; Katiusca Yakabi, Pontificía Universidad Católica de Perú, Lima, Peru.
- Masaki Hayashi, University of Calgary, Canada
- W. J. Hahm, Simon Fraser University, Canada

I am grateful to Amanda Sills and the Formatting Team of The Groundwater Project for their oversight and copyediting of this book. I thank Judith Schenk (JS Hydro Geo LLC, Lakewood, Colorado, USA) and Eileen Poeter (Colorado School of Mines, Golden, Colorado, USA) for reviewing, editing, and producing this book.

The sources of figures and/or tables are cited in their captions. Where a citation does not appear, the figures and/or tables are original to this book.

1 Recharge and Discharge in the Flow System

1.1 What Is Groundwater Recharge?

Put simply, groundwater recharge is the replenishment of the groundwater system. Recharge is measured as a rate (e.g., mm/year). Healy (2010) defines recharge as the downward flow of water that reaches the water table and adds to groundwater storage. Freeze and Cherry (1979) adopted a similar definition, associating recharge with the addition of water to the groundwater system at the water table but also with the associated flow of water away from the water table within the saturated zone. Other sources, including this book, adopt a broader definition of recharge to include 1) water that is exchanged between aquifers (i.e., *interaquifer flow* or *interaquifer exchange*, as defined by Healy, 2010), 2) recharge via irrigation return flow and artificial recharge (discussed in Sections 5.2 and 5.3), and 3) anthropogenic sources of recharge such as leaking infrastructure in cities (e.g. sewers and water mains). The varied definitions of groundwater recharge suggest that we be very clear about what we do and do not consider recharge in our groundwater investigations, particularly when we are calculating water balances. This book focuses on recharge by precipitation, but other types of recharge are discussed.

Recharge occurs through two main mechanisms: *diffuse recharge* and *focused recharge* (Figure 1). Diffuse recharge, sometimes referred to as *direct recharge* (e.g., Simmers, 1997), is recharge that is distributed across the land surface. The recharge rate, usually quantified in mm per year or mm per month, is not uniform in space or time. Diffuse recharge occurs in response to precipitation that infiltrates the geologic materials at the ground surface. The term *precipitation* is used explicitly here because in cold regions, precipitation falls in the form of snow; only when the snow melts can it infiltrate the ground. Some of the water that infiltrates will percolate down to the water table and recharge the groundwater system.

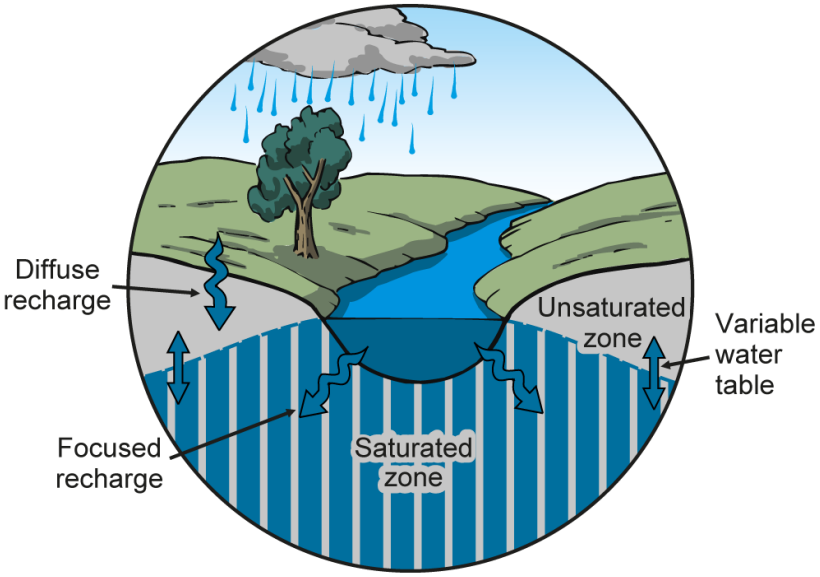

Figure 1 - Diffuse recharge occurs directly from precipitation (rainfall, snowmelt) when water enters the unsaturated zone and percolates downward to the saturated zone. Focused recharge occurs from streams, rivers, and lakes, contributing water to the saturated zone. In both cases, the water table responds dynamically, and its height varies seasonally (modified from Rivera, 2013, Figure 4.2).

Focused recharge is recharge within a localized area. Focused recharge is typically associated with the inflow of water from a surface water body (e.g., a stream or lake) to the groundwater system. These surface water bodies are referred to as *influent* or *losing*. Influent conditions occur when the water table in the adjacent groundwater system is lower than the water level, or stage, of the water body (Figure 1).

Focused recharge can occur in topographic depressions on the land surface and is referred to as *depression-focused recharge* (discussed in Section 4). Focused recharge can also occur along fracture zones and permeable faults. Some authors (e.g., Lerner et al., 1990) distinguish different types of focused recharge, with *localized recharge* defined as concentrated recharge from small depressions, joints, cracks, and other macropores, and *indirect recharge* defined as recharge from mappable features, such as streams and lakes. In this book, the general term *focused recharge* is adopted.

Both diffuse and focused recharge can occur in a groundwater system. They can occur in different areas or in the same area but at different times of the year, depending on the climate and other hydrological factors (such as stream discharge). Figure 2 shows a three-dimensional groundwater flow system that developed due to variable topography and geology. Diffuse recharge occurs across the landscape. The high-elevation area contains a small lake where focused recharge contributes water to both the *confined* and the *unconfined aquifer*. The relative contributions of diffuse and focused recharge change throughout the year due to seasonal climate variations. Groundwater discharges from the unconfined aquifer to the large lake. Small upland lakes are often sources of focused

recharge, while large lakes at low elevation are commonly discharge areas (subsection 1.2 presents more details).

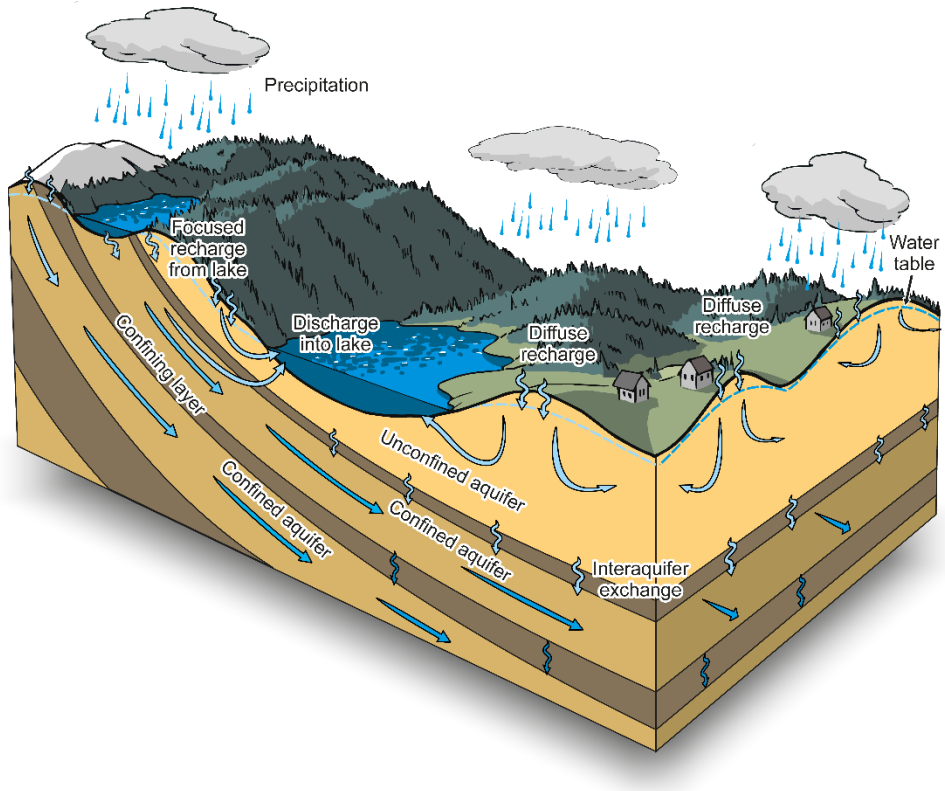

Figure 2 - A three-dimensional groundwater flow system with unconfined and confined aquifers. Groundwater is recharged both at high elevation and lower elevation from precipitation (diffuse recharge from rain and snowmelt), as well as from the upland lake (focused recharge). The confined aquifers receive some recharge by exchange of water through confining units (interaquifer exchange) and from areas at higher elevation where the aquifer outcrops at the surface (modified from Rivera, 2013, Figure 4.1).

Confined aquifers can be recharged in two main ways: 1) from overlying aquifers, via seepage through confining layers; and 2) by diffuse recharge in distant upgradient areas where the confined aquifer outcrops at surface (Figure 2). In some cases, very deep aquifers, such as those found in deep sedimentary basins, may be recharged in remote regions, such as mountains. *Semi-confined aquifers*, with confining layers that are discontinuous, may be recharged in areas where the confining layer is thin to absent or where the confining layer has a localized high permeability due to fracturing, desiccation cracks, or macropores. The geometry of the aquifer system, the permeability of the geologic units, and where these permeable geologic units outcrop determines where recharge occurs.

The term *interaquifer exchange* is used to describe the exchange of groundwater between one aquifer and another. Because one aquifer is losing water and one is gaining water, interaquifer exchange is technically both a recharge and a discharge process. Pumping from a deep confined aquifer can induce recharge by drawing water downward from a shallower aquifer. This can occur if the hydraulic head in the deeper aquifer is reduced sufficiently to cause a downward vertical gradient inducing downward flow.

Regardless of whether recharge is diffuse or focused, the annual replenishment of a groundwater system is fundamental for ensuring a sustainable groundwater resource for human use and for the environment.

1.2 What Is Groundwater Discharge?

Groundwater discharge is the loss of groundwater from the subsurface to the surface environment. Discharge is typically measured as a volumetric-flow-per-unit time (e.g., m^3/s). The most common form of natural discharge is water that leaves the groundwater system and enters a surface water body, such as a stream or a lake or the ocean. Groundwater discharge to a stream, for example, can occur along the length of the stream through the cross-sectional area of the saturated zone that is in contact with the stream (Figure 3). Discharge to the stream may also occur in a localized area, perhaps through a gravel lens or a fracture in bedrock that intersects the stream. Springs and seeps are dominant forms of groundwater discharge, too. Springs and seeps occur where the water table intersects the land surface (Figure 3). Springs are focused discharge points, while seeps (or seepage faces) cover a larger area.

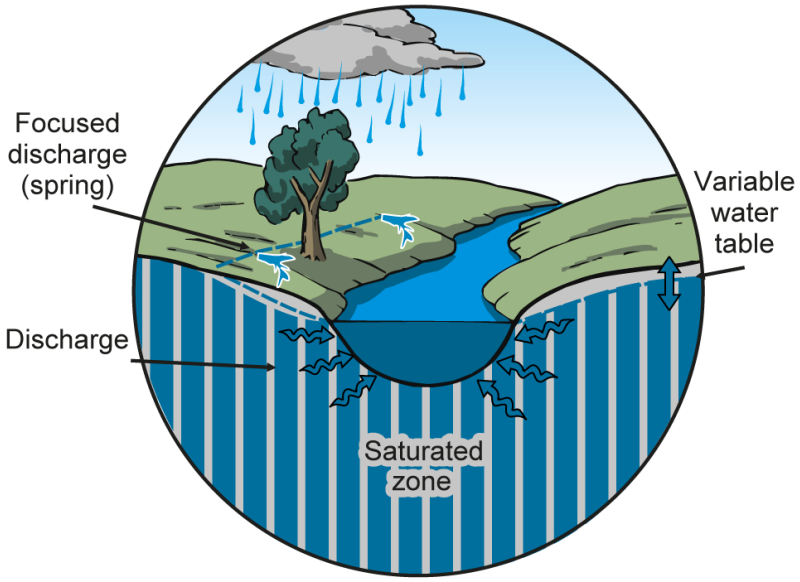

Figure 3 - Diffuse discharge to a stream (or other surface water body) occurs where the saturated zone comes into contact with the stream. Focused discharge from springs occurs where the water table intersects the land surface. In both cases, the water table responds dynamically, and its height varies seasonally (adapted from Rivera, 2013, Figure 4.2).

Woessner (2020) uses the terms *diffuse exchange* and *concentrated* [or focused] *exchange* when referring to exchanges of water between the groundwater system and surface water bodies. In the broad context of Figure 3, discharge (either diffuse or focused) occurs where the saturated zone is in contact with the stream, while focused discharge occurs at the point where the spring issues.

Surface water bodies are not only locations of groundwater discharge. Surface water bodies can also recharge groundwater systems as focused recharge, as described in subsection 1.1. The exchanges of water between the groundwater system and surface water body vary spatially and temporally, as explored in detail by Woessner (2020).

Groundwater discharge is an important source of water for many ecological systems. In particular, groundwater-dependent ecosystems (GDEs) depend on groundwater discharge, meaning that the ecosystem relies on groundwater for some or all its water requirements. Without groundwater, the ecosystem cannot function properly. In such GDEs, not only can the groundwater discharge rate be relatively constant throughout the year but so can the groundwater temperature. The relatively constant temperature of the discharging groundwater acts as a thermal buffer to seasonal variations in stream temperature, providing a more stable habitat for aquatic ecosystems. Some ecosystems may be groundwater influenced, meaning that groundwater discharge has an important influence on the health of the ecosystem.

1.3 Recharge and Discharge Areas in the Groundwater Flow System

Where recharge and discharge occur depends on the characteristics of the groundwater flow system. Groundwater flow systems, encompassing the three-dimensional flow of groundwater in the subsurface, have been explored in several other books in this series. For example, Poeter and others (2020) introduce the concept of groundwater flow systems and how they are a critical component of the water cycle, while Cohen and Cherry (2020) build a conceptual understanding of hydraulic head and the associated intuitive capacity for visualizing groundwater flow in one- and two-dimensional space based on head data and information about basic geologic conditions such as hydraulic conductivity. The topic of groundwater flow systems is covered so broadly because understanding groundwater flow at a variety of scales, both spatially and temporally, is central to understanding the various processes that drive the flow system naturally (e.g., recharge and discharge) and that alter it (e.g., groundwater pumping). This section provides an overview of groundwater flow systems, specifically as they relate to identifying groundwater recharge and discharge areas.

Groundwater flow systems range from simple to highly complex. An example of a simple flow system is shown in Figure 4. Here, the ground surface slopes gently from an area of higher elevation toward a stream at lower elevation. Diffuse recharge occurs across the landscape, adding water to the groundwater system and maintaining the height of the water table within the unconfined aquifer while the water discharges to the stream, such that the water table slopes to the stream. Without the addition of recharge to this system, the water table would drop, eventually becoming horizontal. There would be no hydraulic gradient, so there would be no flow. Over the long term, under natural conditions, there is a balance between the rate at which water is added to the system (recharge rate) and the

rate at which water exits the system (discharge rate). This balance maintains the water-table profile, which often mimics the topography.

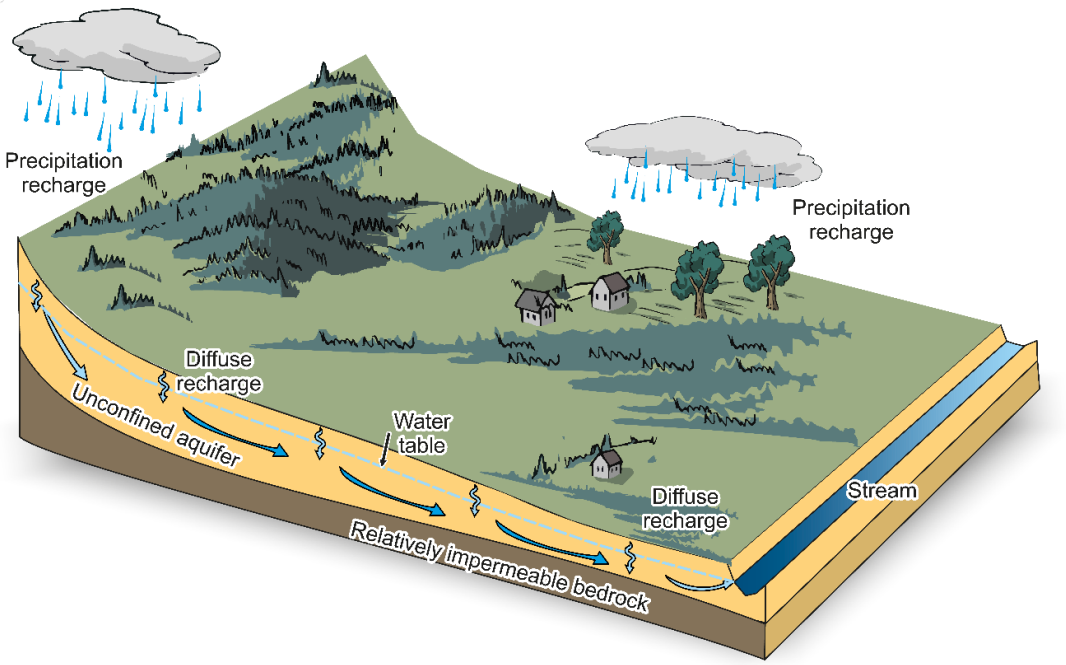

Figure 4 - A simple groundwater flow system within an unconfined aquifer. Diffuse recharge to the unconfined aquifer occurs across the landscape, maintaining a sloping water table that drives groundwater flow from high elevation to low elevation, where it ultimately discharges into the stream. In this simple system, groundwater flow is shown to be exclusively within the unconfined aquifer, because the underlying bedrock is relatively impermeable (adapted from Rivera, 2013, Figure 4.1).

In Figure 4, the underlying bedrock is assumed to be impermeable relative to the overlying materials forming the unconfined aquifer. However, bedrock is permeable to some degree, depending on the rock type (sandstone versus igneous rock) and the intensity and interconnectedness of fractures. Groundwater flow systems in bedrock can be complex. For example, Welch and Allen (2012) explored geometries of mountain catchments with homogenous bedrock and demonstrated that groundwater can flow from one catchment to an adjacent catchment if the catchments have different surface topographies (Figure 5). Figure 5a shows three adjacent catchments with the same bedrock hydraulic conductivities but different surface topographic expressions. The central valley of each catchment contains a main second-order stream that is fed by a series of first-order streams. In this example, the main stream is deeply incised into the mountain block, so most of the groundwater will discharge into the stream network and exit the mountain system as surface *mountain front recharge* (MFR) (red arrows in Figure 5a). A relatively smaller proportion of groundwater will discharge as subsurface *mountain block recharge* (MBR) (green arrows in Figure 5a). Figure 5b shows only the groundwater flow path lines that move from one catchment to the adjacent one; the flow direction is noted by the arrow. Groundwater originating in one catchment can discharge into an adjacent (or even next adjacent) catchment when there are differences in topography. The greater the differences

in catchment symmetry and relief, the more significant is cross-catchment groundwater flow.

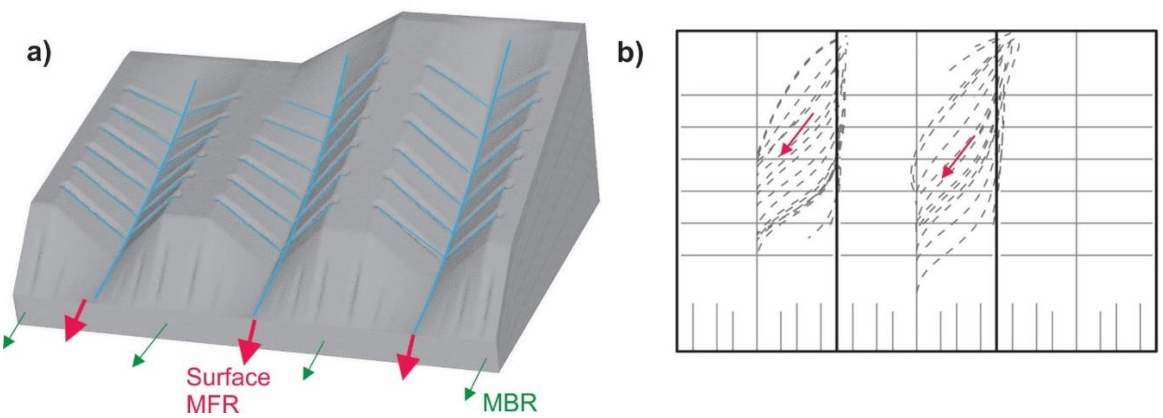

Figure 5 - a) Conceptual catchments with nonsymmetric topography showing surface mountain front recharge (surface MFR) and mountain block recharge (subsurface MBR). b) Projected ridge lines (black) with groundwater flow path lines (dashed dark gray lines) showing only cross-catchment flux. The red arrows indicate general flow direction.

Mountain precipitation is an important source of recharge to adjacent valley aquifers (Figure 6) as observed by Feth (1964) and explored further in Box 1. Valley aquifers can receive contributions from both *surface* MFR and *subsurface* MBR (Feth, 1964; Markovich et al., 2019; Wilson & Guan, 2004). While MBR is commonly associated with diffuse recharge in the mountain block, groundwater entering the valley bottom via faults or fracture zones in the mountain bedrock represents focused MBR.

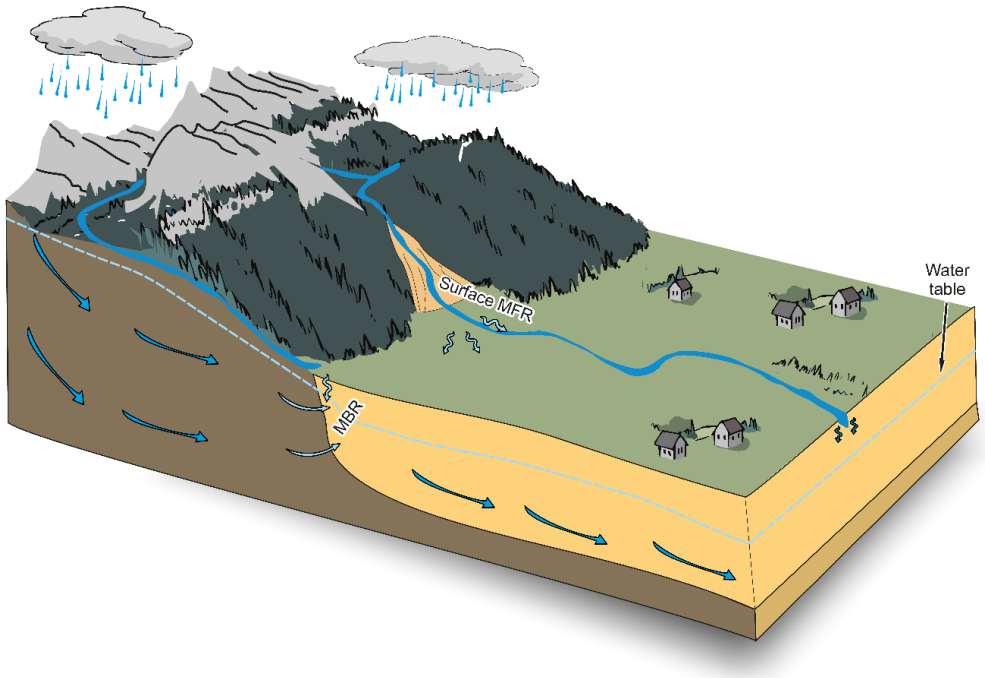

Figure 6 - Mountain front recharge (MFR) is an important source of recharge to valley-fill aquifers. MFR includes recharge from stream loss at mountain fronts (surface MFR), along with subsurface transfer of groundwater from the mountain block to the adjacent alluvial aquifer (mountain block recharge, or MBR) (adapted from Rivera, 2013, Figure 4.1).

Aquifers can extend for hundreds of kilometers beneath the land surface, often crossing natural surface watershed boundaries or jurisdictional boundaries. As such, groundwater may recharge in one watershed and discharge in another or perhaps recharge in one state or nation and discharge in another. For example, the Nubian Sandstone Aquifer System (NSAS) extends over Egypt, Libya, Sudan, and Chad (Figure 7). The NSAS is one of the largest aquifer systems in the world, covering approximately 2.6 million square km in Northeast Africa. The aquifer system is mostly confined; some parts are unconfined. The aquifer receives minimal recharge (<2 mm per year), and groundwater demand is met through extraction of *fossil* groundwater (discussed in Section 4) that was recharged during past wet periods (pluvial periods) associated with the Holocene African Humid Period. Groundwater in the NSAS beneath Egypt originates largely from inflow at the Sudan border (Massoud et al., 2013).

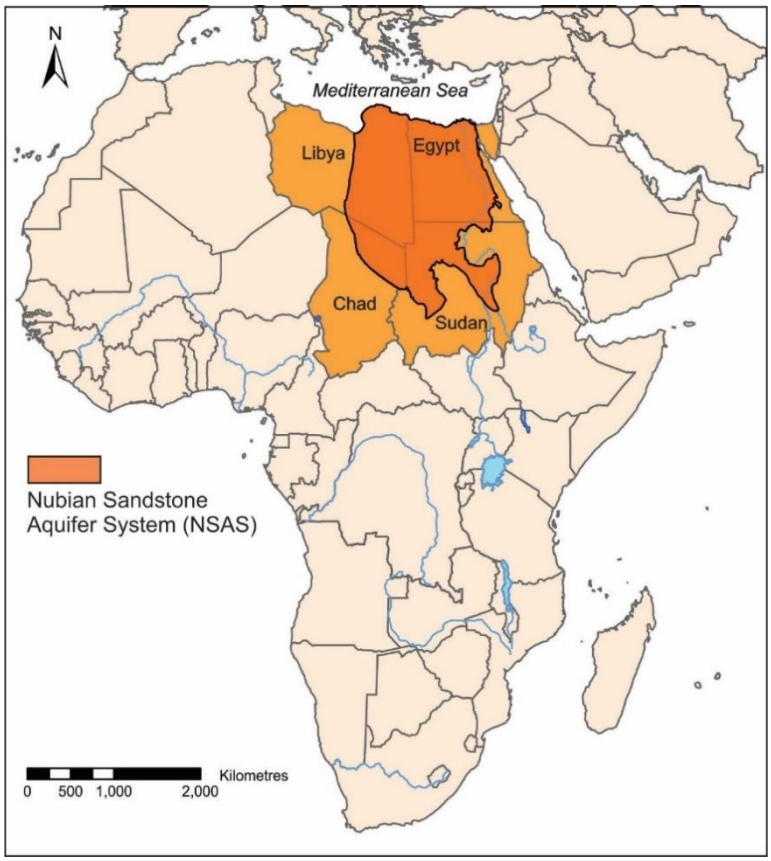

Figure 7 - The Nubian Sandstone Aquifer System in northeastern Africa extends over Egypt, Libya, Chad, and Sudan (modified from original found in IGRAC, 2020).

Transboundary aquifers↗ (International Groundwater Resources Assessment Centre (IGRAC), 2020) are of multinational importance because extensive development of groundwater reservoirs in the recharge area in one country can impact groundwater and surface water quantity and quality downgradient. For this reason, quantitative assessments of groundwater fluxes and sources of recharge are essential for common use of local groundwater resources in transboundary aquifers. The worldwide Internationally Shared

Aquifer Resources Management (ISARM) is a United Nations Educational, Scientific and Cultural Organization–Intergovernmental Hydrological Programme (UNESCO-IHP), Food and Agricultural Organization (FAO), United Nations Economic Commission for Europe (UNECE), and IAH (International Association of Hydrogeologists) initiative on transboundary aquifers. ISARM aims to improve understanding of scientific, socio-economic, legal, institutional, and environmental issues surrounding the management of transboundary aquifers.

Groundwater flows from high hydraulic head to low hydraulic head. Using nested piezometers, vertical groundwater flow components (up or down) can be measured. Piezometers placed at different geographical locations allow us to measure horizontal groundwater flow; Cohen & Cherry (2020) provide a detailed explanation of these fundamental principles. Where we have numerous measurements of hydraulic head in an area, we can map the equipotential lines in plan view or in cross section, or indeed map the equipotential surfaces in three dimensions, to generate a flow net that represents the groundwater flow in the system (Poeter & Hsieh, 2020); Exercise 1.

Freeze and Cherry (1979) define recharge and discharge areas as follows.

- A recharge area is an area where the *net direction of saturated groundwater flow is vertically downward* being directed away from the water table into the flow system.
- A discharge area is an area where the *net direction of saturated groundwater flow is upward.*

Based on these definitions, the recharge areas and discharge areas can be identified using hydraulic head data. In a recharge area, hydraulic head values will decrease with increasing depth, while in discharge areas, the hydraulic head is greater at depth than near the surface. Tóth (1962) noticed this phenomenon in a small drainage basin in central Alberta, Canada where wells in a *definite recharge area* showed a decrease in head of about 0.5 m per m of depth. Wells in a definite discharge area showed virtually no change in head to a depth of about 36.5 m, suggesting lateral flow, beyond which depth the head decreased as much as 0.70 m per m (Tóth, 1962, Fig. 5). Other approaches can be used to identify recharge and discharge areas, including examining the topography, geological substrate, vegetation type (or lack thereof), and groundwater salinity (discussed in Sections 2 and 3); Exercise 2.

Recharge and discharge areas are usually mapped on the land surface. Such maps are being increasingly used in support of land-use decision-making for identifying areas that should be protected from development that may impact the quantity or quality of groundwater in the aquifer. A common misconception is that recharge occurs only in these recharge areas. However, examination of Figure 2 reveals a sloping water table. If the water table is sloping, there must be some component of vertical flow, even though the net

direction of flow is horizontal. Recharge can take place across most of the land surface but may be more concentrated in some areas.

Hydraulic gradients vary in space and time, so it is not surprising that recharge areas and discharge areas might also vary in space and time. Figure 8 shows a conceptual model of how the seepage (i.e., discharge of groundwater at the land surface) changes as the water table rises. Following a long, dry period with no precipitation, the water table is at its maximum depth (red dashed line). When the water table is deep, seepage occurs only at the base of the slope where the water table intersects the land surface. As the water table rises to reach its maximum height following a prolonged period of recharge (blue dashed line), the seepage area expands to form a larger seepage face. Any changes to the groundwater system that might result in altered volume or timing of flow may result in changes to the extent of recharge and discharge areas. Section 4 explores the dynamic nature, both spatially and temporally, of recharge and discharge.

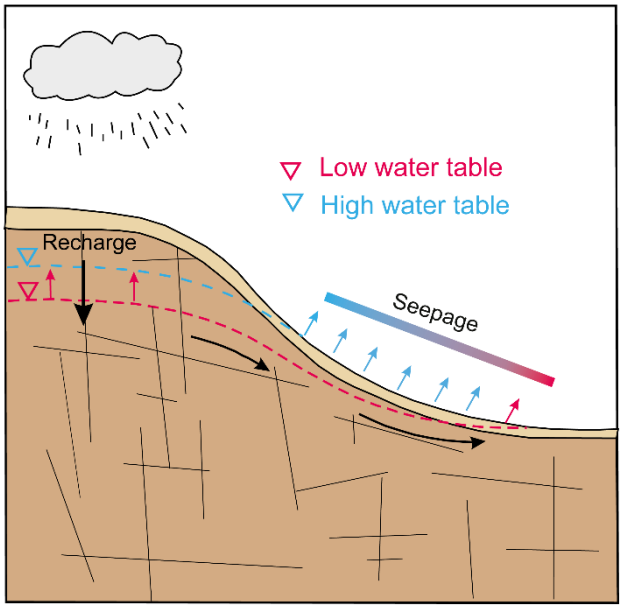

Figure 8 - Conceptual model of diffuse recharge in an area with a relatively shallow water table. The net available precipitation will either infiltrate or form overland flow. The aquifer response to infiltration is shown as a rise in groundwater level (inverted triangle). Intersection of the water table with the land surface results in seepage where groundwater discharges to the surface.

1.4 Summary

This section introduced the concepts of recharge and discharge and, importantly, how they relate to the groundwater flow system. Key takeaways include that groundwater recharge is the replenishment of the groundwater system and that there are two main mechanisms for this replenishment: diffuse recharge and focused recharge.

Both mechanisms can occur in different parts of the groundwater flow system. The replenishment of confined aquifers can occur from overlying aquifers, via seepage through

confining layers, and by recharge in distant upgradient areas where the confined aquifer outcrops at the surface. Interaquifer exchanges also result in the replenishment of one aquifer via the loss of water from another. Section 2 explores the processes controlling diffuse recharge in more detail, specifically the factors that influence how precipitation partitions at the land surface into evapotranspiration, overland flow, infiltration, and, ultimately, diffuse recharge.

Another key takeaway is that discharge is the loss of groundwater from the subsurface to the surface environment and that, like recharge, discharge can be diffuse or focused. Groundwater discharges to surface water bodies as well as to springs and seeps. Groundwater discharge to surface water bodies sustains the flow needed to support aquatic ecosystems. Section 3 explores groundwater discharge and exchange with surface water in more detail.

Based on an understanding of the groundwater flow system, recharge and discharge areas can be mapped, recognizing that their extent might vary in space and time as groundwater pathways change seasonally or over the longer term. Knowledge of the location of important recharge areas can support land-use decision-making to identify areas that should be protected. Section 4 examines recharge and discharge processes in different hydrogeological settings.

2 Processes Controlling Diffuse Recharge

Several processes control diffuse recharge; each process is influenced by different factors, such as climate, topography, geological materials, and type of vegetation. This section begins with an overview of how precipitation partitions at the land surface into evapotranspiration, infiltration, and overland flow. Next, climate variables and some fundamentals about the formation of precipitation are discussed, because these relate to the moisture-holding capacity of the atmosphere, which drives many important meteorological phenomena. Atmospheric moisture also influences evapotranspiration, which is the next topic discussed in some detail. Then follows an overview of infiltration and redistribution of water in the unsaturated zone and, ultimately, recharge to the water table. Streamflow generation as it relates to surface water hydrology is discussed briefly at the end of the section.

Factors controlling focused recharge are discussed in the context of water exchanges between surface water bodies and the groundwater system in Section 3, as well as in Woessner (2020).

2.1 Partitioning of Precipitation at the Earth's Surface

Precipitation landing on the ground surface will *partition*. In the absence of vegetation, the water arriving at the ground surface can 1) be lost to evaporation, 2) infiltrate and potentially form diffuse recharge, and/or 3) form overland flow as illustrated in the conceptual model in Figure 9. In this conceptual model, the land surface has a gentle slope, the ground is bare—that is, no vegetation, and the substrate consists of a thick soil zone with a water table at some depth. During heavy rainfall events, small-scale variations in topography, or microtopography, can lead to water collecting in small depressions, termed *depression storage* (as illustrated by the small blue puddle in Figure 9), where *evaporation* may occur. If precipitation falls in the form of snow, some water will be held on the land surface as snowpack, from which sublimation can occur. If the depression storage capacity is exceeded, the depressions will overflow, and the water will form *overland flow* and be directed down the topographic gradient, where it may collect in other depressions and evaporate or be routed to streams or other surface water bodies as *surface runoff*. The water that is not lost to evaporation or overland flow *infiltrates* and is held in the soil as *soil moisture*. If there is an upward gradient of soil moisture within the soil zone, then moisture can be routed back to surface and lost to evaporation. Ultimately, if sufficient water enters the soil zone, it will percolate downward under the force of gravity through the unsaturated (i.e., vadose) zone to the water table, where it is added to the saturated zone as *diffuse recharge*. The rate at which diffuse recharge occurs is thus determined by a complex interaction between climate and various characteristics of the land surface, such

as topography, vegetation, soil type, and geology, which collectively affect the timing and amount of water available for infiltration (Scanlon et al., 2002).

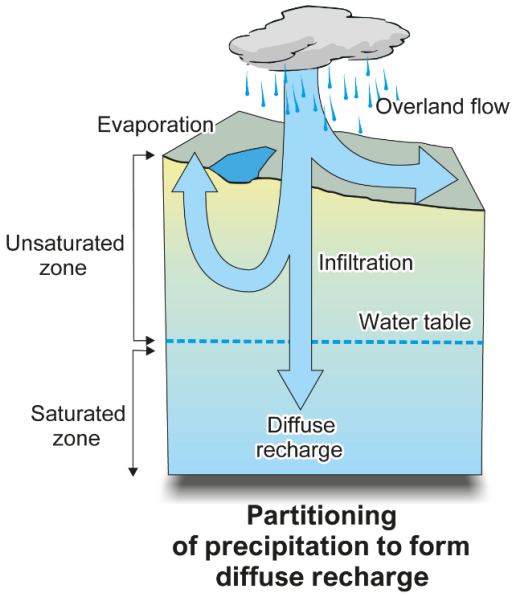

Figure 9 - Precipitation (shown here as rain) falling on a bare ground surface partitions into evaporation, infiltration, and overland flow. Water held in small depressions in the land surface (shown here as a blue puddle) can evaporate. Some water that infiltrates can move back up to surface and evaporate. Infiltrated water that passes the water table is diffuse recharge. Overland flow directs surface water down the topographic gradient.

The processes controlling how precipitation partitions at the land surface are interdependent, and the relative proportion of each component is determined by a variety of factors, including the climate, topographic slope, geologic substrate, and vegetation (if present) as shown in Figure 10. Figure 10a is the same as that shown in Figure 9 except that evapotranspiration occurs due to the presence of vegetation (as discussed in subsection 2.4). In Figure 10b and c, the partitioning for two extreme cases is shown. Figure 10b represents conditions that favor low diffuse recharge, including a warm, dry climate, steep topography with sparse vegetation, and low-permeability geologic materials. Figure 10c represents conditions that favor high-diffuse recharge, including a cool, wet climate, generally flat topography with sparse vegetation, and high-permeability geologic materials. A brief overview of the role of each factor is given below. A detailed examination of climate, precipitation, evapotranspiration, infiltration, overland flow, and percolation to the saturated zone follows in subsequent sections of this book.

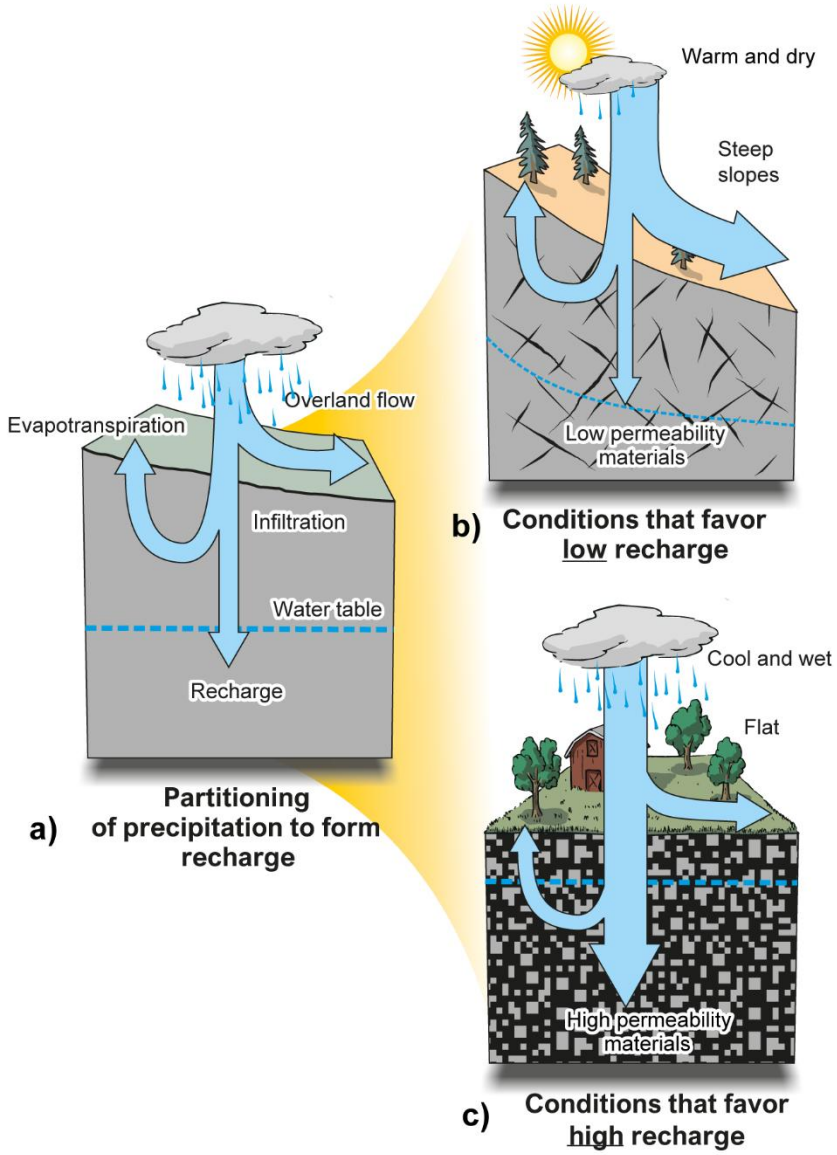

Figure 10 - a) Partitioning of precipitation into overland flow, evapotranspiration, and infiltration. b) Warm and dry regions with a deep-water table, steep slope, and low-permeability geologic materials favor low recharge. c) Cool and wet regions with a shallow water table, flat terrain, and high-permeability materials favor high recharge. The arrow widths in the figures at the right represent the relative magnitude of each component (modified from Rivera, 2013, Figure 4.6).

Climate is the dominant factor in partitioning precipitation at the land surface. Areas that have a warm and dry climate typically have a deeper water table because the limited soil moisture evaporates rapidly. In such climates, the amount of precipitation is the limiting factor for recharge. In contrast, areas with a cool and wet climate have plenty of precipitation, and so the water table is shallower. In these areas, the geological substrate is the limiting factor for recharge due to its ability to transmit and store water.

Geologic materials of high permeability, such as sand and gravel, favor groundwater recharge because the water percolates rapidly. For this reason, unconfined aquifers comprised of sand and gravel typically have high groundwater recharge rates, assuming

there is adequate precipitation. In contrast, geologic materials of low permeability, such as crystalline rock and clay-rich sediments, tend to inhibit groundwater recharge. Consequently, groundwater yields from fractured rock aquifers are generally low, and the groundwater resource can become unsustainable if pumped for long periods. Fractures and faults, however, have been observed to act as conduits for groundwater recharge. If fractures are intersected by a well, the fractured rock will often yield higher quantities of groundwater compared to unfractured rock.

The *slope* of the land surface (topographic slope) and the permeability of the sediments or rocks that lie within the unsaturated zone exercise strong control over the amount and timing of groundwater recharge. Steeper topographic slopes promote more overland flow, particularly when the geologic substrate has a low permeability.

Vegetation type and cover influence recharge through the processes of interception and transpiration and other less-commonly characterized, yet potentially significant, processes such as stemflow and throughfall (e.g., Le Maitre et al., 1999). Practically, transpiration is difficult to separate from evaporation, so the two processes are usually combined as evapotranspiration. Factors that affect evapotranspiration include the plant's growth stage or level of maturity, the percentage of soil cover, solar radiation, humidity, temperature, and wind. Through evapotranspiration, forests reduce the water available for recharge.

Different *anthropogenic factors*, such as pavement (e.g., roads), buildings, agriculture, or forest harvesting, can affect natural infiltration and groundwater recharge. Indeed, our modification of the land surface has led to significant alterations of natural recharge rates in many areas; Exercise 3↴.

2.2 Climate and Weather

The climate and weather of an area exercise the most important control over recharge, determining not only the seasonal patterns of precipitation but also the temperature, relative humidity, as well as wind and air movement, which are important factors influencing evapotranspiration (subsection 2.4). The weather and climate of an area vary seasonally, interannually, and at longer timescales, and these changes invariably affect the timing and amount of groundwater recharge.

2.2.1 Describing Climate and Weather

Climate is described by many meteorological variables: surface air temperature, precipitation, solar radiation, air pressure, wind, and humidity including a statistical description of these variables over a large time scale, typically 30 years (Table 1). These same variables are used to describe the *weather*, or current atmospheric conditions at a particular place and time. Weather changes from day to day according to changing atmospheric circulation patterns. Many countries operate weather stations at which daily (or hourly) measurements are made and reported (Table 1). Hourly air temperature varies

diurnally, being warmer during the day and cooler at night (Figure 11). The maximum and minimum daily temperatures (and thus the mean daily temperature[1]) differ from day to day and from season to season (*seasonally*). Over a longer time, the average daily temperature also varies from year to year (*interannually or interdecadally*). These are expressions of natural *variability* of meteorological conditions and climate (Figure 11).

Table 1 - Descriptions of climate variables as summarized from the National Oceanic and Atmospheric Administration (NOAA).

Climate variable	Description	
Surface air temperature (measured in °C)	The temperature of the air around us	Thermometers, shielded from direct solar energy, are used to measure surface air temperature generally at a height of around 2 m above the surface.
Precipitation (measured in mm)	Liquid or solid water that falls to Earth's surface from clouds. It can be in the form of drizzle, snow, ice, freezing rain, or hail	Rain gauges are the most common instrument used to measure rainfall. A rain gauge is a container (open at the top) that is calibrated to measure the depth of liquid caught. Satellite instruments can also detect and estimate precipitation amounts.
Solar radiation or solar irradiance (measured in W/m^2)	The energy from the sun	On the ground, an instrument called a solar pyranometer measures the amount of incoming solar radiation that reaches Earth. Instruments on satellites measure solar radiation at the top of the atmosphere.
Air pressure (measured in Pa)	The weight-per-unit area of the column of air above the surface	A barometer is used to measure air pressure. Changes in atmospheric pressure can signal a change in weather.
Wind (measured as wind speed in km/hour horizontal to the surface)	Air in motion relative to the earth's surface	Anemometers are used to measure wind speed. Wind vanes and windsocks measure wind direction. Wind directions refer to where the wind is coming from; for example, a north wind is coming from the north and blowing toward the south.
Relative humidity (measured in percent)	The amount of humidity in the air relative to the amount it has the potential to hold at a given temperature and pressure	The instrument used to measure water-vapor content in the air is called a hygrometer.

[1] The mean daily temperature is calculated as the average of the maximum daily temperature and the minimum daily temperature.

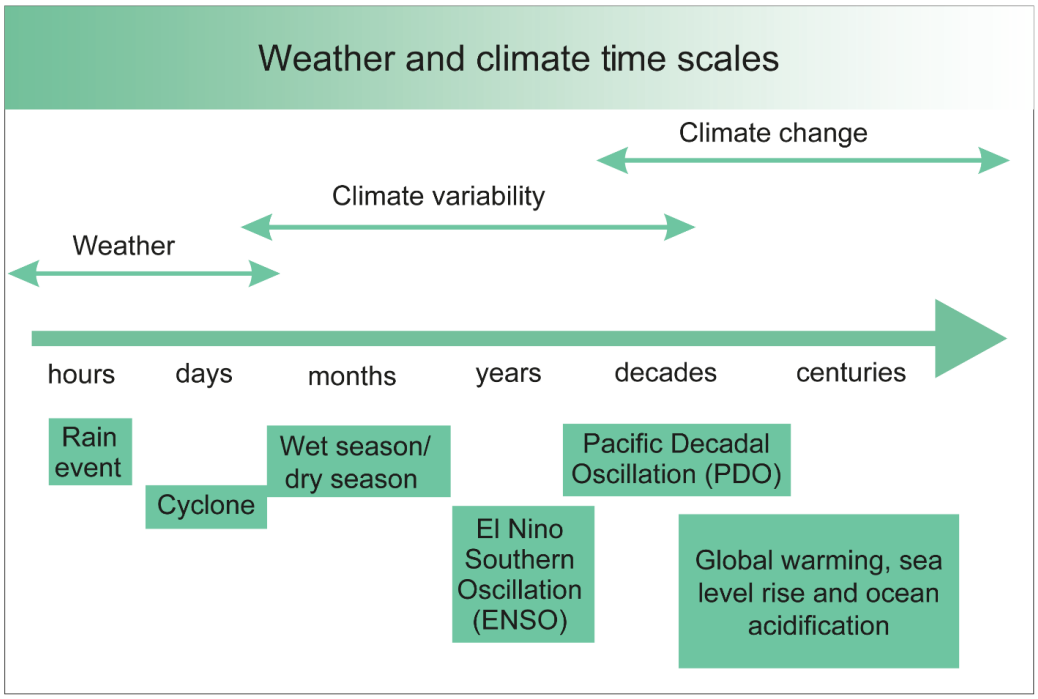

Figure 11 - Time scales applicable to weather, climate variability, and climate change (adapted from Australian Government, n.d.).

The climate of a region is characterized by the average weather conditions. These average conditions reflect the long-term, accumulated data derived from weather observations (e.g., long-term average temperature, humidity, cloud cover, and precipitation). Climatologists define a *climatic normal* as the arithmetic average of a climate variable, such as air temperature or precipitation, over a prescribed 30-year period (e.g., 1961–1990, 1971–2000, 1981–2010). A 30-year interval was selected by international agreement based on the recommendations of the International Meteorological Conference in 1933. A 30-year interval is sufficiently long to filter out many of the short-term interannual fluctuations and anomalies but is sufficiently short to be used to reflect longer-term climatic trends. Climate generally changes relatively slowly due to long-term changes in various factors controlling climate. Climate change, whether driven naturally or by humans, varies over much longer periods of centuries or longer (Figure 11).

Thought Question: Climate normals are often calculated by climatologists using meteorological data collected over 30-year intervals. These climate normals (for monthly mean daily temperature or monthly precipitation) can often be found online. For example, Environment and Climate Change Canada reports climate normals for many climate stations across Canada (Canadian Climate Normals↗). What are the climate normals for a nearby climate station in your country?

2.3 Precipitation

2.3.1 Moisture-Holding Capacity of the Atmosphere

Earth's atmosphere is composed of many gases, including *water vapor*. Water vapor absorbs and emits infrared radiation, which traps heat energy near Earth's surface. Half of the water vapor in the atmosphere is found within two kilometers of the earth's surface. Atmospheric water vapor drives many important meteorological phenomena, notably precipitation. Therefore, a good starting point for understanding precipitation is to consider how much water vapor the air can hold.

As a gas, the concentration of water vapor in the air is measured as a *partial pressure* (specifically the *vapor pressure*). The sum of all the partial pressures of the different gases in the atmosphere is the total *atmospheric (or air) pressure*.

Absolute humidity, also called vapor density, is the measure of the amount of water vapor in air. It is measured as a mass concentration of water vapor in a volume of air. The Ideal Gas Law relates the vapor pressure and the absolute humidity as shown in Equation (1).

$$d_v = \frac{e}{R_v T_a} \tag{1}$$

where:

d_v = absolute humidity (ML^{-3}) often as kg/m^3

e = vapor pressure ($ML^{-1}T^{-2}$) often as kPa

R_v = gas constant for water vapor ($ML^2\ T^{-2}\Theta^{-1}$) for d_v, e, and T in the units noted as often used here, R_v=0.463 kJ m kg^{-1} K^{-1}

T_a = air temperature (Θ) often as K

The maximum water vapor pressure that is thermodynamically stable is the *saturation vapor pressure*, e_s. The saturation vapor pressure is only a function of temperature (Equation D-7 in Dingman, 2002), as shown in Equation (2).

$$e_s = 0.611 exp\left(\frac{17.3\,T}{T + 273.3}\right) \tag{2}$$

where:

e_s = saturation vapor pressure ($ML^{-1}T^{-2}$) for the constants used here e_s is in kPa

T = Temperature, for the constants used here T is in °C (Θ)

Under natural conditions, e_s represents the maximum amount of water vapor that the atmosphere can hold at any temperature (T). The addition of more water vapor or the lowering of temperature results in *condensation* (subsection 2.3.2).

If the vapor pressure and the temperature are below those needed for saturation, then the air is unsaturated. The *relative humidity* (RH) is the ratio of air's actual water vapor pressure (e_a) to the saturated vapor pressure (e_s), typically expressed as a percent as shown in Equation (3).

$$RH = \frac{e_a}{e_s}(100) \tag{3}$$

where:

e_a = actual vapor pressure ($ML^{-1}T^{-2}$) for the constants used here e_a is in kPa

***Thought Question**:* What is the relative humidity at saturation?

The *dew point* (T_{dew}) is the temperature to which air must be cooled to become saturated with water vapor. When cooled further, the water vapor in the air will condense to form liquid water (dew). The dew point can be calculated for unsaturated conditions (Equation D-11 in Dingman, 2002), as shown in Equation (4).

$$T_{dew} = \frac{\ln(e) + 0.4926}{0.0708 - 0.00421\ln(e)} \tag{4}$$

The dependence of saturation vapor pressure on temperature, as in Equation (2), is an important relationship. Under typical atmospheric conditions, the denominator of the exponent in Equation (2) depends weakly on T. Thus, the saturation water vapor pressure changes approximately exponentially with temperature under typical atmospheric conditions. Hence, the water-holding capacity of the atmosphere increases by about 7 percent for every 1°C rise in temperature. Global warming is causing surface air temperatures to increase globally. A warmer atmosphere can hold more moisture, leading to a higher absolute humidity, which enhances the atmospheric circulation of water vapor. This can result in an increased frequency of extreme rain events and increased cloud cover in regions that are not moisture limited.

2.3.2 Characteristics of Precipitation

Precipitation is the source of all water that enters the land surface. Most regions around the world have some seasonal variability in precipitation, but the *precipitation intensity* (how much precipitation falls in one hour, for example) and duration (how long the precipitation event lasts) can be quite different depending on whether the region has a temperate, continental, tropical, dry, or polar climate (more information at Köppen-Geiger climate classification system↗) For example, in regions with a temperate marine climate such as London, United Kingdom, the proximity to the ocean moderates air temperatures and delivers lower intensity rainfall throughout the year (Figure 12a). In contrast, regions with a tropical climate such as Kampala, Uganda, have generally high temperatures and often a dry season and a wet (rainy) season (Figure 12b). During the rainy season, the rain events can be of high intensity and long duration. The intensity and duration of

precipitation events play important roles in how precipitation partitions at the earth's surface (subsection 2.6).

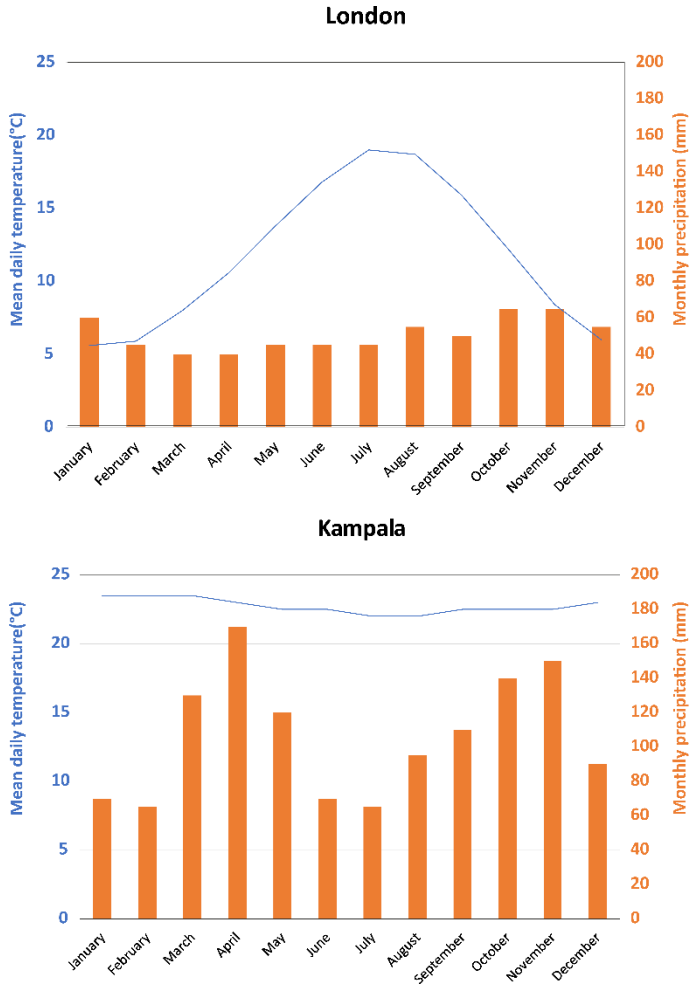

Figure 12 - Climate normals for London, UK (temperate marine climate), and Kampala, Uganda (tropical rainforest climate) The blue line is the average temperature, and the orange bars show the average monthly precipitation. (Data from https://www.climatestotravel.com↗).

Thought Question: Following the Köppen-Geiger climate classification system↗, three letters are used to describe the climate zone: 1) the first letter is the main climate, 2) the second letter is precipitation and 3) the third letter is temperature. For example, BWh is dry, desert, and hot. Which climate zone do you live in?

2.4 Evapotranspiration

While temperature plays an important role in humidity and precipitation generation (as discussed in subsection 2.3), its influence on recharge is primarily through *evapotranspiration*, a collective term for all the processes by which water in the liquid or solid phase at or near Earth's surface becomes atmospheric water vapor (Dingman, 2002). Evapotranspiration, or ET, includes the evaporation of liquid water from surface water bodies, bare soil, and vegetative surfaces; the sublimation from snow and ice surfaces; and

the evaporation from within the leaves of plants (*transpiration*). Evaporation and transpiration occur simultaneously, and there is no easy way of distinguishing between the two processes, so they are often considered together, particularly in recharge and water balance estimations.

Understanding the factors controlling ET is important for understanding the dynamics of recharge. This section begins with a brief overview of energy transfers at the earth's surface and then explores the physics of evaporation and transpiration, how different surfaces can affect ET rates, and how ET is estimated. A detailed treatment of the physics of evaporation and methods used to estimate ET can be found in hydrology textbooks (e.g., Dingman, 2002).

2.4.1 Energy at the Earth's Surface

Solar radiation is the main source of energy at the earth's surface (Figure 13). Incoming shortwave radiation (S_d) can be reflected by the atmosphere or the land surface, or it can be absorbed. The global average of incoming solar radiation is 342 W/m^2. A portion of this incoming solar radiation is reflected at the earth's surface. The amount reflected is a function of the *surface albedo*, α, defined as the ratio between solar radiation reflected by Earth's surface and solar radiation incident at the surface. Light-colored surfaces, such as snow and clouds, tend to reflect most solar radiation, while darker surfaces, such as oceans, forests, or soils, tend to absorb more solar radiation. The absorbed solar radiation warms Earth's land, water, and atmosphere. Natural changes in albedo occur seasonally due to changes in snow cover and vegetation. As a whole, the Earth has an albedo of roughly 30 percent, meaning that 70 percent of the solar radiation is absorbed.

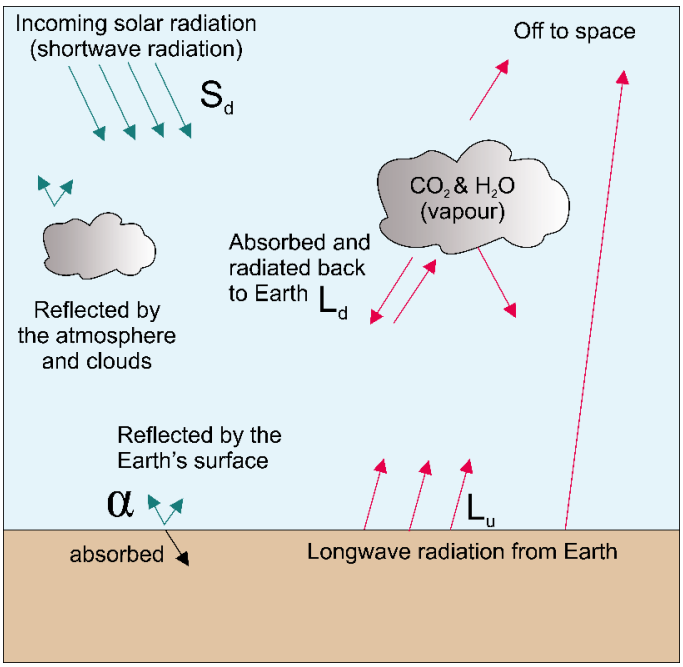

Figure 13 - Incoming and outgoing radiation in the atmosphere and near Earth's surface. Shortwave radiation is shown in green, and longwave radiation is shown in red.

Long-wave radiation (or thermal radiation) emitted from Earth (L_u) can similarly be absorbed by the atmosphere and clouds and radiated back to Earth (L_d) (Figure 13). The *net all-wave radiation* (i.e., incoming versus outgoing radiation) determines whether the earth's surface warms or cools. One hundred percent of energy entering Earth's atmosphere comes from the sun, and approximately 70 percent of this energy is absorbed by Earth's surface, clouds, and atmosphere, causing warming. Without this warming, Earth would be a very cold planet.

Equation (5) shows the net radiation at the earth surface as illustrated in Figure 13.

$$R_n = S_d(1 - \alpha) + L_d - L_u \quad (5)$$

where:

R_n = net all-wave radiation (MT^{-3}) typically as W/m^2

S_d = incoming short-wave radiation at the earth surface (MT^{-3}) typically as W/m^2

α = albedo (dimensionless)

L_d = the downward long-wave radiation (MT^{-3}) typically as W/m^2

L_u = the upward long-wave radiation (MT^{-3}) typically as W/m^2

Ultimately, the net radiation at the earth's surface is the source of energy for evaporation as explored in subsection 2.4.2. Importantly, there is considerable variation in the net radiation over space and time. Distance from the equator (essentially, the angle of the sun providing less solar energy at lower angles) affects the amount of incoming shortwave radiation reaching Earth's surface. Surface albedo can vary seasonally due to factors such as changing vegetation and snow cover, and variable cloud cover and greenhouse gases in the atmosphere trap radiation. Therefore, variations in net radiation daily, seasonally and over the longer term—for example, due to climate change—can impact evaporation rates.

2.4.2 Evaporation

Evaporation is a form of vaporization that involves the transition of liquid particles on a surface into the gaseous phase. Evaporation requires energy to excite the water molecules so they can leave the water surface. However, for evaporation to occur, the surrounding gas (air) must not be saturated with the substance that is evaporating. Energy is transferred as the molecules of the heated liquid collide with the surrounding gas. The liquid particles escape and enter the surrounding air as a gas when a molecule near the surface consumes enough energy to overcome the vapor pressure. The energy extracted from the vaporized liquid as evaporation occurs will decrease the temperature of the liquid, resulting in a process known as *evaporative cooling*.

Fundamentally, evaporation is a diffusion process. The vapor pressure of a wet evaporating surface is equal to the saturation vapor pressure at the surface temperature, e_s (kPa) as in Equation (2). The vapor pressure of the overlying air, e_a (kPa) depends on the relative humidity, as in Equation (3), as well as the temperature. If there is a difference between the two vapor pressures, then there is a gradient in the vapor pressure. Equation (6) gives the evaporation rate E in m s^{-1}.

$$E = K_E \, v_a \, (e_s - e_a) \tag{6}$$

where:

E = evaporation rate (LT^{-1})

K_E = coefficient that reflects how efficiently the water vapor is transported vertically into the air by turbulent eddies in the wind (LT^2M^{-1})

v_a = wind speed (LT^{-1})

The value of K_E can be estimated from the density of the air, the atmospheric pressure, and parameters that represent the surface roughness, which influences the intensity of the turbulent eddies at a given windspeed (Appendix D6 in Dingman, 2002).

The transfer of water vapor from the evaporating surface to the air is accompanied by a transfer of energy in the form of latent heat (*latent heat of evaporation, LE*). The heat transfer results in a decrease in the temperature of the surface, as in Equation (7).

$$LE = \rho_w \, \lambda_v E \tag{7}$$

where:

LE = latent heat of evaporation (ML^2T^{-2})

ρ_w = density of water (ML^{-3})

λ_v = latent heat of vaporization ($MT^{-2}\Theta^{-1}$)

The latent heat of vaporization decreases as the temperature of the evaporating surface increases according to Equation (8).

$$\lambda_v = 2.50 - 2.36 \times 10^{-3} \, T \tag{8}$$

where:

T = temperature in °C

λ_v = latent heat of vaporization in MJ/kg

Sensible heat transfer can also occur if there is a temperature difference between the surface and the air. The sensible heat transfer rate is proportional to the difference in temperature and is influenced by the wind speed, increasing as wind speed increases.

Finally, gradients in air velocity, v_a, above the surface give rise to a momentum gradient (momentum is mass times velocity). Velocity always increases with height due to frictional drag, which is greatest near the surface and thereby slows air movement near the surface. Therefore, momentum is transferred downward via turbulent eddies from where velocities are high to where they are lower.

Ultimately, evaporation is controlled by four transfer processes: 1) transfer of water vapor, 2) transfer of latent heat, 3) transfer of sensible heat (with 2 and 3 being transfer of energy), and 4) transfer of momentum. These transfer processes can be coupled mathematically as shown in Appendix D6 of Dingman (2002).

Considering meteorological conditions, the rate of evaporation is controlled by

- the amount of energy available (net radiation),
- vapor pressure deficit of the air which is a function of moisture content (i.e., relative humidity) and T, and
- the rate of removal of air from the evaporating surface (windspeed).

These meteorological conditions vary spatially and at different time scales, so evaporation rates also vary. The type of evaporating surface also plays an important role, as explored in Section 2.4.3.

2.4.3 Evaporation from Different Surfaces

Evaporation is influenced by the type of surface: a) open water, b) bare soil, or c) leaf or leaf canopy if vegetation is present.

Evaporation from open water is commonly estimated. Hydrometeorologists developed the theoretical concept of free-water evaporation, which would occur from an open-water surface in the absence of advection and changes in heat storage. Lake evaporation is determined by adjusting the free-evaporation estimate to account for advection (driven by wind) and heat storage effects in a specific water body (Dingman, 2002).

Bare soil evaporation occurs in the absence of vegetation. Following a rain event, snowmelt, or irrigation, the soil gradually dries due to evaporation and drainage. Two stages are commonly observed: 1) atmosphere-controlled evaporation, which occurs at the free-water evaporation rate; 2) soil-controlled evaporation, in which the rate of evaporation is determined by the rate at which water can move upward under potential gradients (soil water potential gradients—subsection 2.5.4). The soil-controlled stage is strongly influenced by soil type and occurs only when the surface vapor pressure is not equal to the saturation vapor pressure.

Evaporation can occur from the leaves and stems of plants and from litter on the ground or from anthropogenic features such as building roofs, which intercept water during precipitation events. Here we focus on the natural environment rather than the built environment. The term *interception* is used to describe the precipitation that is retained by,

or absorbed into, the surface of the plant (e.g., bark, leaves) or litter and then evaporated directly back into the atmosphere. Interception is highly variable in space and time and is dependent on vegetation characteristics (seasonal, maturity) and climatic factors.

Stemflow is intercepted water that flows to the ground via the surface of the branches and stems. Litter on the ground surface tends to retain more water than bare soil and improves conditions for infiltration into the soil. Cloud water interception by vegetation can also occur (e.g., along the Chilean coast and in tropical cloud forests). In many parts of the world, *interception loss* is a significant fraction of the total evapotranspiration. Interception loss is the amount of precipitation that is retained by vegetation and evaporates into the atmosphere rather than reaching the ground. Interception is strongly controlled by the type of vegetation, specifically the canopy and the type of bark. Conifers, for example, have small needles (leaves) with a larger surface area than broadleaf trees. Absorbent bark (cedar tress) can also intercept more water than smooth bark. Generally, the greater the canopy cover, the higher the amount of interception.

However, for a particular type of vegetation the proportion of precipitation that is intercepted and evaporated depends on the characteristics of the precipitation event. In general, a greater proportion of precipitation is intercepted in small precipitation events. The rate of interception decreases exponentially with the precipitation amount. Discontinuous, less intense precipitation events (drizzle) lead to a higher proportion of intercepted precipitation because there is an opportunity for intercepted water to be evaporated between precipitation events. This contrasts to short, intense events, where the canopy becomes saturated and water drips off (e.g., tropical forests). In general, if precipitation is in the form of snow, more is intercepted, which will sublimate at negative air temperatures or evaporate at positive air temperatures. However, the snow canopy can *unload*, fall to the ground, and remain as snow.

2.4.4 Transpiration

Transpiration is the evaporation of water from the vascular system of plants into the atmosphere (Figure 14). Transpiration is a physical process rather than a metabolic process like photosynthesis. Water is pulled through the plant by potential energy gradients that originate with the movement of water vapor into the air through the leaf *stomata* in response to vapor pressure differences (as described in subsection 2.4.3 and this video). When vapor exits the stomata, water evaporates from the walls of the stomatal cavity to replace the loss. This loss of liquid water causes a decrease in potential energy that induces the movement of replacement water up through the vascular system of the plant. Ultimately, the movement of water produces a water concentration gradient between the root and the soil, which then induces a movement of soil water into the root.

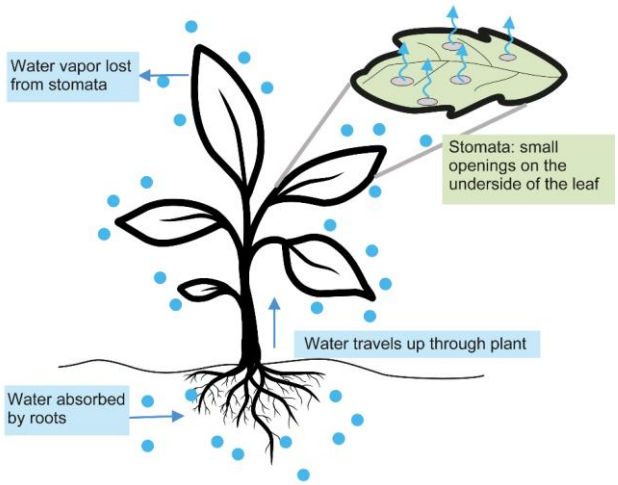

Figure 14 - The transpiration process in a plant (Plant image from Kareemov, the Noun Project↗).

Transpiration rates are influenced by the leaf conductance, the number of stomata per unit area, and the size of the stomata. Leaf conductance (C_{leaf} with dimension of LT^{-1} is typically measured in mm s^{-1}) varies for different types of vegetation (e.g., conifers versus broadleaf forest versus grassland). At a large scale—for example, the scale of a crop—it is necessary to upscale leaf conductance. At this larger scale, the *leaf area index* (LAI) of the vegetation canopy is typically estimated. Effectively, LAI is an equivalent *big leaf* that represents the total leaf conductance for a vegetated area, as in Equation (9).

$$LAI = \frac{Total\ area\ of\ leaf\ surface\ above\ ground\ area\ A}{A} \tag{9}$$

LAI values range from 0 for bare ground to 6 for conifers. A typical crop has an LAI of 3.

The canopy conductance is estimated from

$$C_{canopy} = f_s\ LAI\ C_{leaf} \tag{10}$$

where:

f_s = shelter factor that accounts for some leaves being sheltered from the sun and wind, thus transpire at lower rates

C_{leaf} = leaf conductance (LT^{-1})

Values of f_s decrease with increasing *LAI* and typically range from 0.5 to 1.0 (Allen et al., 1989). Importantly, LAI can vary seasonally depending on foliage (coniferous versus deciduous; maturity of vegetation).

Forests are typically areas of high evapotranspiration because water transpired through leaves comes from the roots, plants with deep-reaching roots can transpire water more continuously, especially during dry periods when the shallow root zone dries out.

Thus, in dry conditions, annual herbaceous plants transpire less than woody plants because herbaceous plants lack a deep root system. Also, woody plants keep their structure over long winters while annual herbaceous plants must grow up from seed in the spring in seasonal climates, contributing little evapotranspiration in the spring.

2.4.5 PET versus AET

As climate is a major driver of evapotranspiration, Thornthwaite (1948) introduced the concept of *potential evapotranspiration* (PET) to classify climate. PET is a measure of the ability of the atmosphere to remove water from the surface of a large area uniformly covered with growing vegetation through the processes of evaporation and transpiration, assuming an unlimited water supply. However, the characteristics of different surfaces (albedo, canopy conductance, and water intercepted by vegetation) can influence ET, as discussed in the previous subsections. Accordingly, Penman (1956) redefined PET as the amount of water transpired by "a short green crop, completely shading the ground, of fairly uniform height, and never short of water" (p. 45). Often a value for PET is calculated at a nearby climate station on a reference surface—conventionally, short grass. This value is called the *reference crop evapotranspiration* (ET_0). Penman's method was further developed by many researchers and extended to estimate ET_0 by introducing resistance factors that describe the resistance of vapor flow through leaf stomata openings, total leaf area, and soil surface (e.g., the FAO Penman-Monteith equation↗).

In regions with abundant rainfall in all seasons, evapotranspiration is energy-limited and the average annual ET can be reasonably estimated by PET. However, in hot, arid regions, evapotranspiration is water-limited, and the calculated PET typically exceeds precipitation. The *actual evapotranspiration* (AET) is the quantity of water that is actually removed by evaporation and transpiration. AET cannot be greater than PET and it usually lower because there is not enough water available for evaporation or because the plants are unable to readily transpire.

AET is affected by several additional factors, including the plant's growth stage or level of maturity, percentage of soil cover, and available water, all of which vary spatially and temporally. To convert the ET_0 to AET, *crop coefficients* are used in many hydrological models. These can be adjusted throughout the year to accommodate the seasonality of crops. Estimation of AET is challenging due to the larger scale of vegetated areas in comparison to the more point-based estimation methods employed for evaporation. Therefore, approaches have been developed to account for the canopy cover of vegetation as discussed in subsection 2.4.6.

The dependence of AET on available energy and water availability means that AET is sensitive to climate change. If only temperature is a factor, then an increase in PET would be expected under global warming. But if the vapor deficit is already high—for example, in semi-arid and arid areas—there will be little effect on AET. An interesting consequence of global warming is that the higher the humidity, the greater the increase in ET for a given

increase in temperature. However, this results in a general increase in atmospheric water vapor contents, which lowers the rate of potential evaporation, thus resulting in negative feedback on the process.

2.4.6 Evapotranspiration Measurement Methods

AET is commonly regarded as the most difficult variable to measure and is a common source of uncertainty for recharge estimation and water balance calculations. Oftentimes, a combination of methods is used (e.g., Prueger et al., 1997). Broadly, these methods are categorized as water balance measurements, water vapor transfer methods, methods that measure the components of evapotranspiration, large scale methods, the Penman method (i.e., combined mass transfer and energy balance), and modeling approaches (Dingman, 2002). Table 2 summarizes some of these methods, along with the general approach and comments on their application. Dingman (2002) and Shuttleworth (2008) provide more details on these and other methods used to estimate AET.

Table 2 - Some common methods for estimating evapotranspiration.

Estimation method	General approach	Comments
Pan evaporation (free-water evaporation)	Fill a shallow pan of well-specified dimensions with water and measure the depth regularly. Total evaporation over a measurement period is the difference in the volume stored minus the amounts added by precipitation.	Evaporation rate can be related to AET if independent measurements of AET are available for calibration. Pans can be used to estimate lake evaporation; however, rates need to be adjusted using a *pan coefficient* (ratio of lake evaporation to pan evaporation).
Lysimetry	The change in weight of a soil is measured along with precipitation and drainage rates. If water additions or drainage occur, the water balance can be calculated, but the additions or drainage must be computed separately to determine AET.	Soil should be undisturbed and the vegetation (if present) representative of the area. Measurements are effectively point-based and may not be representative of larger areas.
Soil moisture measurements	AET is the change in moisture content of the soil over time. Precipitation and drainage rates are also measured.	Various instruments can be used to measure soil moisture, including tensiometers, neutron probes, time-domain reflectometers, and capacitance sensors. Sensor placement is important for accurate measurements.
Plant water use	AET is estimated by measuring diurnal variations in groundwater level caused by plant water use.	A groundwater-level hydrograph is used to estimate the daily evapotranspirative consumption of groundwater by plants (White, 1932).
Water balance	AET is estimated over a particular period for a basin using a water balance equation that includes inflows (precipitation), outflows (surface and groundwater outflows), and changes in storage.	This requires accurate measurements of the other water balance components that have been upscaled to represent the spatial averages for the basin. It is often difficult to measure the individual water balance components, particularly groundwater flow rates.

Estimation method	General approach	Comments
Penman-Monteith equation (or combined equation for mass transfer and energy balance)	Reference Evaporation (ET_0) is calculated as a weighted sum of a rate due to net radiation and a rate due to mass transfer (Penman, 1948) modified to represent the evapotranspiration rate from a vegetated surface by incorporating canopy conductance. See Calculation of ET0↗ is described in the FAO Penman-Monteith manual of Allen and others (1998).	This is the most widely used method for estimating AET from land surfaces. It requires data on net shortwave radiation, net longwave radiation, wind speed, air temperature, and relative humidity. Such data are widely available or can be reasonably well estimated. Several variations of the Penman equation have been proposed. When climate data are not available, the Hargreaves equation can be used (Equation 52 in FAO Penman-Monteith equation↗ of Allen and others (1998).
Bowen ratio	Bowen ratio instrumentation measures temperature and humidity at two heights. The Bowen ratio is derived from the ratio between atmospheric and humidity gradients measured a few meters above the vegetation. AET is calculated as latent heat from the surface energy balance using the Bowen ratio (Prueger et al., 1997).	The method is often used because of the simplicity of data collection and because the robust nature of the system allows for long-term data acquisition.
Eddy covariance (or eddy correlation)	Directly estimates the transfer of water vapor (evapotranspiration) from the land (or canopy) surface to the atmosphere. It uses the time-averaged correlation coefficient between fluctuations in vertical **windspeed,** and atmospheric humidity measured at high frequency (10 Hz) at the same location, a few meters above vegetation.	It can give measurements representative of small (5000 m^2) areas upwind of the sensors. The instrumentation is expensive; typically, the technique is used only for research purposes.
Remote sensing	Remote sensing provides a cost-effective method for estimating evapotranspiration at regional to global scales (Zheng et al., 2016). MODIS (Moderate Resolution Imaging Spectroradiometer) is an instrument aboard the Terra and Aqua satellites, acquiring data in 36 spectral bands. One product of MODIS data is evapotranspiration. The MOD16 ET datasets are estimated using Mu and others (2011) AET algorithm based on the Penman-Monteith equation.	Remote sensing provides a cost-effective method to estimate evapotranspiration at regional to global scales. See MODIS Global Evapotranspiration Project (MOD16)↗.

Thought Questions: Figure 15 shows the global distribution of annual actual evapotranspiration (AET) produced by Abbaspour and others (2019). What is the annual AET in your region? How might a warming climate influence AET?

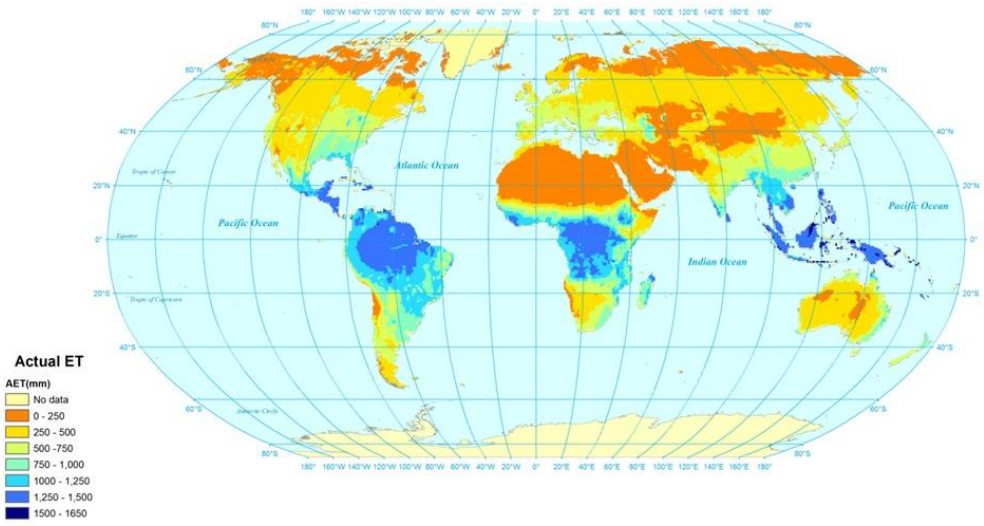

Figure 15 - Annual global map of actual evapotranspiration (From Abbaspour et al., 2019).

2.5 Infiltration Through the Unsaturated Zone

Infiltration is the process by which water arriving at the soil surface enters the soil (Dingman, 2002). Water that infiltrates may be *redistributed* within the unsaturated zone. It may move upward through the soil and evaporate (*exfiltration*), be taken up by plant roots (*transpiration*), move upward from the capillary fringe (*capillary rise*), percolate into the saturated zone (*recharge*), or move downslope (*interflow*) (Figure 16). Water that does not infiltrate typically moves relatively quickly as *overland flow*, where it may infiltrate elsewhere or enter a stream channel.

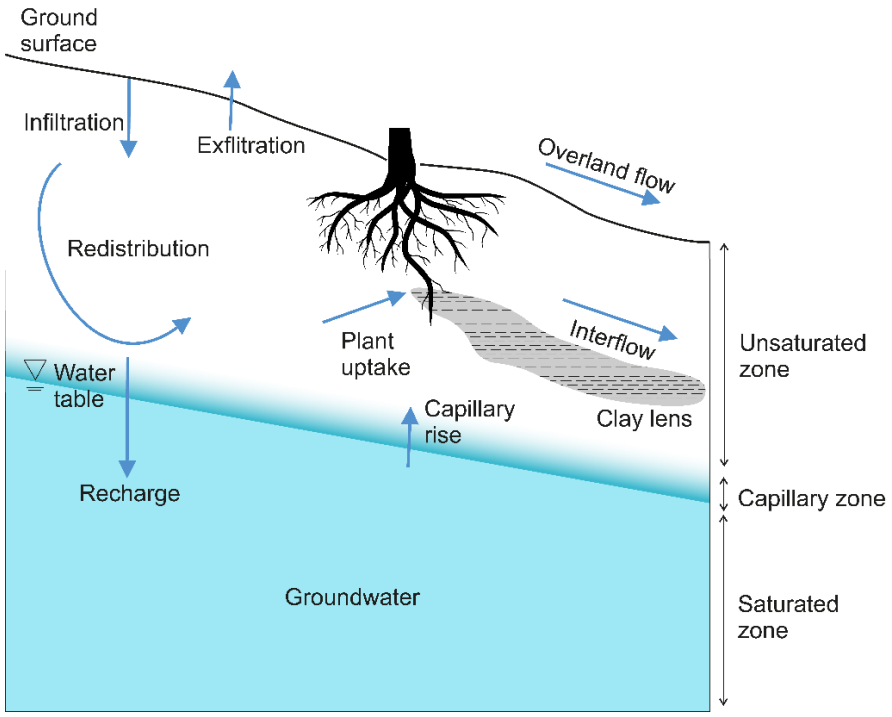

Figure 16 - Processes by which water enters the subsurface and is redistributed in the unsaturated zone (modified from Figure 6-1 of Dingman, 2002).

2.5.1 Capillarity and the Matric Potential

Capillarity is the action by which the surface of a liquid where it is in contact with a solid is elevated or depressed depending on the relative strength of attraction of the liquid molecules to each other and the liquid molecules to molecules of the solid. Consider a small cylindrical glass tube (a capillary tube with a diameter of a few millimeters or less) immersed in a dish of water (Figure 17). Hydrogen bonds at the surface of the water inside the glass tube are attracted to the glass, causing the water molecules to be drawn upward on the glass surface. A meniscus forms between the water and the air, with a *contact angle* α_c between the water surface and the glass. The water will be drawn up the tube until the upward adhesive force—F_u in Equation (11)—is balanced by the downward force—F_d in Equation (12)—due to the weight of water suspended in the tube.

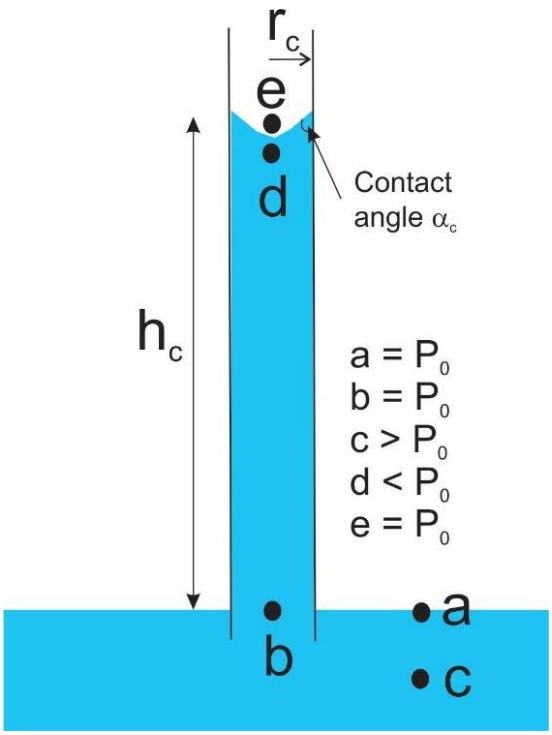

Figure 17 - Water rises in a capillary tube due to capillarity. A fundamental law of hydrostatics is that the pressure of a fluid at rest can vary only in the vertical direction. Thus, the pressure at b must equal the pressure at a and so the pressure at b is atmospheric (P_0). The pressure at d must be less than atmospheric pressure by γh_c.

$$F_u = \sigma \cos(\alpha_c)\, 2\, \pi\, r_c \tag{11}$$

$$F_d = \gamma\, \pi\, r_c^2\, h_c \tag{12}$$

where:

σ = surface tension between water and air (MT^{-2}) often as N m^{-1}

γ = weight density (i.e., specific weight) of the water ($ML^{-2}T^{-2}$) often as 9.8×10^3 N/m^3

r_c = radius of the capillary tube (L) often as m

h_c = height of the water column (L) often as m

For clean glass (as well as most silicate minerals) and pure water, $\alpha_c=0°$, so $\cos(\alpha_c) = 1$. Equating F_u and F_d and solving for h_c gives Equation (13).

$$h_c = \frac{2\,\sigma\cos(\alpha_c)}{\gamma\, r_c} \tag{13}$$

Therefore, water will rise in the tube to a height proportional to the surface tension σ and the cosine of the contact angle; and inversely proportional to the radius of the tube r_c. Water is held under tension within the capillary tube, and the pressure is less than atmospheric (Figure 17)—that is, the pressure is negative or under tension. The narrower the capillary tube, the more negative the pressure. Above the meniscus, the pressure is atmospheric (item e in Figure 17). So, there is a pressure difference across the meniscus.

So, how does this relate to the soil zone? Soils are comprised of particles of different sizes. The size of the pores is related to the grain size; for example, coarse-grained sand will have larger pores than silt. According to Equation (13), we would expect the height of capillary rise to be higher in the silt compared to a sand shown in the Capillary Rise video). An opportunity to calculate capillary rise is provided by Exercise 4.

Soil is typically comprised of a range of grain sizes (i.e., it has a *grain size distribution*) and so has a range of pore sizes. *Soil texture* is described by the proportions of sand, silt, and clay; after particles larger than sand (i.e., >2 mm) are removed. A soil texture triangle is commonly used for identifying the soil texture based on the fraction of sand, silt, and clay. An image of a soil texture triangle is provided by the Science Education Resource Center of Carleton College. Spread-sheet-based soil-texture calculators are provided for download by the US Department of Agriculture.

Another important variable related to capillarity is the moisture content θ of the soil, which is the volume of water V_w in the pores (or voids) divided by the total volume of the soil V_T, expressed as a fraction or percent. Under saturated conditions below the water table, the soil pores are full and $\theta = n$, where n is the porosity of the material. For unsaturated conditions, $\theta < n$.

Consider a soil column comprised of a range of grain sizes (and hence, pore sizes) as illustrated in Figure 18. Pressure is shown as a gauge pressure, whereby atmospheric pressure P_0 has a gauge pressure of $P = 0$. The corresponding pressure head, Ψ, is zero if the datum is chosen as the water table, such that z=0 at the water table. Then, $P = 0$ (as for the point labeled a in Figure 17); and therefore, $\Psi = 0$. Below the water table, $P > 0$ (as for the point labeled c in Figure 17) and $\Psi > 0$. Above the water table, $P < 0$ (as for the point

labeled d in Figure 17) and $\Psi < 0$. Importantly, Ψ becomes increasingly negative at greater heights above the water table, allowing for only the smallest pores to be water filled. Similarly, Ψ becomes increasingly positive below the water table. Pressure head in the unsaturated zone is commonly referred to as the *matric potential head*, or tension head and has the units of length. *Matric potential* has units of energy (J/m^2). Matric potential head and matric potential are used interchangeably hereafter.

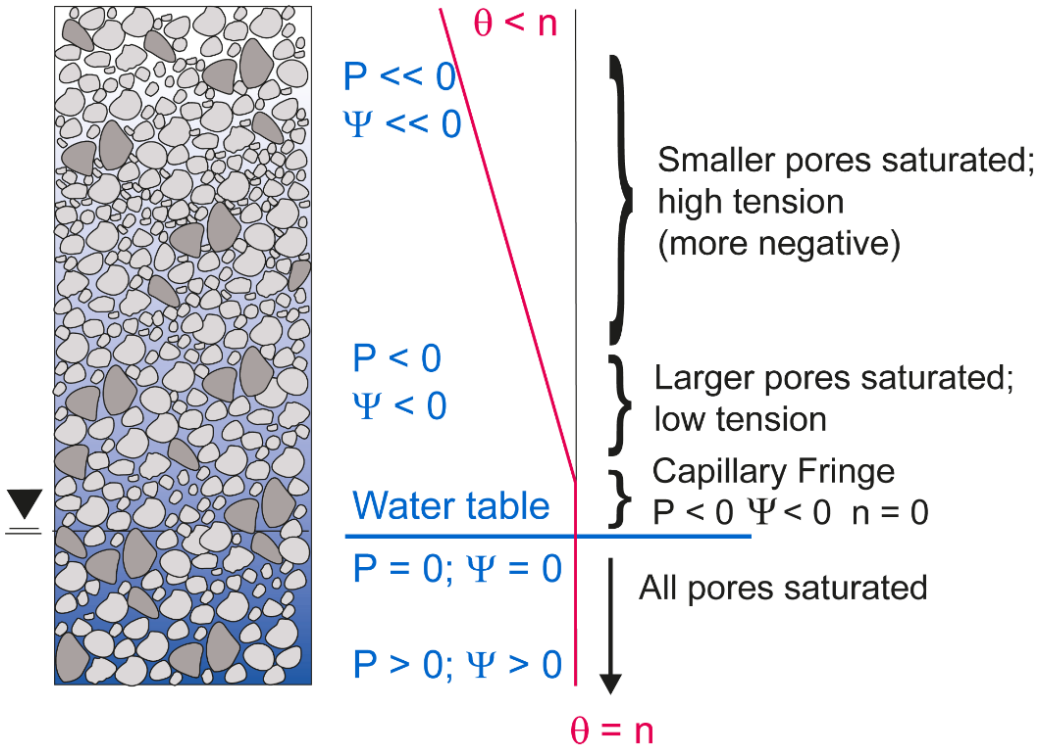

Figure 18 - Soil column showing interconnected water-filled pores. At and below the water table, all the pores are water filled and the moisture content θ is equal to the porosity n. At greater heights above the water table, progressively smaller pores are water filled (illustrated here in faded blue). The graph on the right shows the corresponding pressure and matric potential becoming increasingly negative and the moisture content progressively decreasing at greater heights above the water table.

Considering moisture content θ in Figure 18, at and below the water table, the soil is saturated, and all the pores are filled with water. Water rises upward from the water table due to capillarity. Water will rise to a specific height dependent on the pore radius according to Equation (13). Just above the water table, water rises into the small pores. Above the capillary fringe, water is held in partially filled pores throughout the unsaturated zone. At progressively greater heights above the water table, the water-filled pores become progressively smaller because the water is generally under greater tension (i.e., more negative pressure). The implication of having progressively smaller pores still holding water at greater heights above the water table is that the moisture content θ decreases as the matric potential, Ψ, decreases, as illustrated by the pink line in Figure 18.

2.5.2 Moisture Characteristic Curve

Above the water table, we can represent the relation between the matric potential Ψ and the moisture content θ using a *moisture (or soil-water) characteristic curve* (Figure 19). The y-axis is Ψ, plotted as a reverse axis of negative numbers to represent the soil tension. Smaller, more negative numbers are at the top and represent lower pressure which is greater tension. The x-axis is θ, expressed as a fraction. Figure 19a shows the characteristic curves for both a well-sorted and a poorly-sorted soil that are being wetted from the base of the soil column. Well-sorted (poorly-graded) soils have a narrower range of matric potential over which the moisture content changes as compared to a poorly-sorted (well-graded) soil because the well-sorted soil has a narrow range of pore sizes. Once a well-sorted soil begins to drain, it does so rapidly because most of the pores are the same size. The relationship shifts if the soil column is initially dry and then allowed to imbibe (refill with water). This is caused by larger pore necks preventing entry of water at the same pressure that a draining material retains water because narrow pore necks hold water in underlying large pores (Figure 19b).

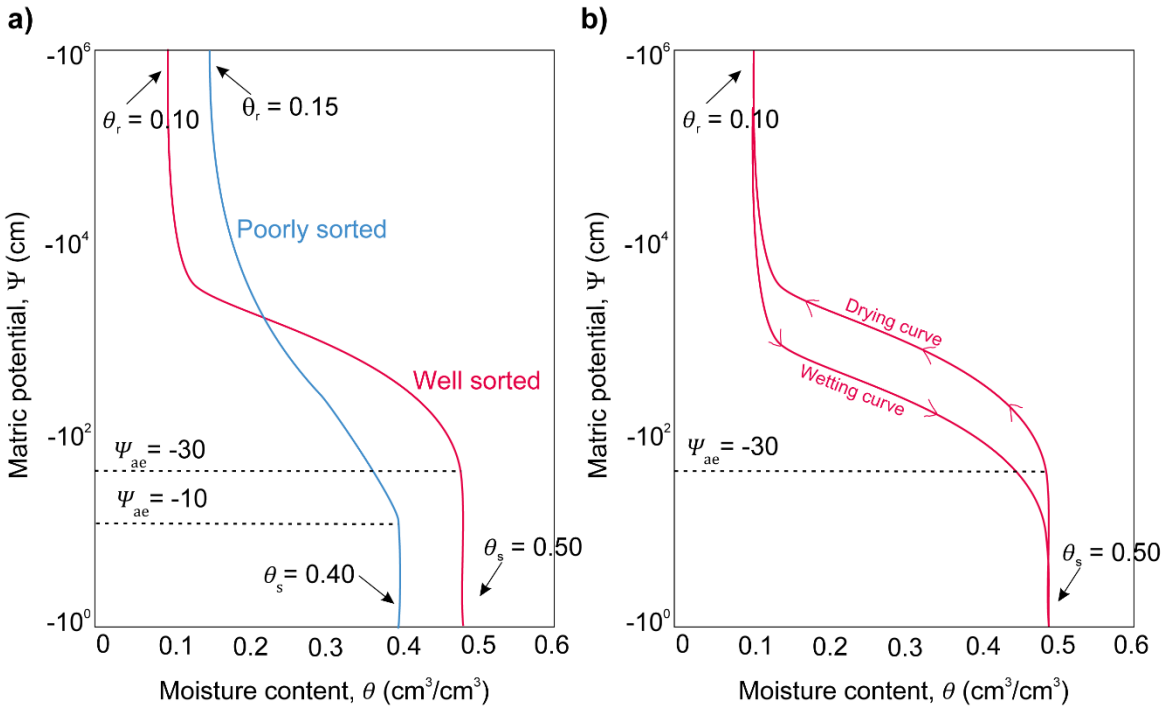

Figure 19 - Moisture characteristic curve for a) both a well-sorted and poorly-sorted soil material, showing air-entry pressure Ψ_{ae}, moisture content at saturation θ_s, and residual moisture content θ_r. b) Moisture characteristic curve of the well sorted material for both drying and wetting, illustrating the hysteresis effect.

At atmospheric pressure (where Ψ is 0), θ is equal to the porosity and the soil is saturated, with the moisture content equal to θ_s=n. The soil will remain saturated as Ψ is gradually decreased (moving up the graph to more negative numbers). At the *air-entry pressure* Ψ_{ae} (or bubbling pressure), there is an abrupt shift to the left where water begins to drain freely from the pores due to gravity. The absolute value of Ψ_{ae} equals the height of the *tension-saturated zone*, or *capillary fringe*. *Field capacity* is the amount of soil moisture

held in the soil when fully drained. Sandy soils have a lower field capacity than clay or loam soils because they have larger pore spaces, allowing water to drain quickly as pressure decreases. The moisture content θ continues to decline as Ψ is lowered until it reaches a residual moisture content, θ_r, where moisture is held very tightly in the soil pores by capillarity and electrochemical forces. θ_r is also referred to as the *irreducible moisture content*.

Moisture characteristic curves are developed in a laboratory using apparatus that applies suction to the sample. A tension plate apparatus is used for the wet soil range (Ψ ranging from -1 to -300 cm) and a pressure plate apparatus for the dry soil range (Ψ ranging from -300 to -15,000 cm). The soil sample is initially saturated and weighed. The sample is placed in the apparatus and weighed after each increase in suction applied. The data points are plotted and fitted to the main drying curve as shown in Figure 19. The reverse process can be carried out to generate the main wetting curve by starting with a sample at residual saturation θ_r and progressively adding water. The wetting curve and the drying curve are not the same and show *hysteresis effects*. Hysteresis occurs for several reasons, but notably due to the pore geometry, whereby the pores fill and drain at different values of Ψ (Hillel, 1980). When θ and Ψ are measured in the field, the values typically plot in a wide region enveloped between the main drying curve and the main wetting curve.

2.5.3 Hydraulic Conductivity of Unsaturated Soils

Hydraulic conductivity, K, represents the relative ease of groundwater flow through soil and geological material. Under saturated conditions, if the fluid properties are constant, then K will increase as the grain diameter increases (Woessner & Poeter, 2020). However, in unsaturated materials, K also varies with the degree of saturation. For a given soil, K is very low at low to moderate soil moisture contents and increases non-linearly to its saturated value, K_{sat}, as the moisture content increases to saturation. In fact, K can increase by several orders of magnitude over a range of moisture content values. Therefore, K is strongly a function of θ. Moreover, K also exhibits hysteresis effects, whereby the different values of K are measured during wetting and drying experiments at the same matric potential because they can be different.

Different approaches have been used to estimate an equation for $K(\theta)$ (e.g., Brooks & Corey, 1964; van Genuchten, 1980). The different equations have been implemented in various computer software for water flow. Equation (14) is one example (van Genuchten, 1980).

$$K(\theta) = K_{sat} S_e^{1/2} \left[1 - \left(1 - S_e^{1/m}\right)^m\right]^2 \quad (14)$$

where:

S_e = effective saturation, calculated as $\frac{(\theta - \theta_r)}{(\theta_s - \theta_r)}$ with θ, θ_r, and θ_s the current, residual, and saturation moisture contents, respectively (dimensionless)

m = van Genuchten parameter derived from fitting a moisture characteristic curve, often estimated as

$1 - \frac{1}{n}$ where n is a measure of pore size distribution and is smaller for a wider range of sizes (values of m range from approximately 0.1 for silty clay to 0.6 for sand)

2.5.4 Darcy's Law

Groundwater flow in the unsaturated zone, specifically in relation to infiltration, is generally in the vertical direction. Both the matric potential and the hydraulic conductivity for a given soil are functions of the moisture content. Therefore, for unsaturated flow, Darcy's law is as shown Equation (15).

$$q_{vz} = -K(\theta)\frac{d(z + \Psi(\theta))}{dz} = -K(\theta)\left(1 + \frac{d\Psi(\theta)}{dz}\right) \quad (15)$$

The matric potential, Ψ, can be measured in the field using a tensiometer. A tensiometer consists of a hollow tube with a porous ceramic cup at the bottom. An example of a tensiometer is presented in Figure 20. The top is fitted with a removable airtight seal that is commonly fitted with a vacuum gauge or pressure transducer. Before being installed in the field, the tensiometer is filled with water. A small auger is used to drill a hole to the desired depth and the tensiometer inserted. A slurry (mix of water and soil) is poured into the annulus to eliminate air space. The water in the tensiometer is slightly above atmospheric pressure, and when the tensiometer is inserted into the unsaturated soil (which is under tension), the water flows from the tensiometer into the soil until a pressure equilibrium is reached. As the water leaves the tube, the negative pressure is measured by the gauge and displayed as a gauge matric potential, Ψ_{gauge}. The soil matric potential, Ψ_{soil}, is calculated from the measured gauge potential using Equation (16).

Figure 20 - A tensiometer, of which the porous cup would be placed in the soil with the pressure gauge exposed at the soil surface (image from the Czech University of Life Sciences Prague website). http://hydropedologie.agrobiologie.cz/images/tenzometr/tenz-foto03.jpg↗.

$$\Psi_{soil} = \Psi_{gauge} + L \tag{16}$$

where:

L = the distance between the tensiometer cup and the height at which the gauge measures

The gauge is *feeling* soil tension plus the weight of the water column. Therefore, by adding L we correct for the weight of the column of water between the gauge and the porous cup—that is, Ψ_{soil} is less negative than the gauge reading. Gauges often measure in units of pressure and, to convert, it helps to know that a pressure of 0.1 kPa is equivalent to a column of water that is 1.02 cm high.

Two or more tensiometers can be installed at different depths to enable measurement of the vertical hydraulic (or soil moisture) gradient. Hydraulic head is calculated using Equation (17).

$$h = \Psi + z \tag{17}$$

The datum is commonly ground surface, so z values are negative. Similarly, matric potential values are negative. An opportunity to explore the relationship of pressure, elevation, matric potential, and hydraulic head is provided by Exercise 5↴.

2.5.5 The Infiltration Process

Infiltration is the process by which water arriving at the soil surface enters the soil. The water input may be from rain, snowmelt, or irrigation. The water input rate is the rate at which water arrives at the ground surface, measured for example in mm/hour. Different soils have different abilities to accept the water as defined by the *infiltration capacity*, also measured, for example, in mm/hour. So, to understand infiltration, we need to consider three scenarios.

1) The water input rate is less than the infiltration capacity. In this case, all the water will infiltrate the soil.
2) The water input rate exceeds the infiltration capacity. As a result, we observe ponding on the ground surface, and the soil is *saturated from above*.
3) There is no infiltration because the water table is at the ground surface before the water input event. The soil is *saturated from below* and ponding occurs at the surface.

Many factors influence the infiltration rate, including the rate at which water arrives at the soil surface, the depth of ponding on the surface, the K_{sat} of the soil profile (it may vary with depth), the antecedent moisture conditions (the moisture content before the event), the initial depth of the water table, and the slope and roughness of the ground surface. When the rate at which water arrives at the surface is less than the infiltration capacity, the rate of infiltration equals the rate of arrival as in scenario (1).

For a single water input event, at any given depth in the soil profile, the rate of infiltration changes over time. When the soil becomes saturated from above, representing scenario (2), infiltration rates during the early stages are usually rapid (Horton, 1933). A wetting front develops and moves vertically downward. The rate of infiltration gradually decreases and becomes asymptotic to a constant value that represents the infiltration capacity and is approximately equal to K_{sat}. Once the infiltration capacity has been exceeded, the excess water accumulates as ponded water on the surface, which is termed *detention storage*. The excess water moves downslope as *infiltration excess* or *Hortonian overland flow* once detention storage is filled (subsection 2.6). The antecedent moisture content therefore plays an important role in infiltration. The higher the antecedent moisture, the higher the K, the more quickly the pores fill with water, and the more rapidly the wetting front advances. If the soil is relatively wet before an event, it will become saturated quickly and the rate of infiltration will decrease.

Sometimes, the soil becomes saturated from below due to the water table rising as in scenario (3); this may be due to seepage from an area upgradient (Figure 10). In this case, because the water table is already at surface, there is no further infiltration, and *saturation overland flow* occurs (subsection 2.6).

Coarse-grained sandy soils allow water to infiltrate quickly. The vegetation canopy and the top layer of undecomposed leaf litter create porous soils by protecting the soil from

pounding rainfall, which can close natural gaps between soil particles. Likewise, *macropores*, created by root growth and decay, and the action of worms, soil insects, and burrowing mammals, can greatly enhance the permeability of fine-grained soils by forming preferential pathways for water. Similarly, fractures, cracks, and solution cavities that provide secondary permeability can act as conduits for groundwater recharge. Where bedrock is exposed at the surface, fractures provide the only means for recharge (Figure 21).

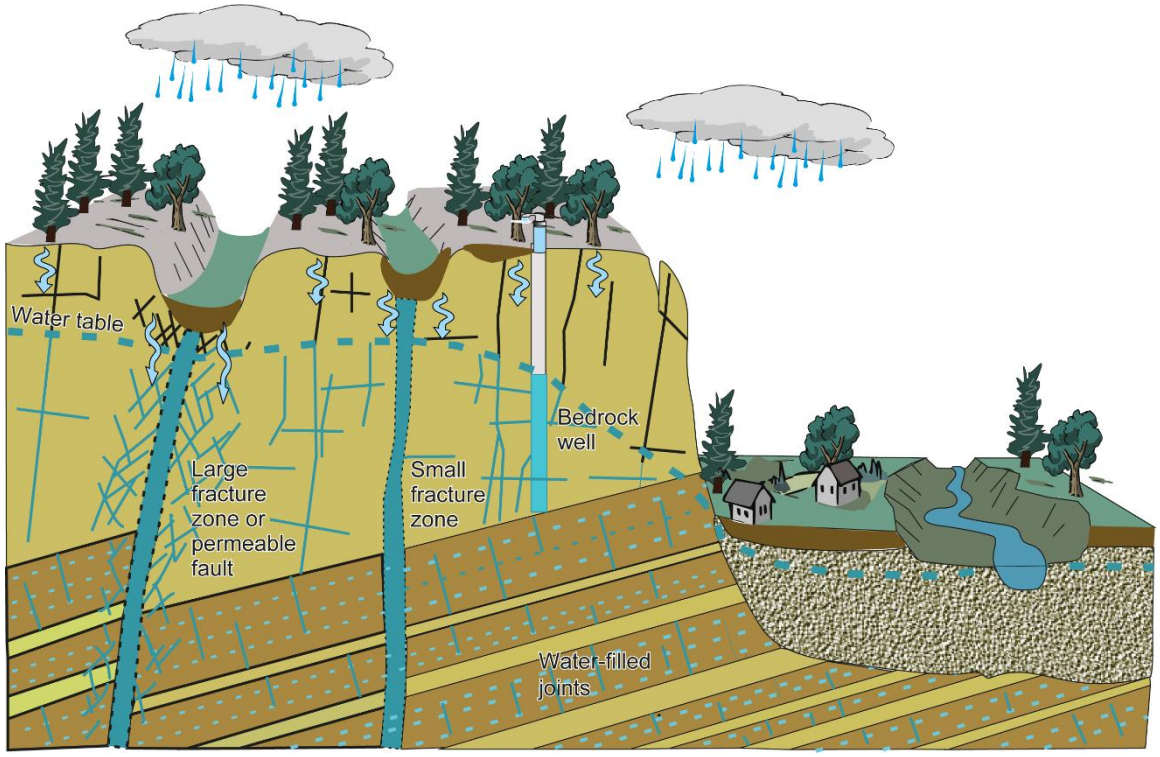

Figure 21 - Conceptualization of recharge to fractured sedimentary rock via large fracture zones, faults, and small fracture zones (Adapted from Canadian Parks and Wilderness Society and Parks Canada, 2005).

The topography of the land surface also plays an important role in determining infiltration. Generally, steep terrain favors overland flow, and flat terrain favors infiltration (Figure 6). However, microtopography creates depressions that hold water or snow, effectively allowing more time for infiltration to occur because runoff water is contained. In southern parts of the Canadian Prairie Provinces, the driest region in Canada, lateral flow of snowmelt and storm runoff concentrates water into topographically closed depressions, causing depression-focused groundwater recharge (subsection 4.2.3).

As a final point, in regions where the temperature of the soil drops to below freezing, a layer of seasonally frozen soil can develop below the ground surface. Frozen soil inhibits infiltration, especially if it is saturated so that the pores are filled with ice, because it effectively lowers the permeability of the soil (Burt & Williams, 1976; Cherkauer & Lettenmaier, 1999). However, macropores remain air filled under partially saturated conditions, allowing preferential flow and meltwater infiltration prior to ground thaw

(Granger et al., 1984; Mohammed et al., 2018). Some regions have permafrost, defined as soil that remains frozen for two or more years. In regions with discontinuous permafrost (patches of permafrost), groundwater recharge occurs only where the ground is not frozen; in regions with continuous permafrost, there is essentially no groundwater recharge except where a *talik* (perennially thawed soil) exists (Box 2↴).

2.5.6 Quantifying Infiltration

The process of infiltration can continue only if there is room available for additional water at the soil surface. The available volume for additional water in the soil depends on the porosity of the soil and the rate at which previously infiltrated water can move away from the surface through the soil. If the water table is relatively deep, the water-table rise during infiltration can be accommodated, but if the water table is already near the surface, any additional rise can result in the water table intersecting the ground surface.

Quantitative methods for estimating infiltration are complex. By combining Darcy's law for the vertical movement of water through the unsaturated zone, as in Equation (15), with conservation of mass, Richards (1931) developed an equation (known as Richards's equation) for calculating the vertical percolation of water into a homogenous soil. Richards's equation has been implemented in various numerical modelling software (e.g., HYDRUS 1D↗). However, the numerical solutions are often computationally intensive. Therefore, other infiltration models have been developed, including the Green-Ampt model (Green & Ampt, 1911). The US Environmental Protection Agency (2023) offers a selection of MathCAD based infiltration codes, including the Green-Ampt model. Box 3↴ illustrates the use of a numerical model used to simulate infiltration.

2.6 Redistribution and Recharge

Once water has infiltrated the subsurface, it can be redistributed by gravity and tension gradients, be removed by evapotranspiration, move downgradient as interflow (subsection 2.7), or continue to flow downward and enter the saturated zone as recharge (Figure 16).

Following an infiltration event, the soil dries both by drainage and by evaporation. There are two stages of *exfiltration* (Phillip, 1957), or evaporation from a soil. In the first stage, the evaporation rate is determined largely by the surface energy balance and the wind and humidity conditions and is largely independent of the soil-moisture content. Evaporation occurs as free-water evaporation (Table 2 – pan evaporation). In stage 2, the evaporation rate is determined by the rate at which water can be conducted up to the surface in response to soil water potential gradients (or tension gradients). The rate of evaporation in phase 2 is less than the free-water evaporation rate.

Plant roots draw water from the unsaturated zone, and some plants called phreatophytes draw water from the saturated zone (Le Maitre et al., 1999). Because water transpired through leaves comes from roots, plants with deep roots can more constantly

transpire water, especially during dry periods when the shallow root zone dries out. Thus, in dry conditions, herbaceous plants generally transpire less than woody plants because herbaceous plants lack a deep root system. However, in dry regions some perennial plants can have roots reaching depths of 4 to 5 m.

The zero-flux plane (ZFP) is the boundary between upward directed moisture movement due to evapotranspiration and the downward directed movement due to drainage. Therefore, the ZFP is a point estimate of potential recharge based on the premise that recharge is equal to changes in the soil-moisture storage below the ZFP. The location of the zero-flux plane changes over time in response to infiltration events and drying. The method requires data on the soil matric potential to locate the ZFP and of soil-moisture content to measure changes in storage. The method is restricted to conditions when a ZFP exists and locations where the water table is deeper than the ZFP.

Soil moisture may also move upward from the capillary fringe (capillary rise) in response to soil matric potential gradients, as discussed in subsection 2.5.4. This results in a redistribution of the soil moisture within the soil profile.

Ultimately, only a portion of the water entering the unsaturated zone during an infiltration event makes it to the water table. This water is referred to as *deep drainage* or as *recharge*. Once the water passes the water table, it begins to flow in the saturated zone as dictated by the hydraulic gradient.

Diffuse recharge rates vary over a range of spatial and temporal scales. Methods for estimating diffuse recharge rates are summarized in Section 4. Commonly, diffuse recharge rates are expressed in mm per year, but for a water balance analysis, a volumetric recharge rate (e.g., m^3 per year) is obtained by multiplying the rate in mm per year by the surface area of the aquifer according to Equation (18). A common error is to make a mistake in converting from km^2 to m^2.

$$\left(diffuse\ rechage\ rate\ \left(\frac{mm}{year}\right)\right)\left(\frac{1\ m}{1{,}000\ mm}\right)$$
$$\left(surface\ area\ of\ aquifer\ (km^2)\right)\left(\frac{1{,}000{,}000\ m^2}{1\ km}\right) \qquad (18)$$
$$= volumetric\ rechage\ rate\ \left(\frac{m^3}{year}\right)$$

Average annual recharge rates are estimated from multiple years of data, ideally with some measure of interannual variation such as the standard deviation. Providing the standard deviation allows the interannual variability to be explicitly reported. Average annual recharge rates are also often reported as a percentage of total annual precipitation. Average monthly or average seasonal diffuse recharge rates can also be reported. An opportunity to calculate diffuse recharge is provided by Exercise 6.

2.7 Streamflow Generation

The dependence of overland flow on the infiltration regime in the unsaturated surface soils was discussed in subsection 2.5. In this section, we focus on where that water ends up. The context explored is a stream, although other surface water bodies also receive inputs following water input events.

Streamflow is generated from a combination of water sources following a water input event such as rain or snowmelt (Figure 22). Dingman (2002) classifies different flow mechanisms that produce event responses. Importantly, their relative importance may vary seasonally or even during single water input events. *Direct channel precipitation*, which is precipitation that falls directly on the stream, generally contributes a small proportion (<5%) of the total event streamflow, but can contribute substantially more to the peak flow (up to 40%) despite the small area of the stream channel itself (Dingman, 2002). *Overland flow* (often referred to as *surface runoff* consists of *infiltration excess overland flow* (i.e., *Hortonian overland flow*) and *saturation overland flow* (Figure 22 inset graph). Hortonian overland flow results from saturation from above where the water input rate exceeds the saturated hydraulic conductivity of the surface layer and for a duration exceeding the time of ponding. Saturation overland flow is flow that occurs via saturation from below due to the water table rising above ground surface, as illustrated near the stream in Figure 22. These two mechanisms may act simultaneously to generate a streamflow response, as depicted by the blue curve in the Figure 22 inset graph. Next is *interflow* (i.e., *subsurface stormflow*), which is water that infiltrated the unsaturated zone upslope, but was redistributed and moved downslope toward the stream. Interflow typically occurs in areas with steep topography and through a permeable geological layer overlying a low permeability layer such as clay layers or bedrock. The presence of macropores that lead to pipe flow may result in a faster response. Return flow (flow from the unsaturated zone to the surface) may also occur. Finally, the groundwater contribution to streamflow (i.e., *baseflow*) is generally maintained year-round and sustains the streamflow during low-flow periods between water input events. Groundwater can also contribute to event flow, as demonstrated by tracer studies (e.g. Newbury et al., 1969). Groundwater discharge to streams is explored further in subsection 3.1.2.

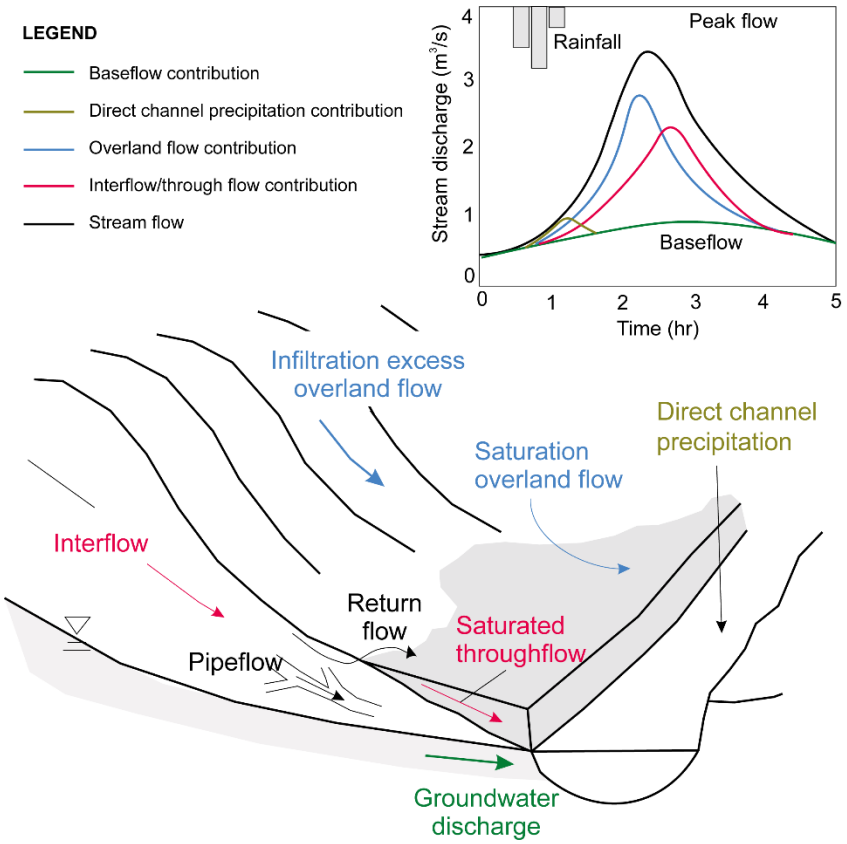

Figure 22 - Mechanisms that generate streamflow (modified from Arnell, 2002).

Streamflow may be generated by different mechanisms in different parts of a watershed. Which mechanism is responsible for generating the greatest amount of streamflow following a water input event depends on several factors, including the topography, particularly whether a slope is concave or convex, and the permeability of the geological substrate and surface materials. Intuitively, one would expect that watersheds that have steep slopes and low-permeability substrates would tend to generate more infiltration excess overland flow (i.e., Hortonian flow); however, classic Hortonian overland flow tends to be a rare occurrence in vegetated humid environments (Freeze, 1972). Hortonian overland flow is an important mechanism in semi-arid to arid regions where rainfall events tend to be intense and natural surface hydraulic conductivities are low (Dingman, 2002).

The topic of streamflow generation in watersheds has been the focus of countless research studies, including recent research on predictions in ungauged basins and an article by Hrachowitz et al., 2013). Understanding these various mechanisms requires robust precipitation, stream discharge, soil, and groundwater data, as well as various chemical and isotope datasets that can be used as indicators. These topics are beyond the scope of this book. Readers are directed to the literature on watershed and hillslope hydrology for a more in-depth treatment of this topic.

Thought Questions: What streamflow generation mechanisms dominate in your region? Do you observe a rapid increase in streamflow during rain events? If so, what

mechanism does this represent? Do you observe streamflow even at times of the year when it has not rained for many weeks? If so, what mechanism does this represent?

2.8 Summary

This section focused on the processes that control diffuse recharge. We began by exploring the partitioning of precipitation at the land surface into evapotranspiration, infiltration, and overland flow, ultimately leading to diffuse recharge. Then we discussed the processes controlling how precipitation partitions at the land surface are interdependent, and the relative proportion of each component is determined by a variety of factors including the climate, topographic slope, geologic substrate, and vegetation (if present).

Next, we considered climate, which exercises the most important control on recharge. The climate of a particular area is determined by the long-term, accumulated data derived from weather observations (e.g., long-term average temperature, humidity, cloud cover, precipitation). We explored the controls on the moisture-holding capacity of the atmosphere and the characteristics of precipitation, specifically its seasonality and the intensity and duration of precipitation events. The characteristics of precipitation have an important influence on how water partitions at the land surface.

We examined in some detail the processes of evaporation and transpiration. Evaporation is influenced by the type of surface (open water, bare soil, or vegetation). For example, water intercepted by the leaves and stems of plants can be evaporated. Evaporation rates are controlled by the amount of energy available (net radiation), the vapor pressure deficit of the air, and aerodynamic factors such as the windspeed, which affects the rate of removal of air from evaporating surfaces. If vegetation is present, water is drawn into the plant from its roots and transpired from the leaf stomata. Practically, evaporation and transpiration are difficult to measure separately and are commonly estimated together as evapotranspiration.

The processes of infiltration, the redistribution of water within the unsaturated zone, groundwater recharge, and the generation of overland flow were then discussed. To understand the infiltration process, we began by examining the process of capillarity. The moisture content of a soil is not uniform but varies according to the matric potential or soil tension; a moisture characteristic curve defines their relationship. The hydraulic conductivity of a soil also depends on the moisture content. Therefore, quantifying the flow of water in the unsaturated zone is more complicated than in the saturated zone because the pore spaces are only partially filled with water. Darcy's law is modified for the unsaturated zone to account for hydraulic conductivity being a function of the moisture content. Quantifying flow in the unsaturated zone requires measurements of the matric potential (measured by tensiometers) and the moisture content for that matric potential.

The infiltration of water into the unsaturated zone following a water-input event (e.g., rain or snowmelt) depends on the initial or antecedent moisture content as well as the infiltration capacity or saturated hydraulic conductivity K_{sat} of a particular soil. If the water-input rate is less than the infiltration capacity, all the water will infiltrate the soil. If the water-input rate exceeds the infiltration capacity, ponding occurs, and saturation overland flow can occur. If the ground is already saturated from below, there is no infiltration. Assuming some water infiltrates the unsaturated zone, not all of it will drain deeply and form recharge. The water may be redistributed by evaporating from the soil, being drawn up from plant roots, or forming interflow.

Ultimately, streamflow is generated through a combination of inputs including overland flow, interflow, and baseflow. While overland flow and interflow are strongly related to water input events and combine to produce peak discharge in a stream, the baseflow is generally sustained year-round and may be the only source of water to the stream during periods with no precipitation.

3 Groundwater Discharge and Exchanges with Surface Waters

As mentioned in Section 1, groundwater discharge is the loss of groundwater from the subsurface to the surface environment. Water that leaves the groundwater system and enters a surface water body, such as a stream or a lake or the ocean, is the most widely recognized form of discharge. But there are many other forms of groundwater discharge.

This section focuses on discharge in different environmental settings and the factors that control discharge, beginning with a more detailed examination of the various discharge mechanisms introduced in Section 1. Following is an overview of the seasonality of discharge, which briefly explores how climate influences discharge and how other effects within the groundwater flow system can modify the discharge environment.

Many ecosystems depend on groundwater discharge in its many forms, particularly groundwater dependent ecosystems (GDEs) and groundwater influenced ecosystems (GIEs) (discussed in Section 5). Understanding the factors that control groundwater discharge is essential for understanding the potential impacts to aquatic habitat and the ecosystems it supports.

3.1 Discharge Mechanisms

This section begins with an overview of groundwater–surface water exchanges, a topic explored in detail by Woessner (2020). Thereafter, the focus is on different types of discharge. Excluded from this section is a discussion of evapotranspiration as a form of groundwater discharge, which was discussed in subsection 2.4.

3.1.1 Exchanges Between Groundwater and Surface Water - An Overview

Before describing the various mechanisms associated with discharge to surface water bodies (streams, lakes, wetlands, oceans), it is important to recognize that these water bodies may not be entirely discharge environments. Two-way exchanges commonly occur between the groundwater system and a surface water body. These exchanges, commonly referred to as *groundwater – surface water interactions*, can occur over a wide range of spatial and temporal scales (subsection 4.4). Groundwater–surface water interactions are more commonly associated with unconfined aquifers. However, there can be exchanges with confined aquifers if the confining layer is thin or if the confined aquifer intersects the water body.

The most widely recognized conceptualization of exchanges between a groundwater system and a surface water body (e.g., a stream) is that of Winter and others (1998), who identified four categories of groundwater-stream interactions (Figure 23). The primary types of exchange occur when groundwater discharges to a stream (a – *gaining stream*) and when the aquifer is recharged by the stream (b – *losing stream*). In addition,

groundwater may pass through a stream laterally (c – *groundwater flow through*), with groundwater inflow occurring on one side of the stream and outflow on the other side. Losing streams may also be disconnected (d – *disconnected stream*) from the water table by an unsaturated zone. For each case, groundwater exchange may differ along a single stream, gaining in some reaches and losing in others, and these exchanges often vary temporally. Exchanges also occur at different scales: from centimeters, to reach scale, to watersheds (Woessner, 2020).

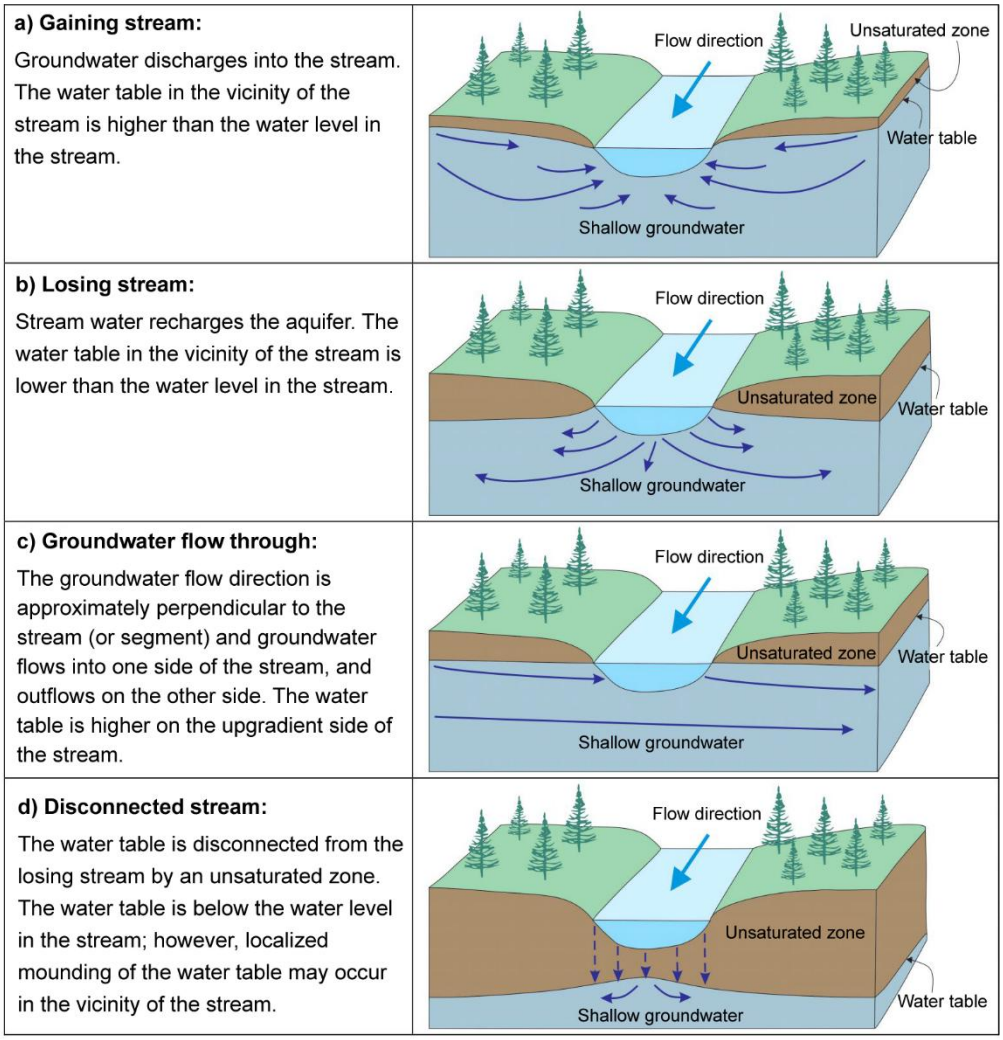

Figure 23 - Types of groundwater-stream interactions (adapted from Winter et al., 1998).

3.1.2 Groundwater Discharge to Streams

Groundwater discharge to streams is perhaps the most widely recognized form of discharge. The term *stream* is used in this section to represent all forms of flowing water along channels (sloughs, ditches, creeks, streams, rivers). While *river* and *stream* are often used interchangeably, streams are of lower order and flow within narrow banks—for example, first order or headwater streams—while rivers are of higher order and flow within wider banks.

Discharge to a stream can occur anywhere along the length of the stream through the cross-sectional area of the saturated zone that is in contact with the stream (Figure 23a, Figure 23c). This means that discharge can occur along the banks of a stream and through the streambed. Discharge may occur in localized areas that are associated with more permeable substrate materials (Figure 24).

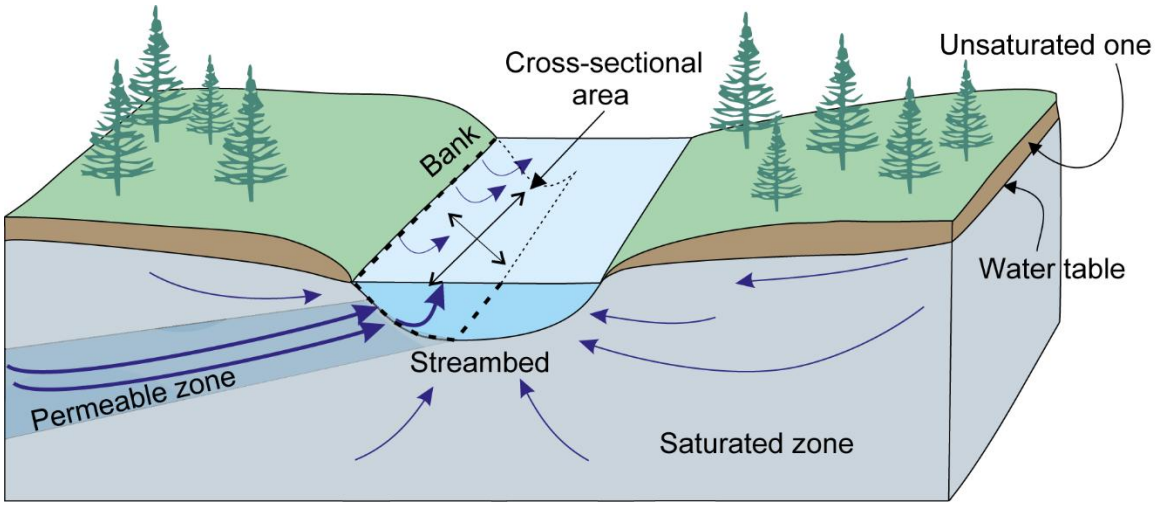

Figure 24 - Discharge to a stream though the cross-sectional area of the saturated zone that is in contact with the stream indicating that a large portion of the discharge may enter through a zone of high permeability substrate.

Groundwater discharge to streams forms the *baseflow* component of the total streamflow. Figure 25 shows a conceptual stream hydrograph. The blue curves show the total streamflow over a 5-year period, while the pink shaded area shows the baseflow contribution to the streamflow. Unlike the total streamflow hydrograph that appears rather flashy in response to precipitation events, the baseflow hydrograph is relatively smooth, reflecting the seasonal variations in groundwater discharge. There is less interannual variability in the baseflow compared to streamflow, suggesting that groundwater discharge is relatively stable from year to year. Of course, if groundwater recharge were to decrease or if groundwater were to be pumped, this could reduce the baseflow.

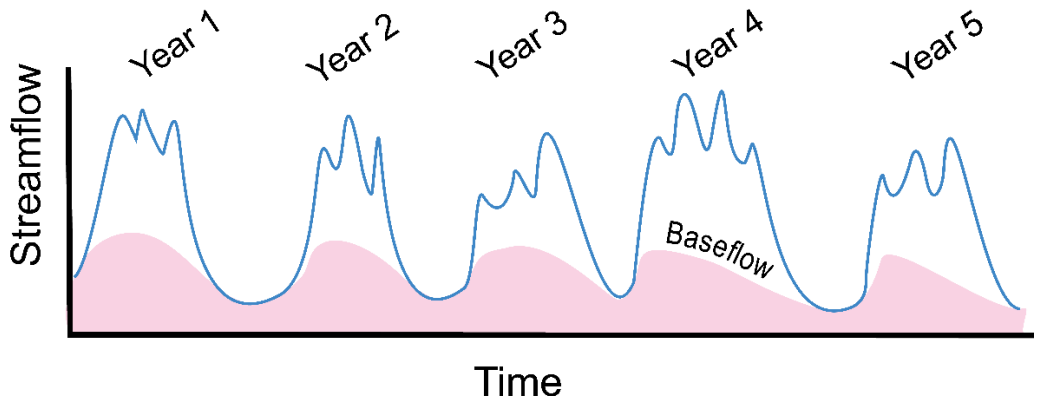

Figure 25 - A streamflow hydrograph showing the baseflow contribution to total streamflow.

Hyporheic exchange occurs as stream water circulates into and out of the stream channel, bed, and banks, to mix with the adjacent groundwater system. The hyporheic zone has important ecological function because, apart from the exchange of water, dissolved gas and solutes, contaminants, microorganisms, and particles are also exchanged.

Steams are often classified as perennial, intermittent, or ephemeral. Streamflow in a *perennial stream* is sustained by the baseflow at times of the year when precipitation is limited or nonexistent, like the example shown in Figure 25. The water table is located above the streambed for most of the year, and so the stream flows year-round during a typical year. Many streams sustain flow during periods of low surface runoff due to the discharge of groundwater. In fact, the sustained contribution of groundwater to streams and other surface water bodies is important for maintaining aquatic habitat.

Intermittent streams (or *seasonal streams*) have flowing water during certain times of the year, when groundwater provides water for stream flow. During dry periods, intermittent streams may not have flowing water. In mountainous regions, steep mountain streams are incised into the bedrock slope and are mostly fed by snowmelt in the spring. Groundwater can discharge into some mountain streams, particularly during the snowmelt season when groundwater recharge to the bedrock is high, raising the water table to the stream level. However, during the summer months, there may be an insufficient amount of groundwater discharge to maintain water in the stream because the water table falls below the streambed and snowmelt runoff ceases, so the stream dries up. Welch and others (2012) modeled groundwater contributions to streams in a mountainous region. They found commonalities in groundwater contributions among small mountain streams but noted that individual streams have unique groundwater contributing areas and discharge patterns, as illustrated in Figure 26a. They found that if recharge changes across the entire watershed, all the streams respond a bit differently (Figure 26b), reflecting topographic uniqueness and the complexity of mountainous terrain.

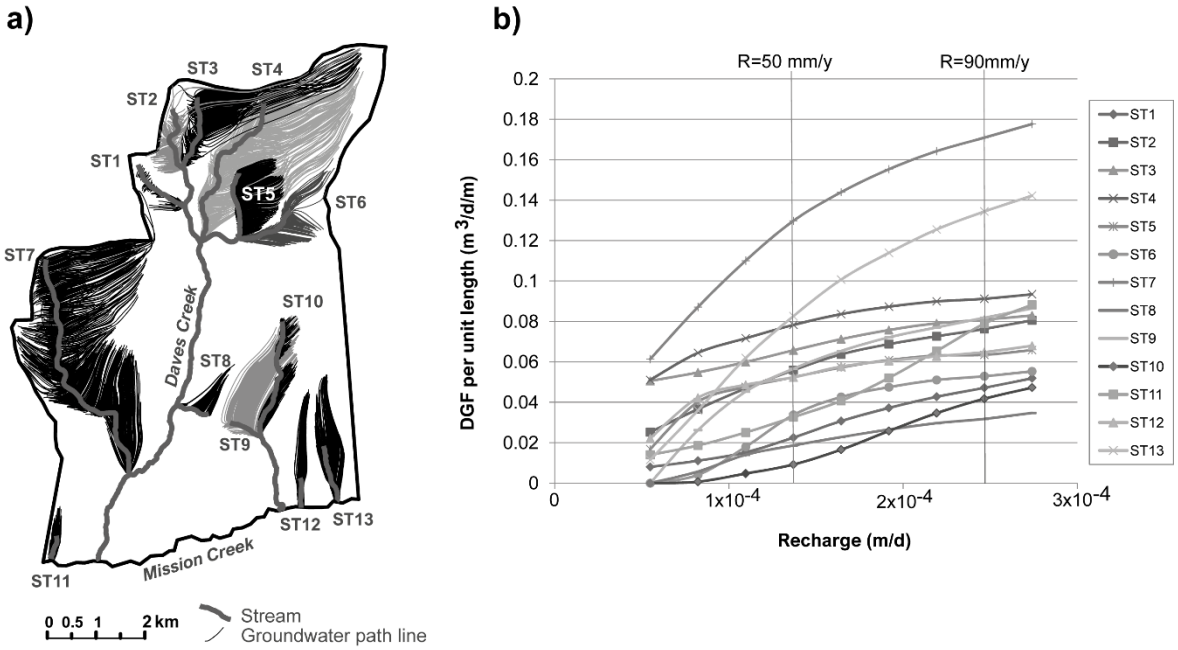

Figure 26 - a) Plan view of modeled groundwater path lines to first-order streams (denoted ST1, ST2, etc.) in a mountain watershed. The recharge rate in the model was 100 mm/y. Path lines are shaded black or gray to ease visualization of the groundwater flow to the different first-order streams and do not denote any particular differences. b) Graph showing changes in groundwater discharge (DGF = deep groundwater inflow in cubic meters per day per meter length of stream) for thirteen first-order streams in the model with a range of recharge between 20 mm/y and 100 mm/y. Due to differences in stream length, the discharge rates are normalized per m stream length for comparison purposes (modified from Welch et al., 2012).

Ephemeral streams have flowing water only during or for a short duration after precipitation or snowmelt events in a typical year. The stream becomes disconnected from the groundwater system as the water table lowers and thus loses its baseflow component. Ephemeral streams are often found in arid and semi-arid areas where streamflow is associated with heavy rain events. Topographic maps often distinguish between perennial (solid-line type) and ephemeral (dashed-line type) stream courses.

3.1.3 Discharge to Lakes and Wetlands

Lakes are bodies of water in which the flow is relatively still compared to a stream. Over time there is a turnover or replacement of the water volume. The hydrologic regime of a lake is strongly influenced by the regional groundwater flow system. Large, permanent lakes are almost always discharge areas for regional groundwater systems; small, permanent lakes in the upland portions of watersheds are usually discharge areas for local flow systems, but can be locations of depression-focused recharge as shown by the recharge from the alpine lake in Figure 2 and discussed in subsection 5.2.1. Lakes can also intercept the regional groundwater flow such that the lake gains water on one side and loses water on the other.

Wetlands are areas of land that are saturated with water, with occasional marshy and soggy areas. There are many kinds of wetlands and many ways to categorize them. Some classifications use the term *wetland* very broadly to encompass all areas where the land is saturated: marine (ocean), estuarine (estuary), riverine (river), lacustrine (lake), and

palustrine (marsh). However, commonly, when we think of wetlands we think of marshes, small ponds, mires, fens, swamps, and bogs. Regardless of the type of wetland, groundwater discharge often plays an important role in maintaining saturated conditions, at least to some degree. A distinguishing feature of a wetland is the slow exchange between the wetland and the groundwater system due to the presence of fine-grained sediments and organic materials. There is a significant pore water exchange in wetlands via roots of plants.

Wetland habitats serve essential functions in an ecosystem, including acting as water filters for contaminants and sediment as well as providing food and habitat for fish and wildlife (Figure 27). Wetlands also absorb excess nutrients and other contaminants before they reach rivers, lakes, and other water bodies. Woessner (2020) examines exchanges between groundwater systems and lakes and wetlands in more detail.

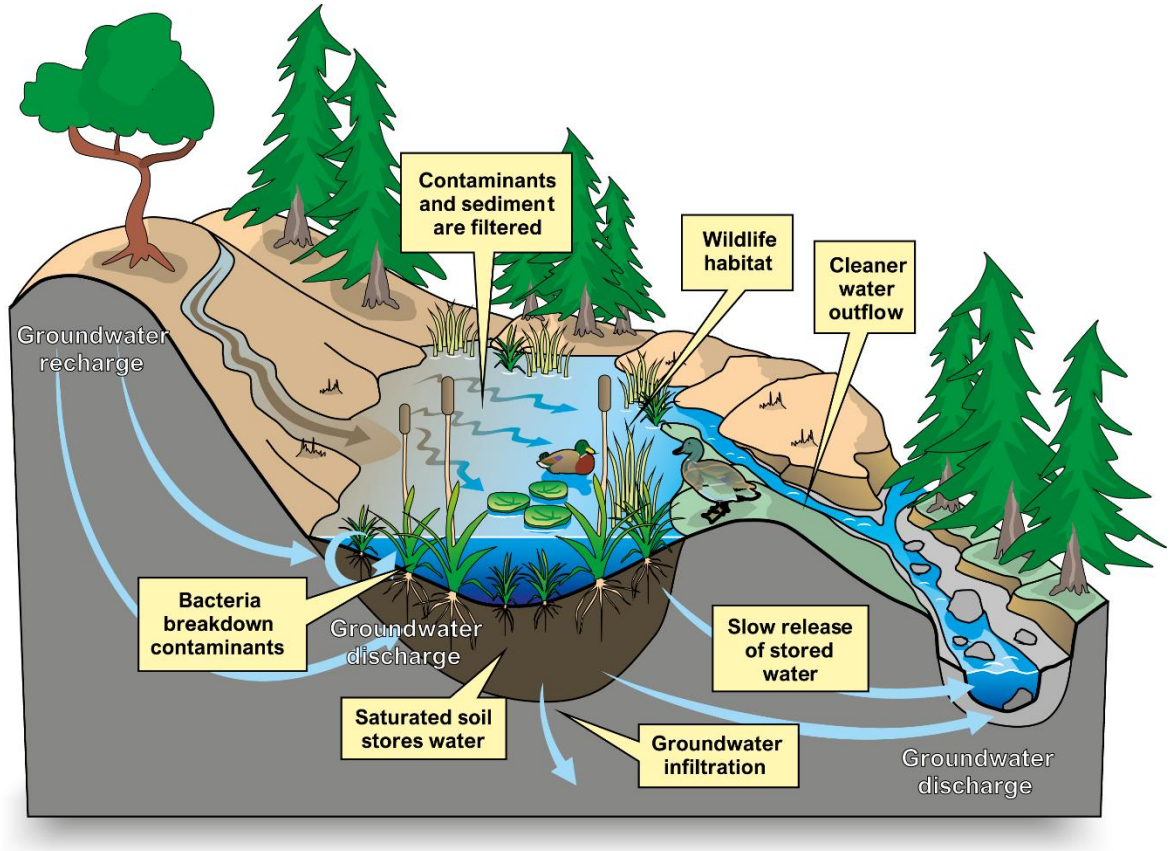

Figure 27 - Schematic of a wetland showing aspects of their ecological function (modified from Turner et al., 2004).

3.1.4 Discharge to Saline Bodies of Water

Coastal aquifers are characterized by a freshwater–saltwater interface. The quintessential model of discharge along the coast is that of an aquifer in which a wedge of seawater extends beneath the land (Figure 28). The landward extension of the wedge is due to the higher density of seawater compared to freshwater. The wedge's presence diverts the freshwater flow in an upward direction; along the contact plane between the freshwater

and the saltwater, mixing by hydrodynamic dispersion and diffusion creates a transition zone—that is, a zone of intermediate salinity between seawater and freshwater. The discharge generally occurs in the intertidal area but can also extend below the seafloor when the rate of freshwater flow is high and the geology permits (i.e., where a confining layer is present).

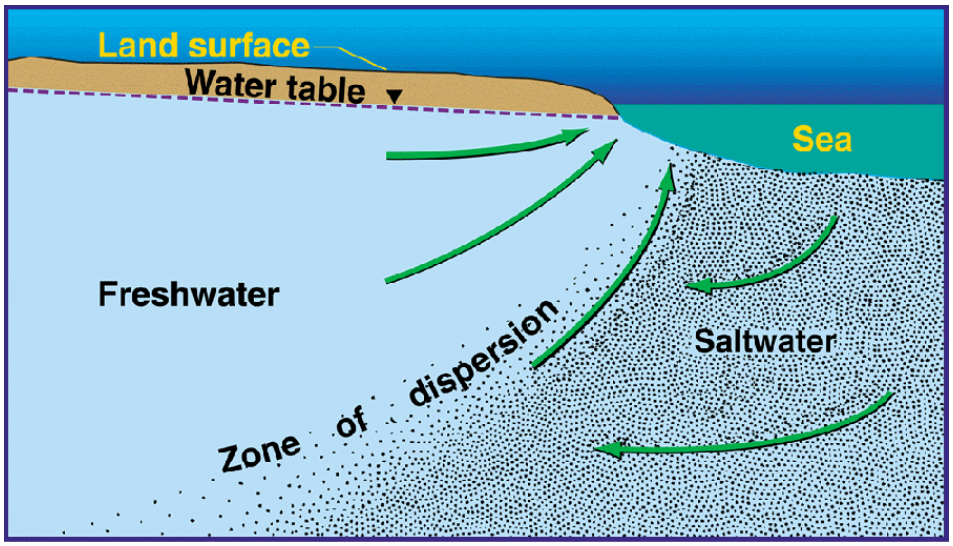

Figure 28 - Coastal aquifer with freshwater discharge along the coastline. The zone of dispersion is a mixing, transition zone of brackish water between the discharging fresh water and the underlying denser sea water (adapted from https://water.usgs.gov/ogw/gwrp/saltwater/salt.html↗).

Most fresh water on small islands is present as a freshwater lens (Figure 29). Like a coastal aquifer as illustrated above, underlying the freshwater lens is a mixing zone of brackish groundwater, which can vary in thickness from less than a meter to tens of meters (Falkland, 1991). The extent and thickness of the freshwater lens on islands depends on the island topography, geology, and climate. Generally, islands that are low-lying have a relatively thin freshwater lens, making them highly vulnerable to groundwater abstraction, sea level rise, and a reduction in recharge. The amount of coastal discharge can be significantly reduced by groundwater abstraction from pumping wells. The increase in coastal groundwater use over past decades have meant that this also has become an important discharge pathway, at the expense of natural discharge features along the coast.

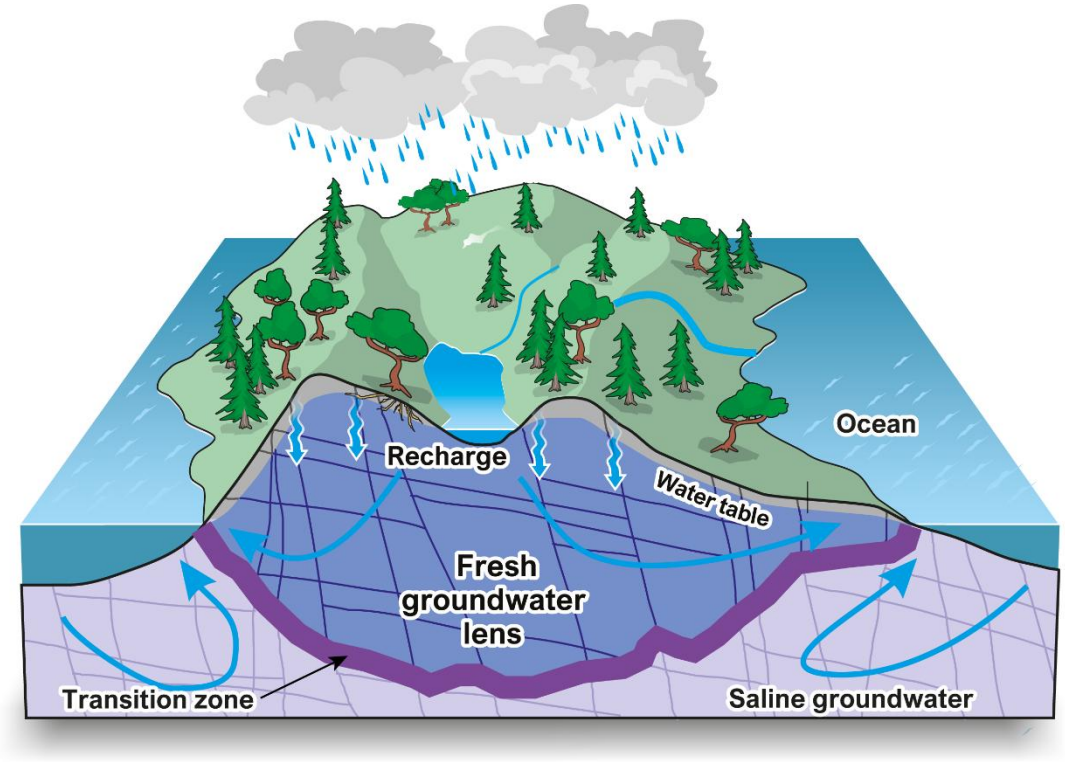

Figure 29 - Groundwater discharge to the ocean on an island.

The position of the freshwater–saltwater interface beneath the coast depends on the groundwater flux toward the ocean (Box 4). If the flux is high, the interface is effectively pushed toward the ocean, but if the flux is low, the interface can be located further inland. Therefore, changes in the flux influence the position of the freshwater–saltwater interface. Studies of coastal aquifers distinguish between *flux-controlled systems* (i.e., *recharge limited systems*) in which groundwater discharge to the ocean is persistent despite a change in sea level, and *head-controlled systems (i.e., topography limited systems)* whereby the water table remains at a fixed elevation regardless of the change in sea level (Werner & Simmons, 2009). In a flux-controlled system, if the sea level rises, the water table rises by the same amount. This suggests that the gradient, and thus the flux, remain the same. Flux-controlled systems require some land capacity for the water table to rise without discharging as springs at low elevations. Werner and Simmons (2009) demonstrate that seawater intrusion due to sea level rise is minimized in flux-controlled systems. In contrast, if the water table is relatively shallow or there are other surface controls such as drains, wetlands, or streams/rivers, sea level rise cannot be accommodated by a rise in the water table. As a result, the groundwater gradient, and thus the flux, are reduced. A change in the salinity of the aquifer or the ocean can also influence the position of the interface, but this effect is generally negligible.

3.1.5 Springs and Seeps

Springs and seeps are important forms of groundwater discharge where groundwater reaches the earth's surface either at or near the land-atmosphere interface or the land-water interface (Springer & Stevens, 2008). Typically, springs are focused

groundwater discharge points, while seeps (or seepage faces) often cover a larger area. However, the terminology distinguishing the two is somewhat vague in the literature.

Springs are found in many different terrestrial (deserts to forests) and aquatic environments (floors of rivers, lakes, and oceans). Classification systems for springs have evolved from schemes based on various physical and chemical variables (Bryan, 1919; Fuller, 1904; Meinzer, 1923) to more comprehensive schemes (Springer & Stevens, 2008). Meinzer distinguished springs whose water is brought to the surface through pressure produced by gravity acting on the water (gravity springs and artesian springs) and springs whose water is brought to the surface through pressure produced by forces originating deep within the earth. He divided gravity springs into depression springs (Figure 30a), contact springs (Figure 30b), fracture springs (shown as a fault in Figure 30c), and tubular springs (shown as dissolution cavities associated with karst in Figure 30d). For artesian springs, the water issues under artesian pressure (i.e., where the potentiometric surface is above the land surface). Springs that originate due to forces at depth are often thermal springs, many of which occur along faults or other structural features that allow water to rise from great depths (Box 5). Springs of this class may be divided into those associated with volcanism and those due to fractures that extend deep into the earth in localities not affected by volcanism (Meinzer, 1923).

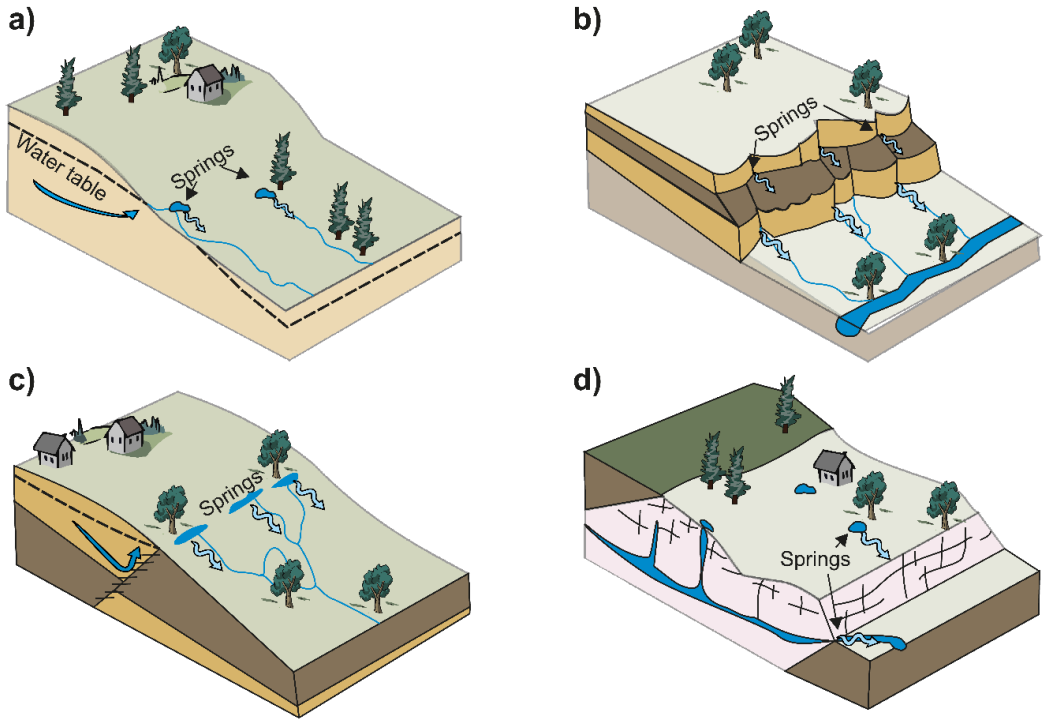

Figure 30 - Common spring types: a) Gravity class – depression type; b) Gravity class – contact type; c) Gravity class – fracture type (here, a fault); and d) Gravity class – tubular type (here, solution cavities associated with karst) (classification from Meinzer, 1923) and schematics modified from Fetter, (2001).

More recent spring classification schemes have been proposed that focus on the *spheres* of discharge of springs (e.g., Springer et al., 2008). Here, in addition to

hydrogeological characteristics, ecological and cultural variables are incorporated. Another prominent classification system that includes springs is for groundwater-dependent ecosystems (GDEs), which focus more on the vegetation aspects (Eamus & Froend, 2006; Kløve et al., 2011).

Spring and seep discharge may be constant or vary over time. They may be perennial (discharge continuously) or intermittent (i.e., only discharge during certain periods but at other times are dry or do not exist). Figure 31 shows thermal, infrared images captured at a fractured sandstone outcrop in coastal British Columbia, Canada (Rathay, 2016). The seep issued from a bedding plane fracture that runs more than half the length of the outcrop (5 m). The seep was warmer at 7 °C (white) relative to the surroundings at 4 °C (dark grey) in November. In June, no seepage was observed. Seepage at the site varies with groundwater recharge as illustrated by the groundwater-level hydrograph from a nearby observation well. The water table begins to rise in November, reaching a maximum in late December, and remains fairly constant until April when the recession begins. Seepage generally occurs when the water table is high but ceases when the water table lowers.

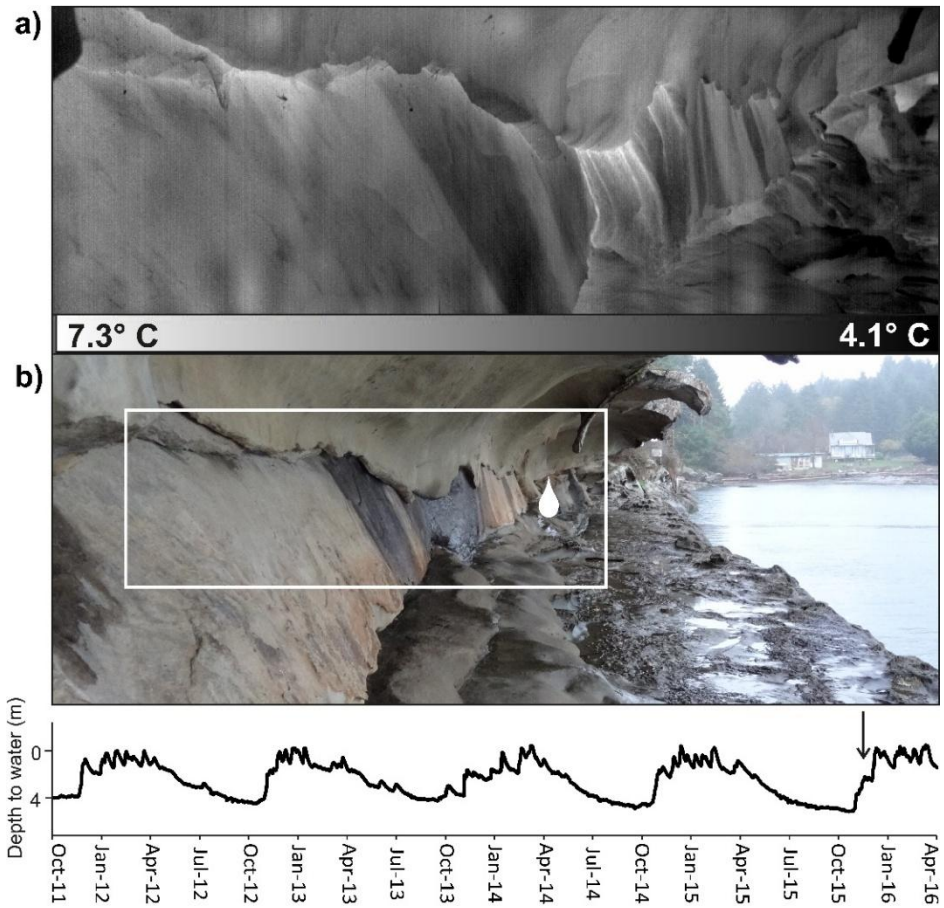

Figure 31 - a) Thermal infrared image, with lighter tones indicating warmer areas as indicated by the thermal scale at the bottom of the image, showing seepage along a bedding-plane fracture in sandstone. The flowing seep appears warmer (white). b) The raindrop in the visible light photograph indicates the site of seepage. The white frame in the photograph delineates the extent of the thermal image (a). The hydrograph at the bottom shows the groundwater level for Provincial Observation Well 196, with the arrow indicating the date of the images (From Rathay et al., 2018).

Spring waters are used for drinking, bathing, and growing food all over the world. Not only have springs provided reliable water for human societies since long before written records began, but springs also have important ecological and cultural significance. Springs support numerous microhabitats and large arrays of aquatic, wetland, and terrestrial plant and animal species. They also sustain rare species of plants and animals, including unique communities of bacteria (Brock, 1994) and even endangered snails (Grasby & Lepitzki, 2002 and Box 5), that often occur nowhere else on earth. Mineral springs (springs rich in dissolved solids) and thermal springs (hot springs) are of particular cultural significance and have played critical roles in the world's Indigenous cultures since time immemorial, serving as reliable water sources, places of healing, and sites of ceremony and religious significance. In Japan, some lucky snow monkeys have their own spa (Monkey Spa | Cousins | BBC Earth).

Perhaps the biggest threat to springs is the overextraction of groundwater from wells (Currell & Katz, 2022), although climate change, urbanization, land-use change, and water-quality degradation due to pollution are also major stressors. The Springs Stewardship Institute (SSI) is an initiative of the non-profit Museum of Northern Arizona. Part of its work is maintaining a springs and springs-dependent species database. The goal of the initiative is to improve the global health of springs. SSI synthesized protocols to inventory and assess the ecological health and functionality of the ecosystems supported by springs. In addition to groundwater chemistry and flow data, the inventory includes information on geomorphology, habitat and soils, flora and fauna, human influences, and administrative (legal and managerial) context.

3.1.6 Geysers

Geysers are geothermal springs that emerge explosively and usually erratically. They are characterized by intermittent discharge of water ejected turbulently and accompanied by a vapor phase (Bryan, 1995). There are over 1,000 geysers worldwide, nearly half of which are located in Yellowstone National Park, Wyoming, USA (video of Yellowstone National Park geysers). The most well known is Old Faithful, so named due to its seemingly regular eruptions. Since records were first taken in the 1870s, Old Faithful has been discharging thousands of gallons of boiling, silica-rich water over 30 m into the air an average of 16 times a day. Other large geyser fields in the world include the Valley of Geysers (200 geysers) on the Kamchatka Peninsula in Russia; El Tatio, in the northern Chilean Andes; Geyser Flat, Whakarewarewa in the Taupo Volcanic Zone in New Zealand; and the shores of Lake Bogoria in Kenya.

The major geyser fields were formed following the last glaciation (<14,000 years ago) (Hurwitz & Manga, 2017). They occur in areas of recent or active magmatism where the supply of heat is abundant, mostly at high latitudes where precipitation rates are high, and where glacial sediments overlie SiO_2-rich volcanic rocks (rhyolite flows or ignimbrites) with abundant fracture networks (Hurwitz & Manga, 2017). Together, these features create

reservoirs that allow hot water to accumulate and then be discharged in discrete events. Deep and large reservoirs provide more water, thus creating larger and longer eruptions. Geysers that are hydraulically isolated, like Old Faithful, tend to be more regular in terms of eruption recurrence. Generally, though, geysers are transient features with periods of activity and dormancy that are affected by earthquakes, changes in water recharge rates, erosion of their cones and/or mounds, and slow silica deposition in flow channels and reservoirs.

Geysers are sensitive to environmental changes; most of the geysers in the Taupo Volcanic Zone and many that were present in Nevada, USA, have vanished due to geothermal energy production (Hurwitz & Manga, 2017). Hurwitz and others (2020) found that Old Faithful was dormant for several decades during the thirteenth century due to a megadrought that gripped much of western North America.

3.1.7 Flowing Wells

Flowing wells, also referred to as flowing artesian wells, are another type of groundwater discharge. Flows can range from a mere trickle to many gallons per minute (Figure 32). Flowing wells are a curiosity for many, but encountering artesian conditions during drilling can pose significant technical and economic challenges for drillers who are unfamiliar with the conditions under which flowing wells can occur.

Figure 32 - Photograph of a flowing well (courtesy Jim Fyfe, Fyfe's Well Drilling). The well is flowing because the elevation of the potentiometric surface, or pressure head, in the zone where the well is screened is above the well head elevation.

The classic conceptual model for the occurrence of flowing artesian wells is a geologically controlled model (Chamberlin, 1885). Chamberlin outlined several requisites necessary for the occurrence of artesian conditions, including a typical sloping confined aquifer where the potentiometric surface is above ground surface at the location of the flowing well (Figure 33a). Here, there is a suitable uphill exposure of the edge of the aquifer (where the aquifer is not confined), so that the aquifer may be recharged. However, modern-day understanding of cross-formational flow through aquitards challenges this requisite, as aquifers do not need to outcrop to receive recharge. A second requisite of Chamberlin's is the presence of an aquitard above the aquifer that prevents the escape upward of water that would otherwise find head relief in that direction. Figure 33b illustrates a conceptual geologically controlled model in which the substrate is fractured bedrock. Fracture pathways intersected by the flowing well are connected to the recharge area. The fractures are effectively confined by the surrounding bedrock matrix, resulting in the potentiometric surface associated with the deep fracture in the well located above ground surface.

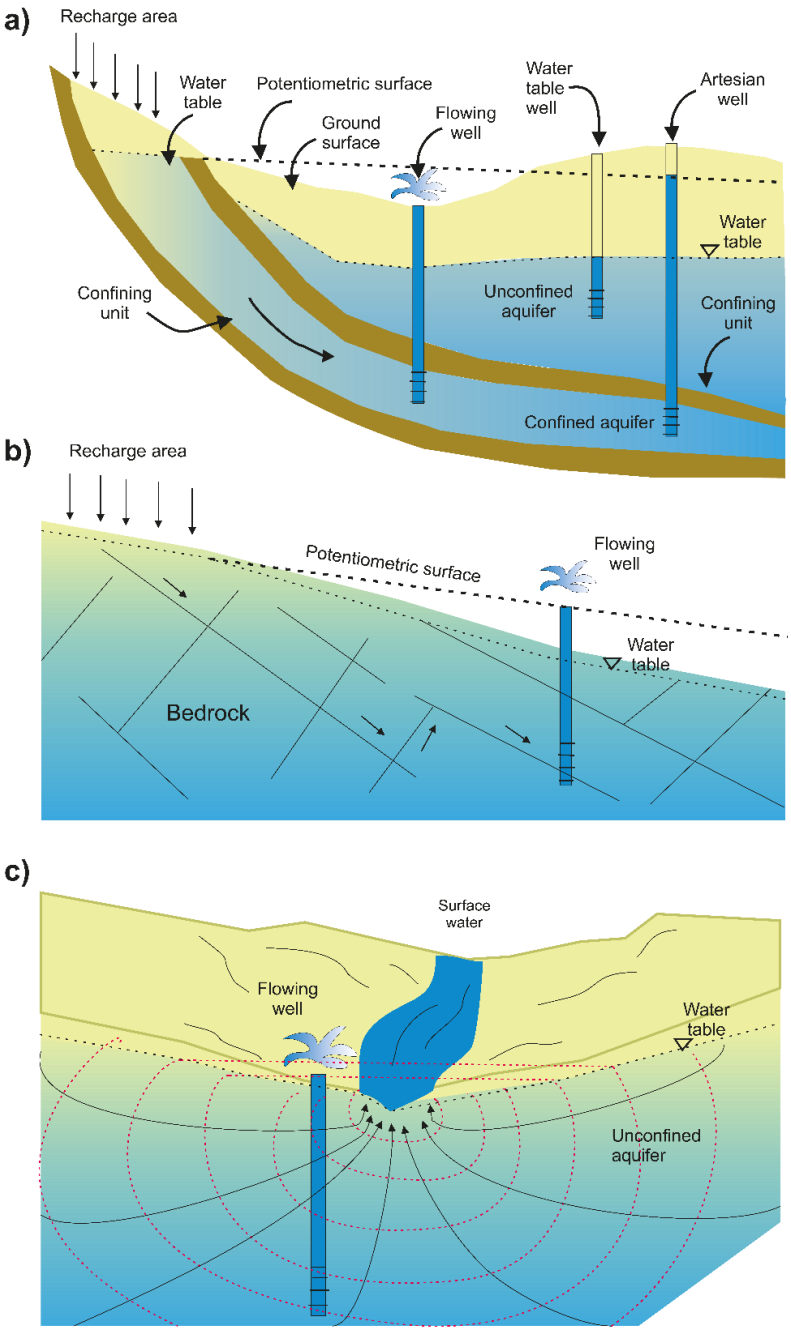

Figure 33 - Flowing wells in three hydrogeological settings. a) Flowing wells due to the potentiometric surface of a confined aquifer above ground surface at the location of the flowing well (adapted from Todd, 1959). b) Fractured bedrock aquifer illustrating flow paths along fractures that connect to a recharge area at higher elevation to result in the potentiometric surface above ground surface at the location of the flowing well. c) Flowing wells in an unconfined aquifer due to the well screen intersecting equipotential lines (hydraulic head contours) with a head value that is above ground surface, as illustrated by the red horizontal dashed lines above the surface (adapted from Gaber, 2005).

While geological conditions are generally better known as controlling conditions for flowing (artesian) wells, Freeze and Cherry (1979) asserted that topography is the primary control. In both of the conceptual models (the confined aquifer in Figure 33a and the fractured bedrock aquifer in Figure 33b), some topographic relief is needed to generate

the high hydraulic head at depth. Indeed, Freeze and Cherry (1979) pointed out the settings that display geologically controlled conditions are not particularly common, despite the widespread use of the geologically controlled model for explaining flowing wells. Topography-controlled flowing wells can essentially occur anywhere the hydraulic head at depth (where the well is screened) is higher than the ground elevation at the well (Figure 33c). Areas where upward flow is common include topographic depressions, such as valley bottoms, where groundwater discharge occurs. Topography-controlled flowing wells are commonly associated with unconfined aquifers and therefore are not strictly defined by the presence or absence of specific geological units, such as confining units. Topographic relief is the reason for the common occurrence of flowing artesian conditions in valleys. Any hydrogeologic system that leads to hydraulic head values in an aquifer exceeding ground surface elevation can result in flowing wells.

In the geologically-controlled model it is the combination of the confined aquifer and a water source at higher elevation (topography) that creates flowing artesian conditions in the aquifer at lower elevation. Whereas in the topography-controlled model, it is primarily the topographic relief that creates upward vertical gradients and a discharge zone. These models are represented as being mutually exclusive in the literature, but they really represent end members of a spectrum of controls on flowing artesian conditions. Therefore, combinations of geological and topographic factors are important to consider when artesian conditions are of concern.

Jiang and Cherry (2024) delve into the history and hydraulics of flowing wells, beginning with classic models for the hydraulics of flowing wells in purely confined aquifers and in semi-confined (leaky) aquifers with a flat initial potentiometric surface and proceed to introduce models for flowing wells in basins—including layered basins and homogeneous basins—with a topographically controlled flow system.

Flowing wells are a known problem in many regions of the world. Allowed to flow uncontrolled, these wells can eventually reduce the long-term sustainability of the aquifer, leading to reduced water yield from wells and springs, and potentially reduce natural groundwater discharge to streams, which can impact aquatic habitat. Moreover, flowing wells may lead to subsidence or sinkholes, potentially resulting in extensive property damage, impacts to infrastructure, loss of property value, and exorbitant costs to the property owner, as well as limit the future use of the land. Uncontrolled flow at the ground surface means this water must be conveyed, in some cases unnaturally, into streams. The low oxygen content of the groundwater entering the stream may impact aquatic habitat.

3.1.8 Groundwater Abstraction

Groundwater *abstraction* (pumping) is an important, albeit unnatural, type of groundwater discharge. In recent decades, the global population has quadrupled, currently standing at around 8.5 billion (United Nations, n.d.). The expansion of irrigated agriculture and economic development driven by this population growth has generated an ever-increasing demand for water worldwide. This increased demand has encouraged the drilling of more wells and the use of groundwater. Consequently, global groundwater withdrawal has seen a significant increase (Famiglietti, 2014; UNESCO, 2022). The total global groundwater withdrawal in 2017 is estimated at 959 km^3, unevenly distributed across the globe (Table 1 in UNESCO, 2022). The bulk of abstracted groundwater is distributed across three primary sectors: agriculture (irrigation), domestic/private use, and industrial/manufacturing purposes (Table 2 in UNESCO, 2022).

Groundwater is abstracted from a variety of well types, including drilled wells, dug wells, and even trench-type wells (Figure 34) that skim fresh water off the top of the water table. These trench-type wells are common on low-lying islands where vertical wells are unsuitable given the shallow depth of the freshwater-saltwater interface (subsection 3.1.4). While water-supply wells are used for providing groundwater for uses such as drinking, livestock watering, and irrigation, other wells pump groundwater for specific purposes, such as dewatering mines and building excavations. While many dewatering projects are non-permanent, others can be permanent. Subsection 4.5.3 explores the effects of groundwater abstraction on the short- and long-term dynamics of recharge and discharge.

Figure 34 - Trench well on Andros Island, the Bahamas. The trench extends to a depth just below the water table and skims water from the freshwater lens on the island.

Thought Question: Considering the different discharge mechanisms (types of discharge) that have been discussed in this section, which ones are present in your region? Attempt to rank them by volume of groundwater discharged annually.

3.2 Factors that Control Discharge

Discharge is inextricably linked to recharge. Whatever water enters the groundwater system will eventually discharge somewhere. If a groundwater system is in equilibrium, then, however much water is recharging the aquifer, the same amount of water will discharge. Otherwise, if there is an imbalance, the groundwater level will rise or fall. The dynamic nature of recharge and discharge are explored in detail in Section 4. Here, an overview of some of the factors that control discharge are discussed briefly.

Fundamentally, under equilibrium (i.e., steady state) flow conditions, the volume of discharge from an aquifer depends on the hydraulic gradient and the hydraulic conductivity and can be described by Darcy's law. Because the hydraulic conductivity of the aquifer typically remains constant, the discharge varies according to the hydraulic gradient (Figure 35). If the hydraulic gradient (d*h*/d*l*) is higher, then discharge is higher, assuming the same hydraulic conductivity. In Figure 35, the land use on the left is a forest with trees that have deep root systems, which would lead to higher evapotranspiration and a deeper water table. In contrast, the land use on the right is irrigated crops. Some irrigation water infiltrates past the shallow root zone of the plants and forms irrigation return flow (subsection 5.2), adding to the natural recharge and subsequently raising the water table. Thus, the additional recharge on the right leads to a steeper hydraulic gradient and, therefore, greater groundwater discharge to the stream along its right bank.

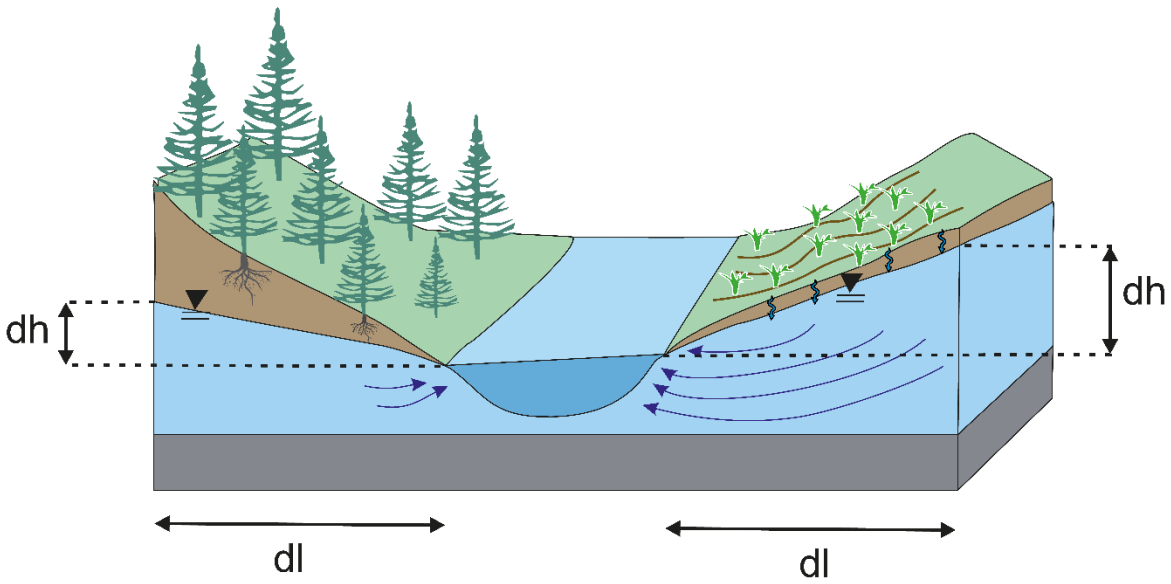

Figure 35 - Groundwater discharging to a stream from an unconfined aquifer. The hydraulic gradient, d*h*/d*l*, on the right is greater than the hydraulic gradient on the left, leading to greater discharge along the right stream bank.

Like recharge, the discharge of groundwater is dominantly controlled by the climate. In humid regions, groundwater recharge can occur throughout the year, although there is usually a dominant recharge season, as explored in more detail in Section 4. Groundwater typically discharges to surface water bodies year-round, even during dry periods with no precipitation, and sustains the streamflow. However, in arid and semi-arid regions recharge events tend to be episodic and highly seasonal; for example, most recharge occurs during the rainy season that coincides with the monsoon. These episodic recharge events can lead to episodic discharge.

Alterations to the groundwater system or the surface-water system can influence discharge. While the hydraulic properties of the aquifer typically do not change, processes such as compaction can lead to a reduction in pore space, which in turn can reduce the amount of recharge to the aquifer and consequently the amount of discharge from that aquifer. Changes in land cover or land use can also affect the amount of recharge and thus discharge. Groundwater pumping, as discussed in subsection 3.1.6, can lower the water table or potentiometric surface and cause springs and seeps to stop flowing. Groundwater pumping captures groundwater that would otherwise have discharged into surface water bodies. Likewise, groundwater pumping from deep confined aquifers can induce recharge from overlying unconfined aquifers and, consequently, reduce the amount of available water to discharge from the upper aquifer. Modifications to the surface water system by dam construction or channelization, for example, can also influence how much groundwater discharges.

As explained earlier, discharge depends on recharge, but recharge also depends on what is happening at the discharge end. In Figure 35, the water table was at different elevations on the left and right sides of the stream, while the stream stage was the same for both sides. But stream discharge and stream stage vary throughout the year, so it is not just the water table rising and falling that can influence the hydraulic gradient, but also the stream stage. In cold mountainous regions, stream discharge increases during the spring melt season (the *spring freshet*). Stream discharge, particularly in high-order streams, can be significant. This results in the stream stage being higher than the water table adjacent to the stream. As a result, the hydraulic gradient between the stream and the aquifer reverses and the stream loses water to the aquifer. When this happens, groundwater discharge to the stream ceases and the stream becomes a source of recharge to the aquifer; Exercise 7.

Ultimately, we need to consider the nature of recharge and discharge together in order to gain an understanding of how an aquifer system functions in and by itself, how it interacts with the surface water systems, and how it is influenced by human intervention.

3.3 Summary

This section explored discharge processes in different environmental settings. Groundwater discharge is the loss of groundwater from the subsurface to the surface

environment, either to the land surface or subaqueously. We began by exploring the exchange of groundwater and surface water, a topic that is expanded upon in detail by Woessner (2020).

We discussed that while many surface water bodies receive groundwater discharge, there can be two-way exchanges, commonly referred to as groundwater–surface water interactions. The concepts of gaining, losing, flow through, and disconnected streams were introduced, noting that the exchanges can be spatially and temporally varying.

We then looked at groundwater discharge in different environments, beginning with discharge to streams, which can occur diffusely or in a more focused manner. The groundwater that enters the stream forms baseflow, which is the portion of streamflow generated by groundwater discharge. The magnitude of baseflow varies seasonally, increasing during periods when groundwater recharge is high and lowering as the recharge wanes. If the baseflow is continuous, then streamflow will be maintained, even during periods when there is no precipitation. Such streams are classified as perennial streams. But there are also intermittent streams that flow only at certain times of the year, indicating that the groundwater discharge becomes insignificant. Ephemeral streams, on the other hand, flow only for short periods, typically after heavy rain events. Such streams are common in arid and semi-arid regions, and the streams effectively become disconnected from the groundwater system.

We then examined discharge to lakes and wetlands, a topic explored by Woessner (2020) in more detail. Importantly, exchange of water between the wetland and the groundwater system is slow due to the presence of fine-grained sediments and organic materials. Wetlands serve an important role in an ecosystem, absorbing excess nutrients and other contaminants before they reach rivers, lakes, and other water bodies.

Groundwater discharge in coastal areas is influenced by the presence of a saltwater–freshwater interface that lies at some depth where the fresh groundwater system meets the saline submarine environment. The interface acts as a sort of barrier, causing the fresh groundwater to circulate upward and discharge close to the coast in the intertidal area. However, groundwater discharge pathways in coastal zones are strongly controlled by the geology, particularly the presence of low-permeability layers, and the morphology of the landscape as discussed in Box 4.

We explored different types of springs, including thermal springs and geysers, as well as groundwater seeps. While springs tend to be focused groundwater discharge points, seeps (or seepage faces) discharge groundwater over a larger area. Regardless, these locations of groundwater discharge have held cultural and spiritual significance for many thousands of years, particularly thermal and mineral springs. Springs are also important from an ecological perspective, with some host to rare and endangered species. Thermal springs commonly issue from faults in mountainous regions, which provide pathways for the rapid upward flow of heated groundwater from great depth as discussed in Box 5. A

particularly fascinating type of episodic groundwater discharge from depth is a geyser. The site of over half the world's geysers, Yellowstone National Park in the USA is home to the Old Faithful geyser, so named because of its seemingly regular eruptions.

The last types of discharge considered in this section are flowing wells and groundwater abstraction. These types of groundwater discharge are caused by human intervention. Flowing wells occur when the water table or potentiometric surface lies above the ground surface (or above the casing). If a well is not capped, water will flow out of it. Two end-member models have been proposed to explain the occurrence of flowing wells: geologically controlled models and topography-controlled models. However, these models represent end members of a spectrum of controls on flowing artesian conditions. Combinations of geological and topographic factors are important to consider. Groundwater abstraction is the active removal of groundwater from aquifers. Groundwater is becoming an increasingly important resource in many regions around the world, largely due to population growth and climate change.

The section ended with a short section on the factors that control discharge. Emphasized was the fact that discharge is strongly influenced by recharge. The two go hand in hand. Importantly, the flow of groundwater is controlled by the hydraulic gradient. Gradients change seasonally, giving rise to differences in the amount of groundwater discharge. But gradients can also be modified by geological variations, changes in land cover or land use, and groundwater pumping.

The following section explores the dynamic nature of recharge and discharge. Recharge and discharge are considered together, because it is important to think about what is happening throughout the entire groundwater system and how it interacts with the surface environment.

4 The Dynamic Nature of Recharge and Discharge

Recharge and discharge are inextricably linked in a groundwater system, as discussed in the previous section. Therefore, it is important to consider the dynamics of these processes together. This section begins by describing how recharge and discharge relate to changes in storage, which is a fundamental concept that relates groundwater-level change to inputs, outputs, and storage properties. An overview of methods of measurement is given. The section then explores the seasonality of recharge and discharge in some detail, with closer examination of recharge and discharge dynamics in different climate regions, beginning with cold regions, temperate regions, and finally arid and semi-arid regions. We discuss the various factors, then explore variability in recharge and discharge at other temporal scales, including daily and subdaily, and over longer timescales such as interannually, and in relation to climate oscillations and climate change. The section ends with a discussion of the influence of the hydraulic connection between aquifers and streams on the dynamics in these systems.

4.1 Recharge and Discharge Lead to Changes in Storage

4.1.1 The Groundwater Level Hydrograph

Both groundwater recharge and discharge influence changes in groundwater storage. The changes in storage are manifested by a change in the groundwater level. Groundwater levels in aquifers vary spatially (by location and depth) and temporally (hourly, daily, seasonally, interannually, and at longer time scales). Observation wells, or groundwater-level monitoring wells, are used to monitor groundwater-level variations over time, and the data are normally graphed on a *well hydrograph* as a time series (Figure 36). Groundwater levels can be expressed either as hydraulic head in meters above sea level (masl) or as a depth in meters below ground surface (mbgs), as illustrated in Figure 36 for Observation well 201 accessible through the British Columbia Groundwater Level Data website↗.

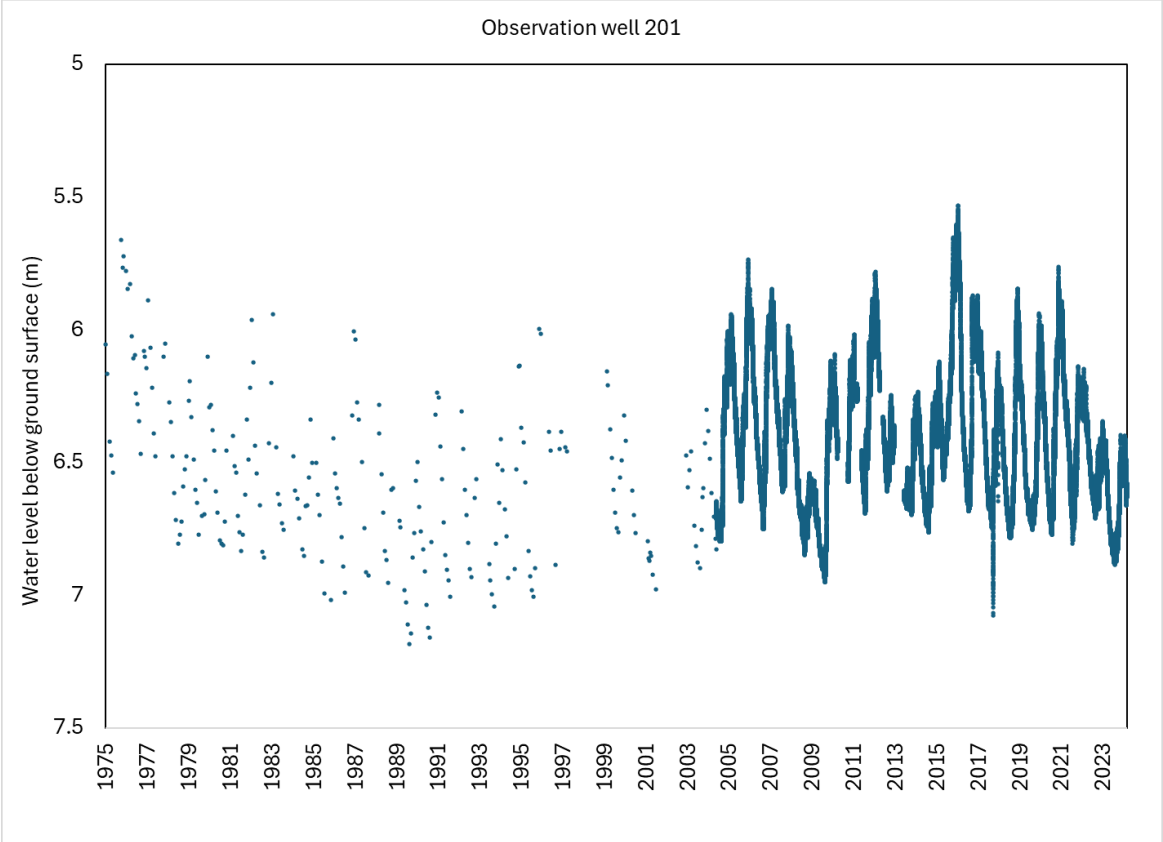

Figure 36 - Example of a well hydrograph for British Columbia, Canada. Observation Well 201, Alert Bay (Fir St.) showing seasonal variations in groundwater level, expressed here as a depth in meters below ground surface (mbgs). Measurements prior to 2005 were made manually approximately once per month, while a water level data logger was used to make hourly measurements since 2005 (adapted from Province of British Columbia, 2024).

A measured groundwater level represents the hydraulic head that is averaged across the depth interval over which the well is open to the zone being monitored. In unconsolidated sediments the well is screened to prevent the hole from collapsing and to keep particles from entering the well. For observation wells that are screened across an entire aquifer, the head represents the depth-averaged head for the aquifer. Similarly, if the well is completed in bedrock, the open borehole length from the base of the surface casing or the water level (whichever is lower) to the bottom of the well is the averaging depth interval. In cases where the hydraulic head is expected to vary with depth, such as in a recharge area or discharge area, a long monitoring interval will obscure the vertical variations in hydraulic head. Only if flow is dominantly horizontal in the monitored zone will a long open interval represent the head at all depths.

A *water year* is a common period for reporting and describing hydrologic data. The water year (or hydrological year as defined in the UK) has been adopted by many countries. North America and Europe have adopted the period October 1 to September 30. A water year differs from the calendar year because the bulk of annual precipitation falls in late autumn and winter recharging aquifers and streams, with accumulated snow not draining until snowmelt occurs in the following spring or early summer, setting up water

availability for the drier summer months. It is a convenient time window for hydrogeologists in the northern hemisphere because it begins when water levels are low then captures the rise and associated fall of water levels for an annual period of recharge and its related discharge.

As illustrated in the well hydrograph in Figure 36, groundwater levels vary over the water year. In this particular aquifer (British Columbia Aquifer #858 with details accessible through the British Columbia Groundwater Wells and Aquifers webpage↗), comprised of silty sand, the annual range in groundwater level is approximately 1 m; however, there is interannual variability in the range and the maximum and minimum groundwater levels. Interannual variability in the well hydrograph is normally related to interannual variability in the weather. However, changes in local conditions can influence interannual variability—for example, when groundwater pumping begins at a nearby well(s), irrigation is introduced, land use or land cover changes, or the discharge environment is modified. Such *permanent* changes in local conditions often lead to a change in the hydrogeologic regime. Accordingly, the well hydrograph may show evidence of an alteration or a long-term trend. In the example shown in Figure 36, there are no observable positive or negative trends. This record has insufficient data to calculate a statistical trend, despite the relatively long record for this well. Normally, 30 years of data are required to calculate a statistical trend, but in this example, the period from approximately 1995 to 2005 is incomplete.

4.1.2 Why do Groundwater Levels Rise and Fall?

The rise and fall of the groundwater level observed on a well hydrograph reflects the addition of water to storage in the aquifer and the release of water from storage, respectively. It is important to remember that groundwater is constantly flowing in the aquifer—what goes in (recharges) drains out (discharges), although the rates of recharge and discharge vary. If the water level is rising, this means that the rate of recharge is greater than the rate of discharge. During seasonal recharge periods, we observe a *groundwater-level rise*. When recharge reduces or stops, we observe a groundwater-level decline, also known as a *groundwater recession* (Figure 37). In an unconfined aquifer, the water-table elevation typically varies seasonally as discussed in subsection 4.3; it rises during the rainy or snowmelt season when most of the annual recharge occurs, usually reaching a peak elevation near the end of that season, and then undergoes a recession. The rise in water table temporarily increases the hydraulic gradient, driving groundwater toward the discharge area. Unless the aquifer system is continually replenished, the water table will gradually lower. This is the groundwater-level recession.

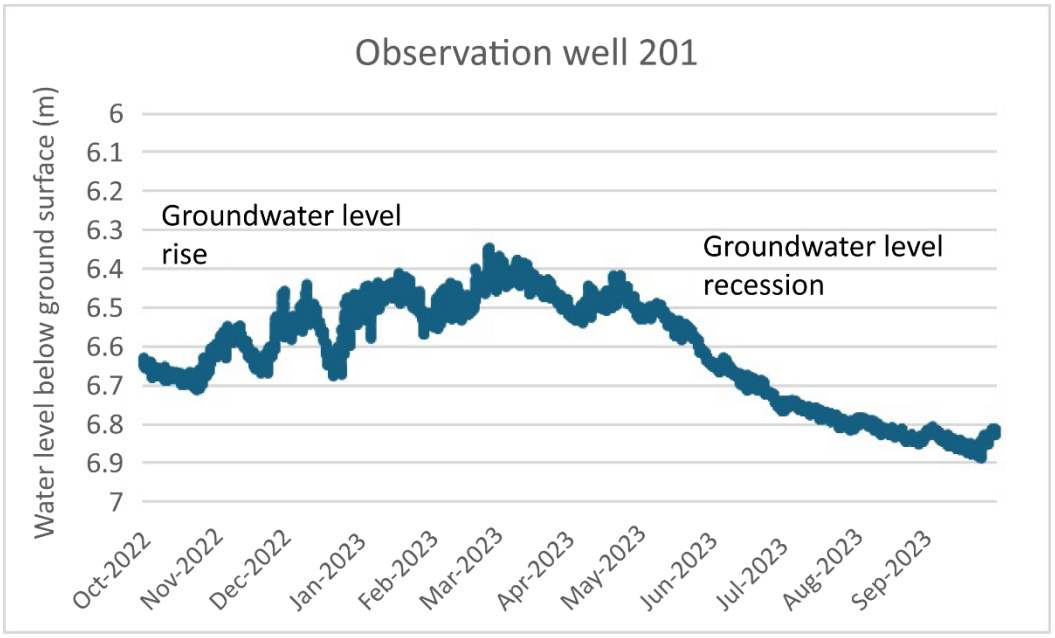

Figure 37 - Example of a well hydrograph (for the water year from October 1, 2022 to September 30, 2023) for British Columbia Observation Well 201, Alert Bay (Fir St.) showing seasonal variation in groundwater level, expressed here as a depth in meters below ground surface (mbgs) (adapted from Province of British Columbia, 2024).

The dynamic range (the difference between the maximum and minimum groundwater levels) observed on a particular well hydrograph varies slightly from year to year depending on the weather. Years with greater precipitation are typically associated with higher recharge and so the aquifer will have higher maximum groundwater levels, while years with little to no precipitation, particularly during the recession period, will have lower minimum groundwater levels. However, the magnitude of rise and fall in groundwater level in any particular aquifer also depends largely on how much water can be accommodated in storage, as defined by the storativity, S (dimensionless). For confined aquifers, Equation (19) applies.

$$S = S_S\, b \tag{19}$$

where:

S_S = specific storage (L^{-1})

b = saturated thickness of the hydrogeological unit

S_S is defined as the volume of water released from (or added to) storage per unit volume of the hydrogeological unit in response to a unit decline (or rise) in hydraulic head.

For unconfined aquifers, Equation (20) applies.

$$S = S_Y + S_S\, b_{average} \tag{20}$$

where:

S_Y = specific yield, which reflects the volume of water that drains by gravity when the water table is lowered or fills with water when the water table is raised (dimensionless)

$b_{average}$ = saturated thickness average thickness before and after the rise or fall (L)

S_Y values typically are much higher than S_S values; therefore, the storativity for unconfined aquifers is dominated by S_Y. As a result, for the same amount of recharge, unconfined aquifers will have a smaller rise in water level compared to the rise in the potentiometric surface in a confined aquifers because the unconfined aquifer can accommodate more water in storage per unit increase of head. This occurs because the recharge physically fills pores in an unconfined aquifer whereas it only increases pressure in pores of a confined aquifer. A more in-depth discussion of these storage terms is provided in section 4.3 of Poeter and others (2020)↗ with greater details in section 6.4 of Woessner and Poeter (2020)↗. An opportunity to explore this is provided by Exercise 8↴.

When considering the water level rise, another factor comes into play, which is how quickly the groundwater is conveyed away from the recharge area. If the water flows quickly, the recharge pulse will travel quickly and the recharge pulse will dissipate quickly. This means that the aquifer's transmissivity (T) is also important and is combined with storage in the hydraulic diffusivity, D, of the aquifer, as shown in Equation (21).

$$D = \frac{T}{S} \tag{21}$$

where:

D = hydraulic diffusivity (L^2T^{-1})

T = transmissivity, product of thickness and hydraulic conductivity (L^2T^{-1})

S = storativity (dimensionless)

The interplay of T and S means that it is not always straightforward to predict how high the water level will rise due to a recharge event, though higher diffusivity leads to more rapid dissipation of water level rise associated with a recharge event. Additionally, the groundwater-level response across an aquifer can depend on the hydraulic connection with surface water bodies (subsection 4.4) as well as aquifer heterogeneity. Nevertheless, when comparing responses across different aquifers, even if the aquifers have the same climate conditions, the groundwater-level range will differ depending on the aquifer diffusivity.

4.1.3 Methods Used to Estimate Recharge, Discharge, and Changes in Storage

This section provides an overview of various methods for estimating recharge, discharge, and changes in storage, which can be broadly categorized into water balance methods, physical methods, chemical and isotopic (tracer) methods, heat (temperature) methods, and remote sensing methods as listed in Table 3. Oftentimes, two or more methods are used to address uncertainty. Scanlon and others (2002) and de Vries and Simmers (2002) reviewed various methods for estimating recharge, and Healy (2010) wrote a book on the topic. Cook and Brunner (2025) provide an overview of different methods for estimating recharge, including water balance approaches, hydrograph analysis, chloride mass balance, unsaturated zone tracers, and groundwater dating. The application of stable isotopes of water and noble gases is also described. Methods used to estimate groundwater exchanges in the context of groundwater–surface water interactions are discussed by Woessner (2020). Kalbus and others (2006) provide a review of methods specific to groundwater–surface water interactions.

Table 3 - Methods for estimating or inferring recharge, discharge, and changes in storage.

Estimation method	Use	Technique
Water balance methods		
Residual water balance method using empirical data	Recharge estimation; site scale; various timeframes	Uses empirical data: precipitation (P), actual evapotranspiration (AET), and runoff (R_{OFF}) to estimate recharge (R_{CH}); reflects infiltration into the subsurface but does not differentiate between unsaturated zone storage and recharge to the water table; the magnitude of error in P, AET, and R_{OFF} can be of similar magnitude to the magnitude of R_{CH}.
Numerical models	Recharge, discharge, and storage change estimation; various spatial scales and timeframes	1D vertical percolation models through to fully integrated 3D land surface – subsurface models used to simulate the water balance from which recharge is obtained; 2D or 3D groundwater flow models can be used to estimate R through calibration; models can be highly parameterized and computationally intensive.
Physical methods		
Unsaturated soil moisture storage	Storage change estimation, recharge; site scale; various timeframes	Lysimeters, neutron probes, time domain reflectometry, and nuclear magnetic resonance techniques are used to estimate soil moisture spatially and temporally. Recharge is estimated based on drainage and changes in soil moisture.
Unsaturated zone moisture flux	Recharge	Darcy's law is used to estimate fluxes within the unsaturated zone, with downward vertical fluxes indicating drainage. Tensiometers are used to measure the matric potential gradient, and soil moisture characteristic curves are used to estimate the hydraulic conductivity needed to employ Darcy's law. K_{sat} can be measured using a Guelph permeameter or ring infiltrometer.
Saturated zone water storage changes	Recharge	Water-table fluctuation method uses the rate of rise of a groundwater-level hydrograph multiplied by S and adds the amount of drainage (rate of decline during a period with zero precipitation). The method is best suited to shallow water tables, where water-table rise from precipitation is more distinct; presence of other drivers of water-table rise (e.g., pumping wells) or connection with surface water may obscure the water-table increases related to recharge.

Estimation method	Use	Technique
Saturated zone water flux	Saturated zone flux	Darcy's law is used to estimate fluxes within the saturated zone; piezometers are used to measure the hydraulic head at specific depths and in different locations to determine hydraulic gradients in 1D, 2D, or 3D. Saturated hydraulic conductivity is needed to determine the flux using Darcy's law.
Spring flow rate	Discharge	Flow measured at a spring outlet; provides a direct measurement of groundwater discharge; allows seasonal assessment of groundwater discharge.
Stream water balance	Recharge and discharge	The gain or loss of water from the stream through exchange with the groundwater system is estimated from the stream water balance. Streamflow is measured upstream and downstream on a reach, and where there are no other sources or sinks of water to the stream, the difference in streamflow is the seepage rate—either recharge to the aquifer from the stream or discharge of groundwater to the stream.
Streambed flux	Recharge and discharge	Vertical gradients measured in nested instream piezometers can be used to calculate the Darcy flux using the streambed hydraulic conductivity. Seepage meters can be used to directly measure the volume of water exchanged between the stream and the groundwater system through the area covered by the seepage meter (either into or out of the stream).
Stream hydrographs	Discharge and recharge	Hydrograph separation techniques can be used to quantify the baseflow contribution to a gaining stream, which represents the groundwater discharge. At a catchment scale, the total baseflow may equate to the recharge, assuming no losses or gains of groundwater elsewhere in the catchment.
Chemical and isotopic methods		
Chloride mass balance (CMB)	Recharge estimation	The CMB method requires precipitation amount, Cl concentration in precipitation, and Cl concentration in groundwater; particularly useful for estimating recharge in arid and semi-arid regions.
Chemical composition	Recharge and discharge	The chemical composition of water, total dissolved solids (TDS), and electrical conductivity (EC) may aid in identifying groundwater recharge and discharge areas; groundwater in recharge areas typically has a $Ca\text{-}HCO_3$ water type, low TDS, and low EC; groundwater discharge is typically associated with high TDS and high EC in water collected from seepage meters or instream piezometers.
Stable isotope composition	Used to infer recharge	Stable isotopes of water (i.e., $\delta^{18}O$ and $\delta^{2}H$) and radiogenic isotopes (e.g., Rn) may provide an indication of groundwater sources and discharge areas; used in the unsaturated and saturated zones; used as an aid for hydrograph separation.
Tracer studies	Recharge	Various chemicals, isotopes, and dyes are used as tracers; they may be naturally occurring or applied in a controlled setting (e.g., as a pulse in the soil column) to measure recharge rates or applied in a flow system to determine velocity.
Noble gases	Recharge	The concentrations of noble gases dissolved in water (e.g., He, Rn) provide information on the temperature and pressure at the time of recharge; noble gases can also be used for age dating.
Age dating	Recharge	Radioactive isotopes, including ^{3}H, ^{14}C, and other "historical" tracers (e.g., ^{36}Cl and chlorofluorocarbons CFCs) are measured in groundwater and used to estimate age based on the decay rate.
Heat (temperature) methods		
Borehole temperature logs	Recharge, discharge	Borehole temperature logs (temperature with depth) are used to estimate groundwater recharge and discharge rates and identify fracture locations in open boreholes.

Estimation method	Use	Technique
In-situ measurement of stream temperature	Exchanges between groundwater and surface water	Commonly used to quantify exchanges between surface water and groundwater; approaches make use of the large, dynamic temperature oscillations (daily and seasonally); measured using small sensors such as Tidbits or fiber optic cables.
Remote sensing and indirect methods		
Unsaturated soil moisture storage	Storage change, recharge; watershed scale; various timeframes	Space-based interferometric synthetic aperture radar observations provide near-global coverage of proxies for soil moisture; time series measurements show the evolution of soil moisture storage.
Saturated zone water storage change	Storage change estimation, recharge; regional scale.	Changes in groundwater storage in the saturated zone are measured at a regional scale (400 km x 400 km) using gravity anomaly data from the Gravity Recovery and Climate Experiment.
Thermal infrared images	Discharge to surface water bodies or seepage	Thermal infrared sensors that are hand-held or drone-mounted or satellite-mounted detect radiation in the infrared range (0.7-1000 μm) that is emitted from a surface; dependent on emissivity of the surface; displayed as a thermal image known as a thermogram.
Vegetation	Primarily identifying discharge areas	Identify areas with comparatively higher photosynthetic activity relative to surrounding areas during the dry mid-summer months; for example, using the Landsat product Normalized Difference Vegetation Index. Local scale vegetation studies to identify specific plants associated with discharge areas; for example, willows.

Healy (2010) describes the importance of developing a conceptual model of the recharge processes, but because recharge, discharge, and changes in storage are connected, a conceptual model of the entire groundwater system and the associated surface water bodies will provide a stronger conceptual model. Such conceptual models typically center on establishing a water balance.

Water balance methods vary from an arithmetic water balance to a water balance calculated based on the simulation results of numerical models, some of which—for example, integrated hydrological models—simulate all aspects of the hydrological cycle. As discussed in subsection 2.1, precipitation partitions at the land surface (Figure 9). An arithmetic water balance for a soil column is of the form in Equation (22).

$$P = ET + OLF + R + \Delta S \tag{22}$$

where:

P = precipitation (L)

ET = evapotranspiration (L)

OLF = overland flow (or runoff) (L)

R = recharge (L)

ΔS = change in water storage in the soil column which is positive when there is an increase in storage and negative when there is a decrease (L)

At a daily time scale, the amount of precipitation that reaches the land surface will partition into ET, OLF, and R, with some amount of water adding to the soil moisture

storage. Over long periods (e.g., 30 years), ΔS should be zero because the soil reaches a state of equilibrium (i.e., the soil does not continue to get wetter or drier).

Water balances can be developed for individual aquifers, watersheds, and even entire basins. Recharge is often inferred based on the other components of the water balance because the other components may be estimated with less uncertainty. This is referred to as a *residual approach*. Developing a water balance is not a trivial exercise. However, a preliminary water balance can be constructed using readily available data and refined over time as greater insight into processes and supporting data become available.

Water balances can also be generated from the output of numerical models. These models simulate the physical processes at the scale of interest and keep an accounting of the water volume over time. One-dimensional models—such as HYDRUS 1D↗ (Simunek and others, 2005) and USEPA HELP↗ (US Environmental Protection Agency, 2020)—are used to simulate water fluxes and changes in storage through a vertical column. One limitation of 1D models is that they do not allow any water at the surface that forms overland flow to be routed elsewhere. Two- and three-dimensional models allow for routing of surface water. Groundwater flow models are commonly used to estimate the water balance of a groundwater system, but they do not simulate recharge directly. Rather, recharge is input to the model and adjusted during model calibration. More complex, integrated (or coupled) hydrological models can simulate all the important hydrological processes that operate in watersheds, including evaporation, transpiration, overland flow, infiltration, surface water flow, groundwater flow, and exchanges between surface water bodies and the groundwater system. These models use precipitation and air temperature time series as input. These models can also simulate snowpack and snowmelt, and accommodate different types of vegetation, soils, and geological materials. Cook and Brunner (2025) provide a more detailed discussion of different types of numerical models.

Physical methods

Physical methods can be broadly categorized into those used in the unsaturated zone, saturated zone, or streams.

In the *unsaturated zone*, the downward vertical flux or changes in soil water storage are targeted for measurement. Most methods provide point measurements of soil water drainage, which is assumed to eventually reach the water table and form recharge. However, because unsaturated zones may be very deep (hundreds of meters in arid regions), it may take time for moisture originating at the land surface to drain to the water table and form recharge. The Zero-flux plane (ZFP) and Darcy methods (described in detail by Healy, 2010) are soil moisture gradient methods and require measurement of the hydraulic gradient, which can be difficult to measure when the hydraulic gradient is small. Hydraulic gradients are determined by measuring the matric potential (subsection 2.5.1) using tensiometers (subsection 2.5.4) or soil moisture probes that use heat dissipation or electrical resistance to measure the matric potential. The ZFP and Darcy methods also

require an estimate of the hydraulic conductivity (subsection 2.5.3), which depends on the moisture content and is described by a moisture characteristic curve (subsection 2.5.2). Drainage of water through the unsaturated zone can also be determined by measuring change in soil moisture over time.

Different instruments can be used to measure moisture content, including lysimeters, neutron probes, and time domain reflectometry (TDR). Lysimeters are tubes of soil that are placed in a snug hole in an effort to mimic conditions of a site. A gauge measures the water that falls on its surface, the water that drains is collected and measured, and the entire tube is weighed to determine the change in volume of moisture in the soil over time. They are placed in the ground so that the top is flush with the ground surface. They can range in size from a few square cm to more than 100 m^2 in surface area.

Neutron probes can be used to obtain measurements of soil moisture with depth, whereby a probe is lowered down an access tube in the soil, or the probe can be inserted into the top few centimeters of soil at the ground surface. Neutrons emitted from the probe collide with hydrogen atoms in the soil water, are slowed, and scattered back to the probe where they are counted. The density of the neutron flux measured by the probe depends on the amount of water in the surrounding soil. For most devices, a higher neutron count indicates a higher water content.

TDR is based on the measurement of the travel time of an electromagnetic wave pulse (usually <1.5 GHz) through a wave guide (also called a probe or sensor) inserted into a porous medium. The travel time of the wave depends on the *apparent relative dielectric permittivity* (ε_a) of the soil, which expresses the ability of a material to polarize under an electric field. The ability of a material to polarize is increased by the presence of water. The soil moisture is estimated by relating ε_a to the moisture content using a calibration equation that is determined by making measurements on samples of known moisture content.

Topp and others (1980) performed laboratory experiments on soils of varying texture to determine empirically the dependence of the moisture content (θ) on ε_a at electromagnetic frequencies of 1 MHz and 1 GHz. TDR works in unfrozen and frozen soils; the electrical conductivity (EC) of the soil is measured at the same time. The TDR probes can be installed in any orientation to obtain vertical profiles or lateral measurements of soil moisture at a particular depth. He and others (2021) provide a review of TDR applications in porous media. Magnetic resonance imaging (MRI), also called magnetic resonance tomography (MRT), is a non-invasive, 3D imaging technique for monitoring water content and water fluxes in the unsaturated zone (Pohlmeier, 2011). MRI uses the effect of nuclear magnetic resonance of certain atomic nuclei, mostly ^1H in H_2O, which is modulated by the chemical and physical environment inside the porous medium. The application of MRI for soil systems started in the 1980s. The methods yield 2D (slices) or 3D (volume graphics) images of the medium under investigation.

In the *saturated zone*, groundwater-level data are the primary data source used for hydrogeological investigations. If measurements are available as a time series, then a groundwater-level hydrograph can be generated, as described in subsection 4.1.2. Groundwater-level hydrographs for unconfined aquifers can be used to estimate recharge using the water-table fluctuation (WTF) method, described in detail in Box 6↴. An opportunity to calculate a recharge rate from hydrograph data is provided by Exercise 9↴. Methods based on Darcy's law are also used to estimate recharge and discharge in groundwater systems. Measurements of hydraulic head are best made using piezometers, because piezometers typically have a short screen section that allows for a *point* measurement of the hydraulic head at a particular depth. Nested piezometers (more than one at approximately the same location with different screen depths) allow for vertical gradients to be measured, while piezometers screened at the same depth but spaced apart can be used to estimate horizontal flow in the groundwater system. Nested piezometers can also be arranged along a cross section, as illustrated in Exercise 1.

The most ideal arrangement uses a network of nested piezometers that are spaced apart laterally to allow for hydraulic heads to be measured in three dimensions. By contouring the hydraulic heads, a flow net can be generated (Poeter & Hsieh, 2020), which will aid in identifying recharge and discharge areas. To obtain estimates of recharge or discharge (as a flux), Darcy's law is used, which requires an estimate of the saturated hydraulic conductivity. To obtain a volumetric flow, the flux needs to be multiplied by the cross-sectional area through which the groundwater flows. Of course, groundwater systems are oftentimes heterogeneous and anisotropic, which can significantly alter the flow pattern (Poeter & Hsieh, 2020).

Recharge to confined aquifers can also be estimated using the hydraulic gradient between either an overlying unconfined aquifer and a confined aquifer, or between two confined aquifers. In this case, the vertical hydraulic conductivity of the confining unit is used to calculate the flow. An opportunity to calculate the recharge rate to a confined aquifer from an overlying layer is provided by Exercise 10↴.

Finally, discharge of groundwater as a spring can be measured directly by timing how much water issues from the spring outlet over a period. In fact, a spring hydrograph can be plotted to show how the discharge changes over time.

Methods based *on surface water data* can be used to estimate recharge and discharge. A water balance can be calculated for a stream reach, as in Equation (23), modified slightly from Healy (2010). The balance is calculated for a given period with the volumetric rate for each component over that period. The sign for evaporation is negative because a positive value is a loss from the reach. The sign is also negative for ΔS because a positive value is a rise in water level of the stream which is a decrease in the downstream outflow.

$$Q_D = Q_U + P - E - \Delta S + Q_{OLF} + Q_{IF} + Q_{Trib} + Q_{Seep} \quad (23)$$

where:

Q_D = stream discharge at the downstream end of a stream reach (L^3T^{-1})

Q_U = stream discharge at the upstream end of a stream reach (L^3T^{-1})

P = precipitation falling on a stream reach (L^3T^{-1})

E = evaporation from a stream reach (L^3T^{-1})

ΔS = change in storage in a stream reach (L^3T^{-1})

Q_{OLF} = overland flow into a stream reach (L^3T^{-1})

Q_{IF} = interflow into a stream reach (subsection 2.7) (L^3T^{-1})

Q_{Trib} = tributary flow into a stream reach (negative for diversions from the reach) (L^3T^{-1})

Q_{Seep} = groundwater inflow into a stream reach (negative for loss from the stream to the groundwater) (L^3T^{-1})

As noted by Healy (2010), measurement times are often selected such that P, Q_{OLF}, and Q_{IF} are zero, and the terms E and ΔS are generally small for naturally flowing streams. Therefore, Equation (23) reduces to Equation (24).

$$Q_D = Q_U + Q_{Trib} + Q_{Seep} \tag{24}$$

Measurements of the streamflow are made upstream, downstream, and in at the entry of any contributing tributaries, and an estimate of Q_{Seep} is calculated. Q_{Seep} can be positive, meaning that the stream reach is gaining (groundwater contribution to baseflow). Not only does the magnitude of Q_{Seep} correspond with a groundwater discharge estimate, but, if there is a well-defined catchment area for the stream, then an estimate of diffuse recharge can be made. However, estimates of recharge may be significantly lower than actual recharge rates due to the partitioning of recharge between multiple groundwater sinks (e.g., ET from riparian vegetation, subsurface transfer to adjacent aquifers). Q_{Seep} can be negative, meaning the stream reach is losing water and recharging the groundwater system. In this case, the loss of water from the stream contributes to focused recharge along the length of the reach.

Measurements should be made on different stream reaches, because some reaches may be gaining and some losing (Woessner, 2020). As well, whether a reach is gaining or losing may change at various timescales. Seepage through the streambed can be measured directly using nested instream piezometers or seepage meters. Darcy's law is used to calculate the vertical flux through the streambed sediment using the vertical hydraulic gradient and an estimate of the hydraulic conductivity of the streambed sediment (i.e., the same approach used for Exercise 7). Seepage meters can be used to measure the seepage rate (through the streambed in either direction). A seepage meter consists of an open-bottom chamber (e.g., the bottom half of a plastic or steel drum) that is inserted a few

centimeters into the streambed sediment, leaving no air space in the chamber (subsection 5.7 in Woessner, 2020↗). A plastic bag connected to tubing is inserted into the top of the chamber. If the stream is gaining at the location of the seepage meter, the bag will fill with water. The volume of water accumulated in the bag over time is equal to the volumetric seepage rate for the area of the bottom of the chamber. To obtain the flux, the volumetric seepage rate is divided by the cross-sectional area of the chamber. If seepage measurements are made at different locations, the average flux can be multiplied by the area of the streambed in the reach to obtain a total seepage rate.

Woessner (2020) briefly describes the use of stream hydrograph separation techniques to estimate the baseflow contribution to surface waters—hence, the groundwater discharge. In principle, at a catchment scale, assuming streams are gaining and there is no cross-catchment groundwater flow (Figure 5), the total baseflow may be used to estimate the groundwater recharge to the catchment. As noted by Scanlon and others (2002), bank storage may complicate the hydrograph separation analysis, because water discharging from bank storage is generally derived from short-term fluctuations in surface water flow and not from areal aquifer recharge and could result in overestimation of recharge. Various methods, including chemical and isotopic tracers, digital filtering (Nathan & McMahon, 1990), and recession curve displacement (Rorabough, 1964), can be used for hydrograph separation (Healy, 2010; Woessner, 2020). The R package grwat↗ provides various filters to separate baseflow and quickflow.

Various *chemical and isotopic methods* can be used to estimate recharge and discharge. They provide both qualitative and quantitative estimates of recharge, identify sources of recharge and groundwater discharge areas, and aid in estimating groundwater velocities and travel times. Collectively, these methods are often referred to as *tracer methods* (Healy, 2010; Scanlon et al., 2002). Here they are categorized as the chloride mass balance (CMB) method, methods based on the chemical composition, methods based on the stable isotope composition, and age dating methods. Cook and Brunner (2025) describe the CMB method in detail. Essentially, the method is premised on the fact that as rainfall evaporates, salt becomes concentrated in the remaining water. Thus, if the concentration of salt (dissolved chloride, Cl, is used as the indicator) in the precipitation is known, and no other sources of Cl are present, the evapotranspiration rate can be calculated by measuring the water salinity. Assuming rainfall is the only source of Cl and there is no runoff that would remove some Cl from the groundwater system, the recharge (R) is as in Equation (25).

$$R = \frac{C_P P}{C_R} \tag{25}$$

where:

C_P = concentration of Cl in the precipitation averaged over time (ML^{-3})

P = precipitation averaged over time (L)

C_R = Cl concentration in the recharge measured either near the base of the unsaturated zone where Cl concentrations tend to be stable if the water table is deep or just below the water table in the saturated zone (ML^{-3})

Importantly, there should be no other sources of Cl—for example, from mineral dissolution or fertilizers or road salt (used for deicing in cold climates) in the soil or the aquifer. Chloride is generally a conservative ion, meaning that it rarely reacts with other ions. For this reason, Cl is useful as a tracer, as is bromide (Br). Whether introduced naturally into the subsurface (i.e., via precipitation), accidentally (i.e., by the application of road salt), or on purpose (i.e., for a tracer experiment), the concentration with depth can be used to estimate the vertical groundwater velocity (Cook, 2020; Cook & Brunner, 2025).

The *chemical composition of groundwater* can aid in identifying recharge and discharge areas and give some indication of the relative age of the groundwater. Many factors influence the chemical composition of groundwater as it flows from recharge to discharge areas (Appelo & Postma, 2005). Groundwater in recharge areas typically has low total dissolved solids (TDS) concentration and, consequently, low electrical conductivity (EC). Groundwater in recharge areas often have a calcium-bicarbonate ($Ca\text{-}HCO_3$) water type but can evolve to a different chemical composition depending on the type of geological formations the groundwater flows through. Therefore, understanding the hydrogeology is important for interpreting the chemistry. The chemical composition of groundwater is often distinct from surface water, with surface water typically having low TDS concentrations and low EC. Therefore, groundwater discharge areas (particularly focused discharge areas) can often be detected by an increase in EC, and by temperature anomalies (a discussion on heat tracer methods follows).

Water chemistry and temperature measurements derived from seepage meters and instream piezometers can be used to identify areas of focused groundwater discharge in surface water bodies. The *stable isotope composition of groundwater*, characterized by the ratios of the oxygen-18 to oxygen-16 (expressed as $\delta^{18}O$ in units of per mil ‰) and hydrogen-2 to hydrogen-1 (δ^2H) in water, can be useful for determining recharge processes (Cook & Brunner, 2025). For example, $\delta^{18}O$ and δ^2H concentrations are particularly useful for estimating the degree of evaporation prior to recharge, as well as recharge temperature and elevation, due to a process called *fractionation* (Clark & Fritz, 1997; Cook & Brunner, 2025).

Box 7 presents a case study in the Andes in Peru where a combination of water chemistry and stable isotopes of water are used to identify groundwater source areas from different elevations in a region with mountain block recharge (subsection 1.3 and Box 1 are relevant to this discussion). The concentrations of noble gases dissolved in water (e.g., helium (He), radon (Rn)) provide information on the temperature and pressure at the time of recharge, which can be used to infer seasonality of recharge, or recharge elevation in mountainous regions.

Some radioactive isotopes can be used for age dating; age is defined as the time since water entered the saturated zone. The concentrations of the *historical* radionuclides, hydrogen-3 (^{3}H or tritium) and chlorine-36 (^{36}Cl), were elevated in Earth's atmosphere during the thermonuclear bomb testing in the 1950s and 1960s, which resulted in the precipitation of that period having elevated concentrations. Therefore, precipitation that entered the groundwater system was *tagged*, and it has been possible to track the movement of this *bomb* water and estimate recharge rates (Clark & Fritz, 1997).

Importantly, radioactive elements have half-lives, meaning that they decay to half their concentration every half-life; ^{3}H, for example, has a half-life of 12.3 years. Today, there is essentially no bomb water left, but there is still some ^{3}H in the atmosphere that can be used to identify young versus old groundwater. Groundwater older than approximately 50 years has no ^{3}H remaining.

Chlorofluorocarbons (CFCs) and $^{3}H/^{3}He$ (Cook & Solomon, 1997) have largely replaced ^{3}H for age dating (Scanlon et al., 2002). Solomon and Gilmore (2024) explore the various methods for age dating young groundwater. Radiocarbon dating using carbon-14 (^{14}C) is employed for age dating older waters (Pearson & White, 1967). However, the method is complex due to dilution effects of dissolved inorganic and organic carbon introduced along the flow path, which results in an artificial aging of groundwater (Afsin et al., 2014; Clark & Fritz, 1997), and correction factors need to be determined in order to estimate the age of the water.

Heat tracer methods are based on temperature, an extremely robust parameter to measure accurately and at relatively low cost. Heat is also a natural tracer. For these reasons, heat tracer methods, which gained popularity in the 1960s, are used for a variety of groundwater-related investigations (Anderson, 2005), ranging from characterizing flow patterns in groundwater systems (Cartwright, 1974; Schneider, 1964; Smith & Chapman, 1983) to quantifying exchanges between surface water and groundwater (Constantz, 2008; Lapham, 1989; Stonestrom & Constantz, 2003).

The utility of heat as a groundwater tracer was perhaps first recognized by Slichter (1905), who identified relatively high groundwater temperatures due to induced infiltration from a pond. Later, building on early work by Bredehoeft and Papadopulos (1965) and Stallman (1965), temperature profiles (or borehole temperature logs, in which temperature measurements are made at fixed intervals down a borehole) were used to estimate groundwater recharge and discharge rates in basins (e.g., Cartwright, 1974; Sorey, 1971; Taniguchi 1993, 1994) and identify fracture locations in open boreholes (Drury, 1990).

Today, heat tracer methods are commonly used in stream settings to quantify exchanges with groundwater. Approaches make use of the large, dynamic temperature oscillations (daily and seasonally) between the stream and underlying streambed (Constantz, 2008). Figure 38 illustrates the thermal and hydraulic responses for each of a

gaining stream (Figure 38a) and a losing stream (Figure 38b). The thermographs on the left show the daily variation in temperature measured at the streambed surface and 1 m deeper into the streambed sediments. A stream hydrograph is shown on the right of each. Each day, the stream surface heats up and then cools down due to variations in incoming solar radiation. Constantz (2008) offers a detailed discussion of the partitioning of this heat energy in the stream system. Some of the heat energy moves vertically downward through the water column and warms the streambed. In the gaining stream (Figure 38a), the vertical hydraulic gradient induces upward flow as evidenced by a hydraulic head that is higher than the stream stage. The temperature sensor at the streambed has a large diurnal variation in water temperature compared to that of the streambed sediment because the stream is gaining groundwater. Groundwater has a relatively stable temperature and so it moderates the streambed temperature, causing a lower amplitude signal. In the losing stream (Figure 38b), the vertical hydraulic gradient inducing downward flow carries heat downward through the sediments. This is *advective transport of heat* by the moving water. Therefore, the streambed sediment has a higher amplitude signal. Also, the streambed temperature is not moderated by any inflowing groundwater, so it, too, has a higher amplitude signal.

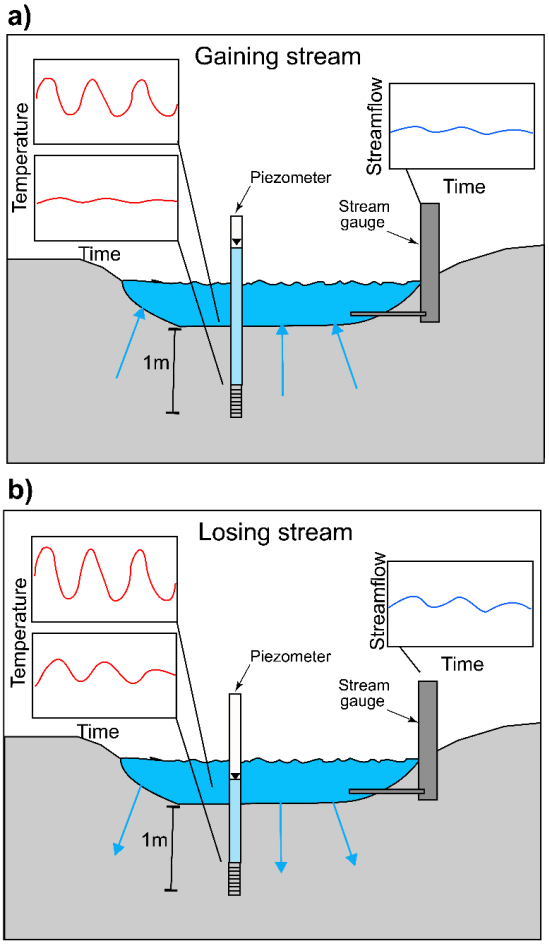

Figure 38 - Thermal and hydraulic responses in the streambed for a) a gaining stream and b) a losing stream (modified from Constantz, 2008).

Temperature can be measured using a variety of devices, depending on the application. Borehole logging employs a temperature sonde that is lowered down a well using a winch. Instream applications can involve point measurements made using individual temperature sensors such as tiny (3 cm *x* 4 cm) data loggers (e.g., Onset HOBO TidbiT loggers or Thermochron iButton loggers). Temperature over a larger area (e.g., at the streambed surface) can be measured using high-resolution fiber-optic, distributed, temperature sensors or using remote sensing, as discussed later.

These methods are increasingly being used to measure attributes of the earth's surface that are relevant to estimating recharge, discharge, and storage change. Space-based interferometric synthetic aperture radar (InSAR) observations provide near-global coverage of proxies for soil moisture. While InSAR has not been used extensively to date for soil moisture monitoring, the method is promising. Scott and others (2017) analyzed a 1.5-year-long InSAR time series spanning the March 2015 extreme precipitation event in the hyper-arid Atacama Desert of Chile. They demonstrated the use of InSAR for capturing the time evolution of soil moisture storage over different surface types. Changes in groundwater storage in the saturated zone can be measured at a regional scale using gravity anomaly data from the Gravity Recovery and Climate Experiment (GRACE), as described in Box 8↴. Water temperature can be remotely detected by a sensor that receives thermal radiation (in the thermal infrared or TIR range of 0.7-1000 μm) that is emitted from a surface, depending on the emissivity of the surface (Anderson & Wilson, 1984). The resulting TIR images or thermograms provide spatially distributed temperature measurements of the water surface—for example, the stream surface (Handcock et al., 2006), a groundwater seep (Rathay et al., 2018; Figure 31), or springs (Roeper et al., 2014).

In stream settings, the locations where groundwater is discharging can be identified. These areas offer thermal refugia (cooler in summer and warmer in winter relative to other areas along the stream) for fish (Hare et al., 2021). TIR sensors can be housed in portable cameras (e.g., FLIR cameras), mounted on drones or helicopters, or even on satellites (Landsat 8 and 9).

Lastly, vegetation can be mapped, and the distribution of a particular species or presence/absence of vegetation can be used to identify potential recharge or discharge areas. Vegetation differences can be observed on the ground by using aerial photographs and other remote sensing products such as the normalized difference vegetation index (NDVI). NDVI is a widely-used metric for quantifying the health and density of vegetation. It is calculated from spectrometric data obtained from satellites at two specific bands: red and near-infrared. NDVI identifies areas with comparatively higher photosynthetic activity relative to surrounding areas, particularly during the dry mid-summer months. For example, Upwanshi and others (2023) used NDVI as one criterion in a multicriteria decision analysis (MCA) method based on an Analytic Hierarchical Process (Saaty, 1980) to generate a groundwater potential map.

4.2 Seasonal Variations in Timing and Distribution of Recharge and Discharge

Climate is the primary driver for seasonal variations in groundwater level. Given that precipitation (subsection 2.3.2) and AET (subsection 2.4) vary seasonally, there are certain times of the year when recharge tends to occur, or at least when there is more recharge. If rainfall is high at a time of the year when the evapotranspiration demand is low (i.e., when the plants are not actively growing), then most recharge will occur at this time. In regions with a cold climate that experience significant snowfall, the most significant recharge occurs during spring melt.

In many arid and semi-arid areas, PET exceeds total precipitation on an annual basis. Such regions experience an annual precipitation deficit. However, this does not necessarily mean that there is no recharge. Recharge may occur only at certain times of the year when the evapotranspirative demand is lower than precipitation. Ultimately, the timing and magnitude of the water level response typically varies depending on antecedent conditions (e.g., how much moisture is held in the soil), evapotranspiration demand, soil and aquifer hydraulic properties, and the depth to the water table (Cuthbert, 2010).

The following subsections explore seasonal variations in regions with a cold continental climate, a temperate climate, and an arid or semi-arid climate (the Köppen-Geiger climate classification system↗ provides climate zone characteristics).

4.2.1 Cold Continental Climate

Seasonal variations of recharge and discharge in cold regions are largely controlled by freeze-thaw processes and the timing of snow and glacier melt. Figure 39 illustrates a conceptual model for the seasonal variation of diffuse recharge in a region with seasonal snow cover (northern latitude). During the winter months, the ground is frozen, and precipitation falls as snow. Streamflow is at a minimum. Water levels in the aquifer, however, may still be high because of recharge the fall and early winter of the previous year that occurs before the ground is frozen. These conditions remain until spring, when the ground thaws and meltwater from snow and/or spring rain infiltrate(s) the soil. Typically, streamflow increases at this time and may persist into the summer depending on the source of water. For example, snowpack or glaciers at high elevation melt late in the spring and, consequently, deliver water via streams to lower elevations well into the summer. In unconfined aquifers, this rise in the water table coincides with higher streamflow, but the peak groundwater level is often delayed with respect to peak level in the stream. Throughout most of Canada and other middle-to-high latitude countries, the summer season is warm, and evapotranspiration rates are high. Apart from contributions to streamflow from the occasional summer precipitation event, streamflow is generally low. These conditions result in a gradual decline in the water table, which persists into the fall. During the summer, there is a higher water demand for plant growth. This, combined with higher evaporative losses from the soil and surface water bodies, results in a declining

water table. The fall season generally brings somewhat wetter conditions, with consequent small increases in streamflow and rising water tables. In colder regions, fall precipitation may be in the form of snow and recharge may not take place until the snow melts.

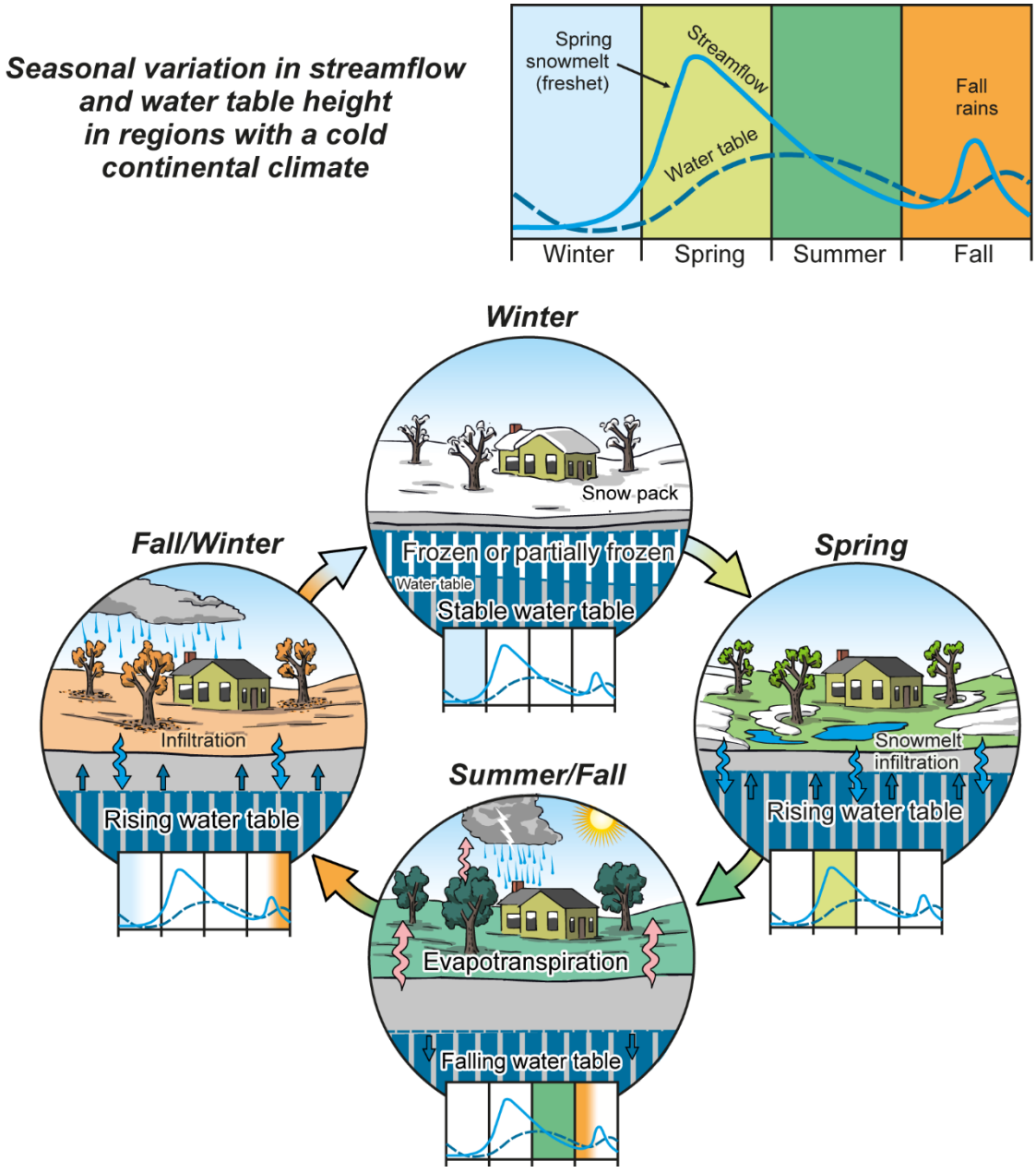

Figure 39 - Conceptual model for the seasonal variation of diffuse recharge in a region with seasonal snow cover typical of a cold continental climate.

4.2.2 Temperate Climate

Seasonal variations in recharge and discharge in regions with a temperate climate largely reflect the timing of precipitation, which primarily falls as rain. Box 9 illustrates a case study of how recharge and discharge areas on a small island (Gabriola Island in British Columbia, Canada) vary in space and time. As illustrated in Box 9, overland flow closely

matches precipitation; when rainfall is high in winter, overland flow is also high. The start of the increase in overland flow (September) coincides with the increase in precipitation. This increase continues until January, after which both precipitation and overland flow begin to decrease, reaching a low in July and August. Evapotranspiration is generally low from November to February and begins to increase in March. Evapotranspiration rises gradually through the summer and begins to decrease in August through to October. Recharge increases from October to January, when it reaches a pseudo-stable rate, before declining from April through to September. The recharge response matches the water-table dynamics, with the water table following the same seasonal trend. There is a lag between the increase in precipitation (and overland flow) and the increase in recharge and the water table. The increase in precipitation starts in September, while the recharge rate and water table do not begin to increase until November, representing an approximate 2-month lag. This lag is caused by the low vertical hydraulic conductivity of the vadose zone, which slows the vertical movement of the infiltrating water. Due to the low storage capacity of the bedrock, once the infiltrating water reaches the water table, the pore space quickly fills up and the water table rises rapidly.

4.2.3 Arid and Semi-Arid Climate

In regions with an arid or semi-arid climate, precipitation amounts are exceeded by potential evapotranspiration. Therefore, almost all of precipitation infiltrating to the surface soil layer is returned to the atmosphere by soil evaporation and plant root uptake, leaving little, if any, water for groundwater recharge. As a result, the magnitude of diffuse recharge is often negligible or a minute fraction of precipitation. Recharge potential is greater in those parts of the landscape that receive lateral inputs of water from surrounding areas by surface or subsurface runoff, in addition to vertical precipitation input. Therefore, groundwater recharge in these regions tends to be focused recharge in a small fraction of the landscape.

Mechanisms and locations of focused recharge vary depending on physiographic settings (Box 10↴). However, a common requirement seems to be a relatively short duration of lateral water input causing ponding, which allows effective percolation of infiltrated water to the water table before it is taken up by plant roots. For example, in some dry regions, the water table may be very deep and perennially disconnected from streams (Figure 40). During periods of heavy rainfall, stream channels fill with water and the water in the channel percolates downward, eventually contributing to recharge. This type of recharge is commonly observed in ephemeral streams called *wadis* in the Middle East and Africa (e.g., Subyani, 2004), as well as ephemeral/seasonal streams in many dry regions of the world (e.g., Izbicki et al., 2000; Villeneuve et al., 2015).

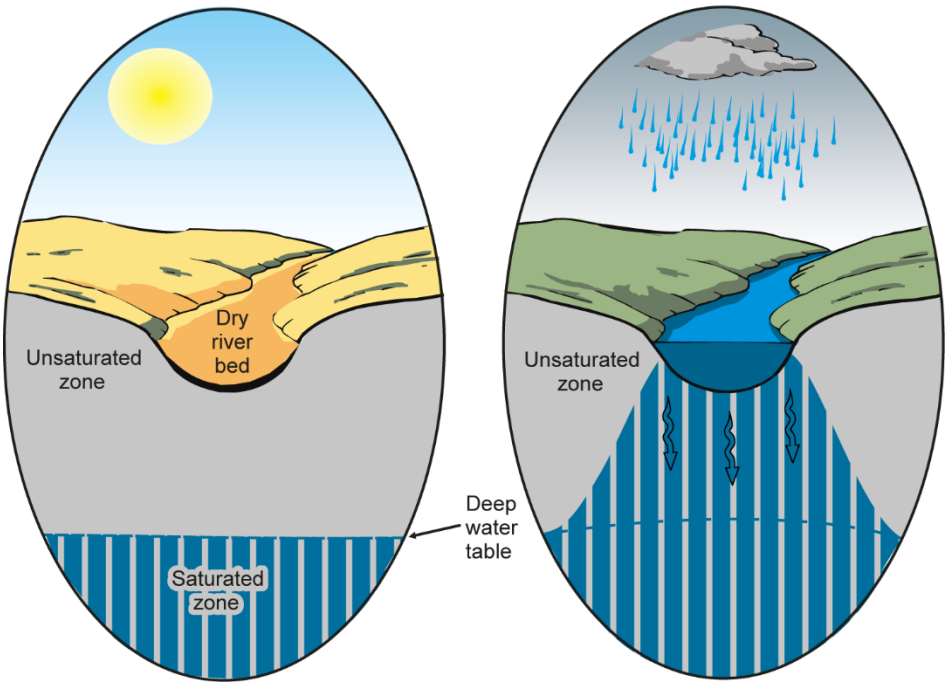

Figure 40 - Seasonality of focused recharge under an ephemeral/seasonal stream in a semi-arid or arid region that receives highly seasonal or episodic precipitation.

While the dominant recharge mechanism in arid and semi-arid regions is focused recharge, diffuse recharge can still dominate. For example, recharge to the Williston Basin (102,400 km^2) consists almost entirely of diffuse recharge, with a small amount of focused recharge through streambeds (Meixner et al., 2016). The climate in the Williston Basin is arid cold steppe, and the aquifer is dominantly sand and gravel. Average annual precipitation is 380 mm and annual PET is 1440 mm, so the basin is significantly water limited, yet diffuse recharge is 4.6 mm/year (97 percent) and focused recharge is 0.13 mm/year (3 percent).

4.3 Variability of Recharge and Discharge at Other Temporal Scales

4.3.1 Subdaily to Daily Variability

On short (hourly to daily) time scales, the water-table height varies, although these variations depend on the nature of the precipitation event(s), the depth to the water table, the permeability of the material, and the available storage. All other factors being equal, a deeper water table results in a delay in the response of water level. This is because it takes time for the infiltrating water to make its way down to the water table. High-permeability materials transmit water more readily than low-permeability materials and, consequently, the response is faster. The amount of available groundwater storage mediates the response. Materials with a high specific yield (Sy), such as coarse sands and gravels, have a much smaller overall change in water level following a recharge event. The pore space in high-specific-yield materials occupies a larger portion of the material as compared to low-specific-yield materials thus more water can be held in storage for a given change in water

table elevation, so the water table does not rise as much in high-specific-yield materials. Because of all these factors, some aquifers reflect rainfall events effectively, showing high-frequency variation, while others record long-term changes in water level accompanying seasonal or longer-term variations in precipitation. Fractured bedrock aquifers, with high permeability and low Sy values, can show distinct responses to recharge events. Figure 41 shows a groundwater-level hydrograph for an observation well in fractured sedimentary rock. The water table is relatively shallow (<1.8 m), so the water table responds quickly to rain events.

Importantly, the ability to measure the response in an observation well also depends on the diameter of the well because the rising water in the porous media has to flow into the well and fill a volume that has a 100% porosity, so the larger the well, the longer the time required to equilibrate to the water table elevation. To minimize the time lag between fluctuations of the water table and those in the observation well, the well diameter should be smaller in materials with lower permeability.

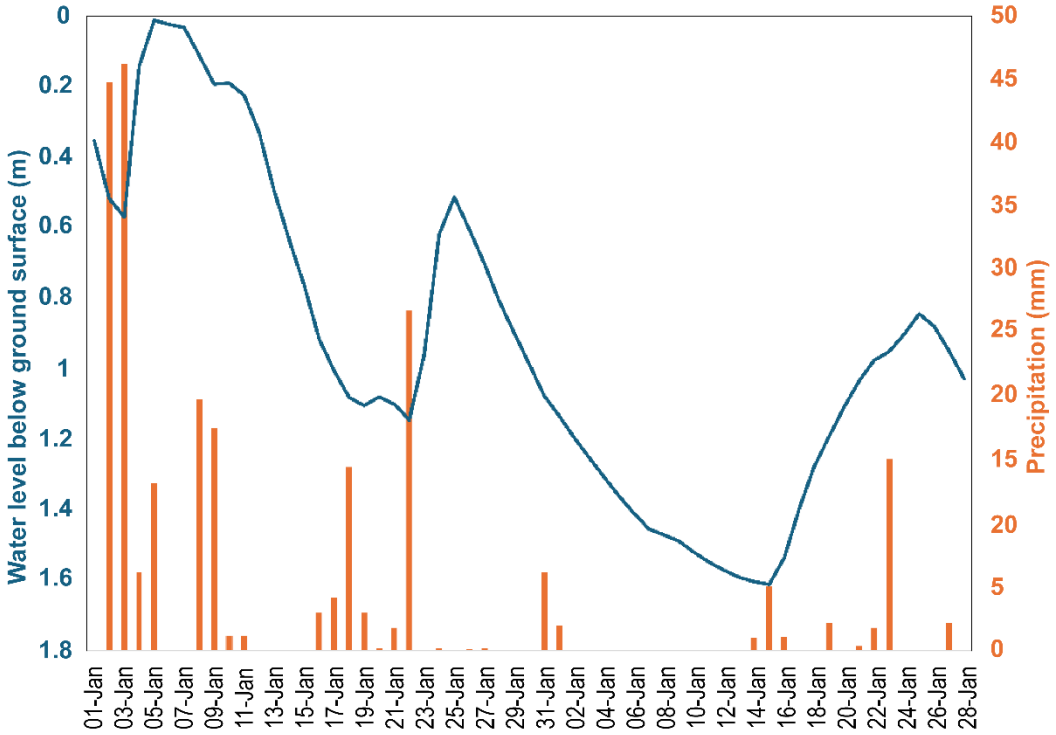

Figure 41 - Example of a well hydrograph (January 1, 2019 to February 28, 2019) for Observation Well 196 in Gabriola Island, British Columbia, Canada, showing the groundwater-level response (blue line) to rain events (orange bars). Groundwater level is expressed as depth in meters below ground surface (mbgs) (groundwater data from Province of British Columbia, 2024); precipitation data from Nanaimo City Yard Station ID 10253G0. The data are accessible via Environment and Climate Change Canada (2024)↗.

Precipitation intensity (subsection 2.3.2) is also an important factor controlling the groundwater-level response. Intense rain events are referred to as heavy rain events. There are few examples in the literature that demonstrate the response to varying precipitation intensity. Most studies appear to focus on either tropical regions or arid/semi-arid regions.

For example, Owor and others (2009) examined groundwater recharge from intense rainfall in the Upper Nile Basin in Uganda (tropical climate) and found that the magnitude of groundwater-recharge events is better correlated to heavy rainfall events, defined as those exceeding 10 mm/day, than total rainfall. Taylor and others (2013) examined statistically extreme months and seasons of rainfall in Tanzania (semi-arid, tropical climate) and found that the increase in recharge from anomalously intense rainfall can be attributed to high rates of evapotranspiration that need to be surpassed for potential recharge to reach the water table in deeply weathered granite. Rathay and others (2018) examined the groundwater-level hydrographs for 14 observation wells in the Gulf Islands, British Columbia, Canada (temperate climate). Of the 14 wells, only three showed pronounced responses to heavy rain events. A detailed analysis at one well suggested that rises in groundwater level were better correlated to all rain events than exclusively heavy rain during summer and that the strength of the correlation to all rain events decreased as the rainfall intensity increased. Nott (2024) analyzed the groundwater-level response in southwest British Columbia (temperate climate) to intense precipitation associated with atmospheric river (AR) events, which are a type of extreme precipitation event (Box 11↴). Nott found that regardless of whether ARs occurred during dry periods or wet periods, the average monthly groundwater levels increased as the AR fraction of monthly precipitation increased.

Intense rain events are a natural phenomenon in many regions of the world. In arid and semi-arid regions, these intense rain events are the only major source of recharge to aquifers. However, the soil infiltration capacity may be exceeded during intense rain events, resulting in more overland flow and less infiltration (Dingman, 2002). If the overland-flow water cannot be adequately conveyed away, flooding can occur. Whether or not the infiltration capacity is exceeded depends on the water-input rate, saturated hydraulic conductivity, soil water-retention properties and moisture content of the ground surface layer, and duration of rainfall (Dingman, 2002). Measuring the groundwater-level rise in response to rain events can be challenging due to natural fluctuations in atmospheric pressure and to air entrapment (Box 12↴).

Understanding how recharge responds to intense precipitation events is particularly important considering future climate change. According to the Intergovernmental Panel on Climate Change (IPCC) 6th Assessment Report (AR6), heavy precipitation events have increased in central North America and northern Europe (with medium and high confidence, respectively). Moreover, it is very likely that heavy precipitation events will intensify and become more frequent in most regions of the world with additional global warming. At the global scale, extreme daily precipitation events are projected to intensify by about 7 percent for each 1 °C of global warming (high confidence; IPCC, 2021).

In groundwater discharge areas, such as the riparian zone next to lakes and streams, the water table is generally near the land surface or at least within the reach of phreatophyte roots. Phreatophytes are deep-rooted plants that extract water directly from the saturated zone (Figure 42). Examples include trees such as cottonwood, willow, elm, and Russian olive, and smaller plants such as tamarisk and alfalfa. The roots of phreatophytes accommodate low oxygen concentrations in the aquifer and can exploit a source that is more generous and steadier than that supplied by ordinary soil moisture. This helps them survive in dryland areas where soil moisture is scarce (Wang et al., 2023). Transpiration of groundwater commonly results in a drawdown of the water table, much like the effect of a pumped well (i.e., a cone of depression as shown by the dotted line surrounding the plant roots in Figure 42). Phreatophytes are known to deplete baseflow in streams, and at times water levels in lakes, via high transpiration rates when they grow near water bodies.

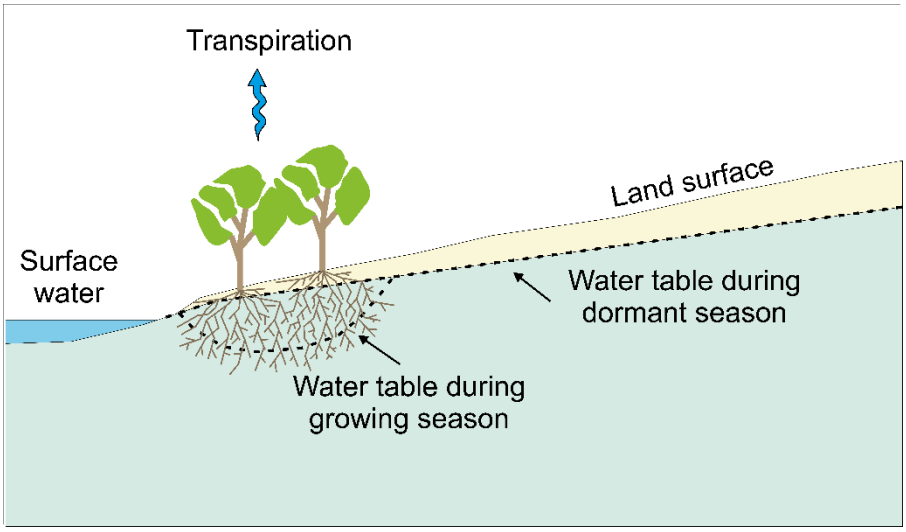

Figure 42 - Water-table decline during the growing season due to phreatophyte consumption near a stream.

White (1932) observed regular diurnal water-table fluctuations during the growing season in response to plant transpiration and devised an empirical method of estimating evaporative loss based on a water-table hydrograph. Figure 43 (reproduced from Meyboom, 1967) illustrates a groundwater-level hydrograph acquired from a monitoring well near a Manitoba maple tree, a type of phreatophyte found in southern Saskatchewan, Canada. The difference in water-level elevation between the beginning and the end of the graph is part of the summer decline of the water table. During the night, the leaf stomata are closed and water losses from the plant are at a minimum. Transpiration is assumed to be practically zero during this time. To determine the rate of recharge, a tangent to the rising limb of the groundwater-level curve is drawn for a 4-hour period (typically midnight to 4 in the morning). This is shown as 4r on Figure 43 between the 6th and 7th of July. The slope is the rate of recharge for that period. If this rate continued throughout a period of 24 hours with no transpiration (or other losses), the water table would rise by an amount equivalent to the distance marked 24r. In the morning, with increasing light intensity, the

stomata open and photosynthesis begins. Transpiration is occurring and, instead of rising, the water table drops a distance marked as s during the day. Consequently, the total transpiration loss is the sum of recharge water plus the transpired water, which is indicated by the sum of the lengths (24r+s) multiplied by S_Y as shown in Equation (26).

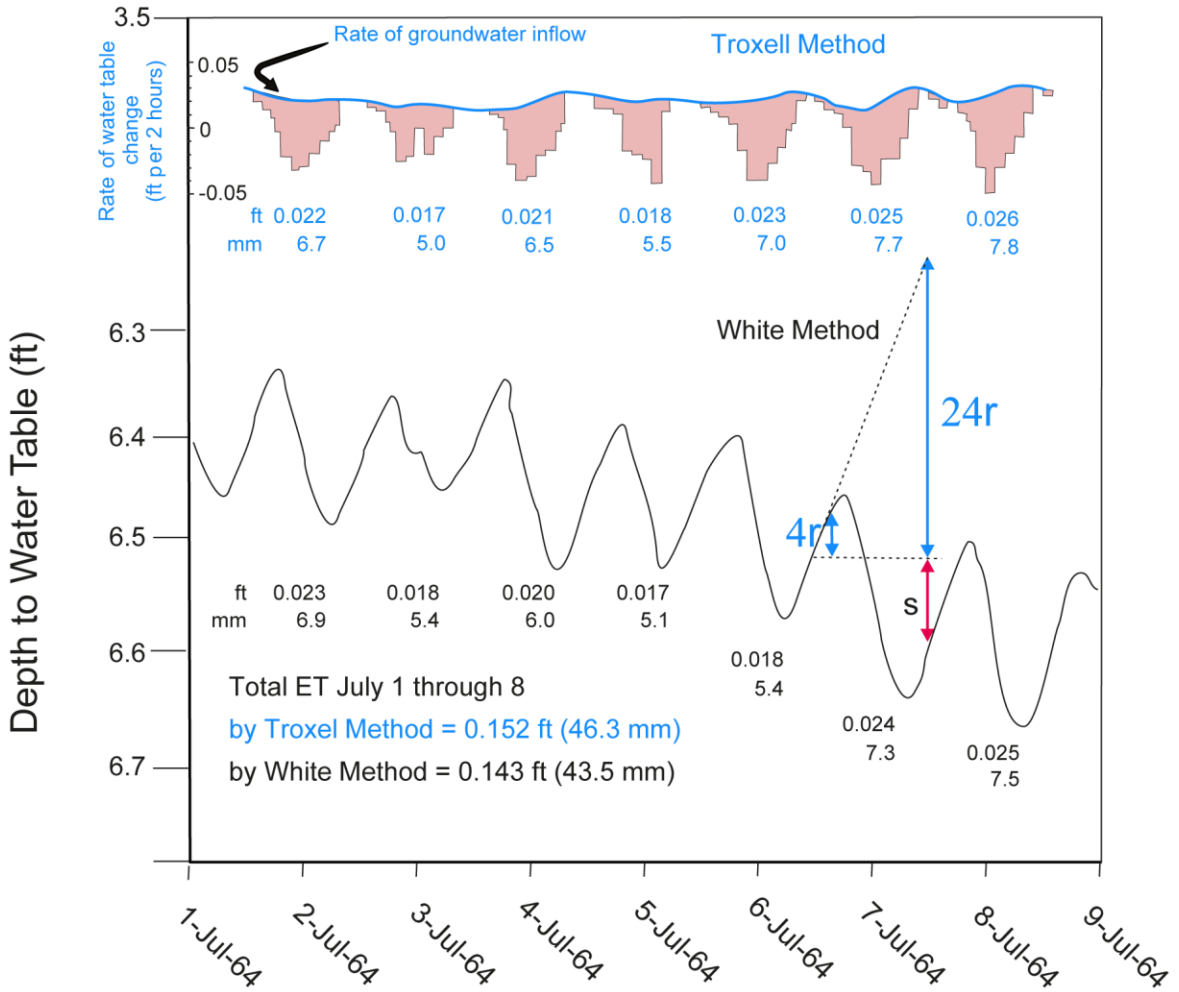

Figure 43 - A water-table hydrograph in the Assiniboine River basin is displayed as a black line. Troxell's (1936) method for estimating evapotranspiration is illustrated above White's (1932) method. Values under each graph represent daily ET (in ft and mm) calculated by each method. Red bars represent Troxell's estimated ET for 2-hour periods (modified from Meyboom's 1967 presentation for observation well No. 3 which is near a Manitoba maple tree by the Arm River near Chamberlain, Saskatchewan, Canada).

$$ET_g = S_Y\,(24r + s) \tag{26}$$

where:

ET_g = daily evapotranspiration from the groundwater (L)

S_Y = specific yield (dimensionless)

r = average recovery of the groundwater level (L) over 24 hours

s = net change in groundwater level over 24 hours, with a positive value for a rise in groundwater and a negative for a decline (L)

As an example, ET_g for the 24-hour period from July 6th to 7th is calculated as follows.

$$ET_g = 0.0825\ (0.24\ \text{ft} + 0.07\ \text{ft}) = 0.026\ \text{ft}$$

The Troxell (1936) method is based on the concept that the groundwater level hydrograph is combines the groundwater inflow and the transpiration. Troxell stated, "*It is impossible by this method to determine the actual rates of recharge during the transpiration period. However, the rates for this period can be sketched in with sufficient accuracy to give hourly distribution of the transpiration losses*" (1936, p. 501). Accordingly, first the rate of groundwater inflow as determined by the White (1932) method is plotted to define the rate of groundwater inflow (i.e., the water that is either drawn upward or in from storage by the plants) as shown in the upper blue line of Figure 43. This is a positive contribution to the budget. Then the first derivative of the groundwater hydrograph using 2-hour increments is plotted as the red bars extending down from the inflow curve to represent water lost by transpiration, which is a negative contribution to the budget. The values at the bottom of each red bar (some are positive and some negative) are summed to obtain the net evapotranspiration for the 24-hour period which is displayed as a number below the curve for each day in Figure 43. Values of daily ET noted on Figure 43 are uncorrected for readily available S_Y, which was estimated by Meyboom (1967 as shown in his Table 1) to be 0.0825 for sandy loam. *Readily available specific yield* is 50 percent of the true or ultimate specific yield (Meyboom, 1967).

There are four main assumptions underlying both the White and the Troxell methods: 1) the decline in groundwater level is caused by plant transpiration; 2) plant transpiration is negligible during the night so the tangent is drawn at 4:00 a.m.; 3) the average rate of groundwater-level recovery at 4:00 a.m. is equal to the average rate of groundwater-level recovery for that 24-hour period; and 4) a representative value of specific yield is available.

The methods presented above have been widely used to estimate the rate of groundwater consumption by plants in arid regions. The greatest uncertainty comes from the S_Y value, which White (1932) noted is exceedingly difficult to determine, as it differs from the traditional definition of S_Y under adequate drainage conditions. Meyboom (1965) introduced the concept of the *readily available specific yield*, which is empirically taken as 50 percent of S_Y, to differentiate it from the traditional yield.

Meyboom (1966a, 1967) undertook a groundwater-flow-system study in south central Saskatchewan, Canada, within the Assiniboine River basin. The region is dominated by rolling topography, with groundwater flowing to low-lying areas where it may or may not discharge onto the surface. Groundwater is consumed in the low-lying area by patches of phreatophytes, such as willows, that grow in rings around small circular depressions about 30 to 150 m in diameter (see Box 13↴). Meyboom measured daily fluctuations in groundwater level of over one meter each day in response to the opening and closing of

leaf stomata. Meyboom (1967) used White's (1932) method and Troxell's (1936) graphical method to estimate ET as illustrated in Figure 43.

4.3.2 Variability Over Longer Periods

The magnitude of groundwater levels also varies over long periods (from interannual to paleo time scales). At an interannual time scale, variations depend on the climatic conditions. Some years are wetter than others, and some are colder. Generally, the long-term average water level is dynamically stable as illustrated for observation well 357 in Figure 44, even though a long term trend might occur due to climate change or over pumping of the system as illustrated for observation well 359 in Figure 44.

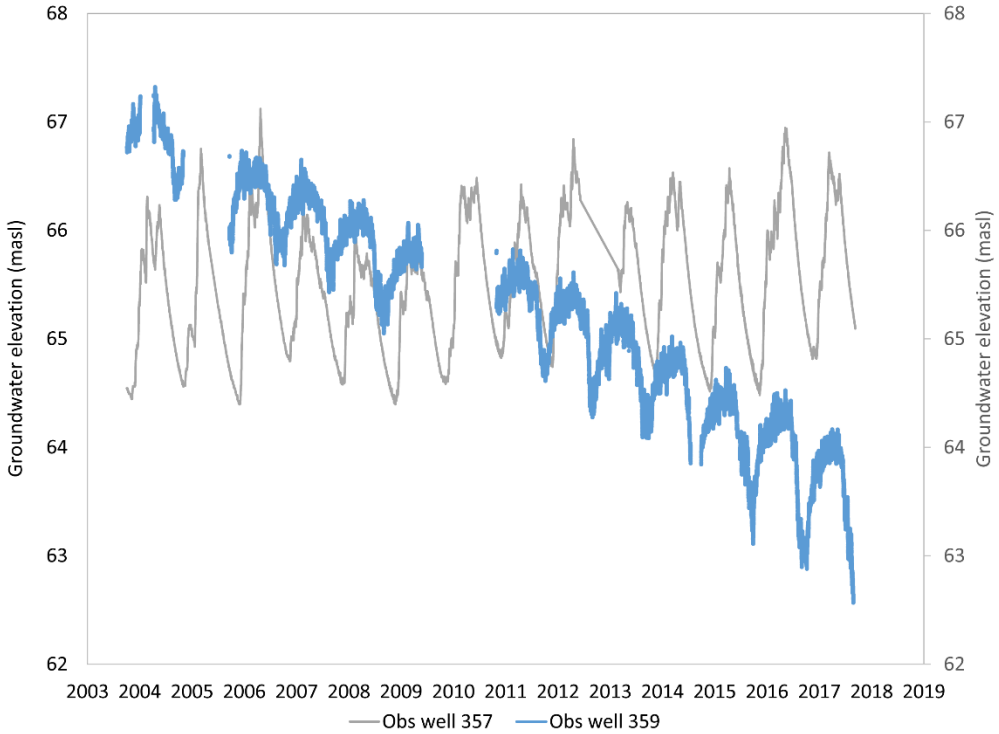

Figure 44 - Groundwater hydrographs for two Province of British Columbia observation wells located in the south coast region near Vancouver, Canada. Water levels have been recorded since 2004. Data are shown from October 1, 2014, to July 26, 2018. Observation Well 357 is in a shallow unconfined aquifer that is screened from 17 to 19 m and exhibits a dynamically stable situation. Observation Well 359 is in a shallow confined aquifer, screened from 39 to 42 m, and shows a decreasing trend in groundwater level.

If there is some significant change in the aquifer system causing a long-term decline (or increase) in recharge, perhaps due to introduction (or cessation) of pumping, then a trend in groundwater level may be observed. Trends are an indicator of a shift in the system, as illustrated for observation well 359 in Figure 44. Determining the cause of the trend requires careful analysis. Groundwater pumping is an obvious reason for groundwater levels in an aquifer to have a declining trend. But interannual variability in precipitation (e.g., multi-year droughts) can also be a cause. Statistical analysis of trends in time series data, such as groundwater levels, normally requires a suitably long period of record (e.g., 30 years) to conclude the trend is statistically significant.

Groundwater levels can also vary due to cyclical changes of Earth's climate. Those related to major changes in the orbit of the earth around the sun have a periodicity of tens of thousands of years, while those related to one orbit of Earth around the sun have an annual pattern associated with the seasons. Superimposed on these are *climate oscillations* (or climate cycles). These are less regular than the cycles mentioned above and have periods from a few months up to several decades. Climate oscillations include, for example, the El Niño Southern Oscillation (ENSO), Pacific Decadal Oscillation (PDO), Madden-Julian Oscillation (MJO), the Atlantic Multidecadal Oscillation (AMO), and the Pacific North American (PNA) pattern. The website titled Earth's Climate Oscillations↗ provides a detailed discussion of climate oscillations, also known as climate cycles and teleconnection patterns. Global weather patterns are highly influenced by the combined variations in air pressure, ocean temperature, and wind direction, which affect regional air temperature and precipitation patterns. Climate oscillations are commonly described as having positive (warm), neutral, or negative (cool) phases (also called states). For example, during a positive phase of the ENSO, termed an El Niño, ocean temperatures are warmer than typical in the tropical Pacific Ocean, disrupting the wind and rainfall patterns across the region. These changes bring a cascade of global side effects. Climate oscillations are recurring and quasiperiodic (not perfectly periodic). ENSO, for example, cycles every 2 to 7 years, while the AMO cycles about every 55 to 70 years. Climate oscillations also have associated climate indices↗. A climate index is a simple diagnostic quantity used to characterize the state of the oscillation. The indices are calculated using observed data (e.g., sea surface temperature) and are reported monthly as anomalies. The Oceanic Niño Index (ONI) is the rolling 3-month temperature anomaly relative to a 30-year moving average of normal sea surface temperatures in the central Pacific's Niño 3.4 region (Figure 45). It is used by the USA's National Oceanic and Atmospheric Administration (NOAA) as the primary indicator for monitoring the ocean's contribution to ENSO. NOAA considers El Niño conditions to be present in the ocean when the ONI is +0.5 or higher, meaning sea surface waters in the east-central tropical Pacific are 0.5 °C, or more, warmer than average. Oceanic La Niña conditions exist when the ONI is -0.5 or lower, indicating the region is 0.5 °C, or more, cooler than average.

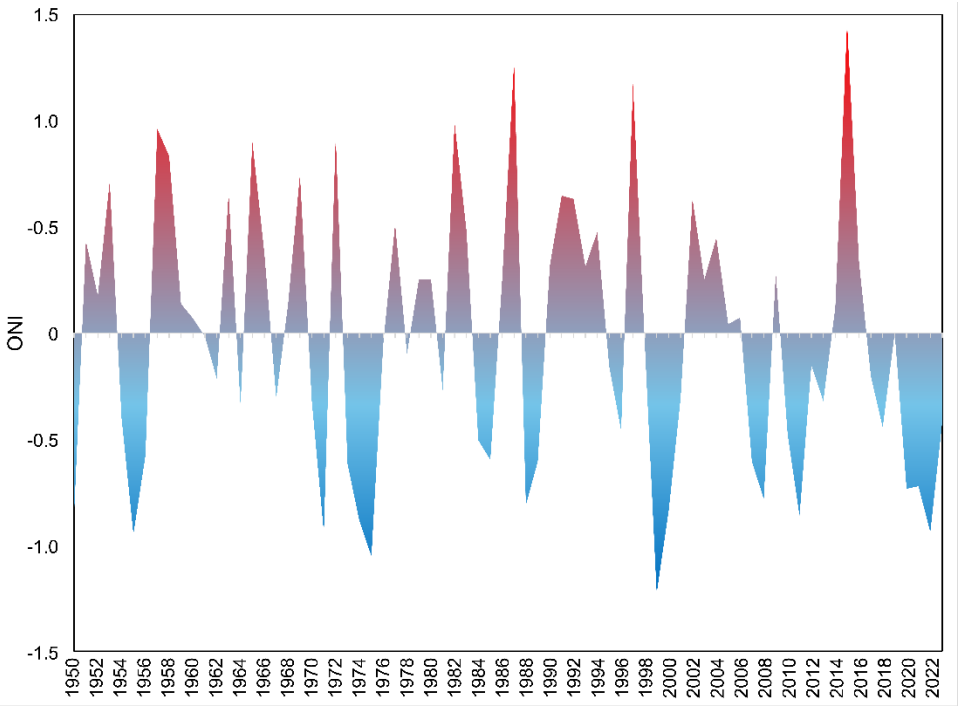

Figure 45 - The Oceanic Niño Index ONI from the year 1950 to 2022 (Data from National Oceanic and Atmospheric Administration↗). The ONI is the rolling 3-month temperature anomaly relative to a 30-year moving average of normal sea surface temperatures in the central Pacific's Niño 3.4 region.

The links between groundwater levels and specific climate indices have been investigated in many countries—for example, Canada (Tremblay et al., 2011), the United States (Gurdak et al., 2009; Hanson et al., 2006); the United Kingdom (Holman et al., 2009), and Spain (Luque-Espinar et al., 2008). In southwest British Columbia, Canada, Fleming and Quilty (2006) established that groundwater levels tend to be higher during La Niña years and lower during El Niño years, with the strongest correlation observed in the winter and spring. This aligns with general conclusions that El Niño is associated with less precipitation and La Niña with more precipitation in southwest British Columbia, Canada, and the Pacific Northwest of the USA (Shabbar et al., 1997). Graham and others (2014) showed that monitoring wells display unique, nonuniform cyclical variability in nitrate concentrations that appears to correspond with seasonal (1-year) cycles in precipitation as well as longer-period cycles (5 years), possibly due to ENSO or the PNA pattern. These precipitation cycles appear to influence nitrate concentrations in groundwater by approximately ± 30 percent of the maximum allowable concentration (10 mg/L NO_3–N). Not all wells showed direct correlation due to complex local-scale factors that influence nitrate leaching, including spatially and temporally variable nutrient management practices and soil/crop nitrogen dynamics (anthropogenic and agronomic factors). Across the Canadian Prairies, Perez-Valdivia and others (2012) found significant variability in groundwater levels at frequencies of 2 to 7 and 7 to 10 years that negatively correlated with the ENSO index, while strong relationships existed with the PDO between the 18 and 22 year frequency.

Groundwater levels have also changed over long periods due to natural climate change, alternations to the natural environment, and many other anthropogenic factors such as pumping, land use, and land cover change. Global rainfall patterns have changed over the last 10,000 years, since the Late Pleistocene. The presently hyper-arid regions in the Northern African region (e.g., the Sahara) received significant rainfall in the past (de Menocal et al., 2000; Lézine et al., 2011), and that rainfall provided paleo recharge to many of the large aquifers that today have large groundwater reserves. Glacial meltwater also recharged the Canadian Shield aquifers (Clark et al., 2000). Modern-day global warming occurring primarily due to the burning of fossil fuels is altering temperature and precipitation patterns globally, and ultimately affects groundwater systems. Green and others (2011), Taylor and others (2013), as well as Amanambu and others (2020) provide thorough reviews on the topic of climate change impacts on groundwater systems.

4.4 Dynamic Interactions between Streams and Aquifers

The focus of this section is on dynamic interactions between streams and aquifers. The nature of these interactions can be extended to other surface water bodies. The focus here is on interactions with unconfined aquifers. Similar interactions occur with confined aquifers if the confining layer is thin or if the confined aquifer intersects the stream.

As discussed in subsection 3.1.1, streams are not only groundwater discharge environments; two-way exchanges can also occur. These exchanges, commonly referred to as groundwater–surface water interactions, can occur over a wide range of spatial and temporal scales. The degree to which exchange occurs depends on several factors, specifically the magnitude of the difference between the water-table height near the stream and the stream stage and the hydraulic properties of the aquifer and streambed materials. Collectively, these factors affect the *hydraulic connectivity* between aquifers and streams.

Allen and others (2010) proposed a framework for evaluating the responses of aquifers and local streams that intersect the aquifer (Figure 46). They classified observation wells according to end-member *aquifer–stream system types* based on the dominant *response mechanism*.

- **Recharge-driven**: In these systems, groundwater is recharged solely by precipitation (diffuse recharge) and groundwater discharges to streams throughout the year. The water levels in the aquifer are predominantly higher than the stream stage, so groundwater drains to the stream at lower elevation. (Figure 46a).
- **Streamflow-driven**: In these systems, groundwater flow to and from the stream is bi-directional and varies seasonally depending on stream stage. These aquifer–stream systems are commonly found in association with major streams/rivers (Figure 46b).

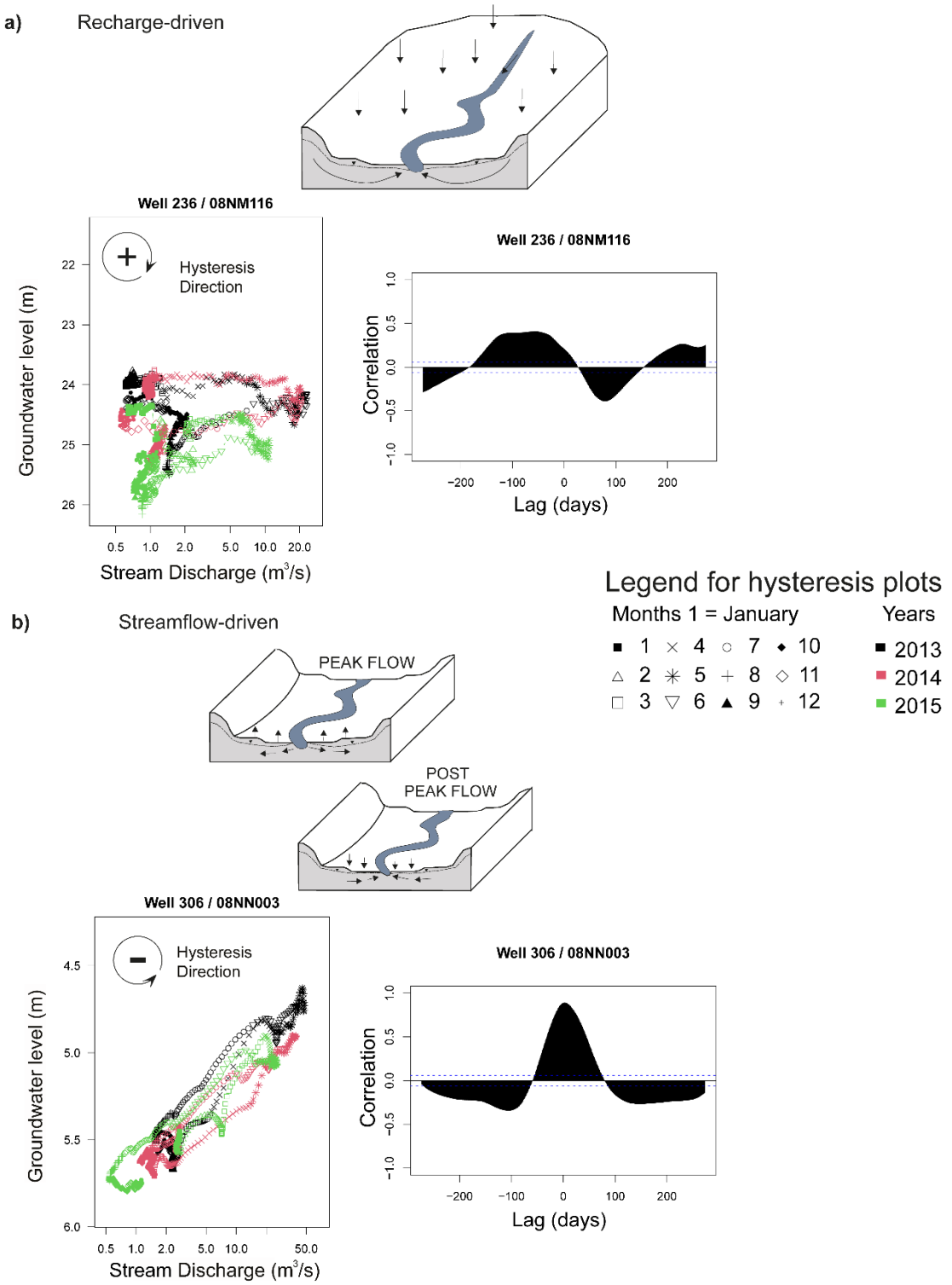

Figure 46 - Response mechanisms, their associated hysteresis plots of groundwater level versus stream discharge, and their cross-correlation plots for which the maximum deviation on the y-axis is associated with the lag time on the x-axis. a) A recharge-driven system with clockwise hysteresis (i.e., high groundwater levels lead to high stream discharge early in the year and as the year proceeds and the groundwater level drops, the streamflow also drops). In this case the streamflow signal lags the groundwater signal by approximately 75 days. b) A streamflow-driven system with counter-clockwise hysteresis (i.e., high streamflow levels lead to high groundwater levels early in the year and as the year proceeds, the lower streamflow leads to lower groundwater levels). In this case the streamflow signal leads the groundwater signal by a few days. Both examples are in a snowmelt hydrologic regime where winter precipitation is stored as snowpack and streamflows peak in spring and early summer.

The fundamental difference between recharge-driven and streamflow-driven systems is whether the streamflow signal or the groundwater signal leads the response. For example, in the recharge-driven system, the groundwater signal will lead throughout the year because groundwater replenished from precipitation (i.e., diffuse recharge) flows in one direction: from the aquifer to the stream (Figure 46a). In the streamflow-driven system, the streamflow signal leads the response; a rise in streamflow is followed by a rise in groundwater level and a decline in streamflow is followed by a decline in groundwater level (Figure 46b). During the spring freshet in mountain regions, streamflow (and stage) is high, and water can recharge the aquifer, causing the groundwater level to rise. Once the freshet ends, streamflow decreases and the groundwater flow system reverses to discharge into the stream (Figure 46b). The system in this second scenario is bi-directional.

The hysteresis graphs show groundwater level measured in an observation well (plotted on an arithmetic scale) against stream discharge measured at a nearby hydrometric station (plotted on a log scale). Each month in the hysteresis graph is given a separate symbol and each year is a different color. By tracking the symbols, the direction of hysteresis can often be determined: CW (clockwise) is denoted by a positive loop and CCW (counter-clockwise) by a negative loop, as illustrated in the upper left corner of the hysteresis graphs.

In some cases, the direction is difficult to identify. Hysteresis is due to the lag between stream discharge and groundwater level, which generates a loop structure that repeats itself in general shape but not in position between years. The shape of the hysteresis differs depending on the lag; small lags result in tight, almost linear, loops. The cross-correlation graphs show the degree of correlation between the two signals. Cross-correlation is a measure of similarity of two signals as a function of a time lag applied to one of them. Values of the correlation coefficient (y-axis) at 0 lag (x-axis) indicate how well correlated the two signals are if no lag in the response is introduced. By looking at the peaks (and troughs) and noting the lag, here in days, when these occur, the leading signal can be identified.

For example, in Figure 46a, the maximum peak occurs at a negative lag of approximately -75 days. So, the streamflow signal lags behind the groundwater signal, as would be expected in a recharge-driven system. In Figure 46b, the peak is located at slightly greater than 0 lag, meaning that the streamflow signal leads the groundwater signal, but only slightly (by a few days). Both examples are from a snowmelt hydrologic regime where winter precipitation is stored as snowpack and streamflows peak in spring and early summer.

Observation Well 236 (Figure 46a) is completed in a confined sand and gravel aquifer situated at the base of a mountain slope. The aquifer is recharged from infiltration of snowmelt runoff during the spring and groundwater discharges into a nearby small stream. Observation Well 306 (Figure 46b) is completed in an unconfined sand and gravel

aquifer through which a major river flows, whose annual hydrograph is generated by snowmelt processes remote from the aquifer (i.e., an allogenic source). Unsurprisingly, due to the high hydraulic connectivity of the aquifer with the river, the response is negative (CCW) and the system is streamflow-driven. In both systems, there may be localized bank storage effects following flood events where the elevated stream stage induces flow into the stream bank (Todd, 1956). As the stage declines, the flow is reversed.

Groundwater-level changes may also be driven by oscillating changes in the water elevation of surface water bodies, an obvious driver is ocean tides. Near the ocean, groundwater levels fluctuate with the tide, although the amplitude of the variation is lower and there is a time lag. The closer to the shoreline and the greater the hydraulic diffusivity of the aquifer (D=T/S, where T is transmissivity and S is storativity), the greater the amplitude of the response and the shorter the time lag. In addition to tidal variations that occur on a subdaily timescale, changes in mean sea level also impact groundwater systems, although over much longer timescales.

Box 13 explores the dynamics of climate-groundwater-stream interactions and introduces the concepts of the *water-table ratio* (WTR) and *groundwater response time* (GRT).

4.5 Summary

This section explored the dynamics of recharge and discharge. Importantly, these dynamics cause changes in groundwater storage, which are manifested as a change in groundwater level. First, we considered a groundwater-level hydrograph, which shows graphically the rise and fall of groundwater, either as hydraulic head elevation or as depth to groundwater. The fluctuations in groundwater level vary spatially (by location and depth) and temporally (hourly, daily, seasonally, interannually, and at longer timescales). A water year is a common period for reporting and describing hydrologic data. Interannual variability in the well hydrograph is normally related to interannual climate variability, but changes in groundwater pumping or irrigation can influence the natural variability.

We discussed that the rise and fall of the groundwater level reflects the addition of water to storage in the aquifer and the release of water from storage while the groundwater continues to flow from recharge to discharge areas. If the groundwater level is rising, the rate of groundwater recharge is greater than the rate of groundwater discharge. When recharge reduces or stops, the groundwater level declines; this is termed *groundwater recession*. The maximum and minimum water levels in a particular well (reflecting the maximum and minimum aquifer water levels) vary slightly each year, depending on the weather. However, different aquifers have different ranges for the same amount of recharge, depending on the aquifer properties. Aquifers with low storativity values, such as confined aquifers or fractured bedrock aquifers, typically have a greater annual range in groundwater level compared to unconfined aquifers. Proximity to surface water bodies also influences the groundwater levels.

Many methods are used to estimate recharge, discharge, and changes in storage. These range from point-based estimates obtained using in situ instrumentation to regional scale estimates from satellite data and span water balance methods, physical, chemical, and isotopic methods, heat methods, and remote sensing methods. Specific techniques are used for the unsaturated zone and the saturated zone and in surface waters. Table 3 summarizes the various methods.

Climate is the primary driver for seasonal variations in groundwater level. Examples of seasonal variations were explored for cold climate regions, temperate climate regions, and arid/semi-arid climate regions. In cold climate regions, seasonal variations of recharge and discharge are controlled largely by freeze-thaw processes and the timing of snow and glacier melt, while in temperate climate regions, they largely reflect the timing of precipitation, which primarily falls as rain. In regions with an arid or semi-arid climate, precipitation amounts are exceeded by evapotranspiration leaving little, if any, water for groundwater recharge. Groundwater recharge in these regions tends to be focused recharge in a small fraction of the landscape such as surface depressions and surface water bodies.

Recharge and discharge also vary at other timescales, including subdaily to daily, interannually, and over longer periods. At the subdaily to daily timescales, some aquifers record precipitation (i.e., rainfall) events very effectively, showing high frequency variation, while others record long-term changes in water level accompanying seasonal or longer-term variations in precipitation. Precipitation intensity is an important factor controlling the groundwater-level response. Intense rain events are referred to as extreme or heavy rain events. In arid and semi-arid regions, these intense rain events are the only major source of recharge to aquifers.

Groundwater levels can vary over longer periods (interannually to paleo timescales). A significant change in the aquifer system, such as long-term decline (or increase) in recharge or the introduction (or cessation) of pumping, can lead to positive or negative trends in the groundwater level. Groundwater levels can also vary due to climate oscillations (or climate cycles), such as the El Niño Southern Oscillation (ENSO) and several others. Groundwater levels have also changed over very long periods due to natural climate change, alterations to the natural environment, and many other anthropogenic factors such as pumping, land use, and land cover change. For example, global rainfall patterns have changed over the last 10,000 years, since the Late Pleistocene. Current hyper-arid regions in northern Africa received significant rainfall in the past to providing paleo recharge to many of the large aquifers that today have large groundwater reserves.

Finally, groundwater levels can vary due to the dynamic interactions between streams and aquifers. Two-way exchanges of water between aquifers and surface water bodies, commonly referred to as groundwater–surface water interactions, can occur over a wide range of spatial and temporal scales. The degree of interaction depends on the

hydraulic connectivity between the two systems. Groundwater-level changes can be caused by changes in stream stage (streamflow-driven response mechanism) or groundwater-level changes can cause changes in stream stage (diffuse recharge-driven response mechanism). Groundwater levels can oscillate in response to tidal oscillations.

5 Alteration of Natural Recharge and Discharge

Changes in groundwater level, in terms of year to year and season to season variability, as discussed in the previous section, are most associated with relatively short-term variability in precipitation and temperature. However, groundwater level and, by association, groundwater storage also respond to anthropogenic influences. The addition of water to a groundwater system is, over the long term (perhaps tens of years or less), balanced by similar amounts of outflow to a surface system such that most groundwater systems are in equilibrium with surface water systems. Unless the aquifer is overdrafted by pumping, overirrigated, impacted by a change in climate or land cover, or has had some alteration of its hydraulic properties (e.g., a reduction in storage capacity by compaction), the aquifer is in dynamic equilibrium with the environment. For this reason, ecological systems are also in equilibrium with the groundwater system. Many ecological systems adapt to changing environmental conditions, but some do not.

While many human interventions can influence recharge and discharge, this section focuses on groundwater abstraction, irrigation, and managed aquifer recharge, highlighting some consequences of these interventions. The section ends with an overview of how recharge and discharge are associated with ecological systems and how climate change is impacting these processes.

5.1 Groundwater Abstraction

As discussed in subsection 3.2.6, the abstraction of groundwater has significantly increased globally, largely due to the expansion of irrigated agriculture and economic development driven by population growth (Famiglietti, 2014; UNESCO, 2022). Here, we explore some of the consequences of groundwater abstraction.

The main consequence of groundwater pumping is the lowering of hydraulic head (water table or potentiometric surface), which creates a cone of depression around the well. Initially, the entirety of the pumped groundwater originates from depletion of the aquifer storage. However, as pumping continues and the cone of depression broadens and deepens, a portion of the water is captured, where capture includes both increases in recharge from induced infiltration from surface water bodies and decreases in discharge to surface water bodies (Konikow & Leake, 2014; Theis, 1940). Because most capture translates into streamflow depletion, there can be significant impacts on aquatic ecosystems (Figure 47a). Konikow and Leake (2014) examined a large sample of real aquifer systems with a long history of development and found that the fractions of depletion of storage and capture of induced infiltration and decreased discharge are highly variable in time and space, but the depletion fraction averages about 15 percent, and the capture fraction averages about 85 percent based on cumulative volumes pumped. These results suggest that capture is a critical consequence of groundwater pumping. To mitigate the effect of

pumping on streamflow, Gleeson and Richter (2018) suggest that "high levels of ecological protection will be provided if groundwater pumping decreases monthly natural baseflow by less than 10 [percent] through time" (p. 89).

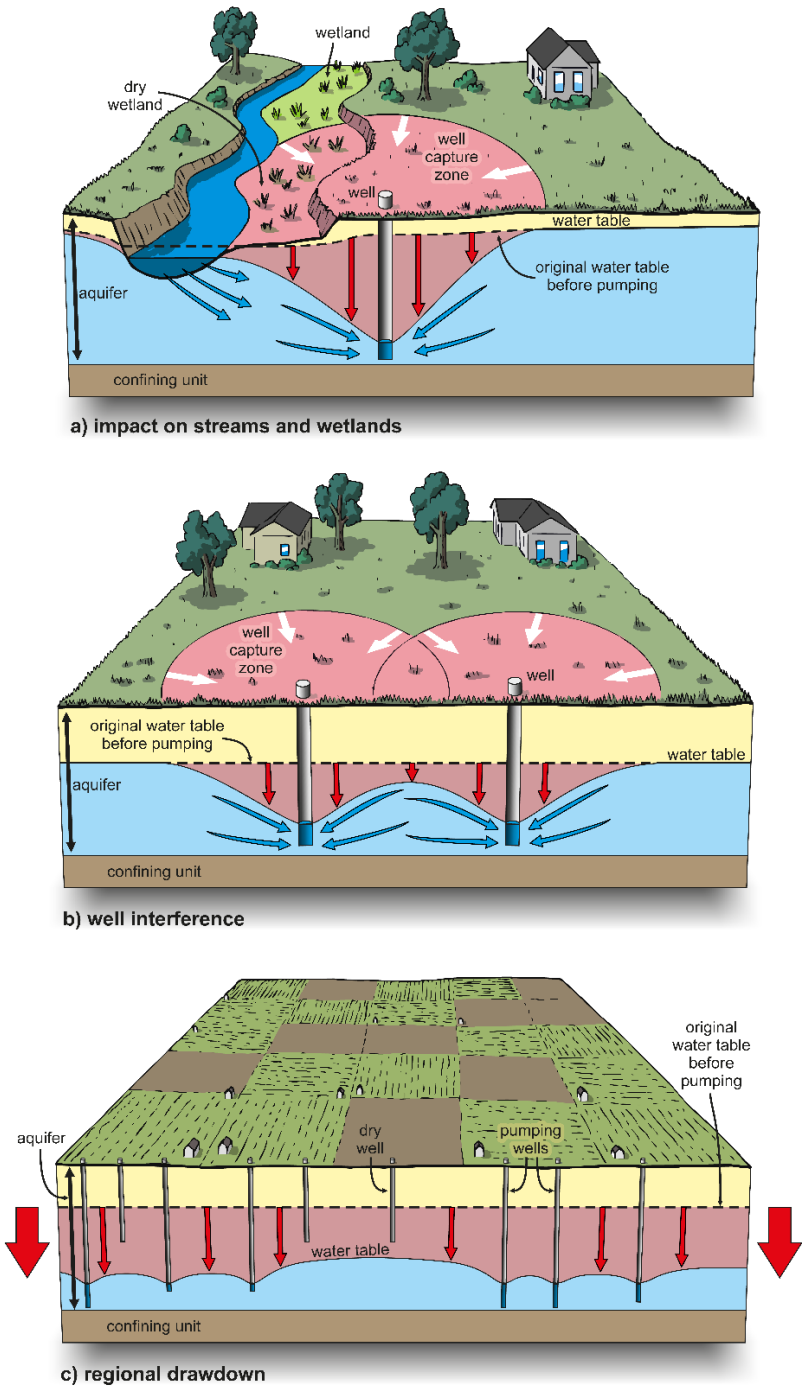

Figure 47 - Groundwater abstraction may lead to a) impacts on streams and wetlands due to induced infiltration and capture, b) superposed cones of depression due to well interference, and c) regional drawdown due to the cumulative effects of pumping (modified from Rivera, 2013's Figure 6.5).

The effects of pumping are cumulative, meaning that if two or more adjacent wells are pumped simultaneously, their cones of depression can grow large enough to overlap (Figure 47b). This is known as well interference, and it results in a combined drawdown effect in the overlapping region. If many wells are pumped and the cumulative pumping volume exceeds the amount of water from the combined depletion of storage and capture, then the pumping is unsustainable, the aquifer becomes depleted, and regional drawdown will occur (Figure 47c). Groundwater depletion is a significant problem in many aquifers globally. The most prominent examples of this effect are the Central Valley of California and the High Plains of the midwestern USA, the North China Plain, western India and a part of eastern Pakistan, central Mexico, Iran, southeast Spain, and the Middle East (Bierkens & Wada, 2019; Werner et al., 2013). Groundwater in deep, confined aquifers is particularly at risk of depletion because this groundwater can be hundreds, or even millions, of years old. If this old groundwater is abstracted, it may take millions of years to replenish the aquifer by natural processes because recharge rates are very low. This is referred to as *groundwater mining*. Groundwater development is discussed in more detail by Konikow and Bredehoeft (2020).

5.2 Irrigation

Irrigation is a dominant source of anthropogenic or incidental recharge in many regions. Globally, irrigated agricultural land area expanded by 480 percent from 1900 to 2000 and was projected to increase by 20 percent (202 – 242 Mha) from 2005 to 2030 in developing countries (Scanlon et al., 2007). Agricultural areas often require at least some irrigation during the dry months to replenish the soil moisture for the plants, but too much irrigation (more than the plants can use) can result in rising water tables and unnecessary water recharging the aquifer.

Irrigation return flow (IRF) is the surplus amount of irrigation water; that is, the amount of water not lost to evapotranspiration or surface runoff that percolates below the plant root zone and contributes to groundwater recharge (Figure 48). Some of this water may be intercepted by tile drains and conveyed to agricultural ditches surrounding fields, but IRF can occur if tile drains are not installed. The proportion of water returned from the cultivated area to the groundwater system relative to the amount of water abstracted for irrigation is referred to as the *irrigation return flow coefficient* (IRFC), which varies depending on crop type and irrigation method. Dewandel and others (2008) used a hydrologic model to simulate irrigation return flow and the IRFCs for different irrigated crops in the 53 km^2 Maheshwaram pilot watershed located 35 km south of Hyderabad (Ranga Reddy District, state of Andhra Pradesh, India). In the Maheshwaram watershed, more than 700 borewells support the irrigation of crops; rice cultivation uses 87 percent of the pumped groundwater. Indeed, rice cultivation requires huge amounts of water (with 1500 to 2000 mm of irrigation water applied per cultivation) and usually requires a continuously maintained depth of a

few centimeters of free-standing water in the field. Dewandel and others (2008) estimated that the IRFC ranged from more than 50 percent for rice cultivation using standing water irrigation to 0 percent in the case of a drip irrigation technique.

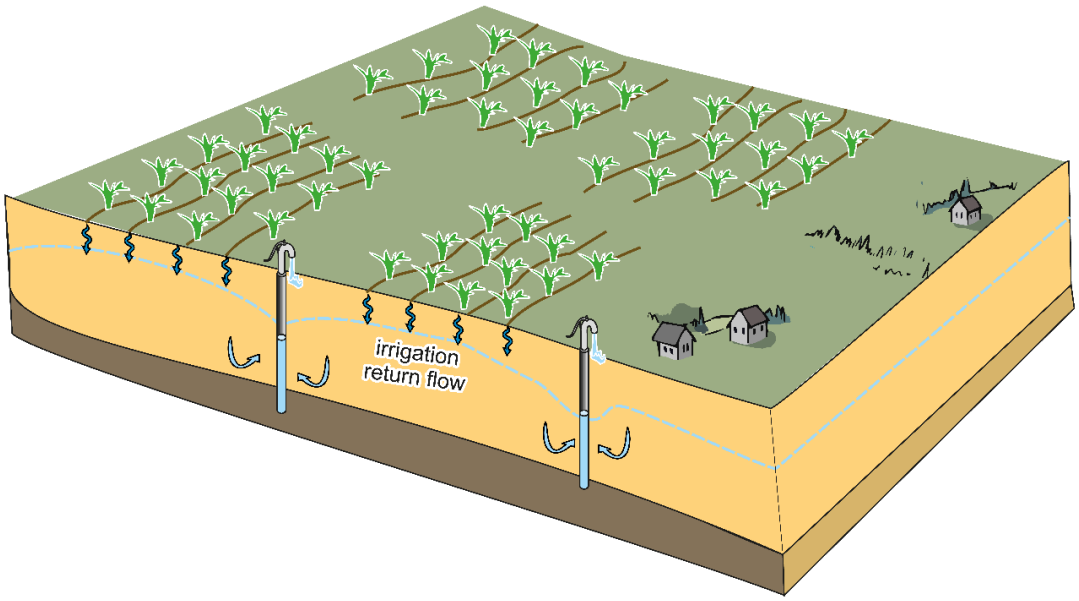

Figure 48 - Irrigation return flow raises the water table beneath the areas where the irrigation is applied.

Irrigation may cause a redistribution of water between surface water and groundwater. Irrigation based on surface water has resulted in groundwater-level rises due to water losses along conveyance structures and deep percolation on irrigated fields. Groundwater-fed irrigation also may result in transfer of surface water to groundwater because groundwater pumping may induce infiltration from streams, as discussed in subsection 5.1. Large groundwater-level rises can result in extensive waterlogging and soil salinization. This irrigation-induced (or secondary) salinization arises from poor-quality irrigation water, inadequate leaching due to insufficient irrigation water application to facilitate flushing or low hydraulic conductivity soils, and high evaporation rates (Rengasamy, 2006). Salt accumulation in soils has damaged 45 Mha of agricultural land, representing approximately 20 percent of the world's total irrigated land. Each year, 1.5 Mha of land are damaged due to salinization globally (Wood, 2000). The leaching of agricultural chemicals can also be enhanced because of irrigation. For example, in the central High Plains (USA), water-quality degradation has been attributed to irrigation, based on higher TDS (median 675 mg/L, relative to 374 mg/L for water samples collected in areas not affected by irrigation), higher nitrate-N levels (median 7.1 mg/L relative to 2.5 mg/L), and detection of pesticides (Bruce et al., 2003).

Another important and well-recognized example of the effects of irrigation return flow is non-point-sourced arsenic pollution in the groundwater of the Bengal Basin in Bangladesh and India, which is regarded as one of the largest public health concerns in human history (Acharyya et al., 2000; Chakraboty et al., 2015). The source of arsenic in the

Bengal Basin groundwater is thought to be the Himalayas, brought down by river systems to sites of recent sedimentation. When anoxic groundwater is pumped from these deeper sediments and exposed to the atmosphere, the arsenic is sequestered to the oxidized ferric iron in the soils of the agricultural fields. Edmunds and others (2015) reported that irrigated soils have higher arsenic concentrations (on the order of tens of mg/Kg) than non-irrigated soils (5 to 10 mg/Kg). This arsenic can be subsequently recirculated to the groundwater, particularly in the dry seasons via irrigation return flow, thereby adding to the groundwater arsenic problem.

5.3 Managed Aquifer Recharge

Many regions around the word receive recharge at times of the year when demand for water is lowest. Managed aquifer recharge (MAR), also called *groundwater replenishment*, *water banking*, and *artificial recharge*, is the purposeful recharge of water to aquifers for subsequent recovery or environmental benefit (IAH, International Association of Hydrogeologists↗, 2020). *MAR* has replaced the term *artificial recharge*, which traditionally focused only on augmenting the quantity of recharge, with little consideration to how water quality might result in negative impacts on human or ecosystem health. MAR is an increasingly important water-management strategy, alongside demand management, to maintain, enhance, and secure stressed groundwater systems, to protect and improve water quality, and to secure drought and emergency supplies (Dillon et al., 2019).

MAR uses natural water sources and appropriately treated urban stormwater, sewage, and other waste waters to increase groundwater storage. Use of natural water sources occurs primarily at times of the year when surface water sources are plentiful—for example, during the monsoon season. If not captured for storage underground, these water resources form runoff. The various MAR schemes make use of natural water resources during times of plenty, as well as other sources of reclaimed water, to augment water supplies during times of need.

Gale (2005) broadly classifies MAR under the following schemes, some examples of which (*in italics*) are shown in Figure 49.

- **Spreading methods** including *infiltration ponds and basins*; soil aquifer treatment (SAT) involving wastewater recharge and recovery; controlled flooding of the land surface; incidental recharge from irrigation (as discussed in the previous subsection)
- **In-channel modifications** including *percolation ponds behind check-dams*, gabions; sand storage dams; subsurface dams; leaky dams and recharge releases
- **Well, shaft, and borehole recharge** including *aquifer storage and recovery (ASR)*; open wells and shafts
- **Induced bank filtration** including *bank filtration*; interdune filtration

- **Rainwater harvesting** including *roof-top rainwater harvesting*; field bunds (berms along topographic contours that control erosion and foster infiltration)

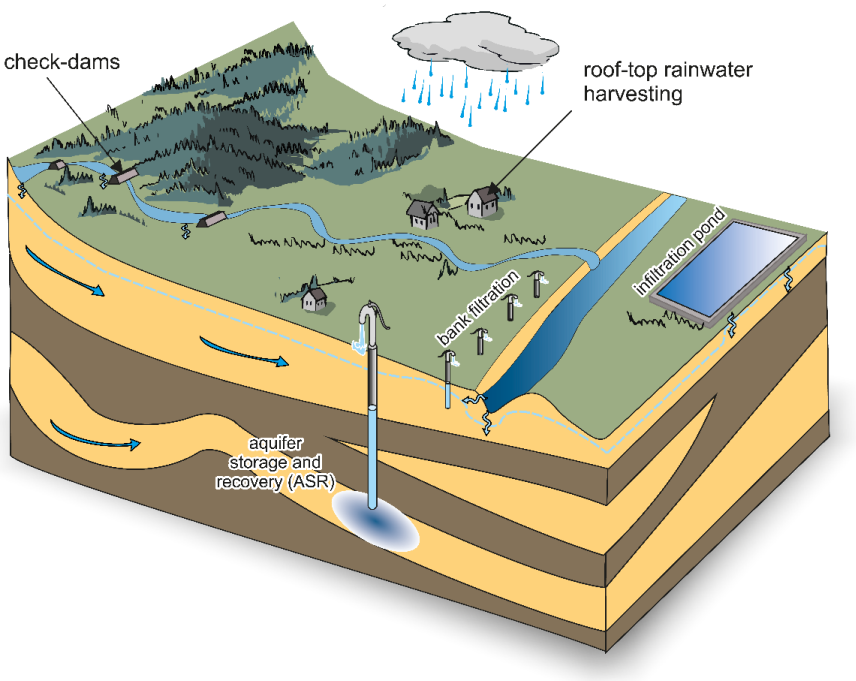

Figure 49 - Managed aquifer recharge (MAR) schemes (adapted from Gale, 2005).

The physical success of a MAR scheme depends largely on the local hydrogeological conditions. These conditions determine the ability of the recharge water to percolate through the unsaturated zone and the ability of the aquifer to store the recharge water (Gale, 2005). Braune and Israel (2021) discuss MAR in southern Africa.

Since the 1960s, global implementation of MAR has accelerated at a rate of 5 percent per year and by 2015 reached an estimated recharge of 10 km^3/year globally (Dillon et al., 2019). Given the changing climate and more frequent extreme weather conditions, the use of MAR is expected to increase significantly.

5.4 Recharge, Discharge, and Ecological Systems

Recharge and discharge are inextricably linked to many ecological systems (or ecosystems). Recharge is moderated by vegetation through transpiration (subsection 2.2.4), and variations in recharge lead to variations in discharge and changes in storage (subsection 4.2.2), which ultimately impact ecosystems. Ecosystems that rely on groundwater for some or all their water requirements are classified as *groundwater dependent ecosystems* (GDEs). Not all GDEs draw on groundwater directly and not all rely solely on groundwater. However, in many cases, groundwater provides an important and reliable source of water to many ecosystems and can be the main factor controlling the distribution of ecosystem types. Examples of GDEs include the following.

- Terrestrial vegetation that relies on the availability of shallow groundwater (e.g., phreatophytes, as discussed in subsection 4.3.1 on vegetation demand)
- Wetlands whose function depends on sustained high-water levels in aquifers
- River systems where groundwater discharge provides a significant baseflow component to the river
- Estuarine and near-shore marine systems, such as coastal mangroves, salt marshes, and seagrass beds, which rely on the submarine discharge of groundwater

Eamus and others (2016) give an excellent overview of GDEs, including their classification, identification techniques, and threats.

Several factors influence the source of groundwater to GDEs. The most significant is recharge. A reduction in recharge can lead to groundwater-level declines and, consequently, a reduction in discharge that contributes to baseflow. But groundwater abstraction can also be a factor. In Western Australia, for example, the combination of climate change, abstraction, and land use changes have led to significant declines in groundwater levels in the Gnangara Groundwater Mound over the last few decades (Barreteau et al., 2016). The Gnangara Mound supplies approximately half of the water needs of the city of Perth (Barreteau et al., 2016). A rainfall reduction of 10 to 15 percent and fewer high-intensity rainfall events since the mid-1970s has led to reduced streamflow sourced by runoff and groundwater discharge (Petrone et al., 2010). A significant increase in groundwater abstraction from the Gnangara Mound was associated with a decline in available surface water supplies. Land use changes, particularly in the case of pine plantations, had the strongest influence on groundwater levels, particularly in areas with a high density of plantations due to increased evapotranspiration and reduced recharge (Yesertener, 2008).

Among other impacts, such as saltwater intrusion in some coastal areas and the acidification of wetlands by being exposed to sulphate-rich soils (Barreteau et al., 2016), the lowered groundwater levels in the Gnangara Mound caused declines in total abundance of groundwater–dependent plants and shifts in species composition toward more drought-tolerant species (Froend & Sommer, 2010). In the United States, groundwater abstraction in the Edwards Aquifer since the early 1900s has diminished spring flow and threatened GDEs (Sharp & Green, 2022). The lowered water tables have negatively impacted habitat for invertebrate species endemic to the Edwards Aquifer's karstic formations (Zektser et al., 2005).

The impact of changes in groundwater quantity and quality on GDEs is determined by the degree and nature of their groundwater dependency. The sensitivity of a GDE is often viewed from the perspective of volumetric water requirements, commonly referred to as *environmental flow needs* (EFNs). Only a small decline in groundwater level is needed to affect streamflow (de Graaf et al., 2019). However, decreases in groundwater inflows or

levels, especially during seasonal low flows and dry conditions, may also have implications from a physiochemical perspective—for instance, if groundwater inflows are insufficient to maintain required temperature or nutrient conditions of a GDE. The relatively stable thermal regimes of some groundwater discharge zones can buffer stream temperatures against long-term air temperature trends and short-term hot and cold extremes (Boulton & Hancock, 2006).

Depth to groundwater (from the land surface) is considered one of the most important groundwater attributes for GDEs, particularly for terrestrial ecosystems that rely on subsurface provision of groundwater (Eamus et al., 2016). An increased depth to groundwater may result in reduced plant growth, mortality, and a change in species compositions (Shafroth et al., 2000). Reduced groundwater pressure and flux cause reduced groundwater discharge and, subsequently, reduced surface water availability to wetlands and GDEs that depend on baseflow and springs (Shafroth et al., 2000). In unconfined aquifers, short-term fluctuations of groundwater level and flux occur naturally in response to time-varying uptake of water by vegetation, while seasonal fluctuations often reflect time-varying groundwater recharge related to wet and dry season cycles (Box 14). Longer-term trends in groundwater level and flux caused by climate change and/or land use change can have significant impacts on ecosystems (subsection 5.2). Figure 50 illustrates the potential changes in the ecological status of GDEs over time with increasing pressure from climate change and land use. However, groundwater ecology, the study of phreatic ecosystems (i.e., saturated groundwater ecosystems in porous and fractured-rock aquifers) as a scientific discipline is in its infancy (Larned, 2012), and little is known about how climate change will affect GDEs and their biota (Kløve et al., 2014).

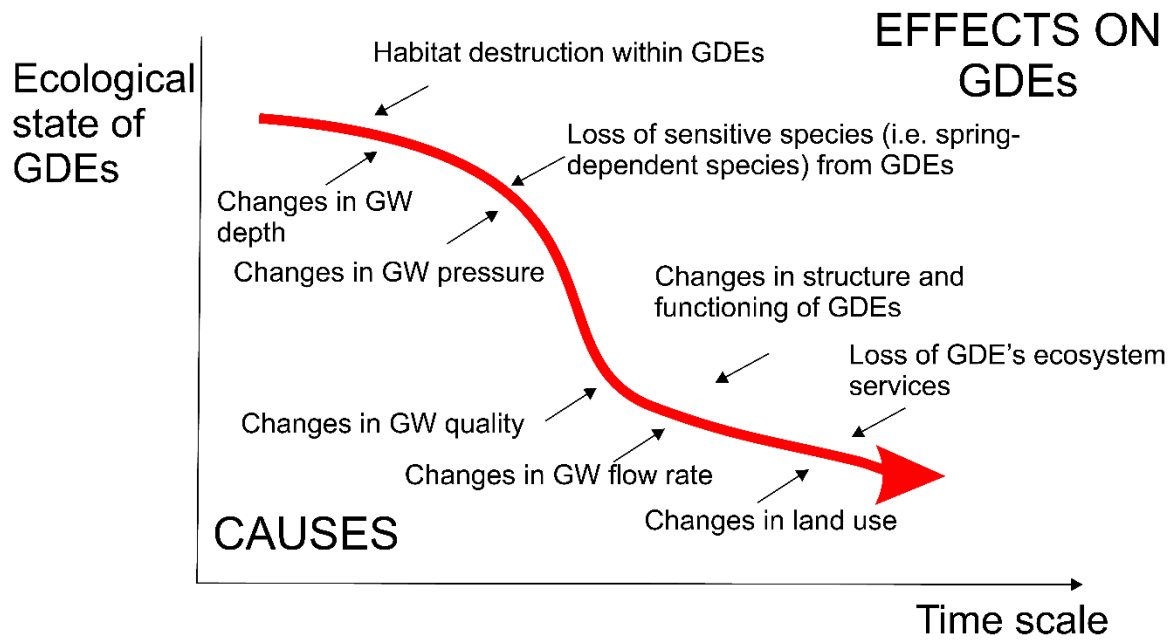

Figure 50 - The potential changes in the ecological status of groundwater-dependent ecosystems (GDEs) over time with increasing pressure from climate change and land use (adapted from Kløve et al., 2014).

Thought Question: Identify a potential groundwater dependent ecosystem in your region. How might a change in groundwater level (depth to groundwater) or flux influence that GDE?

5.5 Impacts of Climate Change on Recharge and Discharge

Groundwater has always been affected by changes in climate, but only in recent years have we focused on the impacts of global warming on groundwater. Over the past few decades, a wide array of scientific research was carried out to better understand how water resources might respond to global climate change, but the focus was largely on surface water systems, as noted by Green and others (2011), who wrote the first comprehensive review on groundwater and climate change. Taylor and others (2013) emphasized that the strategic importance of groundwater for global water and food security will likely intensify as more frequent and intense climate extremes, such as droughts and floods, affect surface water resources.

Central to understanding climate change's impact on groundwater is the ability to predict how recharge might change, because a change in recharge affects the amount of water held in storage and how much discharges. As discussed in Section 2, the rate at which diffuse recharge occurs is determined by a complex interaction between climate and various characteristics of the land surface such as topography, vegetation, soil type, and geology, which collectively affect the timing and amount of water available for infiltration. If we consider only climate variables, we need to consider the increase in air temperature alongside changes in the amount and timing of precipitation; the form of precipitation (i.e., rain or snow); wind patterns; relative humidity, among other factors. The projected shifts in the distribution and timing of precipitation based on global climate models are uncertain; there are, nevertheless, significant regional differences.

Generally, high-latitude land masses are projected to receive more precipitation due to the additional water-carrying capacity of the warmer troposphere, while the dry belt that lies just outside the tropics is projected to expand farther poleward, and mid-latitude and subtropical arid and semi-arid regions will receive less precipitation (IPCC, 2021). Evapotranspiration rates also depend on many factors noted previously, including the type of vegetation (subsection 2.4). However, we cannot assume that vegetation in a region will be the same in the future; some species may not be able to adapt to changing climate conditions. Neither can we assume that the land surface and subsurface will remain unaltered. Greater rates of erosion—due to heavy rain events, for example, or alterations to the land surface by humans—may result in modifications to the topography, soil, and sediment.

Groundwater systems are also shaped by their discharge areas, which commonly comprise streams, lakes, and wetlands. A change in the stage of a stream or lake influences the groundwater discharge environment and thus the water-table height (subsection 4.4).

Surface water systems can also be sources of recharge (both diffuse and focused). Therefore, it is important to consider both recharge and discharge processes. Moreover, we need to consider the seasonality of recharge and discharge. In regions with snow, less snowpack will accumulate, and melt will occur earlier in the spring.

Figure 51 illustrates the shift in the timing of groundwater levels in a small valley bottom aquifer in southern British Columbia, Canada. Here, the river meandering through the valley is sourced from snowmelt high in the mountains. Streamflow peaks during the spring freshet and undergoes a recession throughout the summer. By the 2050s, the snowmelt will occur earlier relative to the historical baseline period of 1961 to 1992. It has already begun to shift, and the peak streamflow occurs earlier (Scibek et al., 2007).

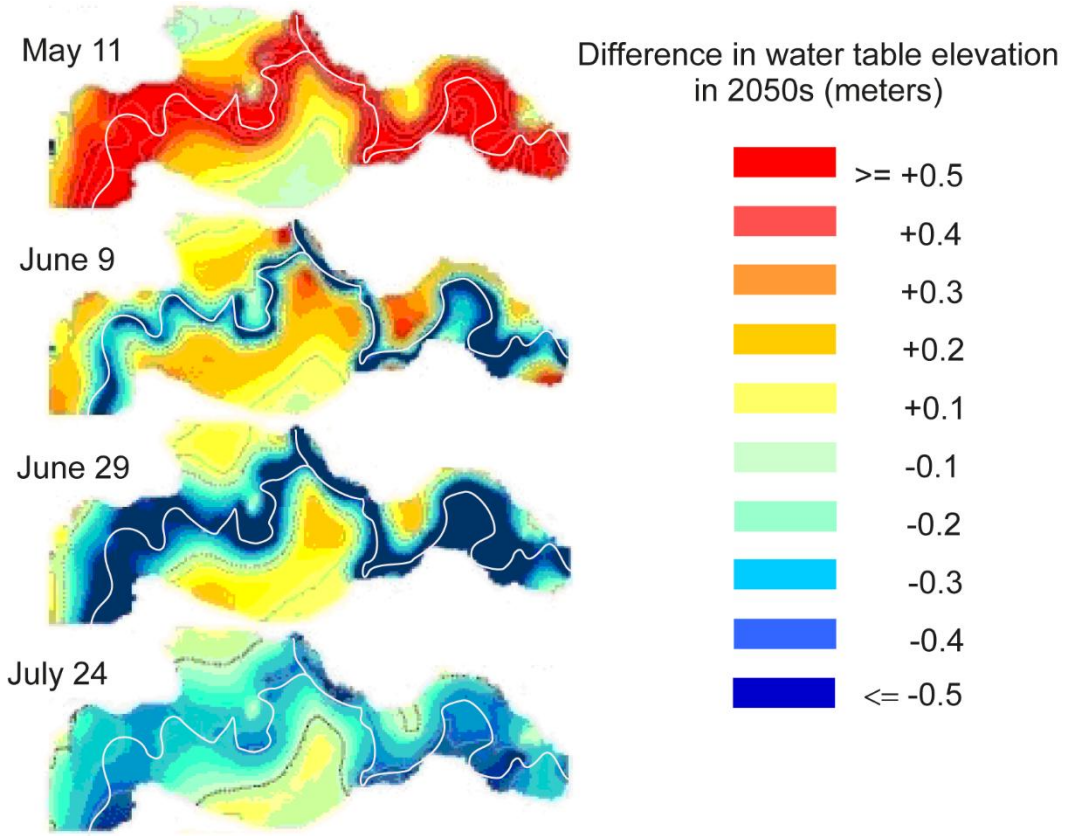

Figure 51 - Simulated water-table differences between future (2050s) and historical (1961–1992) climates on a specific day each month. The shift in groundwater levels reflect an earlier spring melt (higher groundwater levels earlier in the year) and an earlier onset of the summer low-flow period (modified from Scibek et al., 2007).

Likewise, the timing of peak groundwater levels is projected to shift to earlier in the year due to the earlier spring freshet. This shift in groundwater levels occurs because the stream stage influences the groundwater levels (subsection 4.4, streamflow-driven systems). By the 2050s, the groundwater levels on May 11 will be higher compared to the same day in the historical baseline period. By June 9, the groundwater levels will have fallen near the river as the freshet has passed. By July 24, almost the entire aquifer has lower groundwater levels compared to this historical period. By the 2050s, climate-induced changes in water-table elevations are on the order of 0.5 m.

Some regions will experience a complete loss of snowpack as the climate warms. Glaciers have begun to retreat in many regions and, although stream discharge is currently high, it will gradually lessen. This means many regions will undergo a shift in the hydrologic regime. Snowmelt-dominated hydrologic regimes may shift to rainfall-dominated regimes, and the timing of recharge and discharge will likewise shift.

Much of the research to date has been modeling-based and focused on the effect of climate change on the magnitude and timing of recharge (Döll, 2009; Green et al., 2011; Treidel et al., 2012), with less emphasis on whether recharge mechanisms may change (e.g., shift from diffuse to focused recharge). Moreover, few papers have addressed how groundwater will be indirectly affected by the changing patterns of groundwater abstraction and/or land use (Treidel et al., 2012). Increasing abstraction with reduced recharge can reduce groundwater levels significantly. Furthermore, groundwater quality has received far less attention than groundwater quantity (Treidel et al., 2012). Climate change impacts on GDEs have received limited attention (Taylor et al., 2013), despite the importance of GDEs. de Graff and others (2019) estimated that, by 2050 (incorporating climate change), environmental flow limits will be reached for approximately 42 to 79 percent of the watersheds worldwide in which there is groundwater pumping, and that this will generally occur before substantial losses in groundwater storage are experienced. Overall, aquifers and GDEs face increasing pressure from climate change and land use change (Kløve et al., 2014).

Finally, it is important to understand that the response of the groundwater system to a change often lags behind the driver of that change as illustrated by the investigations presented in Box 15↴. This means that changes in a groundwater system due to a change in climate may not be evident for a long time.

Thought Question: The World Bank Climate Change Knowledge Portal↗ offers a global summary on current climate, climate projections, extreme events, risk, and sea level. Under climate projections, you can explore climate variables for different time periods. These projections are derived from global climate models. Typically, outputs from several models are averaged—this is a model ensemble. Emissions scenarios are also available. The output data are shown as an anomaly (or change) relative to historical baseline conditions.

Considering the projected changes in air temperature and precipitation for the region of your choice, what impact might these have on groundwater recharge?

5.6 Summary

In this section, we explored alterations of natural groundwater recharge and discharge. First, we considered groundwater abstraction, that is, human-controlled discharge. Groundwater pumping lowers the water table (or potentiometric surface), giving rise to a cone of depression centered around the well. However, if there are multiple pumping wells, then the drawdown cones coalesce, leading to widespread lowering of the

groundwater level, which may lead to groundwater depletion. Equally important is the potential capture of water from streams during pumping, which can lead to streamflow depletion. Most capture translates into streamflow depletion, which can lead to significant impacts on aquatic ecosystems.

The next two sections considered irrigation and managed aquifer recharge (MAR). Irrigation return flow (IRF) is the surplus amount of irrigation water that percolates below the plant root zone and contributes to recharge. Irrigation may redistribute surface water and groundwater—for example, induced infiltration for streams due to groundwater pumping for irrigation. Groundwater levels may increase, and soil salinization may occur if irrigation water is of poor quality. Various MAR schemes make use of natural water resources during times of plenty, as well as other sources of reclaimed water, to augment water supplies during times of need. With climate change and more frequent extreme climate conditions, the use of MAR is expected to increase significantly.

We then explored some connections between recharge, discharge, and ecosystems, focusing on groundwater-dependent ecosystems (GDEs). While not all GDEs draw on groundwater directly and not all are solely reliant on groundwater, groundwater often provides an important and reliable source of water to many ecosystems (e.g., terrestrial, aquatic, cave, and coastal). Changes in the depth to groundwater and the flux—for example, due to a reduction in recharge or groundwater abstraction—can severely compromise the health of GDEs in terms of both water quantity and quality.

Finally, we briefly explored the topic of groundwater and climate change. Most studies have focused on how the magnitude and timing of recharge might change, and some have considered the broader impacts to surface water and groundwater. Relatively few studies have examined potential impacts to groundwater quality or GDEs, and even fewer studies have attempted to assess the cumulative effects of increased groundwater abstraction coupled with land use change and climate change. Such holistic studies are needed considering the various connections and feedbacks between groundwater systems and the natural and built environments.

6 Wrap-up

Recharge and discharge are perhaps the most critical components of a groundwater system. They are vital to the sustainability of groundwater resources and surface water resources. They sustain and maintain the flow system; if there is no recharge, no water replenishes the aquifer system and no water discharges. With no groundwater discharge, many surface water bodies would become completely dry during the dry season, with significant detrimental effects on ecosystems. However, as noted in subsection 5.4, groundwater ecology as a scientific discipline is in its infancy, and little is known about how climate change will affect GDEs and their biota. Groundwater ecology, therefore, is a discipline ripe for research.

This book aimed to examine recharge and discharge in sufficient detail for readers to understand the factors that influence them and how they are linked to other components of the hydrologic cycle. This knowledge should be sufficient to enable more in-depth reading on specific processes as well as broader reading on other groundwater-related topics, such as groundwater contamination, groundwater sustainability, groundwater–surface water interactions, and groundwater dependent ecosystems (GDEs).

With a growing global population, there will be increased demand for food and water. However, our warming climate is altering the distribution and timing of precipitation in many regions. Surface water resources are highly sensitive to these alterations, while groundwater resources are considered more resilient. Consequently, many regions are looking to groundwater to meet water demands. As the use of groundwater increases, so will the risks of groundwater depletion and, by association, streamflow depletion. It is critical that groundwater be used sustainably. This requires regional (or even local) knowledge and quantification of recharge and discharge.

Our understanding of recharge and discharge in specific areas, including their quantification, should be revisited, because climate change and other human alterations are potentially changing their dynamics and even their mechanisms. These dynamics should be re-examined at a range of spatial and temporal scales. Particularly, for larger spatial and temporal scales, numerical models will likely continue to be key tools for exploring impacts, but new technologies such as machine learning and new data sources such as from satellites will add to our hydrogeological toolbox.

As noted in subsection 5.4, while a growing number of studies attempt to project how recharge might be altered due to climate change, relatively few studies have addressed how groundwater will be indirectly affected by the shifting patterns of groundwater abstraction and/or land use in a changing climate. Water quality may also be impacted, although relatively less research has been conducted on the effects of climate change. Neither has there been much research on the impacts of extreme weather events on recharge and discharge.

Also, because the climate is not stationary, the statistics of instrumental data that have been used historically to characterize climate and hydrology are not necessarily valid. This means statistical data once used to quantify recharge and discharge—for example, mean annual (or monthly) groundwater level or mean annual baseflow—may not be representative. Even the characteristics of groundwater-level hydrographs may change. In short, the characteristics of recharge and discharge, and indeed groundwater systems, will evolve.

7 Exercises

Exercise 1

The image below shows a simplified cross section through an unconfined aquifer. The right edge is a groundwater divide, and the bottom is impermeable. The aquifer extends to the left, past the creek. The water table is shown as a dashed line. Assume the aquifer material is homogeneous and isotropic. Using the hydraulic head values (Table Exercise 1) measured in the numbered piezometers completed at different depths, draw and clearly label the equipotential lines and the flow lines for the flow system. Label the recharge and discharge areas.

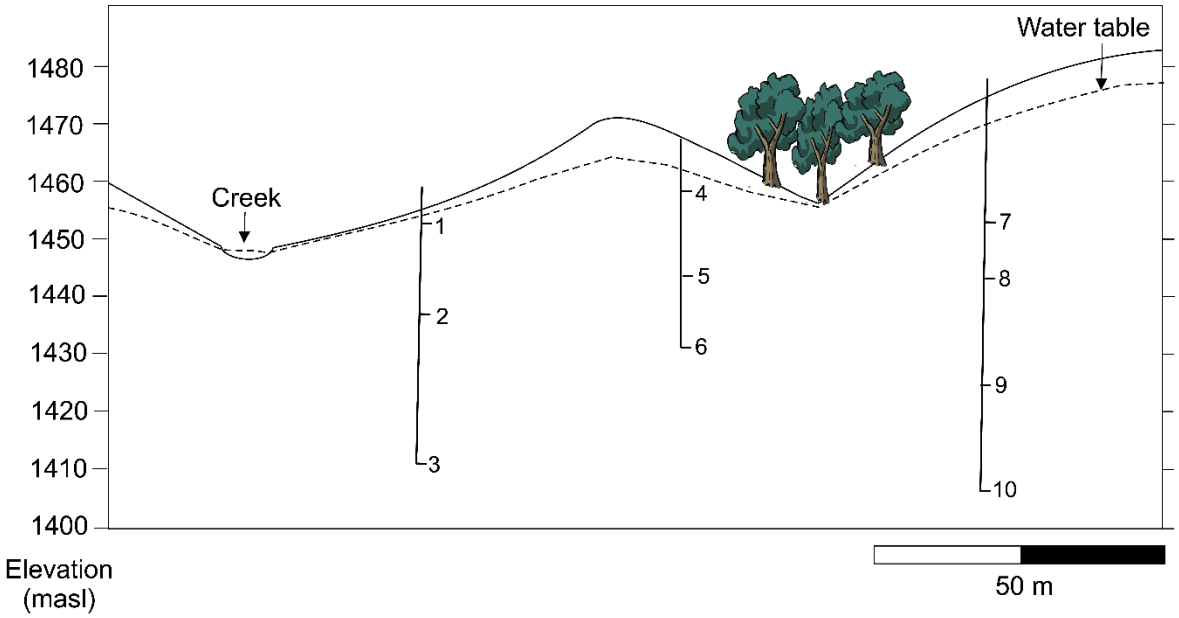

Table Exercise 1 - Hydraulic head values at each piezometer location. Measurements are in meters above sea level (masl).

Piezometer Number	Hydraulic Head (m asl)
1	1453
2	1450
3	1452
4	1460
5	1457
6	1454
7	1464
8	1460
9	1456
10	1454

Solution to Exercise 1

Return to where text linked to Exercise 1

Exercise 2

a) Where are the likely recharge and discharge areas in the simple flow system shown in Figure 4?
b) Where are the likely recharge and discharge areas in the complex flow system shown in Figure 2?

Solution to Exercise 2

Return to where text linked to Exercise 2

Exercise 3

a) How might civil infrastructure like roads and buildings impact recharge?
b) How might agriculture impact recharge?
c) How might forest harvesting (logging) impact recharge?

Solution to Exercise 3

Return to where text linked to Exercise 3

Exercise 4

Using Equation (12), calculate the height of capillary rise, h_c, for each of the soils below. The surface tension of water (at 10 °C) is 0.0742 N/m.

Texture	Grain diameter (cm)	Pore radius (cm)	Capillary rise (m)	Capillary rise in cm and rounded
Fine silt	0.0008	0.0002		
Very fine sand	0.0075	0.0015		
Medium sand	0.03	0.006		
Very coarse sand	0.2	0.1		

Solution to Exercise 4

Return to where text linked to Exercise 4

Exercise 5

Using the image below, calculate the matric potential in each tensiometer. Calculate the hydraulic gradient. Which way is the water flowing?

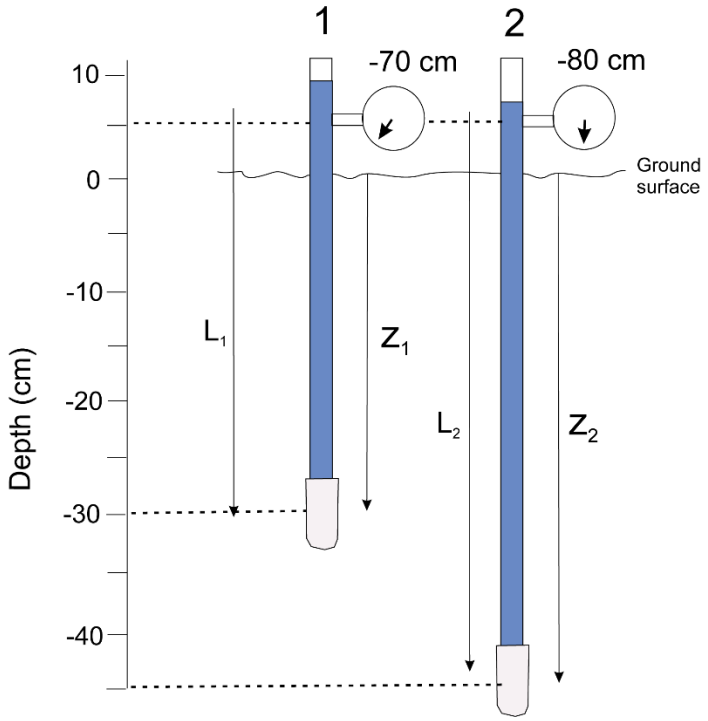

Two tensiometers installed at different depths in the unsaturated zone are shown here with the values displayed on their pressure gauges.

Solution to Exercise 5

Return to where text linked to Exercise 5

Exercise 6

The following diffuse recharge rates were estimated for an aquifer. Calculate the average annual recharge rate and the standard deviation in mm per year. The standard deviation is a measure of how data points are scattered around the estimated mean of a sample data set. A lower standard deviation implies greater confidence in the estimated average whereas the higher standard deviation implies less confidence in the estimate.

If the aquifer has a surface area of 62 km^2, calculate the average annual volumetric recharge rate in m^3 per year.

Table Exercise 6.

Year	Recharge rate (mm/year)
2015	246
2001	312
2017	253
2018	289
2019	320
2020	230

Solution to Exercise 6

Return to where text linked to Exercise 6

Exercise 7

Consider groundwater discharge to a stream as illustrated in Figure 33c. A shallow well is drilled 50 m left of the stream edge (the left edge of the stream). During the rainy season, the water-table elevation in the well is 220 masl and the stream stage is 215 masl. During the dry season, the water-table elevation is 217 masl and the stream stage is 214 masl. If the aquifer has a hydraulic conductivity of 5×10^{-6} m/s, what is the difference in the groundwater discharge (specific discharge or flux) to the stream between the rainy season and the dry season?

Solution to Exercise 7

Return to where text linked to Exercise 7

Exercise 8

The rise and fall of groundwater level observed on a well hydrograph reflects the addition of water to and the release of water from storage, respectively, in the monitored unit. Consider a unit volume (1 m^3) of recently drained aquifer material enclosed in a solid box (1 m x 1 m x 1 m in dimension) with an open top; this would represent an unconfined aquifer open to the atmosphere but with no ability to drain. Ten liters (0.01 m^3) of water are added to the box. The height to which the water level (here, the water table) rises depends on the specific yield (Sy) of the material. If the Sy value is 30 percent (or 0.30), calculate the level to which the water will rise when the 10 liters of recharge is added.

Solution to Exercise 8

Return to where text linked to Exercise 8

Exercise 9

Consider the well hydrograph shown in Figure Box 6-1. The well is completed in an unconfined aquifer with a specific yield value of 0.25. Calculate the recharge rate.

Solution to Exercise 9

Return to where text linked to Exercise 9

Exercise 10

A confined aquifer receives leakage (recharge) from an overlying aquifer through a confining unit (i.e., an aquitard). If the hydraulic head near the bottom of the upper aquifer is 50 masl, the hydraulic head near the top of the confined aquifer is 47 masl, and the confining unit is 30 m thick, calculate the recharge rate in mm per year assuming the hydraulic conductivity of the confining unit is $1x10^{-7}$ m/s.

Solution to Exercise 10

Return to where text linked to Exercise 10

8 References

Abbaspour, K. C., Vaghefi, S. A., Yang, H., & Sriviasan, R. (2019). Global soil, landuse, evapotranspiration, historical and future weather databases for SWAT applications. *Scientific Data*, *6*, 263. https://doi.org/10.1038/s41597-019-0282-4↗.

Acharyya, S., Lahiri, S., Raymahashay, B., & Bhowmik, A. (2000). Arsenic toxicity of groundwater in parts of the Bengal basin in India and Bangladesh: The role of Quaternary stratigraphy and Holocene sea-level fluctuation. *Environmental Geology*, *39*, 1127–1137. https://doi.org/10.1007/s002540000107↗.

Afsin, M., Allen, D. M., Kirste, D., Durukan, G., Gurel, A., & Oruc, O. (2014). Mixing processes in hydrothermal spring systems and implications for interpreting geochemical data: A case study in Cappadocia Region of Turkey. *Hydrogeology Journal*, *22*(1), 7–23. https://doi.org/10.1007/s10040-013-1056-2↗.

Allen, D. M., Grasby, S. E., & Voormeij, D. A. (2006). Determining the circulation depth of thermal springs in the Rocky Mountain Trench, south-eastern British Columbia, Canada using geothermometry and borehole temperature logs. *Hydrogeology Journal*, *14*, 159–172. https://doi.org/10.1007/s10040-004-0428-z↗.

Allen, D. M., Werner, A., & Whitfield, P. H. (2010). Groundwater level responses in mountainous terrain: regime classification, and linkages to climate and streamflow. *Hydrological Processes, 24(23)*, 3392–3412. https://doi.org/10.1002/hyp.7757↗.

Allen, R. G., Jensen, M. E., Wright, J. L., & Burman, R. D. (1989). Operational estimates of reference evapotranspiration. *Agronomy Journal*, *81*(4), 650–662. https://doi.org/10.2134/agronj1989.00021962008100040019x↗.

Allen, R.G., Pereira, L.S., Raes, D., & Smith, M. (1998). Crop evapotranspiration - Guidelines for computing crop water requirements. FAO Irrigation and drainage paper 56. https://www.fao.org/4/X0490E/x0490e00.htm#Contents↗.

Amanambu, A. C., Obarein, O. A., Mossa, J., Li, L., Ayeni, S. S., Balogun, O., Oyebamiji, A., & Ochege, F. U. (2020). Groundwater system and climate change: Present status and future considerations. *Journal of Hydrology, 589*, 125163. https://doi.org/10.1016/j.jhydrol.2020.125163↗.

Anderson J. M., & Wilson, S. B. (1984). Review article: The physical basis of current infrared remote-sensing techniques and the interpretation of data from aerial surveys. *International Journal of Remote Sensing*, *5*(1), 1–18. https://doi.org/10.1080/01431168408948786↗.

Anderson, M. P. (2005). Heat as a ground water tracer. *Groundwater*, *43*(6), 951–968. https://doi.org/10.1111/j.1745-6584.2005.00052.x↗.

Appelo, C. A. J., & Postma, D. (2005). *Geochemistry, groundwater and pollution* (2nd ed.). CRC Press.

Arnell N. (2002). *Hydrology and Global Environmental Change*. Prentice Hall.

Australian Government. (n.d.). *Understanding climate variability and change* (Figure 1). https://www.pacificclimatefutures.net/en/help/climate-projections/understanding-climate-variability-and-change↗.

Autoridad Nacional del Agua. (2015). *Huella hídrica del Peru: Sector agropecuario*. https://repositorio.ana.gob.pe/handle/20.500.12543/197↗.

Bam, E. K. P., Ireson, A. M., van der Kamp, G., & Hendry, J. M. (2020). Ephemeral ponds: Are they the dominant source of depression-focused groundwater recharge? *Water Resources Research*, *56*(3), e2019WR026640. https://doi.org/10.1029/2019WR026640↗.

Baraer, M., McKenzie, J., Mark, B., Gordon, R., Bury, J., Condom, T., Gomez, J., Knox, S., & Fortner, S. (2015). Contribution of groundwater to the outflow from ungauged glacierized catchments: A multi-site study in the tropical Cordillera Blanca, Peru. *Hydrological Processes*, *29*(11). https://doi.org/10.1002/hyp.10386↗.

Barreteau, O., Caballero, Y., Hamilton, S., Jakeman, A. J., & Rinaudo, J.-D. (2016). Disentangling the complexity of groundwater dependent social-ecological systems. In A. J. Jakeman, O. Barreteau, R. J. Hunt, J.-D. Rinaudo, & A. Ross (Eds.), *Integrated groundwater management: Concepts, approaches and challenges*. Springer Open. https://doi.org/10.1007/978-3-319-23576-9_3↗.

Bierkens, M. F. P., & Wada, Y. (2019). Non-renewable groundwater use and groundwater depletion: A review. *Environmental Research Letters*, *14*, 063002. https://doi.org/10.1088/1748-9326/ab1a5f↗.

Boulton, A., & Hancock, P. (2006). Rivers as groundwater-dependent ecosystems: A review of degrees of dependency, riverine processes and management implications. *Australian Journal of Botany*, *54*, 133–144. https://doi.org/10.1071/BT05074↗.

Box, J. E., Colgan, W. T., Christensen, T. R., Schmidt, N. M., Lund, M., Parmentier, F.-J. W., Brown, R., Bhatt, U. S., Euskirchen, E. S., Romanovsky, V. E., Walsh, J. E., Overland, J. E., Wang, M., Corell, R. W., Meier, W. N., Wouters, B., Mård, J., Pawlak, J., & Olsen, M. S. (2019). Key indicators of Arctic climate change: 1971–2017. *Environmental Research Letters*, *14*(4), 045010. https://doi.org/10.1088/1748-9326/aafc1b↗.

Braune, E., & Israel, S. (2021). *Managed aquifer recharge: Southern Africa*. The Groundwater Project. https://doi.org/10.21083/978-1-77470-006-8↗.

Bredehoeft, J. D., & Papadopulos, I. S. (1965). Rates of vertical ground-water movement estimated from the Earth's thermal profile. *Water Resources Research*, *1*(2), 325–328. https://doi.org/10.1029/WR001i002p00325↗.

Brock, T. D. (1994). *Life at high temperatures*. Yellowstone Association for Natural Science, History and Education, Yellowstone National Park. https://archive.org/details/lifeathightemper0000broc↗.

Brooks, R. H., & Corey, A. T. (1964). *Hydraulic properties of porous media*. Hydrology Papers, No. 3, Colorado State U., Fort Collins, Colorado.

Bruce, B. W., Becker, M. F., Pop, L. M., & Gurdak, J. (2003). *Groundwater quality beneath irrigated agriculture in the Central High Plains aquifer 1999–2000, Water-resources investigations report, 03–4219*. US Geological Survey. https://doi.org/10.3133/wri034219↗.

Bryan, K. (1919). Classification of springs. *Journal of Geology*, *27*(7), 522–561. https://doi.org/10.1086/622677↗.

Bryan, T. S. (1995). *Geysers of Yellowstone*. University Press of Colorado.

Burgess, R., & Allen, D. M. (2016). *Groundwater recharge model for Gabriola Island*. Simon Fraser University. gabriola_groundwater_recharge_modelling_report_2016.pdf↗.

Burgess, R. O. (2017). Characterizing recharge to fractured bedrock in a temperate climate. [Master's thesis, Simon Fraser University]. https://summit.sfu.ca/item/17573↗.

Burt, T. P., & Williams, P. J. (1976). Hydraulic conductivity in frozen soils. *Earth Surfaces Processes*, *1*(4), 349–360. https://doi.org/10.1002/esp.3290010404↗.

Caine, J. S., Evans, J. P., & Forster, C. B. (1996). Fault zone architecture and permeability structure. *Geology*, *24*(11), 1025–1028. https://doi.org/10.1130/0091-7613(1996)↗.

Canadian Parks and Wilderness Society and Parks Canada (2005). *Gulf Islands Ecosystem Community Atlas*. Canadian Parks and Wilderness Society – BC Chapter.

Cartwright, K. (1974). Tracing shallow groundwater systems by soil temperatures. *Water Resources Research*, *10*(4), 847–855. https://doi.org/10.1029/WR010i004p00847↗.

Chakraborty, M., Mukherjee, A., & Ahmed, K. M. (2015). A review of groundwater arsenic in the Bengal Basin, Bangladesh and India: From source to sink. *Current Pollution Reports*, *1*, 220–247. https://doi.org/10.1007/s40726-015-0022-0↗.

Chamberlin, T. C. (1885). The requisite and qualifying conditions of artesian wells. *US Geologic Survey Annual Report*, *5*, 131–175.

Chen, X., Leung, L. R., Wigmosta, M., & Richmond, M. (2019). Impact of atmospheric rivers on surface hydrological processes in western U.S. watersheds. *Journal of Geophysical Research: Atmospheres*, *124*(16), 8896–8916. https://doi.org/10.1029/2019JD030468↗.

Cherkauer, K. A., & Lettenmaier, D. P. (1999). Hydrologic effects of frozen soils in the upper Mississippi River basin. *Journal of Geophysical Research*, *104*(D16), 19599–19610. https://doi.org/10.1029/1999JD900337↗.

Clark, I. D., Douglas, M., Raven, K., & Bottomley, D. (2000). Recharge and preservation of Laurentide glacial meltwater in the Canadian Shield. *Groundwater*, *38*(5), 735–742. https://doi.org/10.1111/j.1745-6584.2000.tb02709.x↗.

Clark, I. D., & Fritz, P. (1997). *Environmental isotopes in hydrogeology*. Lewis Publishers.

Cochand, M., Molson, J., Barth, J. A. C., van Geldern, R., Lemieux, J.-M., Fortier, R., & Therrien, R. (2020). Rapid groundwater recharge dynamics determined from hydrogeochemical and isotope data in a small permafrost watershed near Umiujaq (Nunavik, Canada). *Hydrogeology Journal*, *28*(3), 853–868. https://doi.org/10.1007/s10040-020-02109-x↗.

Cohen, A. J. B., & Cherry, J. A. (2020). *Conceptual and visual understanding of hydraulic head and groundwater flow*. The Groundwater Project. https://gw-project.org/books/conceptual-and-visual-understanding-of-hydraulic-head-and-groundwater-flow/↗.

Constantz, J. (2008). Heat as a tracer to determine streambed water exchanges. *Water Resources Research*, *44*(4). https://doi.org/10.1029/2008WR006996↗.

Cook, P. (2020). *Introduction to isotopes and environmental tracers as indicators of groundwater flow*. The Groundwater Project. https://gw-project.org/books/introduction-to-isotopes-and-environmental-tracers-as-indicators-of-groundwater-flow/↗.

Cook, P., & Brunner, P. (2025). *Quantification of Groundwater Recharge*. The Groundwater Project. https://doi.org/10.62592/BAUS7081↗.

Cook, P. G., & Solomon, D. K. (1997). Recent advances in dating young groundwater: Chlorofluorocarbons, $^{3}H^{3}He$ and ^{85}Kr. *Journal of Hydrology*, *191*(1–4), 245–265. https://doi.org/10.1016/S0022-1694(96)03051-X↗.

Corringham, T. W., Ralph, F. M., Gershunov, A., Cayan, D. R., & Talbot, C. A. (2019). Atmospheric rivers drive flood damages in the western United States. *Science Advances*, *5*(12), eaax4631. https://doi.org/10.1126/sciadv.aax4631↗.

Currell, M. J., & Katz, B. G. (Eds.). (2022). *Threats to springs in a changing world: Science and policies for protection*. American Geophysical Union Monograph Series. https://doi.org/10.1002/9781119818625↗.

Cuthbert, M. O. (2010). An improved time series approach for estimating groundwater recharge from groundwater level fluctuations. *Water Resources Research*, *46*(9). https://doi.org/10.1029/2009WR008572↗.

Cuthbert, M. O., Gleeson, T., Moosdorf, N., Befus, K. M., Schneider, A., Hartmann, J., & Lehner, B. (2019). Global patterns and dynamics of climate–groundwater interactions. *Nature Climate Change*, *9*, 137–141. https://doi.org/10.1038/s41558-018-0386-4↗.

de Graaf, I. E. M., Gleeson, T., van Beek, L. P. H., Sutanudjaja, E. H., & Bierkens, M. F. P. (2019). Environmental flow limits to global groundwater pumping, *Nature, 574*, 90–94. https://www.nature.com/articles/s41586-019-1594-4↗.

de Menocal, P., Ortiz, J., Guilderson, T., Adkins, J., Sarnthein, M., Baker, L., & Yarusinsky, M. (2000). Abrupt onset and termination of the African Humid Period: Rapid climate responses to gradual insolation forcing. *Quaternary Science Reviews*, *19*(1–5), 347–361. https://doi.org/10.1016/S0277-3791(99)00081-5↗.

Desconnets, J. C., Taupin, J. D., Lebel, T., & Leduc, C. (1997). Hydrology of the HAPEX-Sahel Central Super-Site: Surface water drainage and aquifer recharge through the pool systems. *Journal of Hydrology*, *188–189*(1–5), 155–178.

Dettinger, M. (2013). Atmospheric rivers as drought busters on the U.S. West Coast. *Journal of Hydrometeorology*, *14*(6), 1721–1732. https://doi.org/10.1175/JHM-D-13-02.1↗.

de Vries, J. J., & Simmers, I. (2002). Groundwater recharge: An overview of processes and challenges. *Hydrogeology Journal*, *10*(1), 5–17. https://doi.org/10.1007/s10040-001-0171-7↗.

Dewandel, B., Ganolfi, J. M., de Condappa, D., & Ahmad, S. (2008). An efficient methodology for estimating irrigation return flow coefficients of irrigated crops at watershed and seasonal scale. *Hydrological Processes*, *22*(11), 1700–1712. https://doi.org/10.1002/hyp.6738↗.

Dillon, P., Stuyfzand, P., Grischek, T., Lluria, M., Pyne, R. D. G., Jain, R. C., Bear, J., Schwarz, J., Wang, W., Fernández, E., Stefan, C., Pettanati, M., van der Gun, J., Sprenger, C., Massmann, G., Scanlon, B. R., Xanke, J., Jokela, P., Zheng, Y., … Sapiano, M. (2019). Sixty years of global progress in managed aquifer recharge. *Hydrogeology Journal*, *27*, 1–30. https://doi.org/10.1007/s10040-018-1841-z↗.

Dingman, S. L. (2002). Physical hydrology (2nd ed.). Prentice-Hall Inc.

Döll, P. (2009). Vulnerability to the impact of climate change on renewable groundwater resources: A global-scale assessment. *Environmental Research Letters*, *4*(3), 035006. https://doi.org/10.1088/1748-9326/4/3/035006↗.

Dralle, D. N., Hahm, W. J., Rempe, D. M., Karst, N. J., Thompson, S. E., & Dietrich, W. E. (2018). Quantification of the seasonal hillslope water storage that does not drive streamflow. *Hydrological Processes*, *32*(13), 1978–1992. https://doi.org/10.1002/hyp.11627↗.

Dralle, D. N., Rossi, G., Georgakakos, P., Hahm, W. J., Rempe, D. M., Blanchard, M., Power, M. E., Dietrich, W. E., & Carlson, S. M. (2023). The salmonid and the subsurface: Hillslope storage capacity determines the quality and distribution of fish habitat. *Ecosphere*, *14*(2), e4436. https://doi.org/10.1002/ecs2.4436↗.

Dralle, D. N., Rossi, G., Georgakakos, P., Hahm, W. J., Rempe, D. M., Blanchard, M., Power, M., Dietrich, W. E., & Carlson, S. M. (2024). Salmon and the subsurface. *California WaterBlog*. https://californiawaterblog.com/2024/06/09/salmon-and-the-subsurface/↗.

Drury, M. J. (1990). Fluid flow in the crystalline crust: Detecting fractures by temperature logs. In A. E. Beck, G. Garven, & L. Stegena (Eds.), *Hydrological regimes and their subsurface thermal effects*. Geophysical Monograph 47, International Union of Geodesy and Geophysics and American Geophysical Union. https://doi.org/10.1029/GM047p0129↗.

Eamus, D., & Froend, R. (2006). Groundwater-dependent ecosystems: The where, what and why of GDEs. *Australian Journal of Botany*, *54*(2), 91–96. https://doi.org/10.1071/BT06029↗.

Eamus, D., Fu, B., Springer, A. E., & Stevens, L. E. (2016). Groundwater dependent ecosystems: Classification, identification techniques and threats. In A. J. Jakeman, O. Barreteau, R. J. Hunt, J.-D. Rinaudo, & A. Ross (Eds.), *Integrated groundwater*

management: Concepts, approaches and challenges. Springer Cham, https://doi.org/10.1007/978-3-319-23576-9_13↗.

Edmunds, W. M., Ahmed, K. M., & Whitehead, P. G. (2015). A review of arsenic and its impact in groundwater of the Ganges-Brahmaputra-Meghna delta, Bangladesh. *Environmental Science: Processes & Impacts*, *17*(6), 1032–1046. https://doi.org/10.1039/c4em00673a↗.

Eldardiry, H., Mahmood, A., Chen, X., Hossain, F., Nijssen, B., & Lettenmaier, D. P. (2019). Atmospheric river–induced precipitation and snowpack during the western United States cold season. *Journal of Hydrometeorology*, *20*(4), 613–630. https://doi.org/10.1175/JHM-D-18-0228.1↗.

Falkland, A. (Ed.). (1991). Hydrology and water resources of small islands: A practical guide. United Nations Educational, Scientific, and Cultural Organization (UNESCO). https://www.ircwash.org/resources/hydrology-and-water-resources-small-islands-practical-guide↗.

Famiglietti, J. S. (2014). The global groundwater crisis. *Nature Climate Change*, *4*(11), 944–948. https://doi.org/10.1038/nclimate2425↗.

Famiglietti, J. S., Lo, M., Ho, S. L., Bethune, J., Anderson, K. J., Syed, T. H., Swenson, S. C., de Linage, C. R., & Rodell, M. (2011). Satellites measure recent rates of groundwater depletion in California's Central Valley. *Geophysical Research Letters*, *38*(3). https://doi.org/10.1029/2010GL046442↗.

Fernández-Escalante, E., Foster, S., & Navarro-Benegas, R. (2020). Evolution and sustainability of groundwater use from the Ica aquifers for the most profitable agriculture in Peru. *Hydrogeology Journal*, *28*, 2601–2612. https://doi.org/10.1007/s10040-020-02203-0↗.

Feth, J. H. (1954). Investigation of geology and occurrence of water in the Weber Basin Project area, Farmington to Willard, Utah: A progress report. *Utah State Engineer, Technical Publication*, *9*, 121–128.

Feth, J. H. (1964). Hidden recharge. *Groundwater*, *2*(4), 14–17. https://doi.org/10.1111/j.1745-6584.1964.tb01780.x↗.

Fetter, C. W. (2001). Applied hydrogeology (4th ed.). Prentice Hall.

Fleming, S. W., & Quilty, E. J. (2006). Aquifer responses to El Niño-Southern Oscillation, southwest British Columbia. *Groundwater*, *44*(4), 595–599. https://doi.org/10.1111/j.1745-6584.2006.00187.x↗.

Forster, C., & Smith, L. (1988). Groundwater flow systems in mountainous terrain: 2. Controlling factors. *Water Resources Research*, *24*(7), 1011–1023. https://doi.org/10.1029/WR024i007p01011↗.

Fournier, R. O. (1977). Chemical geothermometers and mixing models for geothermal systems. *Geothermics*, *5*(1–4), 41–50. https://doi.org/10.1016/0375-6505(77)90007-4↗.

Fournier, R. O. (1981). Application of water geochemistry to geothermal exploration and reservoir engineering (Ch 4). In L. Rybach, & L. J. P. Muffler (Eds.), *Geothermal systems: principles and case histories*, pp. 109–143. Wiley.

Fournier, R. O., & Truesdell, A. H. (1973). An empirical Na-K-Ca geothermometer for natural waters. *Geochimica et Cosmochimica Acta*, *37*, 1255–1275. https://doi.org/10.1016/0016-7037(73)90060-4↗.

Freeze, R. A. (1972). Role of subsurface flow in generating surface runoff: 2. Upstream source areas. *Water Resources Research*, *8*(5), 1272–1283. https://doi.org/10.1029/WR008i005p01272↗.

Freeze, R. A. (1974). Streamflow generation. *Reviews of Geophysics*, *12*(4), 627–647. https://doi.org/10.1029/RG012i004p00627↗.

Freeze, R. A., & Cherry, J. A. (1979). *Groundwater*. Prentice-Hall. https://gw-project.org/books/groundwater/↗.

Froend, R., & Sommer, B. (2010). Phreatophytic vegetation response to climatic and abstraction induced groundwater drawdown: Examples of long-term spatial and temporal variability in community response. *Ecological Engineering*, *36*(9), 1191–1200. https://doi.org/10.1016/j.ecoleng.2009.11.029↗.

Fuller, M. L. (1904). *Underground waters of eastern United States* [Water Supply Paper 114]. US Geological Survey. https://doi.org/10.3133/wsp114↗.

Gaber, M. S. (2005). *Michigan flowing well handbook*. Michigan Department of Environmental Quality Water Bureau. https://www.michigan.gov/documents/deq/deq-wb-dwehs-wcu-flowwellhandbook_221323_7.pdf↗.

Gale, I. N. (Ed.) (2005). Strategies for managed aquifer recharge (MAR) in semi-arid areas. United Nations Educational, Scientific and Cultural Organization (UNESCO). https://recharge.iah.org/files/2017/01/Gale-Strategies-for-MAR-in-semiarid-areas.pdf↗.

Gillett, N. P., Cannon, A. J., Malinina, E., Schnorbus, M., Anslow, F., Sun, Q., Kirchmeier-Young, M., Zwiers, F., Seiler, C., Zhang, X., Flato, G., Wan, H., Li, G., & Castellan, A. (2022). Human influence on the 2021 British Columbia floods. *Weather and Climate Extremes*, *36*, 100441. https://doi.org/10.1016/j.wace.2022.100441↗.

Gleeson T., & Richter, B. (2018). How much groundwater can we pump and protect environmental flows through time? Presumptive standards for conjunctive management of aquifers and rivers. *River Research and Applications*, *34*(1), 83–92. https://doi.org/10.1002/rra.3185↗.

Graham, G., Allen, D. M., & Finkbeiner, B. (2014). Climate controls on nitrate concentration variability in the Abbotsford-Sumas aquifer, British Columbia, Canada. *Environmental Earth Sciences Journal*, *73*(6), 2895–2907. https://doi.org/10.1007/s12665-014-3072-5↗.

Granger, R. J., Gray, D. M., & Dyck, G. E. (1984). Snowmelt infiltration to frozen prairie soils. *Canadian Journal of Earth Sciences*, *21*(6), 669–677. https://doi.org/10.1139/e84-073↗.

Grasby, S. E., & Hutchinson, I. (2001). Controls on the distribution of thermal springs in the southern Canadian Cordillera. *Canadian Journal of Earth Sciences*, *38*(3), 427–440. https://doi.org/10.1139/e00-091↗.

Grasby, S. E., Hutcheon, I., & Krouse, H. R. (2000). The influence of water–rock interaction on the chemistry of thermal springs in western Canada. *Applied Geochemistry*, *15*(4), 439–454. https://doi.org/10.1016/S0883-2927(99)00066-9↗.

Grasby, S. E., & Lepitzki, D. A. W. (2002). Physical and chemical properties of the Sulphur Mountain thermal springs, Banff National Park, and implications for endangered snails. *Canadian Journal of Earth Sciences*, *39*(9), 1349–1361. https://doi.org/10.1139/e02-056↗.

Green, T., Taniguchi, M., Kooi, H., Gurdak, J., Hiscock, K., Allen, D., Treidel, H., & Aureli, A. (2011). Beneath the surface of global change: Impacts of climate change on groundwater. *Journal of Hydrology*, *405*(3–4), 532–560. https://doi.org/10.1016/j.jhydrol.2011.05.002↗.

Green, W. H., & Ampt, G. A. (1911). Studies in soil physics, part 1: The flow of air and water through soils. *Journal of Agricultural Science*, *4*(1), 1–24. https://doi.org/10.1017/S0021859600001441↗.

Guo, H., Jiao, J.J., and Weeks, E P. 2008. Rain-induced subsurface airflow and Lisse effect. Water Resources Research, vol. 44, no. 7. pp. 1–9. https://doi-org.mines.idm.oclc.org/10.1029/2007WR006294↗.

Gurdak, J. J., Hanson, R. T., & Green, T. R. (2009). *Effects of climate variability on groundwater resources of the United States* [Fact Sheet 2009-3074]. US Geological Survey. https://doi.org/10.3133/fs20093074↗.

Hahm, W. J., Rempe, D. M., Dralle, D. N., Dawson, T. E., Lovill, S. M., Bryk, A. B., Bish, D. L., Schieber, J., & Dietrich, W. E. (2019). Lithologically controlled subsurface critical zone thickness and water storage capacity determine regional plant community composition. *Water Resources Research*, *55*(4), 3028–3055. https://doi.org/10.1029/2018WR023760↗.

Haitjema, H. M., & Mitchell-Bruker, S. (2005). Are water tables a subdued replica of the topography? *Groundwater*, *43*(6), 781–786. https://doi.org/10.1111/j.1745-6584.2005.00090.x↗.

Handcock, R. N., Gillespie, A. R., Cherkauer, K. A., Kay, J. E., Burges, S. J., & Kampf, S. K. (2006). Accuracy and uncertainty of thermal-infrared remote sensing of stream temperatures at multiple spatial scales. *Remote Sensing of Environment*, *100*(4), 427–440. https://doi.org/10.1016/j.rse.2005.07.007↗.

Hanson, R. T., Dettinger, M. D., & Newhouse, M. W. (2006). Relations between climatic variability and hydrologic time series from four alluvial basins across the

southwestern United States. *Hydrogeology Journal*, *14*, 1122–1146. https://doi.org/10.1007/s10040-006-0067-7↗.

Hare, D. K., Helton, A. M., Johnson, Z. C., Lane, J. W., & Briggs, M. A. (2021). Continental-scale analysis of shallow and deep groundwater contributions to streams. *Nature Communications*, *12*, Article 1450. https://doi.org/10.1038/s41467-021-21651-0↗.

Hayashi, M. (2013). The cold vadose zone: Hydrological and ecological significance of frozen-soil processes. *Vadose Zone Journal*, *12*(4), 1–8. https://doi.org/10.2136/vzj2013.03.0064↗.

Hayashi, M., van der Kamp, G., & Schmidt, R. (2003). Focused infiltration of snowmelt water in partially frozen soil under small depressions. *Journal of Hydrology*, *270*(3–4), 214–229. https://doi.org/10.1016/S0022-1694(02)00287-1↗.

He, H., Aogu, K., Li, M., Xu, J., Sheng, W., Jones, S. B., González-Teruel, J. D., Robinson, D. A., Horton, R., Bristow, K., Dyck, M., Filipović, V., Noborio, K., Wu, Q., Jin, H., Feng, H., Si, B., Lv, J. (2021). Chapter 3 - A review of time domain reflectometry (TDR) applications in porous media. *Advances in Agronomy*, *168*, 83–155. https://doi.org/10.1016/bs.agron.2021.02.003↗.

Healy, R. W. (2010). *Estimating groundwater recharge*. Cambridge University Press.

Healy, R. W., & Cook, P. G. (2002). Using groundwater levels to estimate recharge. *Hydrogeology Journal*, *10*, 91–109. https://doi.org/10.1007/s10040-001-0178-0↗.

Hillel, D. (1980). *Fundamentals of soil physics*. Academic Press. https://doi.org/10.1016/C2009-0-03109-2↗.

Holman, I. P., Rivas-Casado, M., Howden, N. J. K., Bloomfield, J. P., & Williams, A. T. (2009). Linking North Atlantic Ocean–atmosphere teleconnection patterns and hydrogeological responses in temperate groundwater systems. *Hydrological Processes*, *23*, 3123–3126. https://doi.org/10.1002/hyp.7466↗.

Hooghoudt, S. B. (1947). Waarnemingen van grondwaterstanden voor de landbouw; Commissie voor Hydrologisch Onderzoek TNO. *Verslagen Technische Bijeenkomsten* 1–6, 94–110. The Hague.

Horton, R. E. (1933). The role of infiltration in the hydrologic cycle. *Transactions American Geophysical Union*, *14*(1), 446–460. https://doi.org/10.1029/TR014i001p00446↗.

Hrachowitz, M., Savenije, H. H. G., Blöschl, G., McDonnell, J. J., Sivapalan, M., Pomeroy, J. W., Arheimer, B., Blume, T., Clark, M. P., Ehret, U., Fenicia, F., Freer, J. E., Gelfan, A., Gupta, H. V., Hughes, D. A., Hut, R. W., Montanari, A., Pande, S., Tetzlaff, D., Troch, P. A., Uhlenbrook, S., … Cudennec, C. (2013). A decade of predictions in ungauged basins (PUB): A review. *Hydrological Sciences Journal*, *58*(6), 1198–1255. https://doi.org/10.1080/02626667.2013.803183↗.

Hurwitz, S., & Manga, M. (2017). The fascinating and complex dynamics of geyser eruptions. *Annual Review of Earth and Planetary Sciences*, *45*, 31–59. https://doi.org/10.1146/annurev-earth-063016-015605↗.

Hurwitz, S., King, J. C., Pederson, G. T., Martin, J. T., Damby, D. E., Manga, M., Hungerford, J. D. G., & Peek, S. (2020). Yellowstone's Old Faithful Geyser shut down by a severe thirteenth century drought. *Geophysical Research Letters*, *47*(20), e2020GL089871. https://doi.org/10.1029/2020GL089871↗.

IAH (International Association of Hydrogeologists). 2020. IAH Commission for Managing Aquifer Recharge. https://recharge.iah.org/

IGRAC (International Groundwater Resources Assessment Centre). (2020). Transboundary aquifers of the world. https://ggis.un-igrac.org/view/tba/

IPCC (Intergovernmental Panel on Climate Change). (2021). *Climate Change 2021: The physical science basis*. Cambridge University Press. https://doi.org/10.1017/9781009157896↗.

Izbicki, J. A., Radyk, J., & Michel, R. L. (2000). Water movement through a thick unsaturated zone underlying an intermittent stream in the western Mojave Desert, southern California, USA. *Journal of Hydrology*, *238*, 194–217. https://doi.org/10.1016/S0022-1694(00)00331-0↗.

Jacob, C. E. (1940). On the flow of water in an elastic artesian aquifer. *Eos, Transactions American Geophysical Union*, *21*(2), 574–586. https://doi.org/10.1029/TR021i002p00574↗.

James, I. (2015, December 10). The costs of Peru's farming boom. *Desert Sun*. http://www.desertsun.com/story/news/environment/2015/12/10/costs-perusfarming-boom/76605530/↗.

Jiang, X.-W., & Cherry, J. (2024). *History and hydraulics of flowing wells*. The Groundwater Project. https://doi.org/10.21083/CPET1503↗.

Kalbus, E., Reinstorf, F., & Schirmer, M. (2006). Measuring methods for groundwater-surface water interactions: A review. *Hydrology and Earth System Sciences*, *10*(6), 873–887. https://doi.org/10.5194/hess-10-873-2006↗.

Kane, D. L. (1980). Snowmelt infiltration into seasonally frozen soils. *Cold Regions Science and Technology*, *3*(2–3), 153–161. https://doi.org/10.1016/0165-232X(80)90020-8↗.

Kane, D. L., Yoshikawa, K., & McNamara, J. P. (2013). Regional groundwater flow in an area mapped as continuous permafrost, NE Alaska (USA). *Hydrogeology Journal*, *21*(1), 41–52. https://doi.org/10.1007/s10040-012-0937-0↗.

Kløve, B., Ala-aho, P., Bertrand, G., Boukalova, Z., Erturk, A., Goldscheider, N., Ilmonen, J., Karakaya, N., Kupfersberger, H., Kvœrner, J., Lundberg, A., Mileusnić, M., Moszczynska, A., Muotka, T., Preda, E., Rossi, P., Siergieiev, D., Šimek, J., Wachniew, … Widerlund, A. (2011). Groundwater dependent ecosystems. Part I: Hydroecological status and trends. *Environmental Science & Policy*, *14*(7), 770–781. https://doi.org/10.1016/j.envsci.2011.04.002↗.

Kløve, B., Ala-Aho, P., Bertrand, G., Gurdak, J., Kupfersberger, H., Kværner, J., Muotkaet, T., Mykra, H., Preda, E., Rossi, P., Uov, C., Velasco, E., & Pulido-Velazquez, M.

(2014). Climate change impacts on groundwater and dependent ecosystems. *Journal of Hydrology*, *518*, 250–266. https://doi.org/10.1016/j.jhydrol.2013.06.037

Konikow, L. F., & Bredehoeft, J. D. (2020). Groundwater resource development: Effects and sustainability.https://gw-project.org/books/groundwater-resource-development/↗.

Konikow, L. F., & Leake, S. A. (2014). Depletion and capture: Revisiting "the source of water derived from wells." *Groundwater*, *52*(S1), 100–111. https://doi.org/10.1111/gwat.12204↗.

Lapham, W. W. (1989). Use of temperature profiles beneath streams to determine rates of vertical ground-water flow and vertical hydraulic conductivity [Water Supply Paper 2337, pp. 1–35]. US Geological Survey. https://doi.org/10.3133/wsp2337↗.

Larned, S. (2012). Phreatic groundwater ecosystems: Research frontiers in freshwater ecology. *Freshwater Biology*, *57*(5), 885–906. https://doi.org/10.1111/j.1365-2427.2012.02769.x↗.

Le Maitre, D. C., Scott, D. F., & Colvin, C. (1999). A review of information on interactions between vegetation and groundwater. *Water SA*, *25*(2), 137–152.

Lemieux J.-M., Fortier. R., Talbot-Poulin, M. C., Molson, J., Therrien, R., Ouellet, M., Banville, D., Cochand, M., & Murray, R. (2016). Groundwater occurrence in cold environments: Examples from Nunavik. *Hydrogeology Journal*, *24*(6), 1497–1513. https://doi.org/10.1007/s10040-016-1411-1↗.

Lerner, D. N., Issar, A. S., & Simmers, I. (1990). Groundwater recharge: A guide to understanding and estimating natural recharge (Vol. 8, International Contributions to Hydrogeology). *Journal of Environmental Quality*, *21*(3), 512. https://doi.org/10.2134/jeq1992.00472425002100030036x↗.

Lézine, A.-M., Hély, C., Grenier, C., Braconnot, P., & Krinner, G. (2011). Sahara and Sahel vulnerability to climate changes: Lessons from Holocene hydrological data. *Quaternary Science Reviews*, *30*(21–22), 3001–3012. https://doi.org/10.1016/j.quascirev.2011.07.006↗.

Liakopoulos, A. C. (1965). Theoretical solution of the unsteady unsaturated flow problems in soils. *Bulletin, International Association of Scientific Hydrology*, *10*, 5–39. https://doi.org/10.1080/02626666509493368↗.

Link, P., Simonin, K., Maness, H., Oshun, J., Dawson, T., & Fung, I. (2014). Species differences in the seasonality of evergreen tree transpiration in a Mediterranean climate: Analysis of multiyear, half-hourly sap flow observations. *Water Resources Research*, *50*(3), 1869–1894. https://doi.org/10.1002/2013WR014023↗.

Liu, P.-W., Famiglietti, J. S., Purdy, A. J., Adams, K. H., McEvoy, A. L., Reager, J. T., Bindlish, R., Wiese, D. N., David, C. H., & Rodell, M. (2022). Groundwater depletion in California's Central Valley accelerates during megadrought. *Nature Communications*, *13*, Article 7825. https://doi.org/10.1038/s41467-022-35582-x↗.

Lock, J., Kelsey, H., Furlong, K., & Woolace, A. (2006). Late Neogene and Quaternary landscape evolution of the northern California Coast Ranges: Evidence for

Mendocino triple junction tectonics. *Geological Society of America Bulletin*, *118*(9–10), 1232–1246. https://doi.org/10.1130/b25885.1↗.

Logan, W. S., & Rudolph, D. L. (1997). Microdepression-focused recharge in a coastal wetland, La Plata, Argentina. *Journal of Hydrology*, *194*(1–4), 221–238. https://doi.org/10.1016/S0022-1694(96)03205-2↗.

Lopez, D. L., & Smith, L. (1995). Fluid flow in fault zones: Analysis of the interplay of convective circulation and topographically driven groundwater flow. *Water Resources Research*, *31*(6), 1489–1503. https://doi.org/10.1029/95WR00422↗.

Lovill, S. M., Hahm, W. J., & Dietrich, W. E. (2018). Drainage from the critical zone: lithologic controls on the persistence and spatial extent of wetted channels during the summer dry season. *Water Resources Research*, *54*(8), 5702–5726. https://doi.org/10.1029/2017WR021903↗.

Luque-Espinar, J. A., Chica-Olmo, M., Pardo-Igùzquiza, E., & García-Soldado, M. J. (2008). Influence of climatological cycles on hydraulic heads across a Spanish aquifer. *Journal of Hydrology*, *354*(1–4), 33–52. https://doi.org/10.1016/j.jhydrol.2008.02.014↗.

Markovich, K., Manning, A. H., Condon, L. E., & McIntosh, J. C. (2019). Mountain-block recharge: A review of current understanding. *Water Resources Research*, *55*, 8278–8304. https://doi.org/10.1029/2019WR025676↗.

Masoud, M. H., Schneider, M., & El Osta, M. M. (2013). Recharge flux to the Nubian Sandstone aquifer and its impact on the present development in southwest Egypt. *Journal of African Earth Sciences*, *85*, 115–124. https://doi.org/10.1016/j.jafrearsci.2013.03.009↗.

McCormick, E. L., Dralle, D. N., Hahm, W. J., Tune, A. K., Schmidt, L. M., Chadwick, K. D., & Rempe, D. M. (2021). Widespread woody plant use of water stored in bedrock. *Nature*, *597*(7875), 225–229. https://doi.org/10.1038/s41586-021-03761-3↗.

McGowan, K. T., & Martin, J. B. (2007). Chemical composition of mangrove-generated brines in Bishop Harbor, Florida: interactions with submarine groundwater discharge. *Marine Chemistry, 104(1-2)*, 58-68.

Meinzer, O. E. (1923). *Outline of ground-water hydrology, with definitions* [Water Supply Paper 494]. US Geological Survey. https://doi.org/10.3133/wsp494↗.

Meixner, T., Manning, A. H., Stonestrom, D. A., Allen, D. M., Ajami, H., Blasch, K. W., Brookfield, A. E., Castro, C. L., Clark, J. F., Gochis, D. J., Flint, A. L., Neff, K. L., Niraula, R., Rodell, M., Scanlon, B. R., Singha, K., & Walvoord, M. (2016). Implications of projected climate change for groundwater recharge in the western United States. *Journal of Hydrology*, *534*, 124–138. https://doi.org/10.1016/j.jhydrol.2015.12.027↗.

Meyboom, P. (1965). Three observations on streamflow depletion by phreatophytes. *Journal of Hydrology*, *2*(3), 248–261. https://doi.org/10.1016/0022-1694(65)90040-5↗.

Meyboom, P. (1966a). Groundwater studies in the Assiniboine River drainage basin, part I, evaluation of a flow system in south-central Saskatchewan. *Geological Survey of Canada, Bulletin, 139*. https://doi.org/10.4095/100701↗.

Meyboom, P. (1966b). Unsteady groundwater flow near a willow ring in hummocky moraine. *Journal of Hydrology, 4*, 38–62. https://doi.org/10.1016/0022-1694(66)90066-7↗.

Meyboom, P. (1967). Groundwater studies in the Assiniboine River drainage basin, part II, hydrologic characteristics of phreatophytic vegetation in south-central Saskatchewan. *Geological Survey of Canada, Bulletin, 139*, 64. https://doi.org/10.4095/101495↗.

Minagri, A. N. A., & Cosude, W. W. F. (2015). *Huella hídrica del Perú. Sector agropecuario* [Peru's water footprint. Agricultural sector]. https://www.wwfca.org/?253691/huella-hidrica-del-peru-sector-agropecuario↗.

Mohammed, A. A., Kurylyk, B. L., Cey, E. E., & Hayashi, M. (2018). Snowmelt infiltration and macropore flow in frozen soils: Overview, knowledge gaps, and a conceptual framework. *Vadose Zone Journal*, *17*(1), 180084. https://doi.org/10.2136/vzj2018.04.0084↗.

Mu, Q., Zhao, M., & Running, S. W. (2011). Improvements to a MODIS global terrestrial evapotranspiration algorithm. *Remote Sensing of Environment*, *115*(8), 1781–1800. https://doi.org/10.1016/j.rse.2011.02.019↗.

Mundhenk, B. D., Barnes, E. A., & Maloney, E. D. (2016). All-season climatology and variability of atmospheric river frequencies over the North Pacific. *Journal of Climate*, *29*(13), 4885–4903. https://doi.org/10.1175/JCLI-D-15-0655.1↗.

Nathan, R. J., & McMahon, T. A. (1990). Evaluation of automated techniques for base flow and recession analyses. *Water Resources Research*, *26*(7), 1465–1473. https://doi.org/10.1029/WR026i007p01465↗.

Navarro, R. (2015). Recarga artificial en el acuífero del valle de Ica durante 2014–15 [Artificial recharge in the Ica Valley Aquifer during 2014–15]. *JUASVI Informe, Ica, Peru*.

Negm, A., Abdrakhimova, P., Hayashi, M., & Rasouli, K. (2021). Effects of climate change on depression-focused groundwater recharge in the Canadian Prairies. *Vadose Zone Journal*, *20*(5), e20153. https://doi.org/10.1002/vzj2.20153↗.

Newbury, R. W., Cherry, J. A., & Cox, R. A. (1969). Groundwater-streamflow systems in Wilson Creek Experimental Watershed, Manitoba. *Canadian Journal of Earth Sciences*, *6*, 613–623. https://doi.org/10.1139/e69-060↗.

Newton, B. W., Farjad, B., & Orwin, J. F. (2021). Spatial and temporal shifts in historic and future temperature and precipitation patterns related to snow accumulation and melt regimes in Alberta, Canada. *Water*, *13*(8), 1013. https://doi.org/10.3390/w13081013↗.

Nott, A. H. (2024). *Groundwater response to extreme weather events in various hydrogeological regimes across southern British Columbia* [Master's thesis, Simon Fraser University]. Summit Research Repository. https://summit.sfu.ca/item/38215↗.

Oshun, J., Dietrich, W. E., Dawson, T. E., & Fung, I. (2016). Dynamic, structured heterogeneity of water isotopes inside hillslopes. *Water Resources Research*, *52*(1), 164–189. https://doi.org/10.1002/2015WR017485↗.

Owor, M., Taylor, R. G, Tindimugaya, C., & Mwesigwa, D. (2009). Rainfall intensity and groundwater recharge: Empirical evidence from the upper Nile basin. *Environmental Research Letters*, *4*(3), 035009. https://doi.org/10.1088/1748-9326/4/3/035009↗.

Pavlovskii, I., Hayashi, M., & Cey, E. E. (2019). Estimation of depression-focussed groundwater recharge using chloride mass balance: Problems and solutions across scales. *Hydrogeology Journal*, *27*, 2263–2278. https://doi.org/10.1007/s10040-019-01993-2↗.

Payne, A. E., Demory, M. -E., Leung, L. R., Ramos, A. M., Shields, C. A., Rutz, J. J., Siler, N., Villarini, G., Hall, A., & Ralph, F. M. (2020). Responses and impacts of atmospheric rivers to climate change. *Nature Reviews Earth & Environment*, *1*, 143–157. https://doi.org/10.1038/s43017-020-0030-5↗.

Pearson, F. J., & White, D. E. (1967). Carbon 14 ages and flow rates of water in Carrizo Sand, Atascosa County, Texas. *Water Resources Research*, *3*(1), 251–261. https://doi.org/10.1029/WR003i001p00251↗.

Penman, H. L. (1948). Natural evaporation from open water, bare soil, and grass. *Royal Society of London Proceedings, Series A*, *193*, 120–145. https://doi.org/10.1098/rspa.1948.0037↗.

Penman, H. L. (1956). Evaporation: An introductory survey. *Netherlands Journal of Agricultural Sciences*, *4*, 9–29. https://doi.org/10.18174/njas.v4i1.17768↗.

Perez-Valdivia, C., Sauchyn, D., & Vanstone, J. (2012). Groundwater levels and teleconnection patterns in the Canadian Prairies. *Water Resources Research*, *48*(7). https://doi.org/10.1029/2011WR010930↗.

Petrone, K. C., Hughes, J. D., van Niel, T. G., & Silberstein, R. P. (2010). Streamflow decline in southwestern Australia, 1950–2008. *Geophysical Research Letters*, *37*(11). https://doi.org/10.1029/2010GL043102↗.

Phillip, J. R. (1957). Evaporation, and moisture and heat fields in the soil. *Journal of Meteorology*, *14*(4), 354–366. https://doi.org/10.1175/1520-0469(1957) ↗.

Poeter, E., Fan, Y., Cherry, J., Wood, W., & Mackay, D. (2020). *Groundwater in our water cycle: Getting to know Earth's most important fresh water source*. The Groundwater Project. https://doi.org/10.21083/978-1-7770541-1-3↗.

Poeter, E., & Hsieh, P. (2020). *Graphical construction of groundwater flow nets*. The Groundwater Project. https://gw-project.org/books/graphical-construction-of-groundwater-flow-nets/↗.

Pohlmeier, A. (2011). Magnetic resonance imaging in soil science. In J. Gliński, J. Horabik, & J. Lipiec (Eds.), *Encyclopedia of agrophysics*. Encyclopedia of Earth Sciences Series. Springer. https://doi.org/10.1007/978-90-481-3585-1_255↗.

Province of British Columbia. (2024). *Groundwater level data*. Provincial Groundwater Observation Well Network. https://governmentofbc.maps.arcgis.com/apps/webappviewer/index.html↗.

Prueger, J. H., Hatfield, J. L., Aase, J. K., & Pikul J. L, Jr. (1997). Bowen-ratio comparisons with lysimeter evapotranspiration. *Agronomy Journal*, *89*(5), 730–736. https://doi.org/10.2134/agronj1997.00021962008900050004x↗.

Ralph, F. M., & Dettinger, M. D. (2011). Storms, floods, and the science of atmospheric rivers. *Eos, Transactions American Geophysical Union*, *92*(32), 265–266. https://doi.org/10.1029/2011EO320001↗.

Rasmussen, T. C., & Crawford, L. A. (1997). Identifying and removing barometric pressure effects in confined and unconfined aquifers. *Groundwater*, *35*(3), 502–511. https://doi.org/10.1111/j.1745-6584.1997.tb00111.x↗.

Rathay, S. (2016). *Response of a fractured bedrock aquifer to recharge from heavy rainfall events*. [Master's thesis, Simon Fraser University]. Summit Research Repository https://summit.sfu.ca/item/16943↗.

Rathay, S., Allen, D. M., & Kirste, D. (2018). Response of a fractured bedrock aquifer to recharge from heavy rainfall events. *Journal of Hydrology*, *561*, 1048–1062. https://doi.org/10.1016/j.jhydrol.2017.07.042↗.

Rempe, D. M., & Dietrich, W. E. (2014). A bottom-up control on fresh-bedrock topography under landscapes. *Proceedings of the National Academy of Sciences*, *111*(18), 6576–6581. https://doi.org/10.1073/pnas.1404763111↗.

Rempe, D. M., & Dietrich, W. E. (2018). Direct observations of rock moisture, a hidden component of the hydrologic cycle. *Proceedings of the National Academy of Sciences*, *115*(11), 2664–2669. https://doi.org/10.1073/pnas.1800141115↗.

Rengasamy, P. (2006). World salinization with emphasis on Australia. *Journal of Experimental Botany*, *57*(5), 1017–1023. https://doi.org/10.1093/jxb/erj108↗.

Richards, A. L. (1931). Capillary conduction of liquids through porous media. *Physics*, *1*(5), 316–333. https://doi.org/10.1063/1.1745010↗.

Riebe, C. S., Hahm, W. J., & Brantley, S. L. (2017). Controls on deep critical zone architecture: A historical review and four testable hypotheses. *Earth Surface Processes and Landforms*, 42(1), 128–156. https://doi.org/10.1002/esp.4052↗.

Rivera, A. (Ed.). (2013). *Canada's groundwater resources*. Fitzhenry & Whiteside.

Rodell, M., Famiglietti, J. S., Wiese, D. N., Reager, J. T., Beaudoing, H. K., Landerer, F. W., & Lo, M.-H. (2018). Emerging trends in global freshwater availability. *Nature*, *557*, 651–659. https://doi.org/10.1038/s41586-018-0123-1↗.

Roeper, T., Greskowiak, I., & Massmann, G. (2014). Detecting small groundwater discharge springs using handheld thermal infrared imagery. *Groundwater*, *52*(6), 936–942. https://doi.org/10.1111/gwat.12145↗.

Rorabough, M. I. (1964). Estimating changes in bank storage and groundwater contribution to streamflow. *International Association of Scientific Hydrology Publication*, *63*, 432–441.

Saaty, T. L. (1980). *The analytical hierarchy process*. McGraw Hill.

Salve, R., Rempe, D. M., & Dietrich, W. E. (2012). Rain, rock moisture dynamics, and the rapid response of perched groundwater in weathered, fractured argillite underlying a steep hillslope. *Water Resources Research*, *48*(11). https://doi.org/10.1029/2012WR012583↗.

Scanlon, B. R., & Goldsmith, R. S. (1997). Field study of spatial variability in unsaturated flow beneath and adjacent to playas. *Water Resources Research*, *33*(10), 2239–2252. https://doi.org/10.1029/97WR01332↗.

Scanlon, B. R., Healy, R., & Cook, P. (2002). Choosing appropriate techniques for quantifying groundwater recharge. *Hydrogeology Journal*, *10*(1), 18–39. https://doi.org/10.1007/s10040-001-0176-2↗.

Scanlon, B. R., Jolly, I., Sophocleous, M., & Zhang, L. (2007). Global impacts of conversions from natural to agricultural ecosystems on water resources: Quantity versus quality. *Water Resources Research*, *43*(3). https://doi.org/10.1029/2006WR005486↗.

Schneider, R. (1964). Relation of temperature distribution to ground-water movement in carbonate rocks of central Israel. *Geological Society of America Bulletin*, *75*(3), 209–216. https://doi.org/10.1130/0016-7606(1964)75[209:ROTDTG]2.0.CO;2↗.

Scibek, J., Allen, D. M., Cannon, A., & Whitfield, P. H. (2007). Groundwater-surface water interaction under scenarios of climate change using a high-resolution transient groundwater model. *Journal of Hydrology*, *333*(2–4), 165–181. https://doi.org/10.1016/j.jhydrol.2006.08.005↗.

Scott, C. P., Lohman, R. B., & Jordan, T. E. (2017). InSAR constraints on soil moisture evolution after the March 2015 extreme precipitation event in Chile. *Scientific Reports*, *7*, 4903. https://doi.org/10.1038/s41598-017-05123-4↗.

Shabbar, A., Bonsal, B., & Khandekar, M. (1997). Canadian precipitation patterns associated with the southern oscillation. *Journal of Climate*, *10*(12), 3016–3027. https://doi.org/10.1175/1520-0442(1997)010%3C3016:CPPAWT%3E2.0.CO;2↗.

Shafroth, P. B., Stromberg, J. C., & Patten, D. T. (2000). Woody riparian vegetation response to different alluvial water table regimes. *Western North American Naturalist*, *60*(1), 66–76. https://www.researchgate.net/publication/271829080↗.

Sharp, J.M., & Green, R.T. (2022). *The Edwards Aquifer*. The Groundwater Project. https://doi.org/10.21083/978-1-77470-029-7↗.

Shuttleworth, W. J. (2008). Evapotranspirtation measurement methods. *Southwest Hydrology, January-February*, 22-23.

Simmers, I. (1997). *Recharge of phreatic aquifers in (semi-)arid areas*. IAH International Contributions to Hydrogeology 19. Routledge.

Simunek, J., Huang, K., Sejna, M., & van Genuchten, M.Th. (2005). Hydrus-1D model, version 3.01. U.S. Salinity Laboratory, USDA-ARS, Riverside, California. https://www.ars.usda.gov/pacific-west-area/riverside-ca/agricultural-water-efficiency-and-salinity-research-unit/docs/model/hydrus-1d-model/↗.

Slichter, C. S. (1905). *Field measurements of the rate of movement of underground waters* [Water Supply Paper 140]. US Geological Survey. https://doi.org/10.3133/wsp140↗.

Smith, L., & Chapman, D. S. (1983). On the thermal effects of groundwater flow: 1. Regional scale systems. *Journal of Geophysical Research*, *88*(B1), 593–608. https://doi.org/10.1029/JB088iB01p00593↗.

Solomon, D. K., & Gilmore, T. E. (2024). *Age dating young groundwater: how to determine groundwater age from environmental tracer data*. The Groundwater Project. https://doi.org/10.21083/LIIU2727.

Sorey, M. L. (1971). Measurement of vertical groundwater velocity from temperature profiles in wells. *Water Resources Research*, *7*(4), 963–970. https://doi.org/10.1029/WR007i004p00963↗.

Spane, F. A. (2002). Considering barometric pressure in groundwater flow investigations. *Water Resources Research*, *38*(6), 14-1–14-18. https://doi.org/10.1029/2001WR000701

Springer, A. E., & Stevens, L. E. (2008). Spheres of discharge of springs. *Hydrogeology Journal*, *17*, 83–93. https://doi.org/10.1007/s10040-008-0341-y↗.

Stallman, R. W. (1965). Steady one-dimensional fluid flow in a semi-infinite porous medium with sinusoidal surface temperature. *Journal of Geophysical Research*, *70*(12), 2821–2827. https://doi.org/10.1029/JZ070i012p02821↗.

Stonestrom, D. A., & Constantz, J. (Eds.). (2003). *Heat as a tool for studying the movement of Ground Water Near Streams* [Circular 1260, pp. 1–96]. US Geological Survey. https://pubs.usgs.gov/circ/2003/circ1260/pdf/Circ1260.pdf↗.

Subyani, A. M. (2004). Use of chloride-mass balance and environmental isotopes for evaluation of groundwater recharge in the alluvial aquifer, Wadi Tharad, western Saudi Arabia. *Environmental Geology*, *46*, 741–749. https://doi.org/10.1007/s00254-004-1096-y↗.

Taniguchi, M. (1993). Evaluation of vertical groundwater fluxes and thermal properties of aquifers based on transient temperature-depth profiles. *Water Resources Research*, *29*(7), 2021–2026. https://doi.org/10.1029/93WR00541↗.

Taniguchi, M. (1994). Estimated recharge rates from groundwater temperatures in the Nara Basin, Japan. *Hydrogeology Journal*, *2*(4), 7–14. https://doi.org/10.1007/s100400050031↗.

Taylor, R. G., Scanlon, B., Doll, P., Rodell, M., van Beek, R., Wada, Y., Longuevergne, L., Leblanc, M., Famiglietti, J. S., Edmunds, M., Konikow, L., Green, T. R., Chen, J., Taniguchi, M., Bierkens, M. F. P., MacDonald, A., Fan, Y., Maxwell, R. M., Yechieli,

Y., … Treidel, H. (2013). Ground water and climate change. *Nature Climate Change*, *3*(4), 322–329. https://doi.org/10.1038/nclimate1744↗.

Theis, C. V. (1940). The source of water derived from wells: Essential factors controlling the response of an aquifer to development. *Civil Engineering*, *10*, 277–280. https://water.usgs.gov/ogw/pubs/Theis-1940.pdf↗.

Thornthwaite, C. W. (1948). An approach toward a rational classification of climate. *Geographical Review*, *38*, 55–94. https://doi.org/10.2307/210739↗.

Todd, D. K. (1956). Ground-water flow in relation to a flooding stream. In *Proceedings of the American Society of Civil Engineers 81*(2), 1–20. ASCE.

Todd, D. K. (1959). *Groundwater hydrology*. John Wiley and Sons.

Topp, G. C., Anaan, A. P., & Davis, J. L. (1980). Electromagnetic determination of soil water content: measurements in coaxial transmission lines. *Water Resources Research, 16,* 574-582.

Tóth, J. (1962). A theory of groundwater motion in small drainage basins in Central Alberta. *Journal of Geophysical Research*, *67*(11), 4375–4387. https://doi.org/10.1029/JZ067i011p04375↗.

Treidel, H., Martin-Bordes, J. L., & Gurdak, J. J. (Eds.). (2012). *Climate change effects on groundwater resources: A global synthesis of findings and recommendations*. CRC Press. https://unesdoc.unesco.org/ark:/48223/pf0000215556↗.

Tremblay, L., Larocque, M., Anctil, F., & Rivard, C. (2011). Teleconnections and interannual variability in Canadian groundwater levels. *Journal of Hydrology*, *410*(3–4), 178–188. https://doi.org/10.1016/j.jhydrol.2011.09.013↗.

Troxell, H. C. (1936). The diurnal fluctuation in the ground-water and flow of the Santa Ana River and its meaning. *Eos, Transactions, American Geophysical Union*, *17*(2), 496–504. https://doi.org/10.1029/TR017i002p00496↗.

Turner, R. J. W., Franklin, R. G., Journeay, J. M., & Denny, S. (2004). *Waterscape Gulf Islands: Protecting and conserving our island water*. Natural Resources Canada. https://waterbucket.ca/wcp/files/2014/07/GulfIslandsWaterscape.pdf↗.

United Nations. (n.d.). *World Population Prospects 2024*. Retrieved September 2, 2025, from https://population.un.org/wpp/↗.

UNESCO. (2022, January 25). *Groundwater: Making the invisible visible in 2022 and beyond*. https://www.unesco.org/reports/wwdr/2022/en↗.

Upwanshi, M., Damry, K., Pathak, D., Tikle, S., & Das, S. (2023). Delineation of potential groundwater recharge zones using remote sensing, GIS, and AHP approaches. *Urban Climate*, *48*, 101415. https://doi.org/10.1016/j.uclim.2023.101415↗.

US Department of Agriculture. (n.d.). *Soil texture calculator*. https://www.nrcs.usda.gov/resources/education-and-teaching-materials/↗.

US Environmental Protection Agency. (2020). Hydrologic evaluation of landfill performance: HELP 4.0 user manual. EPA/600/B-20/219, January 2020. https://www.epa.gov/sites/default/files/2020-

10/documents/the_hydrologic_evaluation_of_landfill_performance_help_4.0_manual_v2.pdf↗.

US Environmental Protection Agency. (2023). *Infiltration models*. https://www.epa.gov/water-research/infiltration-models↗.

Von der Borch, C. C., Lock, D., & Schwebel, D. (1975). Ground-water formation of dolomite in the Coorong region of South Australia. *Geology (May)*: 283-285.

van Everdingen, R. O. (1990). Ground water hydrology. In T. D. Prowse, & C. S. G. Ommanney (Eds.), *Northern hydrology: Canadian perspectives* (pp. 77–101). National Hydrology Research Institute.

van Genuchten, M. T. (1980). A closed form equation for predicting the hydraulic conductivity of unsaturated soils. *Soil Science Society of America Journal, 44*, 892-898. https://doi.org/10.2136/sssaj1980.03615995004400050002x↗.

Villeneuve, S., Cook, P. G., Shanafield, M., Wood, C., & White, N. (2015). Groundwater recharge via infiltration through an ephemeral riverbed, central Australia. *Journal of Arid Environments*, *117*, 47–58. https://doi.org/10.1016/j.jaridenv.2015.02.009↗.

Wang, T., Wu, Z., Wang, P., Wu, T., Zhang, Y., Yin, J., Yu, J., Guan, X., Xu, H., Yan, Dengming, & Yan, Denghua. (2023). Plant-groundwater interactions in drylands: A review of current research. *Agricultural and Forest Meteorology*, *341*, 109636. https://doi.org/10.1016/j.agrformet.2023.109636↗.

Weeks, E. P. (1979). Barometric fluctuations in wells tapping deep unconfined aquifer. *Water Resources Research*, *15*(5), 1167–1176. https://doi.org/10.1029/WR015i005p01167↗.

Weeks, E. P. (2005). The Lisse effect revisited. *Groundwater*, *40*(6), 652–656. https://doi.org/10.1111/j.1745-6584.2002.tb02552.x↗.

Welch, L. A., & Allen, D. M. (2012). Consistency of groundwater flow patterns in mountainous topography: Implications for valley-bottom water replenishment and for defining hydrogeological boundaries. *Water Resources Research*, *48*(5). https://doi.org/10.1029/2011WR010901↗.

Welch, L., Allen, D. M., & Tromp-van Meerveld, I. (2012). Contributions to mountain headwater streams and sensitivity to available recharge. *Canadian Water Resources Journal*, *37*(4), 349–371. https://doi.org/10.4296/cwrj2011-907↗.

Werner, A. D., & Simmons, C. T. (2009). Impact of sea-level rise on sea water intrusion in coastal aquifers. *Groundwater*, *47*(2), 197–204. https://doi.org/10.1111/j.1745-6584.2008.00535.x↗.

Werner, A. D., Zhang, Q., Xue, L., Smerdon, B. D., Li, X., Zhu, X., Yu, L., & Li, L. (2013). An initial inventory and indexation of groundwater mega-depletion cases. *Water Resources Management*, *27*(2), 507–533. https://doi.org/10.1007/s11269-012-0199-6↗.

White, W. N. (1932). *A method of estimating ground-water supplies based on discharge by plants and evaporation from soil: Results of investigations in Escalante Valley, Utah*. [Water Supply Paper 659A]. US Geological Survey. https://doi.org/10.3133/wsp659A↗.

Wilson, J. L., & Guan, H. (2004). Mountain-block hydrology and mountain-front recharge. In J. F. Hogan, F. M. Phillips, & B. R. Scanlon (Eds.), *Groundwater recharge in a desert environment: The southwestern United States* (Vol. 9, pp. 113–137). AGU. https://doi.org/10.1029/009WSA08↗.

Wilson, A. M., Evans, T., Moore, W., Schutte, C. A., Joye, S. B., Hughes, A. H., & Anderson, J. L. (2015). Groundwater controls ecological zonation of salt marsh macrophytes. *Ecology, 96(3)*, 840-849. https://doi.org/10.1890/13-2183.1↗.

Winter, T. C., Harvey, J. W., Franke, O. L., & Alley, W. M. (1998). *Groundwater and surface water: A single resource* [Circular 1139]. US Geological Survey. https://doi.org/10.3133/cir1139↗.

Woessner, W. W. (2020). *Groundwater-surface water exchange*. The Groundwater Project. https://gw-project.org/books/groundwater-surface-water-exchange/↗.

Woessner, W. W., & Poeter, E. P. (2020). *Hydrogeologic properties of earth materials and principles of groundwater flow*. The Groundwater Project. https://gw-project.org/books/hydrogeologic-properties-of-earth-materials-↗.

Wood, S., Sebastian, K., & Scherr, S. J. (2000). *Pilot analysis of global ecosystems: Agroecosystems*. World Resources Institute. https://www.wri.org/research/pilot-analysis-global-ecosystems-agroecosystems↗.

Yesertener, C. (2008). *Assessment of the declining groundwater levels in the Gnangara groundwater mound* [Hydrogeological Record Series, Report HG14]. Department of Water, Western Australia. https://www.wa.gov.au/system/files/2022-04/↗.

Zektser, S., Loáiciga, H. A., & Wolf, J. T. (2005). Environmental impacts of groundwater overdraft: Selected case studies in the southwestern United States. *Environmental Geology*, *47*(3), 396–404. https://doi.org/10.1007/s00254-004-1164-3↗.

Zheng, K., Kimball, J. S., & Running, S. W. (2016). A review of remote sensing based actual evapotranspiration estimation. *WIREs Water*, *3*(6), 834–853. https://doi.org/10.1002/wat2.1168↗.

Zhu, Y., & Newell, R. E. (1998). A proposed algorithm for moisture fluxes from atmospheric rivers. *Monthly Weather Review*, *126*(3), 725–735. https://doi.org/10.1175/1520-0493(1998)126<0725:APAFMF>2.0.CO;2↗.

9 Boxes

Box 1 - The Hidden Recharge from Mountains

Feth (1964) was perhaps the first to identify mountain block recharge (MBR) as a significant contributor to valley bottom recharge. Feth coined the term *hidden recharge*, defining it as "*subsurface percolation of water from basin-margin mountains directly into aquifers of the valley basins*" (Feth (1964), p. 14). He challenged the longstanding assumption that groundwater basin margins could be drawn at the contact between alluvium and bedrock and that mountains are barriers between groundwater basins. As evidence, he summarized key findings from several studies in Utah and Southern California and, notably, from his own project on the Weber Delta in the Wasatch Mountains in Utah (Feth, 1954 as cited in Feth, 1964).

He illustrated how recharge by seepage of water along the mountain front results in near parallel equipotential lines along the basin edge. He noted that most of the mountain front streams, and all those of consequence, had been developed as flumes (or gravity chutes) that carried virtually all the streamflow across recharge areas near the mountains and that these streams were effectively isolated from the aquifer. Therefore, the only remaining source of recharge is the subsurface percolation of water from the mountains directly into the unconsolidated valley fill sediments. In semi-arid to arid mountainous regions, contributions to surface water and groundwater from highland precipitation provide an important replenishment source for valley-bottom water supplies, because valley-bottom precipitation and recharge are limited. Feth (1964) emphasized that disregarding this hidden recharge can lead to large imbalances in valley-bottom water budgets.

In more arid basins where mountain-sourced streams infiltrate completely in the valley fill, surface MFR can be reasonably estimated by directly measuring streamflow at the mountain front. However, as is common in most mountainous regions, few streams are equipped with stream gauges, so direct measurements are limited. Furthermore, mountain-sourced streams often do not completely infiltrate in less arid basins due to evapotranspiration, necessitating additional valley gauge measurements (commonly complicated by local diversions and inputs from irrigation canals).

MBR, the hidden recharge, remains difficult to characterize and quantify due to limited hydrogeologic, climatic, and other data in the mountain block and at the mountain front (Wilson & Guan, 2004; Markovich et al., 2019). Meixner and others (2016) estimated that recharge from the adjacent mountains ranged from 20 percent to 100 percent of total recharge in five major aquifer systems in the western United States. On average, the mountain systems delivered 74 percent of the water to the valley bottom as surface MFR and 26 percent as MBR.

Return to where text linked to Box 1

Box 2 - Groundwater Recharge in Cold Regions

Contributed by John Molson, Jean-Michel Lemieux, Rene Therrien, Nathan Young (Université Laval)

Recharge in cold regions occurs in a similar manner to temperate regions. Surficial, unconfined aquifers are primarily fed by infiltrating precipitation or surface water, while deeper, confined, or partially confined systems predominantly receive water from regional flow systems. However, the availability of liquid water in cold regions is strongly controlled by the climate, which in the Arctic and Subarctic (latitudes greater than 50 °N) is marked by cool, wet summers and long, cold, relatively dry winters. Most northern catchments receive a relatively equal proportion of solid (snow) and liquid (rain) precipitation in a given year, although total precipitation tends to decrease with increasing latitude (Box et al., 2019). The spring snowmelt usually represents the single largest annual recharge event, especially for catchments located north of the Arctic Circle (latitudes greater than 66.5 °N). However, because of the occurrence of sublimation in arctic and subarctic environments, the amount of snowpack available to contribute to recharge in the spring is often only a fraction of the total annual snowfall.

The infiltration capacity of meltwater and precipitation in cold regions is often limited by the presence of seasonally and perennially frozen ground (permafrost). In particular, the portion of the shallow subsurface that freezes seasonally, called the *active layer*, strongly influences the infiltration of spring snowmelt, as the presence of ice in the pore spaces of the active layer can render it largely impermeable. Since the active layer can be only partially thawed at the start of the spring snowmelt, infiltration occurring early in the warm season often quickly overwhelms the infiltration capacity of the soil, resulting in the generation of a large volume of surface runoff and a smaller volume of recharge.

Another pathway for recharge in cold regions is the infiltration of precipitation or surface water through perennially thawed regions or *taliks* (Figure Box 2-1, C-D). Open taliks can penetrate to significant depths within the permafrost and can represent unthawed hydraulic connections to the surface. As a result, these features can represent the only available recharge pathway for aquifers located within or beneath the extent of the permafrost, unless these aquifers are fed by a deeper groundwater flow system (Lemieux et al., 2016). In the continuous permafrost zone, taliks are most often located under large bodies of water, such as lakes or rivers that do not freeze completely in the winter.

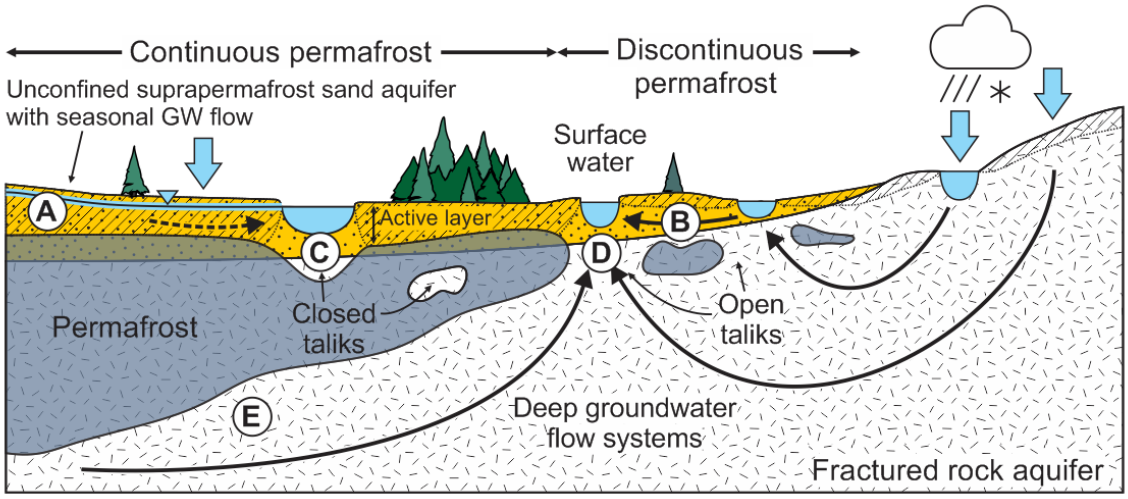

Figure Box 2-1 - Schematic representation of a groundwater flow system in a region containing permafrost. In the continuous permafrost zone, groundwater flow is often restricted to shallow supra-permafrost aquifers contained within the active layer (A, B). However, productive aquifers can also exist within closed taliks beneath large bodies of water (C). Sub-permafrost aquifers can exist within unconsolidated deposits or fractured bedrock beneath the permafrost base (E). These aquifers contribute to deep groundwater circulation that can feed shallower, intrapermafrost aquifers (D) that exist within open taliks or within areas free of permafrost in the discontinuous permafrost zone.

Aquifers in cold regions are generally categorized in three distinct groups, depending on their location relative to the permafrost (van Everdingen, 1990): 1) supra-permafrost aquifers, which overlie the permafrost; 2) intrapermafrost aquifers, located in thawed zones within the permafrost itself; and 3) subpermafrost aquifers, located in the thawed regions beneath the permafrost base.

Supra-permafrost aquifers are thin surficial aquifers that overlie shallow permafrost (Figure Box 2-1, A). Recharge in these aquifers is strongly impacted by the material properties of the aquifer, which control the extent to which it is impacted by seasonal frost. If the unsaturated zone of a supra-permafrost aquifer is composed primarily of sands and gravels, infiltration might occur even when the ground is frozen, as a major fraction of the pore space is filled with air instead of ice (Kane, 1980). However, if the aquifer is composed of finer-grained sediments or sediments prone to ice formation, winter recharge will be negligible. In either case, the bulk of the annual recharge will occur during late spring or summer, after the seasonally frozen ground has thawed (Cochand et al., 2020).

Supra-permafrost aquifers can be divided into three types depending on how extensively they are affected by seasonal frost, and recharge can occur in different ways for each subgroup.

Type I (Figure Box 2-1, A): These are aquifers in which groundwater freezes completely in winter. They are usually shallow, with depths ranging between 1 and 4 m. Recharge in Type I aquifers is largely limited to infiltration of snowmelt and summer precipitation, although small amounts of recharge can occur in winter depending on the material properties of the aquifer.

Type II (Figure Box 2-1, B): These are aquifers in which groundwater partially freezes in winter. Type II aquifers are most frequently found in closed taliks, under small lakes, in alluvial terraces, and in valleys. Since these aquifers do not freeze entirely, active circulation of groundwater is possible during winter, which can provide a pathway for recharge even when seasonal frost is present.

Type III (Figure Box 2-1, C): These are aquifers in which groundwater is not subject to seasonal freezing. These aquifers are primarily located in closed taliks under major rivers. In the continuous permafrost zone, they can represent the only perennial sources of potable water for local communities. Recharge in Type III aquifers occurs primarily by infiltration from the overlying surface water body or, if the talik reopens, via infiltration through the unfrozen sediments.

Intra-permafrost aquifers (Figure Box 2-1, D) are closely related to Type III aquifers, because they are located within the permafrost itself and are not subject to seasonal freezing. However, instead of being located in closed taliks, intrapermafrost aquifers are located in open taliks within the permafrost. Since these aquifers are frequently located beneath large bodies of water, their extent is regulated by the size of the overlying surface water body and the temperature of the water flowing into the talik. Aquifers that exist in perennially unthawed zones within the discontinuous permafrost zone can also be considered intrapermafrost aquifers.

Sub-permafrost aquifers (Figure Box 2-1, E) are confined under the permafrost layer. They can consist of either permeable unconsolidated deposits, if these deposits extend below the permafrost, or bedrock if it is sufficiently permeable, such as sandstone or fractured crystalline rock. Recharge in subpermafrost aquifers occurs primarily either through open taliks that lie beneath large bodies of water, or below glaciers. These aquifers can also be recharged via inflow of water from deeper, regional flow systems (Kane et al., 2013).

Return to where text linked to Box 2

Box 3 - Modeling Hypothetical Infiltration Event and Overland Flow

Freeze, 1974, as presented by Freeze and Cherry, 1979

Figure Box 3-1 shows the results of a representative simulation of a hypothetical infiltration event. The three profiles show the time-dependent response of the moisture content, matric potential, and hydraulic head in the upper 100 cm of a sand with n=30 percent, K_{sat}=0.026 cm/min. The soil moisture characteristic curve used in the modeling is from Liakopoulos (1965) and is shown in Figure 2.13 of Freeze and Cherry (1979) which is in their section 2.6 titled "*Unsaturated Flow and the Water Table*" about half way through Chapter 2↗. The transient behavior occurs in response to a constant-intensity rainfall at the rate R=0.13 cm/min. This rate is 5 times K_{sat}. The initial conditions are shown by the t=0 curves, and subsequent curves are labeled with the time in minutes.

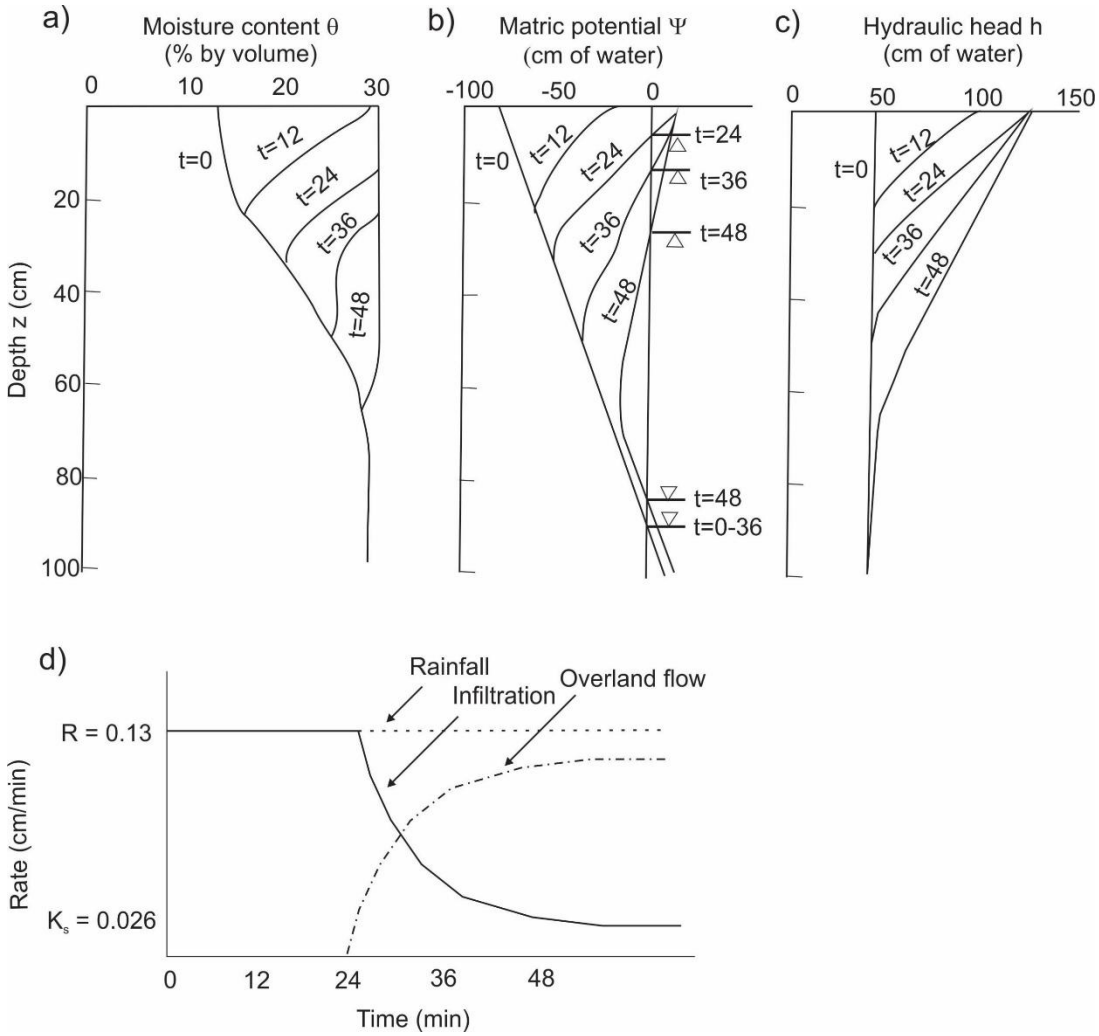

Figure Box 3-1 - Simulated a) moisture content, b) matric potential (i.e., negative pressure head), and c) hydraulic head during d) a hypothetical infiltration event. The matric potential graph uses triangles to show both the regional and the advancing inverted water table of the wetting front.

Figure Box 3-1a shows how the moisture content increases down the profile with time. The surface becomes saturated after 12 min, and the soil pores in the entire profile are

almost filled with water after 48 min. Figure Box 3-1b shows the matric potential changes (Freeze used the term *pressure head* for matric potential). The curve for t=12 min does not reach the ψ=0 point, so the upper few centimeters of surface saturation, indicated by the moisture-content profile, must be *tension-saturated*. By the 24-min mark, the pressure head at the ground surface has reached +10 cm, the indication being that a 10-cm-deep layer of water is ponded on the surface (in their simulation, the maximum allowable ponding depth had been set to 10 cm). There is also an inverted water table 5 cm below the ground surface that propagates down the profile with time (inverted triangles). The true water table, which is initially set at a 95-cm depth, remains stationary through the first 36 min but then begins to rise in response to the infiltrating moisture from above. The hydraulic head profiles in Figure Box 3-1c near the surface provide the hydraulic-gradient values that can be inserted in Darcy's law to calculate the rate of infiltration at various times. The datum for the values appearing on the horizontal scale at the top was arbitrarily chosen as 125 cm below the ground surface.

Figure Box 3-1d shows the time-dependent infiltration rate at the ground surface. The infiltration rate is equal to the rainfall rate until the soil becomes saturated at the surface (and the 10-cm deep pond has been filled); then it decreases asymptotically toward a value equal to K_{sat}. During the early period, as the soil pores are filling up with water, the moisture contents, pressure heads, and hydraulic heads are increasing with time and the downward hydraulic gradient is decreasing. This decrease is balanced by an increase in the hydraulic conductivity values under the influence of the rising pressure heads. The decrease in infiltration rate occurs at the point when the combination of gradients and hydraulic conductivities of the soil can no longer accept all the water supplied by the rainfall. The rainfall not absorbed by the ground as infiltration nor stored in the 10-cm-deep pond is available for land overflow.

Return to where text linked to Box 3 ↑

Box 4 - Coastal Groundwater Discharge

Contributed by Vincent Post

The amount of groundwater that discharges along the coast is primarily a function of the groundwater recharge rate in the inland groundwater catchment and the size of the catchment. Whether all the groundwater flows all the way to the coast depends on the groundwater-surface interaction in the coastal zone. Groundwater discharge pathways in coastal zones are controlled by the rock type and the morphology of the landscape. Groundwater may discharge in lakes, rivers, streams, and swamps before it reaches the shoreline. Figure Box 4-1 shows an example of the Coorong region in Southern Australia where land-derived fresh groundwater discharges into a series of shore-parallel lakes. The lagoon closest to the coast receives both low-salinity groundwater and seawater, and strong evaporation in summer causes the salinity in the lagoon to rise to levels above seawater values. This example shows that flow configurations can be complex, and the complexity increases when the third dimension is considered.

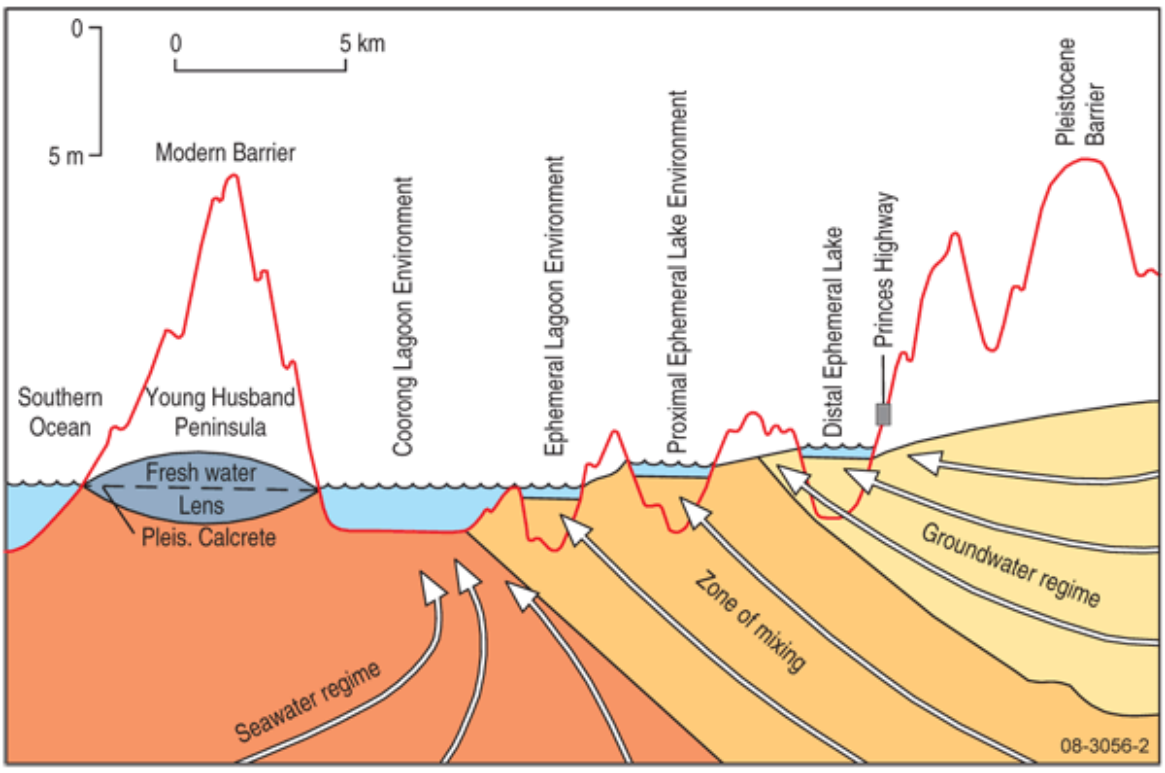

Figure Box 4-1 - (from Von der Borch and others, 1975).

The occurrence of low-permeability layers exerts another strong control on coastal discharge pathways. Their presence can impede the upward movement of the freshwater and force it to continue to flow underneath the seafloor. In extreme cases, the flow can continue for up to 80 km. When multiple aquifers exist above one another, complex flow pathways and salinity distributions can form. The same holds true for heterogeneous systems, such as delta sediments.

Tidal oscillations add further complexity. Depending on the tidal amplitude and the beach slope, an upper saline plume (USP) can form in the intertidal zone (Figure Box 4-2). The flow in the USP is driven by the infiltration of saltwater during high tide and its flow toward the low-water mark during low tide. The flow of freshwater is constrained to a narrow zone between the USP and the deeper seawater wedge, and it discharges near the low-water mark. The configuration of the flow and salinity is not stationary but varies in response to spring-neap tidal cycles, recharge variability, and changes in beach morphology.

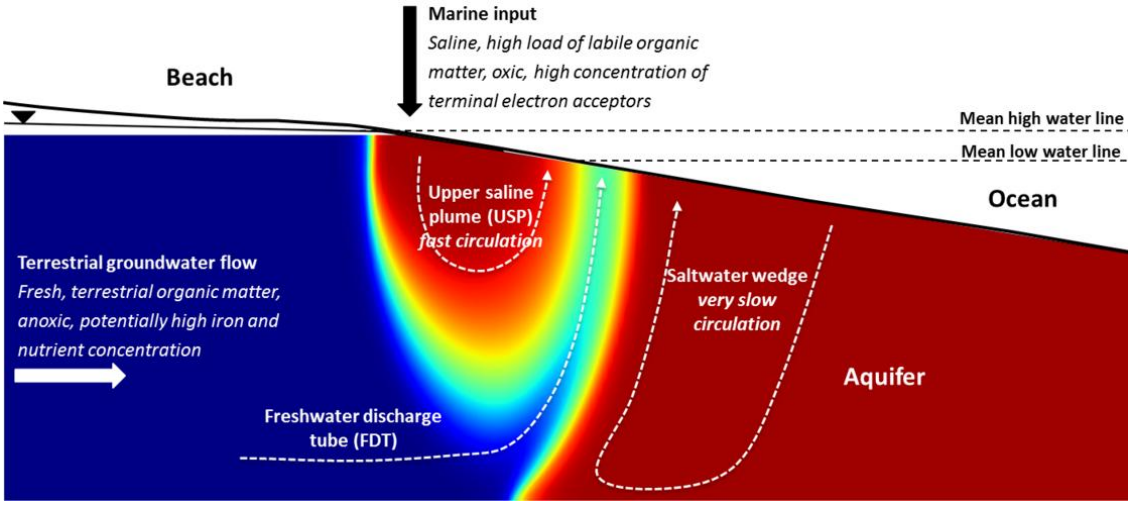

Figure Box 4-2 - Schematic cross section showing salinity distribution and flow paths of fresh and saline groundwater in a beach aquifer.

Numerous cases of focused discharge along high-permeability features have been described in regions with a strongly heterogeneous rock permeability. This can occur in unconsolidated aquifers, but it is especially prominent in consolidated aquifers that are fractured or carbonate rock aquifers with dissolution features. Spectacular examples include large submarine springs—for example, off the coast of Florida in the USA, Croatia, and Indonesia. Such discharge features, albeit mostly smaller in size, can also be observed on beaches and in tidal channels (Figure Box 4-3). They often play an important role in species diversity and are thus a key feature of many groundwater-dependent ecosystems.

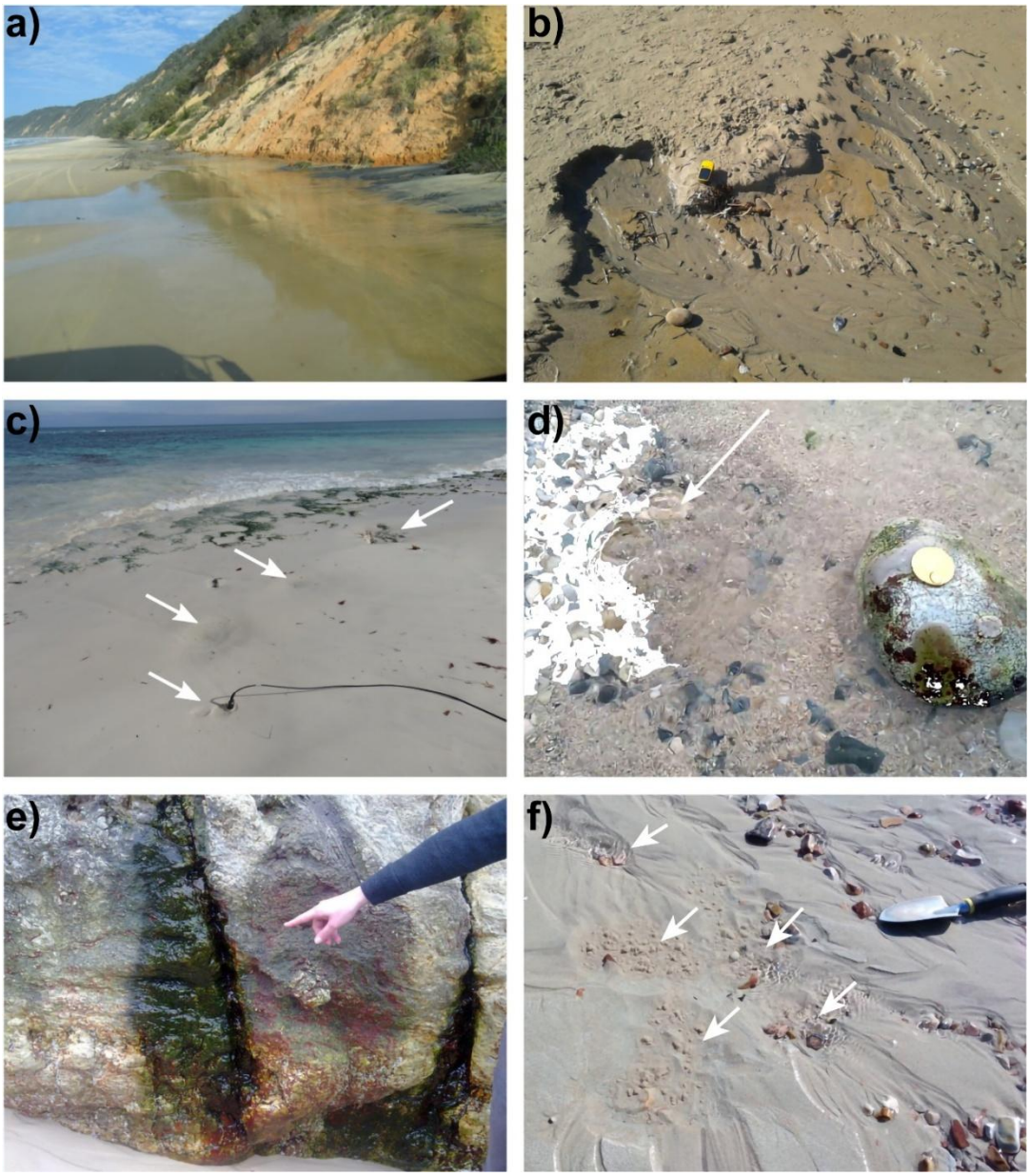

Figure Box 4-3 - Collection of photographs of coastal discharge features: a) diffuse discharge spread across a sandy beach near Noosa, Australia; b) localized discharge on a sandy beach underlain by a fractured rock aquifer in Adelaide, Australia; c) localized discharge from conduits indicated by white arrows in limestone near Seabird, Australia— the electrical conductivity probe provides scale; d) groundwater from a limestone aquifer upwelling in an intertidal area in Yport, France; e) groundwater seeping from a fracture on a beach near Brisbane, Australia; and f) upwelling groundwater forming small *sand volcanoes* at Sellicks Beach, Australia.

Long stretches of coastlines are bordered by salt marshes or mangrove forests. Here, fresh groundwater that derives from further inland can discharge into tidal creeks or via the roots of the vegetation. Fresh groundwater discharge has been shown to play a key role in the zonation of salt marsh ecosystems (Wilson and others, 2015). Strong evapotranspiration can increase the salinity of the discharging groundwater, and complex flow patterns can occur when the salinity of the groundwater near the surface becomes so high that its density causes it to sink deeper into the subsurface (McGowan & Martin, 2007).

Return to where text linked to Box 4 ↑

Box 5 - Thermal Springs in Southwestern Canada

Thermal springs, also referred to as hot springs, assume their temperature according to the circulation depth of groundwater. Thermal waters that issue from springs typically originate as meteoric water (precipitation) that heats as it circulates to great depth. Importantly, once the water is heated at depth, it needs to move upward rapidly to the surface to maintain its high temperature; otherwise, shallower groundwater would mix with the heated water and cool it down. Therefore, some deep-seated structural feature, such as a permeable fault, is required to transport the water rapidly to the surface.

Grasby and Hutcheon (2001) examined the spatial distribution of thermal springs in the southern Canadian Cordillera (spanning British Columbia and Alberta) in relation to geological features. They found that all thermal springs in southern British Columbia are restricted to six major fault systems. In southern Alberta, thermal springs are mostly associated with major thrust faults in the Rocky Mountains. In Banff National Park in Alberta, for example, thermal springs are localized along an anomalously wide portion of the Sulphur Mountain Thrust (Figure Box 5-1).

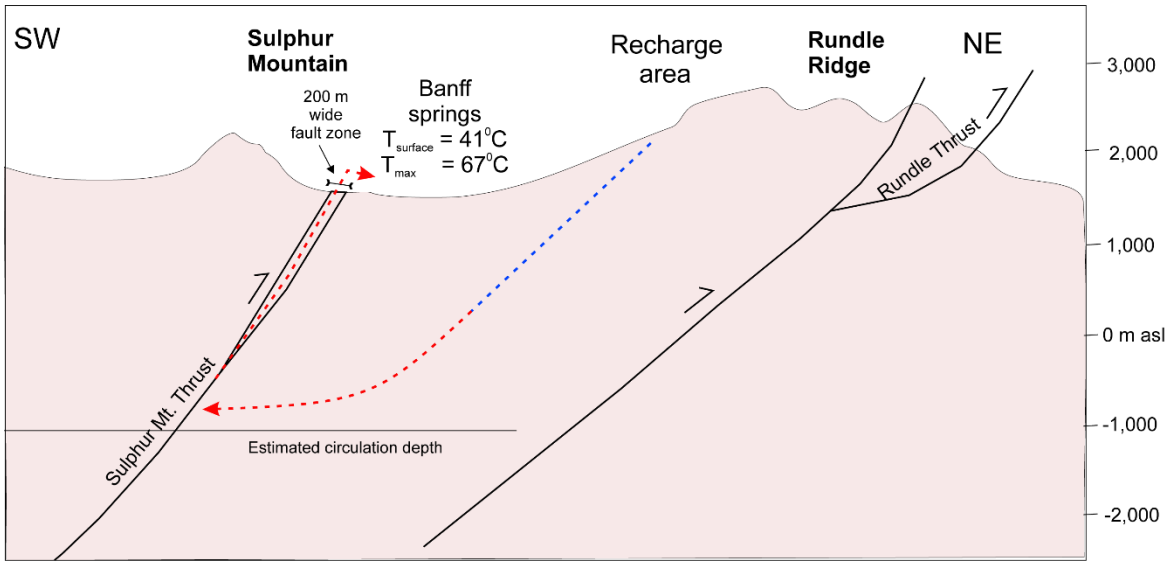

Figure Box 5-1 - Simplified cross section across the Sulphur Mountain Thrust in Banff National Park. The recharge area for the Banff hot springs is thought to be along Rundle Ridge that extends eastward from Mount Rundle. The groundwater warms as it flows deeper (blue to red arrow). $T_{surface}$ is the water temperature at surface and T_{max} is the equilibration temperature calculated with a chalcedony geothermometer. The estimated circulation depth is calculated using T_{max} and an average geothermal gradient of 21 °C/km (modified from Grasby & Hutchinson, 2001).

The fault systems share these common features of (a) penetrating deeply into the crust and (b) having a relatively recent (Eocene or later) component of brittle deformation (Grasby & Hutcheon, 2001). Brittle faults in the upper crust have enhanced permeability that allows preferential fluid flow (e.g., Caine et al., 1996). Using numerical groundwater flow models, Lopez and Smith (1995) illustrated that there is a critical range of permeability (10^{-16} to 10^{-14} m^2) for the host rock that favors the development of thermal springs. If the

permeability is too low, conductive heat flow dominates, whereas at higher permeabilities the groundwater flow is sufficiently high to depress the local geothermal gradient (Forster & Smith, 1988). This critical range of permeability is consistent with that of fractured rock common to deformation belts in mountain regions. While some thermal springs are located in areas of high heat flow in the Canadian Cordillera, some are located in regions of low to moderate heat flow (Grasby & Hutchinson, 2001), suggesting that the normal geothermal gradients of the Cordillera, even in low heat-flow settings, are sufficient for thermal springs to develop.

Grasby and Hutchinson (2001) noted that the faults in the southern Cordillera are associated with major river valleys bordered by high mountain ranges with up to 2500 m of relief. The high relief allows for sufficient hydraulic head in the recharge area to drive the deep groundwater flow. Thermal springs occur in both high and low precipitation regions of the southern Canadian Cordillera, suggesting their occurrence is not constrained by a high recharge rate, although a minimum amount of precipitation is needed to maintain sufficiently high hydraulic head to drive the system.

Using stable isotope data, Grasby and others (2000) demonstrated a meteoric origin for thermal spring waters across the Canadian Cordillera and that the recharge zones are not particularly distant to the spring outlets. They used different chemical geothermometers to estimate the equilibration temperatures of the springs. Geothermometric calculations assume that groundwater equilibrates with minerals in the reservoir rock; by measuring the ion concentrations or ion ratios in the spring water, the source water temperature can be estimated. Common geothermometers include Chalcedony (Fournier, 1977), Quartz (Fournier, 1977), and Na-K-Ca (Fournier & Truesdell, 1973). A fundamental assumption of geothermometry, from the perspective of estimating equilibration temperatures for thermal waters, is that the effects of dilution from surface and/or shallow groundwaters are insignificant and that thermodynamic equilibrium has been attained (Fournier, 1981). Re-equilibration along the flow path and dilution by near-surface mixing can lower the calculated temperatures. Thus, the geothermometers give a minimum estimate of the highest temperature (T_{max}) reached in the system (Figure Box 5-1).

To estimate the circulation depth—that is, how deep the groundwater has traveled before returning to surface—the equilibration temperature is divided by the local geothermal gradient.

Allen and others (2006) used a range of chemical geothermometers to estimate the equilibration temperatures of thermal springs south of Banff, along the southern Rocky Mountain Trench in British Columbia, Canada (Figure Box 5-2). The range of equilibration temperatures is between 24 and 59 °C, assuming there is minimal mixing with colder shallow waters that might lead to a lowering of the calculated equilibration temperature. Temperature logs from 11 boreholes in the vicinity were used to calculate representative

geothermal gradients, which range from 23.8 to 55.7 °C/km with an average of 24.8±8.0 °C/km. Using the average geothermal gradient and the range of equilibration temperatures calculated for each spring, the estimated minimum depths of origin of the thermal waters range from 0.9 to 2.2 km. Heat-flow values range from 90.3 to 155 mW/m^2, with an average of 109.1±21.0 mW/m^2. The moderate to high heat flow and heat generation result in generally higher temperatures at shallow depths, which can explain the occurrence of thermal springs. The alignment of the thermal springs likely relates to the preferred northwest–southeast orientation for major thrust faults along the Rocky Mountain Trench and to waters routed from depth along deep faults.

Figure Box 5-2 - Thermal springs in the Rocky Mountain Trench region of southern British Columbia and Alberta, Canada. The Banff springs described in Figure Box 5-1 are also shown (modified from Allen et al., 2006).

Return to where text linked to Box 5

Box 6 - Water-table Fluctuation Method for Estimating Recharge

Groundwater-level hydrographs for unconfined aquifers can be used to estimate the rate of recharge using the water-table fluctuation (WTF) method. The WTF method is based on the premise that the rise in groundwater level in an unconfined aquifer is due to recharge water arriving at the water table. Recharge is calculated as in Equation Box 6-1 (Healy & Cook, 2002).

$$Recharge = S_Y \frac{dh}{dt} = S_Y \frac{\Delta h}{\Delta t} \qquad \text{(Equation Box 6-1)}$$

where:

$\frac{\Delta h}{\Delta t}$ = the rate of increase of hydraulic head—here, the water table (LT^{-1})

An important assumption is that all the water arriving at the water table goes immediately into storage and that there are no other losses or gains of water at the observation point. To meet this assumption, the WTF method is best used over short periods (hours to perhaps a few days) where the water table is shallow, as illustrated in Figure Box 6-1. To estimate recharge, we begin by measuring the rate of rise of the water table ($\Delta h_1/\Delta t_1$) and then multiply that rate by S_Y.

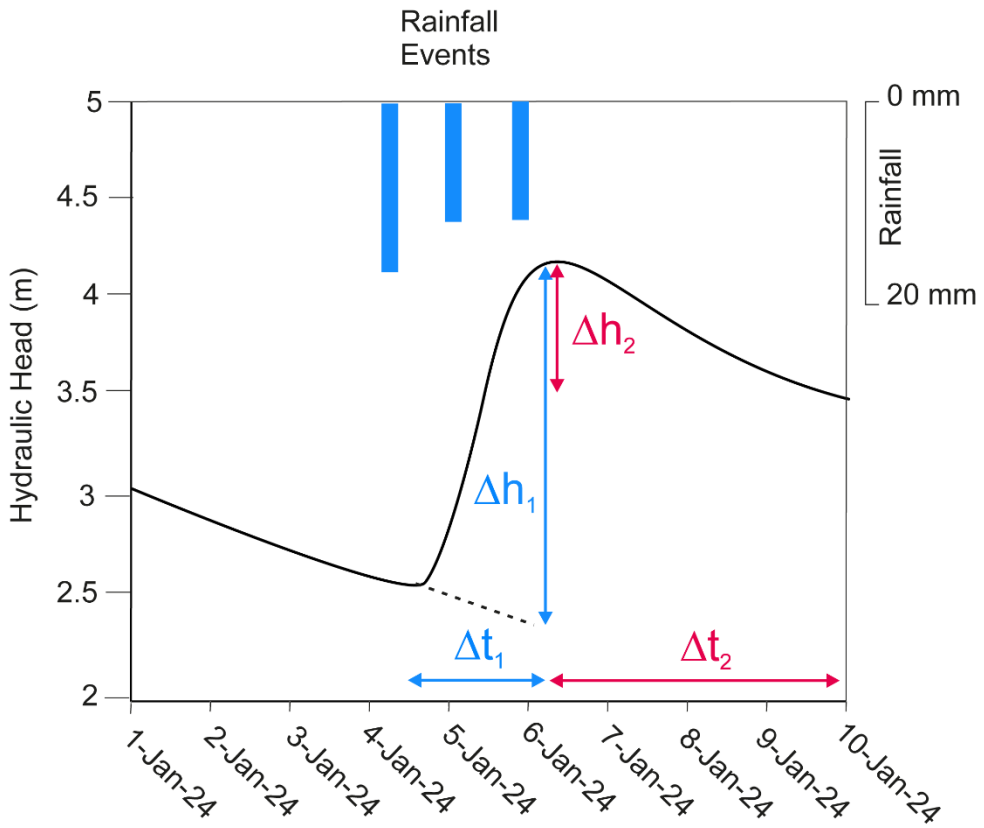

Figure Box 6-1 - Well hydrograph showing the hydraulic head variation over a 10-day period during which there are three daily rain events. All variables are defined in the text. $\Delta h_1/\Delta t_1$ is measured from the start of the rise to the peak, but given that the groundwater level was recessing, the recharge is filling the pores that would have drained if recharge did not enter the system, so the downward trend is extended to obtain Δh_1.

Equation Box 6-1 could be used to determine the total recharge to an unconfined aquifer over a longer period (e.g., seasonally). In this case, the calculation would need to be done for each water level rise event. Making these calculations can be tedious.

In some situations, the water table may be deeper and, consequently, the water-table variation much smoother. This means that individual recharge events are not evident. In this case, we must account for the water draining from the aquifer, because the aquifer continues to drain while it is being recharged. If we do not account for the drainage rate, then recharge will be underestimated. Accordingly, we add the drainage rate, D, to Equation Box 6-1 to obtain Equation Box 6-2 (Cuthbert, 2010).

$$Recharge = S_Y \frac{\Delta h}{\Delta t} + D = S_Y \frac{\Delta h_1}{\Delta t_1} + S_Y \frac{\Delta h_2}{\Delta t_2} \qquad \text{(Equation Box 6-2)}$$

where:

$\frac{\Delta h_1}{\Delta t_1}$ and $\frac{\Delta h_2}{\Delta t_2}$ = changes in head with time as defined in Figure Box 6-2 (LT^{-1})

Unfortunately, estimating the drainage rate is not as straightforward as it might seem. Ideally, we want an estimate of the rate of decline of the water table assuming there is no recharge taking place. One way to do this is to measure $\Delta h_2/\Delta t_2$ during a period with no recharge from precipitation, as illustrated in Figure Box 6-1. In practice, this can be difficult. Oftentimes there is a delay (or lag) between when precipitation ceases and when recharge ceases, given that the water table is not right at ground surface. There may also be a long lag between the last precipitation event and recharge if precipitation has fallen as snow. Recharge would occur during snowmelt—so, in this case, days without precipitation have no bearing on there being no recharge.

Cuthbert (2010) developed a methodology for estimating recharge over long periods that accounts for drainage in a catchment. The catchment aquifer drains to a river located a distance L from a flow divide. The water table is measured in a well positioned a distance x from the flow divide. Recharge is estimated using Equation Box 6-3.

$$Recharge = S_Y \frac{\Delta h_1}{\Delta t_1} + \frac{2\bar{h}T}{(L^2 - x^2)} \qquad \text{(Equation Box 6-3)}$$

where:

$\bar{h}$ = temporally averaged hydraulic head measured at the well over a long period (e.g., years) (L)

T = transmissivity (L^2T^{-1})

Using the WTF method (for any of the equations in this Box) makes several assumptions. Most importantly, recharge rates vary substantially within a catchment due to differences in factors such as topography, geology, land use, and land cover, as discussed in Section 2, thus ideally, water-level data from multiple wells should be analyzed. Other

factors, such as entrapped air during infiltration events (subsection 4.3.1), changes in atmospheric pressure (subsection 4.3.1), and evapotranspiration losses (subsection 4.3.1) can complicate the analysis (Healy & Cook, 2002). Finally, S_Y values are rather difficult to estimate and are uncertain, meaning the recharge estimates are also uncertain.

Return to where text linked to Box 6

Box 7 - Mountain Block Recharge in the Andes of Peru

Contributed by David Bethune, University of Calgary, Alberta, Canada; M. Cathryn Ryan, University of Calgary, Alberta, Canada; Fluquer Peña Laureano, Pontificía Universidad Católica de Perú, Lima, Peru; Katiusca Yakabi, Pontificía Universidad Católica de Perú, Lima, Peru

Peru confronts significant water stress in its desert coastal area, which is in the rain shadow of the Andes. While over 98 percent of Peru's precipitation (hence, water resources) is east of the Andes, the western coastal area is home to more than half of Peru's population and most of the country's economic activities (Minagri & Cosude, 2015). Although dozens of arid western coastal watersheds are in varying stages of water stress in Peru, the Ica Region (Figure Box 7-1) is arguably in the most critical state. This hyper-arid region (<10 mm yr^{-1} precipitation) has no perennial rivers yet is Peru's main agricultural-export production region. Agricultural production relies on irrigation sourced by a combination of water diverted from the Ica River via irrigation canals (70 percent) and the extraction of groundwater (30 percent) from the alluvial aquifer below the Ica Valley (Autoridad Nacional del Agua, 2015). The Ica River's ephemeral (i.e., seasonal) flow is supplemented in the dry season by interbasin transfer of water from Lake Choclococha on the Atlantic side of the continental divide.

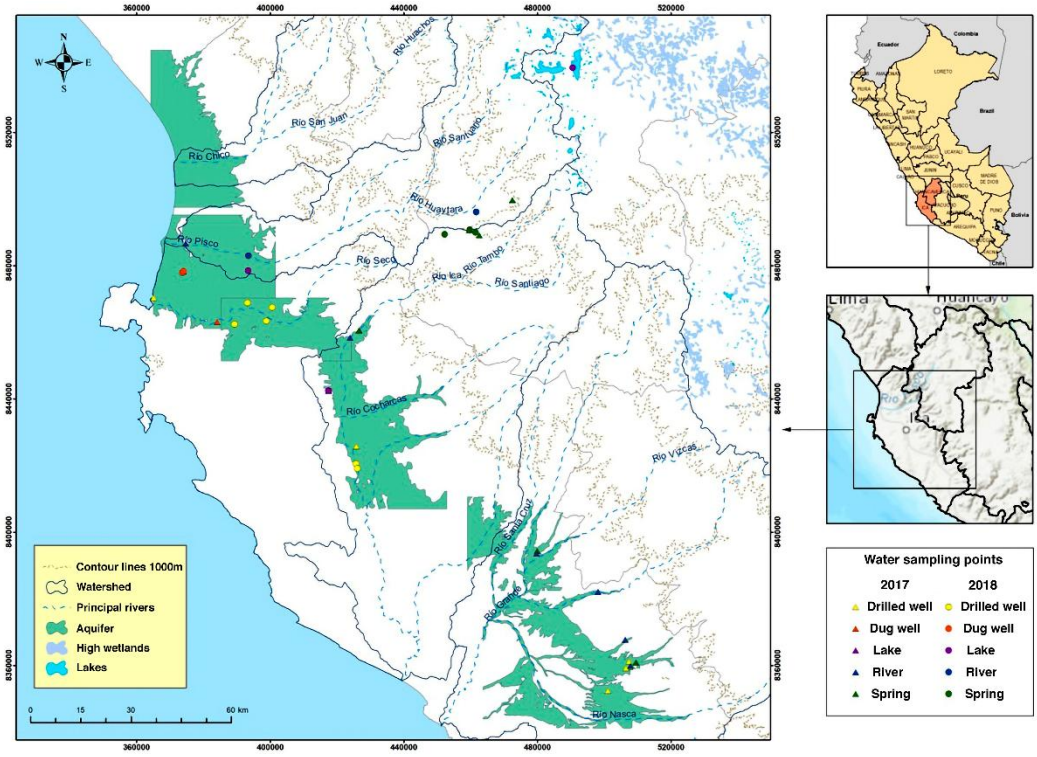

Figure Box 7-1 - Location map showing the Ica (and surrounding) aquifers and groundwater sampling points in Peru. The insets show the study region at a provincial and national scale.

The unconfined Ica Aquifer is comprised of series of Quaternary unconsolidated fluvial-alluvial sediments (gravel, sand, and silt) up to 500 m in depth; however, the thickness of aquifer is, in most areas, 20 to 90 m. Transmissivity varies from 400 to

3,800 m^2/day, hydraulic conductivity (K) varies from 130 to 1,300 m/day, and specific yield ranges up to 12 percent (Autoridad Nacional del Agua, 2015). Bedrock below the valley and in the mountains is comprised of highly faulted igneous, volcanic, and sedimentary rocks. Although the Ica Aquifer is located entirely within the Ica region, the watershed area includes the Ayacucho and Huancavelica regions. Groundwater extraction from the Ica Aquifer has led to a gradual lowering of the water table of up to 2 to 3 m a $year^{-1}$ in some areas (Navarro, 2015), causing increased salinity, reduced yields, and water wells drying up (James, 2015). Concern about the unsustainability of the pumping led to governmental prohibition on new-well drilling in the Ica region (approved in 2009), and several artificial infiltration projects have been undertaken to capture river water and infiltrate it into the aquifer (Fernández-Escalante et al., 2020).

Given the hyper-arid conditions along the Pacific coast of Peru and lack of local groundwater recharge, the groundwater below the Ica Valley must be recharged from either mountain-sourced rivers or deep subsurface groundwater flow, mountain block recharge (MBR), or a combination of the two. This case study sheds light on the following two questions.

1. What can major ion geochemistry and isotopic composition of different water types at different elevations tell us about the importance of MBR for the coastal Ica Aquifer?
2. What is the conceptual model for MBR to the Ica Aquifer and what are the implications for groundwater management?

A total of 52 water samples were collected in December 2017 and May 2018 from the Ica-Huancavelica and Nasca areas for water isotope and geochemical analyses (Figure Box 7-2). Water samples were collected from lakes, rivers, springs, drilled wells, dug wells, municipal water, artificial infiltration ponds, and gallery wells (horizontal wells at surface).

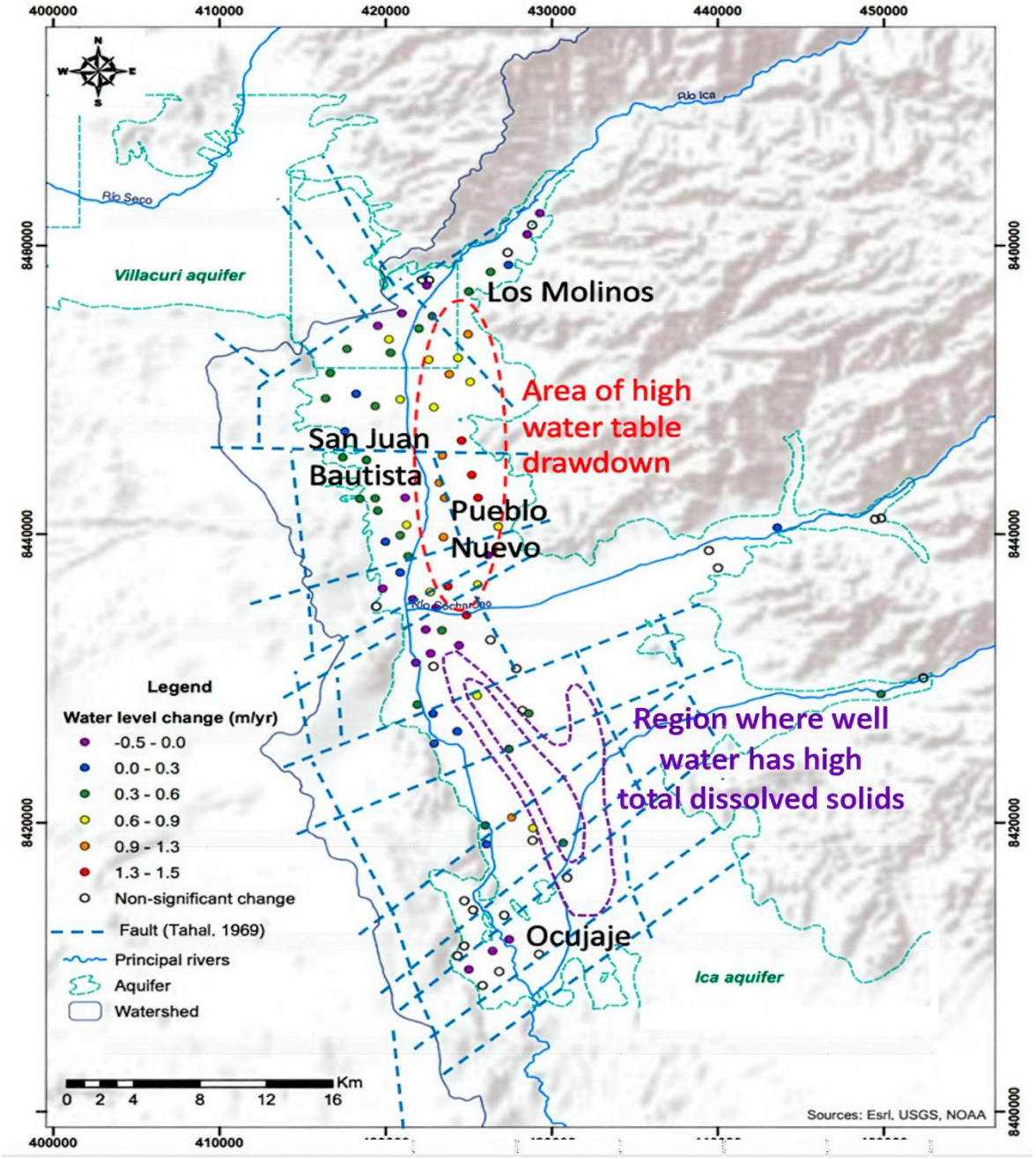

Figure Box 7-2 - Detailed map of Ica (and Villacuri) Aquifer in Peru showing: mapped faults that could transmit groundwater; the location of unpumped wells with statistically significant changes in static water level between 1997 and 2016; and the region where high salt concentrations—i.e., high total dissolved solids concentrations; shown by two isocontours—were observed in water-supply wells.

The water geochemistry results as presented in a Piper plot (Figure Box 7-3) show the varied hydrogeochemical facies, or groups, between the water samples. Three facies are observed, which show a geochemical evolution from Ca-Mg-HCO_3-type water found in higher elevation springs (Figure Box 7-1) to Ca-Cl-type water found in wells and rivers in the coastal valley, and finally to Na-Cl-type water in lakes and drilled wells in the Ica Aquifer. This is a classic geochemical evolution due to rock–water interaction during deep regional groundwater flow (i.e., MBR). If there was no rock–water interaction, the

geochemistry of the river and groundwater would be similar to the high-elevation springs. The Na-Cl waters were observed in the following two water sources

- lakes that were subjected to significant evaporation (discussed later)
- brackish (1,000 to 10,000 mg/L) groundwater in the southern part of the Ica Aquifer

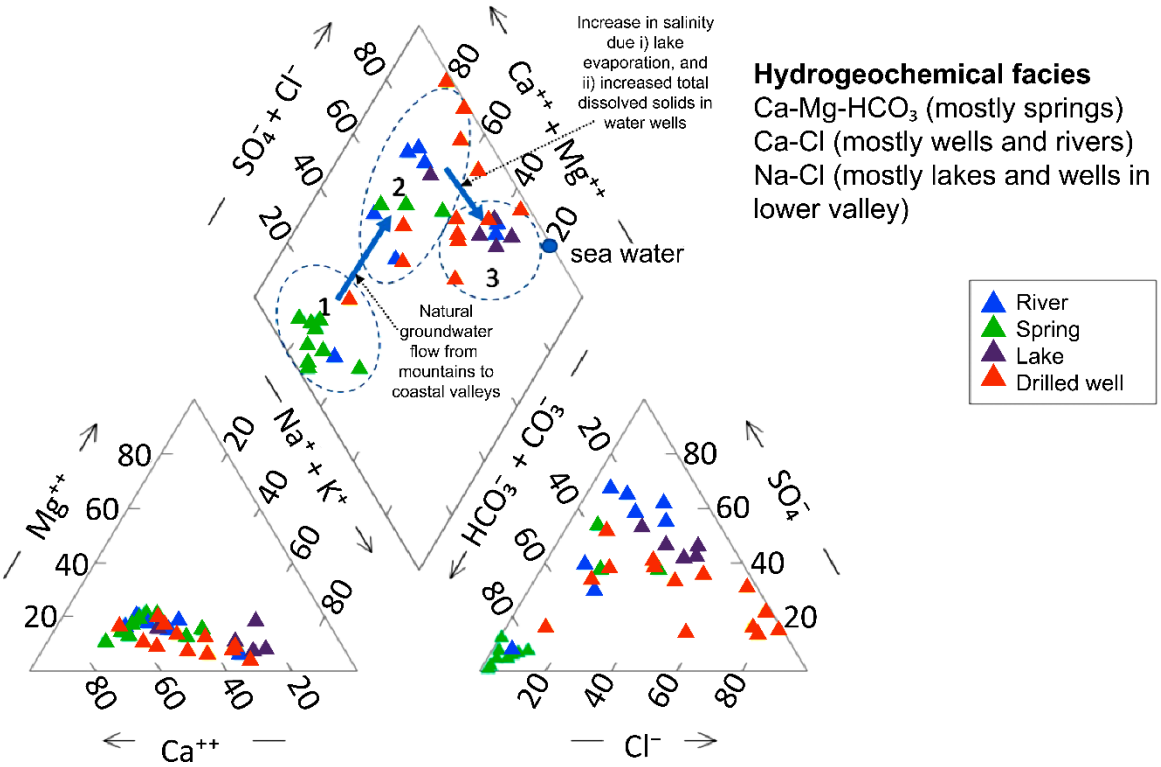

Figure Box 7-3 - Piper diagram showing geochemical composition of river, spring, lake, and drilled well samples. Three hydrogeochemical facies are observed.

Water isotope values (δ^2H and δ^{18}O in H_2O) from precipitation that falls at higher elevations tend to be more depleted and hence plot toward the bottom left of the Global Meteoric Water Line (GMWL) (Clark & Fritz, 1997). Water that remains after increasing evaporation has occurred tends to be more enriched, but more so in δ^{18}O, and plot along a slightly lower slope than the GMWL. Most of the isotope values for water from the Ica river and aquifer plot in a cluster on a dual isotope diagram either directly on the GMWL or to its right, indicating some degree of evaporation (Figure Box 7-4).

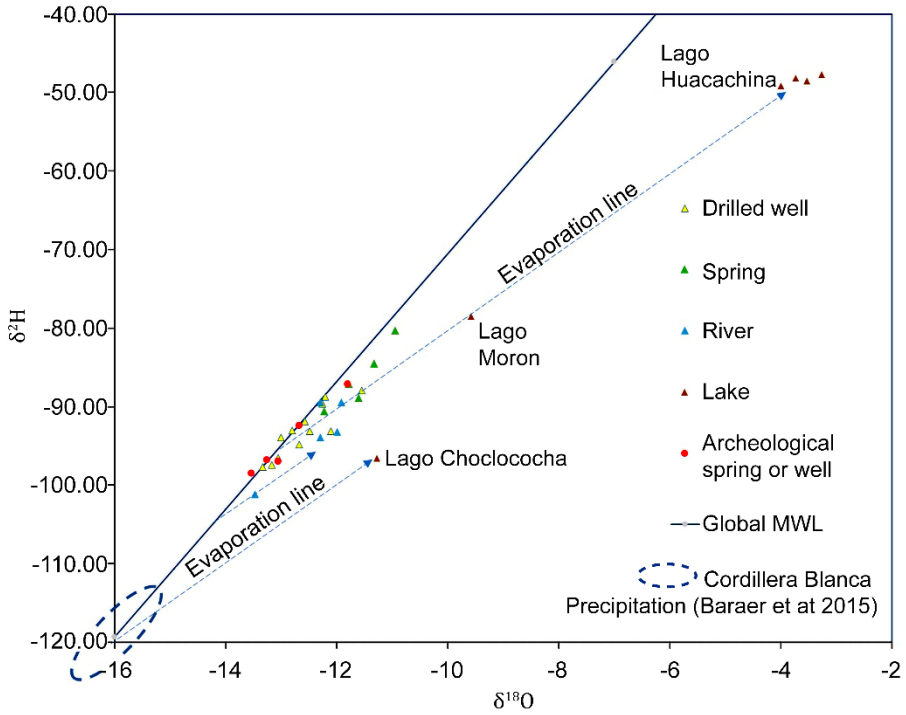

Figure Box 7-4 - Plot of δ^2H vs δ^{18}O for water samples collected from the study area. The Global Meteoric Water Line (GMWL) is indicated, as are evaporation lines. The position to the right of the GMWL of the highest elevation sample (Lago Choclococha) shows evidence of evaporation. When an evaporation line is projected to its intercept on the GMWL, it suggests the precipitation that recharged the lake had an initial isotope concentration on the order of -16‰ for δ^{18}O, and -120 ‰ for δ^2H. A line projected from Lake Huacachina to its groundwater supply well indicates another evaporation line.

The major cluster of samples is observed between δ^{18}O values of -11.5‰ to -13.5‰ and δ^2H values between -100 and -80 ‰. The highest δ^2H and δ^{18}O values were from Lake Huacachina (Figure Box 7-1), a former groundwater-fed *desert oasis* that is now sustained by continual groundwater pumping. Since the groundwater supplying Lake Huacachina was also sampled, an *evaporation line* can be drawn on the dual water isotope diagram by connecting the supply well and the lake.

Notably, one of the few remaining natural lakes in the region (Lake Moron) plots on the same evaporation line on the graph, indicating the slope appears to be robust. The position of most of the river water (and some of the groundwater) samples slightly right of the GMWL indicates they have been subjected to minor evaporation. The lowest isotope values in samples collected for this study were from the Río Pisco during the late rainy season (May), which suggests the river water was sourced at relatively high elevation in the Andes mountains.

A plot of the elevation versus δ^{18}O values (Figure Box 7-5) shows very different elevations for two distinct groupings (i.e., high (>3,800 masl) and low (<800 masl) altitude) but similar δ^{18}O values. The position to the right of the GMWL of the highest elevation sample, collected at the high-altitude Lake Choclococha (4,520 masl), shows evidence of evaporation. When an evaporation line is projected to its intercept on the GMWL, it

suggests the precipitation that recharged the lake had initial isotope values on the order of -15.5‰ for $\delta^{18}O$, and -115‰ for $\delta^{2}H$, which would have fallen at higher altitudes according to results from the high-altitude Cordillera Blanca mountains to the north of this study site (Baraer et al., 2015).

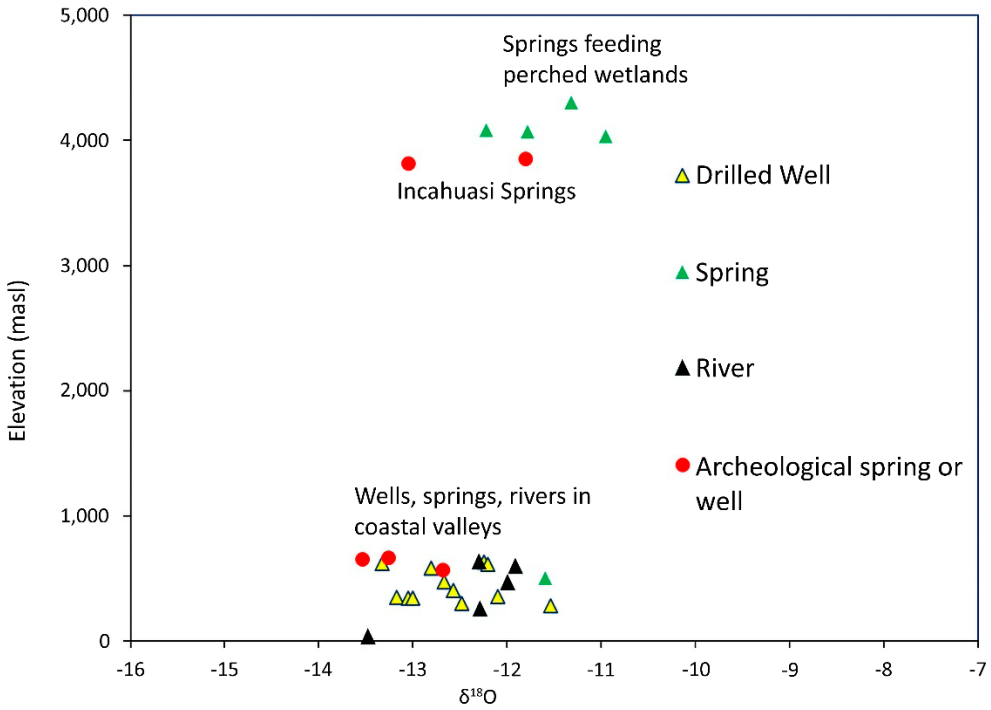

Figure Box 7-5 - Elevation of water sampling points (meters above sea level) versus $\delta^{18}O$ values for water.

These data provide a preliminary hydrogeologic conceptual model where most water precipitates at higher elevations in the Andes then either flows as surface water runoff or infiltrates and migrates downward in rock formations within faults and fractures (Figure Box 7-6). A portion of the surface water runoff infiltrates downward directly into bedrock fractures and faults or through river-connected alluvial aquifers. This water is transmitted as MBR into the deeper groundwater flow that reaches the ground surface at lower elevations feeding springs, seepage faces and river-connected alluvial aquifers. The remainder of the surface water flow continues downward to the coastal valleys, where it discharges to the sea or possibly infiltrates to local aquifers depending on the depth of the water table. The remaining deep groundwater flow that did not discharge at higher elevations flows downward and eventually discharges at the sides of the coastal valleys (along geologic contacts or faults) or deep below the coastal valleys to the alluvial aquifers.

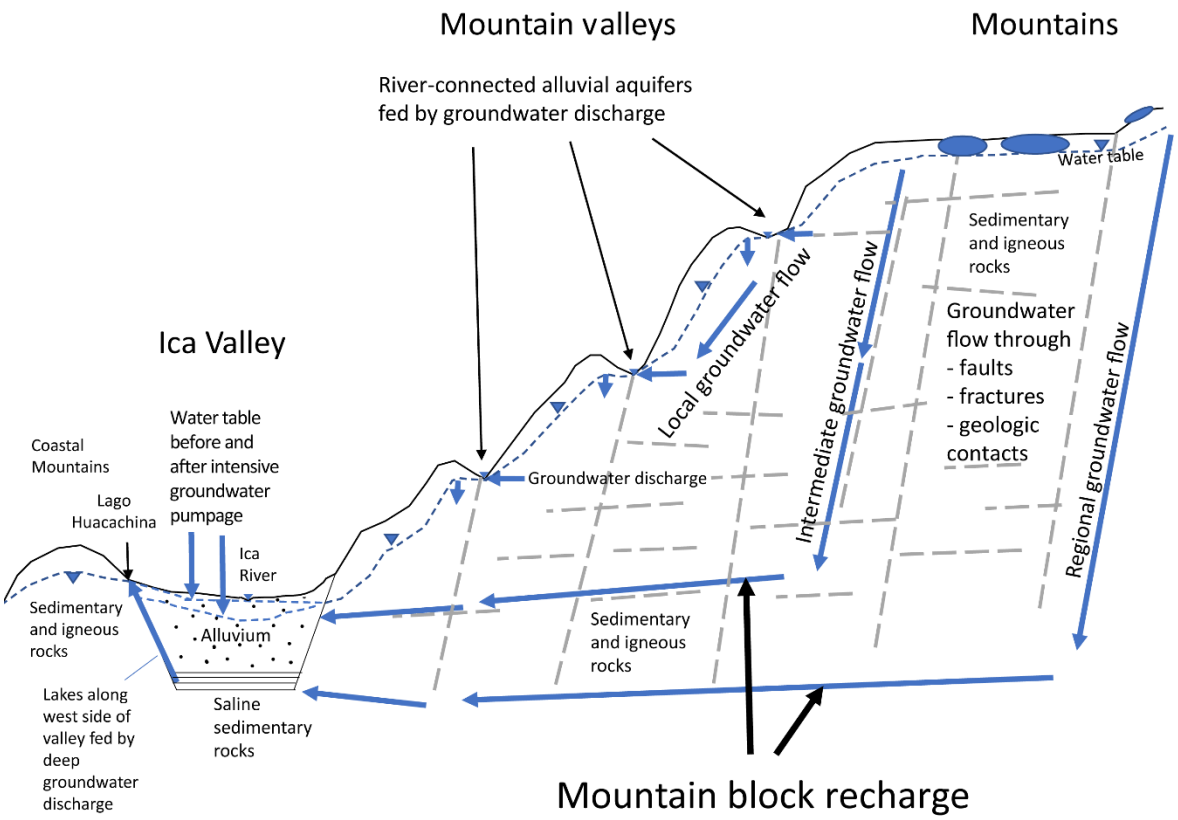

Figure Box 7-6 - Conceptual cross section illustrating local, intermediate, and regional groundwater flow through fractured rock formations in the watershed feeding the Ica Aquifer. Mountain block recharge consists of intermediate and regional groundwater flow systems entering the Ica Aquifer in the subsurface from the mountains.

The sustainability of groundwater in the mountains and coastal valleys depends on maintaining natural groundwater recharge in the mountains to ensure as much water infiltrates into the ground as possible rather than run off downstream, potentially leading to floods, erosion, or loss to the sea. Changing land use in mountain recharge areas (e.g., deforestation for urbanization, industry, or agriculture) can lead to decreased infiltration and groundwater recharge. Land-use management in the mountains needs to ensure natural groundwater recharge is maintained, which will reduce the risk of flooding and feed lower-elevation aquifers. Strong cooperation between communities in the mountains and communities in the lowlands is critical.

Return to where text linked to Box 7

Box 8 - Monitoring Groundwater Storage Changes from Space

NASA's original GRACE (Gravity Recovery and Climate Experiment) mission consisted of twin satellites orbiting the earth between 2002 and 2017. A follow-up mission called GRACE-FO was launched in May 2018 to extend the existing time series. Anomalies in the earth's gravity field due to changes in mass near the earth's surface are detected by continuously measuring the satellites' mutual separation and altitude. These anomalies are mostly attributable to changes in terrestrial water storage (TWS). TWS includes various components: snow storage, canopy storage, surface water storage, soil moisture storage, and groundwater storage. Targeting changes in groundwater storage therefore requires correcting the anomalies for changes in atmospheric moisture, glacier mass loss, soil moisture, and surface water storage. Scanlon and others (2016) suggest that while the accuracy of GRACE total water storage estimates is quite high (order 10 to 30 mm water equivalent), the accuracy of estimated groundwater storage changes is generally much lower because of correction for the other storage terms. As well, the resolution of GRACE data is rather coarse (100,000 km^2), so the data are not suitable for local- to small-scale regional scale studies.

Despite challenges in processing GRACE data, this technology has recently proven invaluable for monitoring groundwater depletion in various regions around the world: Australia, the California Central Valley in the USA, the Middle East (Arabian Aquifer System), and the Indian Subcontinent (the Indus Basin aquifer). More information is available in NASA's video. During the 2006 to 2009 drought in the California Central Valley, GRACE data and ground-based observations revealed that groundwater storage declined by between 24 and 31 km^3, a volume equivalent to the storage capacity of Lake Mead, the largest surface reservoir in the USA (Famiglietti et al., 2011; Lui et al., 2022).

More recently, GRACE data have been used to identify shifts in global freshwater (Rodell et al., 2018). The study was the first attempt to use observations from multiple satellites to assess how freshwater availability is changing. The goal was to distinguish shifts in TWS caused by natural variability in precipitation from trends related to climate change or human impacts. For example, from 2002 to 2016, Saudi Arabia lost 6.1 gigatons per year of stored groundwater (Rodell et al., 2018). The authors examined imagery from Landsat satellites from 1987 to the present, which showed an explosive growth of irrigated farmland in the arid landscape, which may explain the increased drawdown.

Return to where text linked to Box 8

Box 9 - Modeling Recharge and Discharge

Gabriola Island is a small island (60 km^2) located off the southwest coast of British Columbia, Canada. An island is an ideal setting to explore recharge and discharge, because the only source of recharge is local precipitation. The climate is temperate, with cool winters and warm summers. Most of the precipitation falls as rain from October to April. The highest elevations of Gabriola Island occur as cliffs in the southwest , reaching an elevation of 167 m above sea level (masl). Along the coast, the elevation is at sea level (0 masl). The topography is largely controlled by the underlying bedrock, which consists of fractured sandstone- and mudstone-dominant units (Figure 21 conceptualizes the fractured bedrock). The less-competent mudstone units have been preferentially weathered compared to the sandstone units, such that the sandstone forms distinct ridges. The system was modeled with a fully integrated land surface – subsurface numerical model using the MIKE SHE software.

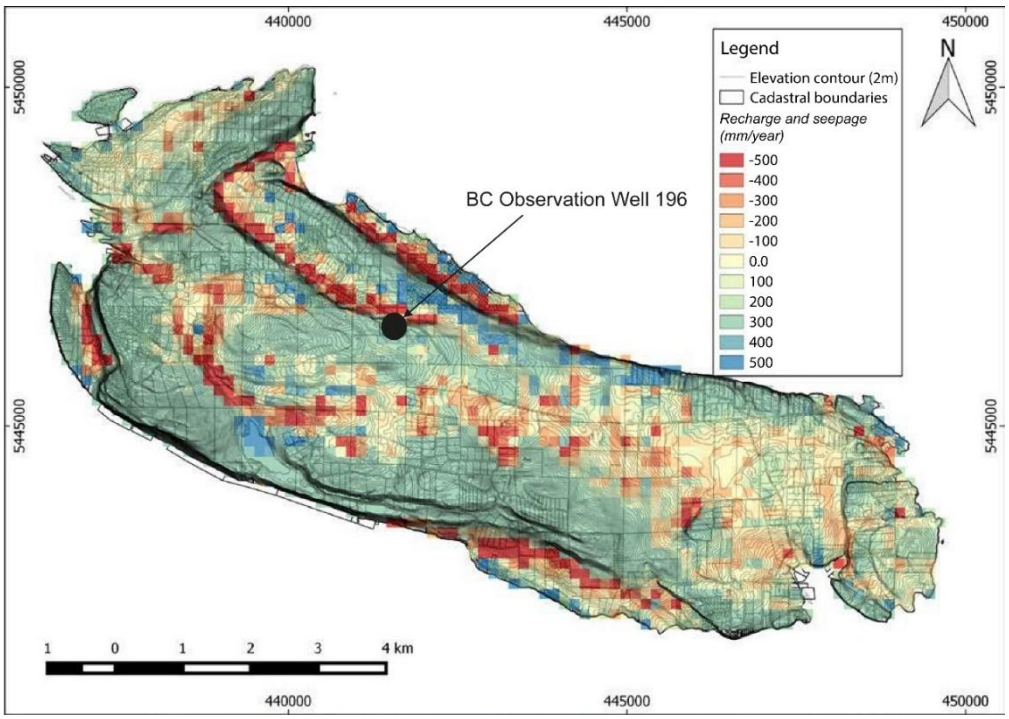

Figure Box 9-1 - Gabriola Island, British Columbia, Canada, showing modeled average annual recharge and seepage (mm/year). The scale shows positive and negative numbers. Positive numbers represent recharge areas on an average annual basis, while negative numbers represent discharge zones on an average annual basis. Values close to zero are neither recharge nor discharge areas. Also shown is the location of British Columbia Observation Well 196. Faint gray contours provide a sense of the topography. They range from a maximum elevation of 167 m above sea level (masl) in the southwest to 0 masl along the ocean. Recharge is concentrated at high elevations on the windward (southwestern) side of the island where storms approach and on sand dunes in the north. Discharge occurs as seepage in low areas (adapted from Burgess & Allen, 2016).

Recharge and discharge were determined using an integrated hydrologic model. The model used climate data for a 20-year period between October 1, 1995, and September 30, 2015. Model calibration spanned October 1, 1995 to September 30, 2005, and model validation spanned October 1, 2005 to September 30, 2015. The results represent a period of

historically high recharge on the island. A description of the model can be found in a report by Burgess and Allen (2016).

Figure Box 9-1 shows recharge areas and discharge (as seepage) areas. Positive values (in blue and green) represent areas where recharge occurs on an average annual basis, while negative values (in red) represent discharge to seepage areas. Recharge generally occurs in areas of higher elevation, while seepage occurs at the base of steep slopes of topographic ridges. Groundwater discharges to the ocean beneath the surface along the coast. Total average annual precipitation from October 1995 to September 2005 (the calibration period) was 984±150 mm and the spatial average annual diffuse recharge was 199 mm/year, varying from 188 to 215 mm/year. Therefore, annual recharge was approximately 20 percent of annual precipitation.

The recharge and discharge patterns vary slightly on a seasonal basis. Figure Box 9-2 shows the distribution of seasonally persistent recharge and discharge areas on the island. Ultimately, groundwater that does not form seepage discharges to the ocean. Approximately 30 percent of the island area is represented by seasonally persistent recharge areas (i.e., recharge areas throughout the year), while only 4 percent is represented by seasonally persistent discharge. Due to the seasonality of precipitation in this coastal region, 66 percent of the island area experiences both recharge and discharge variably throughout the year. Because of local scale variations in topography, recharge and discharge areas are heterogeneously distributed across the island.

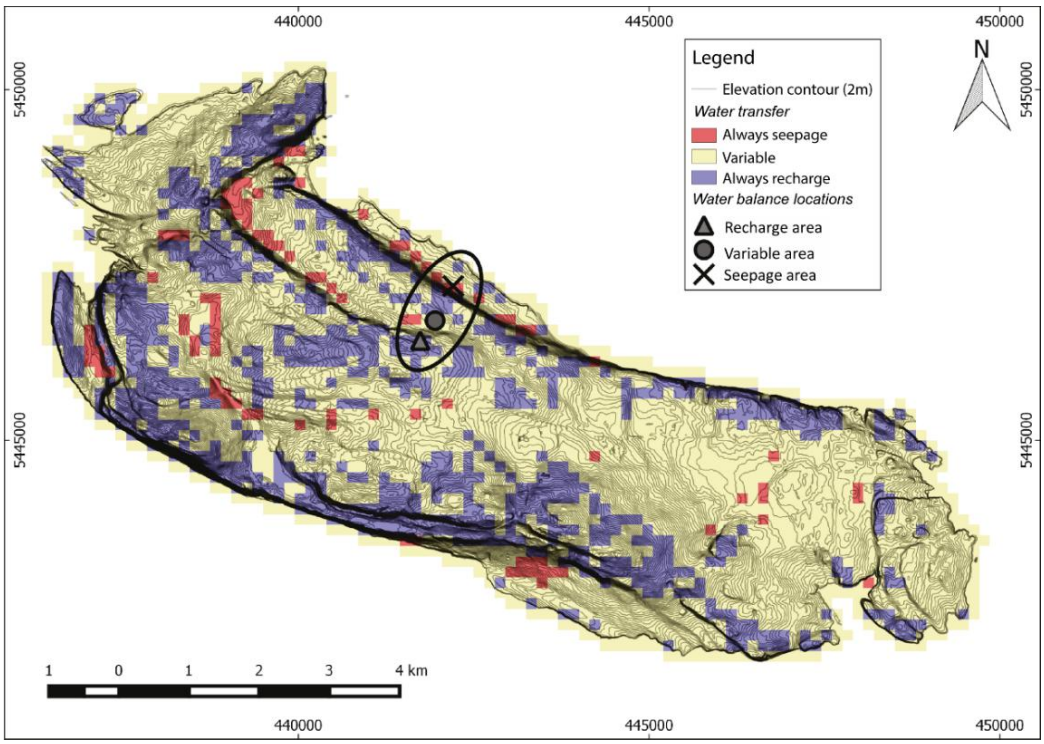

Figure Box 9-2 - Gabriola Island, British Columbia, Canada, showing recharge modeling results. Grid cells displayed as *Always Recharge* have only recharge occurring, while cells displayed as *Always Seepage* have only discharge occurring. Cells designated *Variable* register both discharge and seepage at different times of the year.

Some recharge occurs at low elevation near the coast. Figure Box 9-3 shows the water table in a recharge area remaining below the ground surface (even during the wet season). Conversely, the water table in a seepage area is constantly above the ground surface (even during the dry season). A variable area experiences recharge and seepage depending on the time of year, because the water table varies between being below to above the ground surface. During the summer, the water table is lower than ground surface and only recharge occurs. When the water table is higher in winter, seepage occurs.

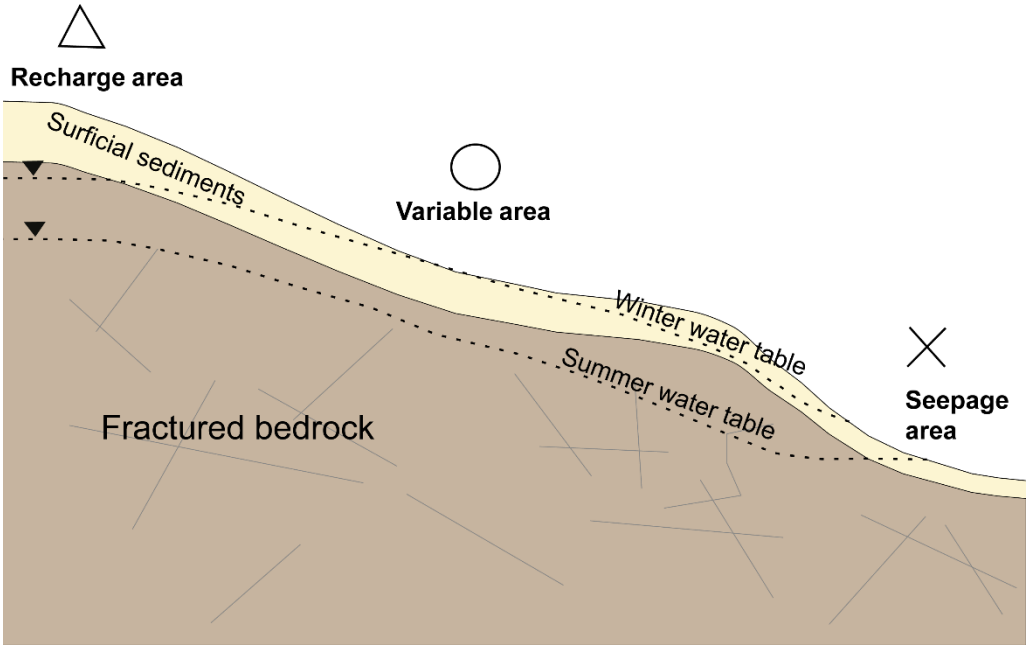

Figure Box 9-3 - Conceptualization of a hillslope showing the location of seasonally persistent recharge and seepage areas. In the variable area, both recharge and seepage occur due to seasonal fluctuations in the water table. The locations of these zones are shown in Figure Box 9-2 (adapted from Burgess, 2017, with permission).

Figure Box 9-4 shows the monthly water balance as average monthly totals. The water table elevation is represented as depth below ground surface (right y-axis) and is expressed as the day-of-year average for a model grid cell that coincides with the location of Observation Well 196 (data accessible from the British Columbia Groundwater Level Data website↗). From January to March, the water table is at its highest, just below ground surface in this temperate region. The water table gradually drops, reaching a low in September. During the rainy months (October to April), the water table rises in response to rainfall. Eventually, the water table stabilizes (January to April) as the amount of infiltration balances the drainage and the storage is full. From May to September, less precipitation falls and the water table declines. Evapotranspiration is higher during the summer, resulting in even less recharge.

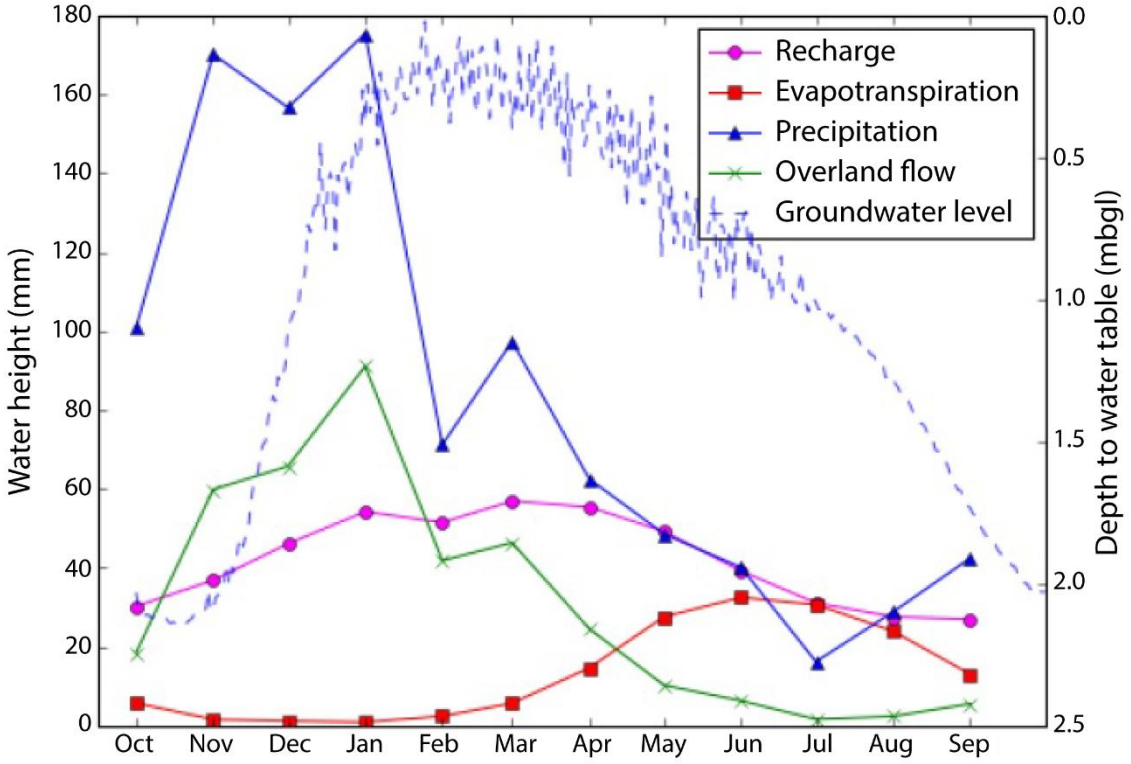

Figure Box 9-4 - Water balance for Gabriola Island. Water balance items are average monthly totals as a water height (in mm), while the groundwater level represents the water table (in meters below ground level, mbgl) and is the day of year average for one grid cell in the model that coincides with the position of Observation well 196 for which data are accessible on the British Columbia Groundwater Level Data website↗ (adapted from Burgess & Allen, 2016).

Return to where text linked to Box 9↑

Box 10 - Depression-focused Recharge

Contributed by Masaki Hayashi, University of Calgary, Alberta, Canada

Focused recharge also occurs in topographic depressions in some regions. Stream-focused recharge and depression-focused recharge are associated with highly seasonal or episodic inputs of water. Surface and subsurface runoff generated in surrounding areas floods the depressions and infiltrates, thereby forming a mound of the water table under the depression (Figure Box 10-1a). These depressions are topographically closed in terms of surface water drainage, which allows the retention of runoff water as it infiltrates into the ground. Therefore, depression-focused recharge is common in semi-arid and arid regions that have low regional topographic gradients, such as the Southern High Plains of Texas, USA (Scanlon & Goldsmith, 1997), the Canadian prairies (Hayashi et al., 2003), the La Plata region of Argentina (Logan & Rudolph, 1997), and the Sahel region of Niger (Desconnets et al., 1997). Each depression may occupy only a small area (e.g., less than a hectare, i.e., $1x10^4$ m^2), but collectively depressions can cover a sizable fraction of the landscape (Figure Box 10-1b,c). Therefore, in regions with a high density of small depressions, such as the Northern Great Plains of North America, depression-focused recharge is the dominant mode of recharge (e.g., Pavlovskii et al., 2019; Bam et al., 2020). Given the importance of depression-focused recharge in these regions, the shorter winter seasons and decreased snowfall amounts projected due to global warming (Newton et al., 2021) have the potential to decrease spring runoff, storage in depressions and, consequently, regional groundwater recharge rates (Negm et al., 2021).

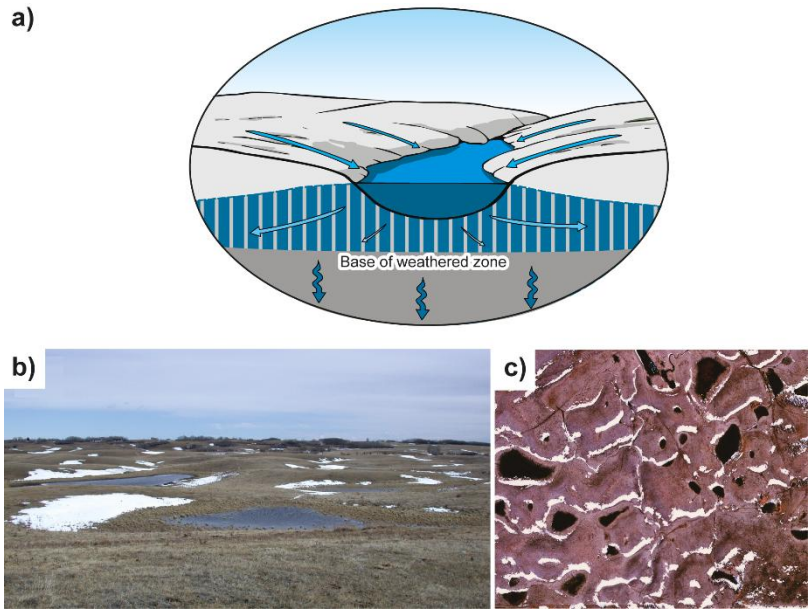

Figure Box 10-1 - a) A schematic diagram showing a flooded depression and the water-table mound formed by depression-focused recharge. b) Depressions flooded by snowmelt runoff in the Canadian prairies. c) Infrared aerial photograph of the area shown in in b). Dark areas indicate standing water in (b) and (c). (modified after Hayashi, 2013).

Return to where text linked to Box 10

Box 11 - Atmospheric Rivers

Atmospheric rivers (ARs) are long plumes of atmospheric moisture, thousands of kilometers long and hundreds of kilometers wide, that transport large volumes of water vapor as a "river" in the atmosphere and deliver intense precipitation to mid-latitude coastlines (Ralph & Dettinger, 2011). They are responsible for over 90 percent of the globe's water vapor flux from the tropics toward the poles (Zhu & Newell, 1998). When AR paths intersect coastal or inland mountain ranges, these storms release intense orographic precipitation (Ralph & Dettinger, 2011), giving way to flooding, landslides, and infrastructure damage (Payne et al., 2020). As a result, ARs were responsible for 84 percent of flood damage in the western USA between 1978 and 2017 (Corringham et al., 2019). In November 2021, a series of ARs made landfall in southwestern British Columbia, Canada (shown in this AR video) and led to extreme flooding on the south coast and the interior of the province causing significant damage to infrastructure (more information at Understanding the November 2021 B.C. Flood Damage↗). To date, these ARs were the costliest natural disaster in British Columbia (Gillett et al., 2022).

ARs also have a significant effect on North American water resources. As predominantly cold-season phenomena (Mundhenk et al., 2016), AR precipitation is generally associated with beneficial snowpack contributions in western North America (Eldardiry et al., 2019) but can degrade snowpacks through rain-on-snow events (Chen et al., 2019; Eldardiry et al., 2019). Warm-season ARs can relieve droughts; ARs have broken 60 to 74 percent of all persistent droughts between 1950 and 2010 in the northwest USA (Dettinger, 2013).

Return to where text linked to Box 11↑

Box 12 - Groundwater-level Responses to Atmospheric Pressure Fluctuations and to Air Entrapment

Barometric Pressure Fluctuations

Atmospheric pressure fluctuations represent a real, wide-spread (blanket) stress applied both directly at land surface and to the water surface in an open well. Atmospheric pressure is the weight of the air over a given location. The average atmospheric pressure at mean sea level (MSL) in the International Standard Atmosphere model (ISA) is 101.325 kPa (1 atm). Pressure decreases smoothly and rapidly from the earth's surface to the top of the atmosphere, where at 10-km elevation it is about 26.4 kPa. In addition, atmospheric pressure has a diurnal (24-hour or circadian) and semidiurnal (12-hour or semi-circadian) cycle caused by global atmospheric tides. This effect is strongest in tropical zones, with an amplitude of a few hectopascals (hPa), and is almost zero in polar areas. Atmospheric pressure also varies with the weather. Low-pressure systems usually bring cloudiness, wind, and precipitation, while high-pressure systems are associated with clear, sunny days.

Let's first consider confined aquifers. Jacob (1940) introduced a model for atmospheric pressure effects on confined aquifers. Jacob's model is premised on the instantaneous transmission of the pressure change, without attenuation through the confining bed, to the interface between the confining bed and the aquifer (Figure 40).

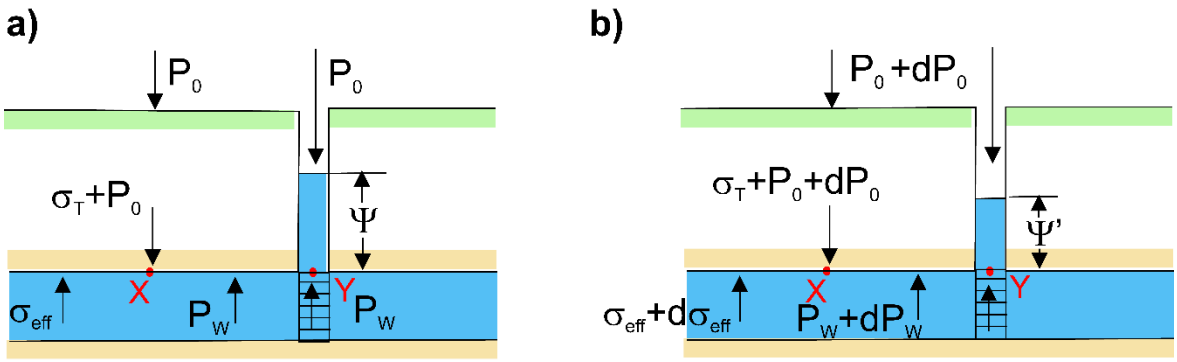

Figure Box 12-1 - The effect of atmospheric pressure change on the water level in a well screened in a confined aquifer. a) Pressure head Ψ under atmospheric pressure P_0. b) Instantaneous reduced pressure head Ψ' due to an increase in atmospheric pressure P_0+dP_0. P_W is water pressure, σ_T is total stress and σ_{eff} is effective stress, where d denotes change in the respective parameter. The water level in the well declines because a portion of the increased stress in the aquifer is borne by the aquifer skeleton while all of the pressure increase is applied to the water level surface in the well.

At equilibrium, the stresses acting downward on the confined aquifer must equal the stresses acting upward. Two stresses act downward: the total stress σ_T and atmospheric pressure P_0. Upward stresses include the fluid pressure (let's assume the fluid is water) P_W and the effective stress σ_{eff} acting on the aquifer skeleton (i.e., the assemblage of grains). So, at equilibrium, it would be as in Equation Box (12-1).

$$\sigma_T T + P_0 = \sigma_{eff} + P_W \qquad (12\text{-}1)$$

We can equally write this equation in terms of changes in each stress variable, as in Equation Box (12-2).

$$d\sigma_T + dP_0 = d\sigma_{eff} + dP_W \quad (12\text{-}2)$$

Normally, σ_T does not change ($d\sigma_T=0$), unless some heavy load such as a train passes over the aquifer; shown in Equation Box (12-3).

$$dP_0 = d\sigma_{eff} + dP_W \quad (12\text{-}3)$$

Now, consider what happens if P_0 changes. According to Equation Box (12-3), part of this change will be manifested in the aquifer though $d\sigma_{eff}$ and part through dP_W. In a well, recall that the water rises up to a height Ψ (the pressure head) where the upward acting fluid pressure P_W just balances the weight of the water column ($\rho g\Psi$) plus P_0, as in Equation Box (12-4).

$$P_W = \rho g\Psi + P_0 \quad (12\text{-}4)$$

Unlike the aquifer, within the well, a change in P_0 is borne entirely by the water because there is no aquifer material in the well. This leads to a pressure imbalance equal to $dP_0 - dP_W$ between the water in the well and the aquifer water, which results in an equivalent change in Ψ, as in Equation Box (12-5).

$$dP_W - dP_0 = \rho g\, d\Psi \quad (12\text{-}5)$$

The new pressure head is denoted Ψ' in Figure Box 12-1. Given the negative sign of dP_0 in this equation, if P_0 increases, then Ψ' decreases.

Observations of atmospheric pressure records and groundwater-level records for confined aquifers indicate that the two signals are synchronous and that the initial change in water level in the well is a constant fraction of the change in pressure (i.e., a linear relationship).

Water levels in wells screened below the water table in unconfined aquifers (Figure Box 12-2) are also affected by changes in atmospheric pressure, but the mechanism is substantially different from that causing such changes in confined aquifers. Weeks (1979) developed a model for atmospheric pressure variations in unconfined aquifers. If atmospheric pressure changes, air (a gas) must first move into or out of the overlying unsaturated materials. But there is some resistance to gas flow imposed by the unsaturated materials due to their finite permeability and their capacity to store or release gas as the pressure changes—that is, the *pneumatic diffusivity* of these materials. This resistance to gas flow slows the transmission of the pressure change to the water table, as illustrated by the wavy arrows in Figure Box 12-2a. Thus, shortly after the atmospheric pressure changes at the land surface by an amount dP_0, only a fraction of the change has been transmitted through the unsaturated zone to the water table. Consequently, the change in gas pressure

at the water table lags behind the change at the land surface. However, atmospheric changes are transmitted instantaneously down a well bore (Figure Box 12-2b). This results in a temporary pressure imbalance between water in the well and water in the adjacent aquifer that results in a decline of Ψ' if P_0 increases by dP_0. As time passes, the entire pressure change is transmitted through the unsaturated zone and the well water level recovers to its initial position. In short, an atmospheric pressure change causes water-level to change in a well before the atmospheric pressure change influences the aquifer (Weeks, 1979).

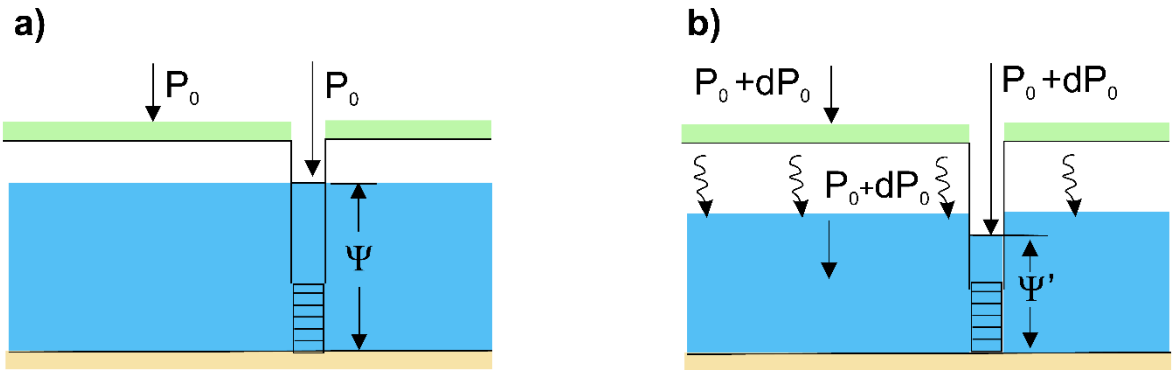

Figure Box 12-2 - The effect of atmospheric pressure change on the water level in a well screened in an unconfined aquifer. a) Pressure head Ψ under atmospheric pressure P_0. b) Delayed response to P_0+dP_0 in the aquifer accompanied by an instantaneous response in the well shown by a decrease in Ψ'.

Practically, for low-gradient, unconfined aquifers with variable unsaturated zone characteristics (e.g., thickness, pneumatic diffusivity), atmospheric pressure fluctuations can cause temporal changes in both the direction and velocity of lateral flow in the unconfined aquifer (Spane, 2002). Rasmussen and Crawford (1997) also identified a delayed well response associated with well characteristics (i.e., wellbore storage and well skin effects).

Finally, although not discussed further here, other loads on the Earth's surface also result in water-level fluctuations (e.g., earth tides, explosions, passing of rail trains). Earth tides have semi-diurnal, diurnal, and longer period fluctuations.

Air entrapment - The Lisse effect

The water table rise due to rain events occasionally can be much greater than would be expected based on the amount of rain that has fallen. As the wetting front advances, even by a few millimeters, air can be trapped between the advancing wetting front and the original water table, leading to an increase in pressure (Figure Box 12-3). The increase in pressure produces a rapid rise in the water level measured in a well screened below the water table that can be up to 50 times greater than the amount of rain producing the rise (Weeks, 2005).

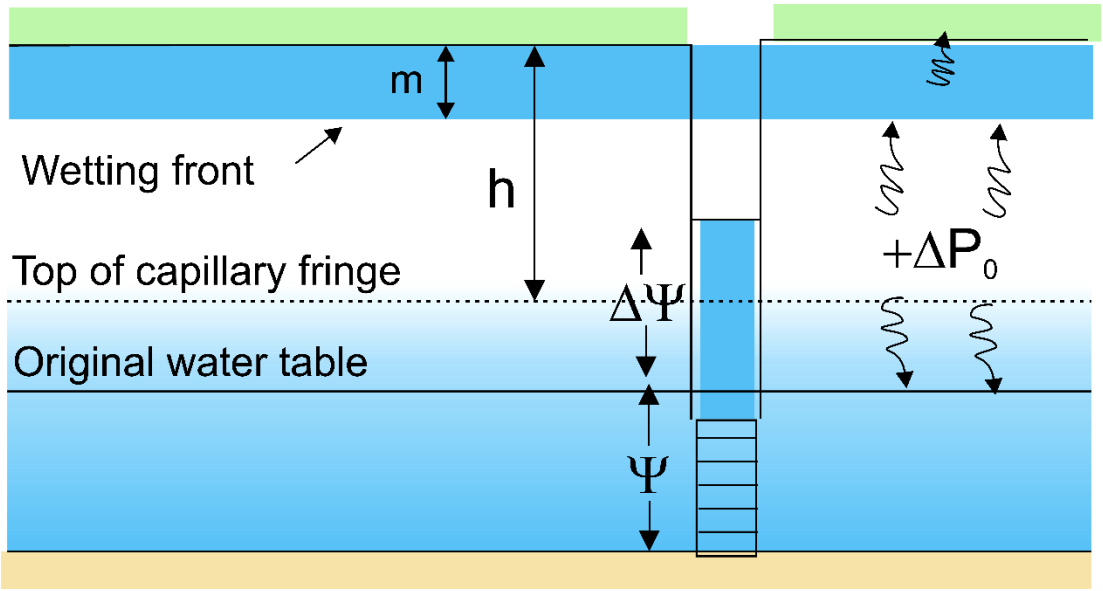

Figure Box 12-3 - Conceptualization of the Lisse effect. Air is trapped (as illustrated by the wavy arrows) between the advancing wetting front during a rain event and the original water table, leading to an increase in air pressure P_0 within the vadose zone. Some air can escape to surface (modified from Weeks, 2005; based on the original figure from Hooghoudt, 1947).

This process is called the *Lisse effect*, first described by Hooghoudt (1947), who named it after the village of Lisse in Holland, where the effect was first witnessed in a shallow observation well by Thal Larsen in 1932.

The original conceptual model by Larsen suggests that during an intense rain event, the wetting front acts as a seal, trapping the air between the advancing wetting front and the water table. This leads to an increase in the unsaturated zone air pressure relative to atmospheric pressure and causes a rise in the water level measured in a well. Larsen's equation for calculating the rise in pressure head $\Delta\psi$ in the well is shown in Equation Box (12-6).

$$\Delta\Psi = P_0\left(\frac{m}{h-m}\right) \qquad (12\text{-}6)$$

where:

P_0 = atmospheric pressure expressed in terms of water column height (L)

m = depth of wetting front penetration (L)

h = distance from the top of the capillary fringe to land surface (L)

Weeks (2005) later revisited Larsen's conceptual model, suggesting that an additional force was needed to balance the back pressure of soil air against the wetting front. Weeks proposed including a capillary pressure gradient imposed by the soil tension due to residual moisture in the soil column immediately below the advancing wetting front. Weeks drew a parallel to Green and Ampt's (1911) capillary pressure head ψ_f used in rainfall-runoff models to explain the decline in the rate of infiltration with time during precipitation events. Effectively, the negative soil tension beneath the wetting front (ψ_f)

adds to the gravitational force driving the advance of the wetting front, so the rate of advancement is faster than that due to gravity alone. Weeks proposed a modified version of Equation Box (12-6) to account for this additional downward force as shown in Equation Box (12-7).

$$\Delta\Psi = P_0\left(1 + \frac{m}{h-m}\right) \tag{12-7}$$

Week's compared observed water-level rises from the Lisse effect (which ranged from 0.10 to 0.55 m) to those calculated using Equation Box (12-7) using published values of ψ_f for similar material types (range 0.10 to 0.60).

In a later study, Guo and others (2008)—in a paper co-authored by Weeks—used numerical simulations to evaluate the reliability of the theory presented by Weeks (2005) to predict the magnitude of the Lisse effect in situations that mimic the physical complexity of real aquifers. The simulations showed a more rapid rate of advancement of the wetting front than proposed by Larsen's equation as shown by Equation Box (12-6). They proposed that the Lisse effect is generally governed by the *air entry pressure* (also referred to as the *bubbling pressure* h_b) rather than the Green and Ampt ψ_f in the conceptual model for the Lisse effect.

Guo and others (2008) found that the magnitude of the Lisse effect increases with soil uniformity and decreases with water-table depth. Meyboom (1967) observed the effect in light sandy soils where the water table depth was less than 0.6 m, with the effect diminishing as the water-table depth increased. Meyboom did not observe the effect where the water table was deeper than 1.3 m. The Lisse effect was also extensively explored by Heliotus and De Witt (1987) in an extensive field study and laboratory column experiments. The phenomenon requires rather specific conditions to occur (e.g., a shallow well screened just below the water table) but could be more widespread in occurrence than recognized. Failure to recognize the Lisse effect could result in overestimation of recharge (Healy & Cook, 2002). Additionally, the effect appears to limit infiltration and increase overland flow during intense rain events.

The Lisse effect leads to a similar magnitude of water level rise as a very different process, known as the *reverse Weiringermeer effect* (Hooghoudt, 1947; Meyboom, 1967) in which the capillary fringe extends to land surface and only a small amount of rain is required to fill the capillary menisci and bring both the water table and the water level in the well close to the surface. The rise in water level is rapid, as is the recession.

Return to where text linked to Box 12

Box 13 - Seasonal Variations in Groundwater Flow Patterns near a Willow Ring

Based on the study by Meyboom (1966a, 1966b)

Using detailed vertical measurements of hydraulic head, Meyboom (1966b) mapped the seasonal variation of groundwater flow in the vicinity of willow rings (Figure Box 13-1). During the winter (Figure Box 13-1a), the groundwater flow direction is obliquely downward, which Meyboom described as *normal* conditions relating to regional groundwater flow pattern that is not influenced by the vegetation or water in depression storage (Box 10 discusses depression-focused recharge). As soon as the snow that had accumulated in the depression melts and starts to infiltrate, a groundwater mound begins to develop underneath the depression. By the time the depression has filled with water, it has attained the highest hydraulic head, driving groundwater flow vertically downward and radially away from the mound (Figure Box 13-1b). In the absence of vegetation, the water table would eventually rise to the position indicated by the dashed line below the depression in (Figure Box 13-1b). However, groundwater is consumed by the willows, creating a cone of depression, which eventually leads to a reversal in the hydraulic gradient, resulting in groundwater discharge to the depressions (Figure Box 13-1c).

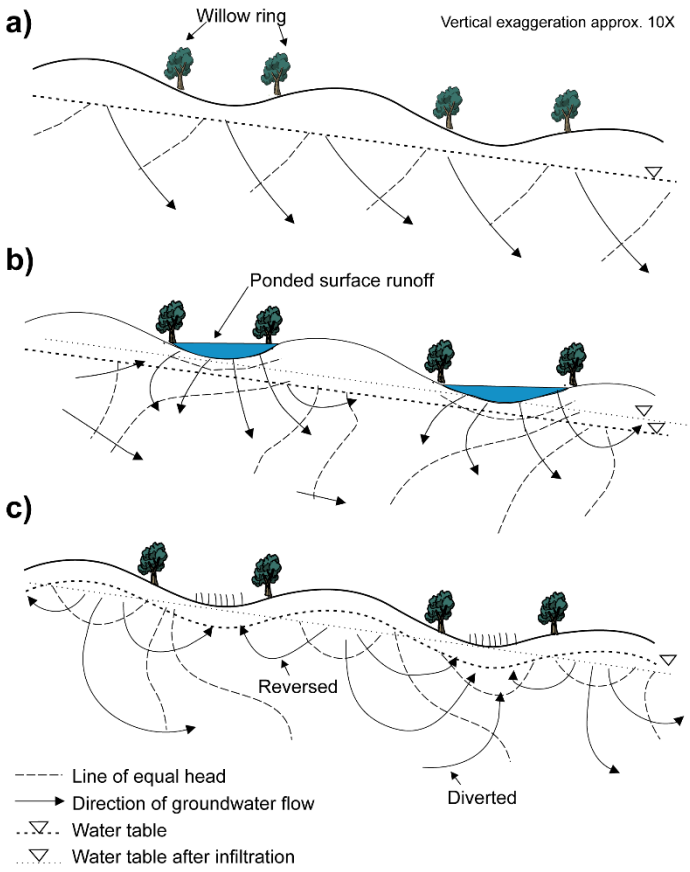

Figure Box 13-1 - Generalized sequence of flow conditions near willow ring: a) *normal* downward flow; b) groundwater mounds produced by infiltrating melt water; and c) inverted water-tables resulting from a cone of depression around the phreatophytic willows (reproduced from Meyboom, 1966b's Figure 5).

Meyboom (1967) measured groundwater salinity in numerous ponds surrounded by willows. Because the willows have a very low tolerance for saline (alkali) conditions (<700 microSiemens per cm), the presence of the willows suggests that most willow rings are located on top of recharge areas.

Return to where text linked to Box 13

Box 14 - Dynamics of Climate–Groundwater Stream Interactions

Based on the study by Cuthbert and others (2019)

Groundwater flow systems exist in dynamic balance with the climate connecting interacting zones of recharge and discharge with multiple feedbacks (Cuthbert et al., 2019). As climate varies, changes in the quantity and location of natural groundwater recharge lead to changes in groundwater storage with consequent changes in water levels and groundwater discharge. Cuthbert and others (2019) explored the sensitivity of groundwater systems to changes in climate and the sensitivity of climate to changes in groundwater systems as well as the timescales over which such changes may occur. They used the concept of the water table ratio (WTR), which is defined as the ratio of the hydraulic head at a groundwater flow divide above the fixed hydraulic head boundary (h_0–b) to the maximum terrain rise above the fixed head boundary, d, as illustrated in Figure Box 14-1a.

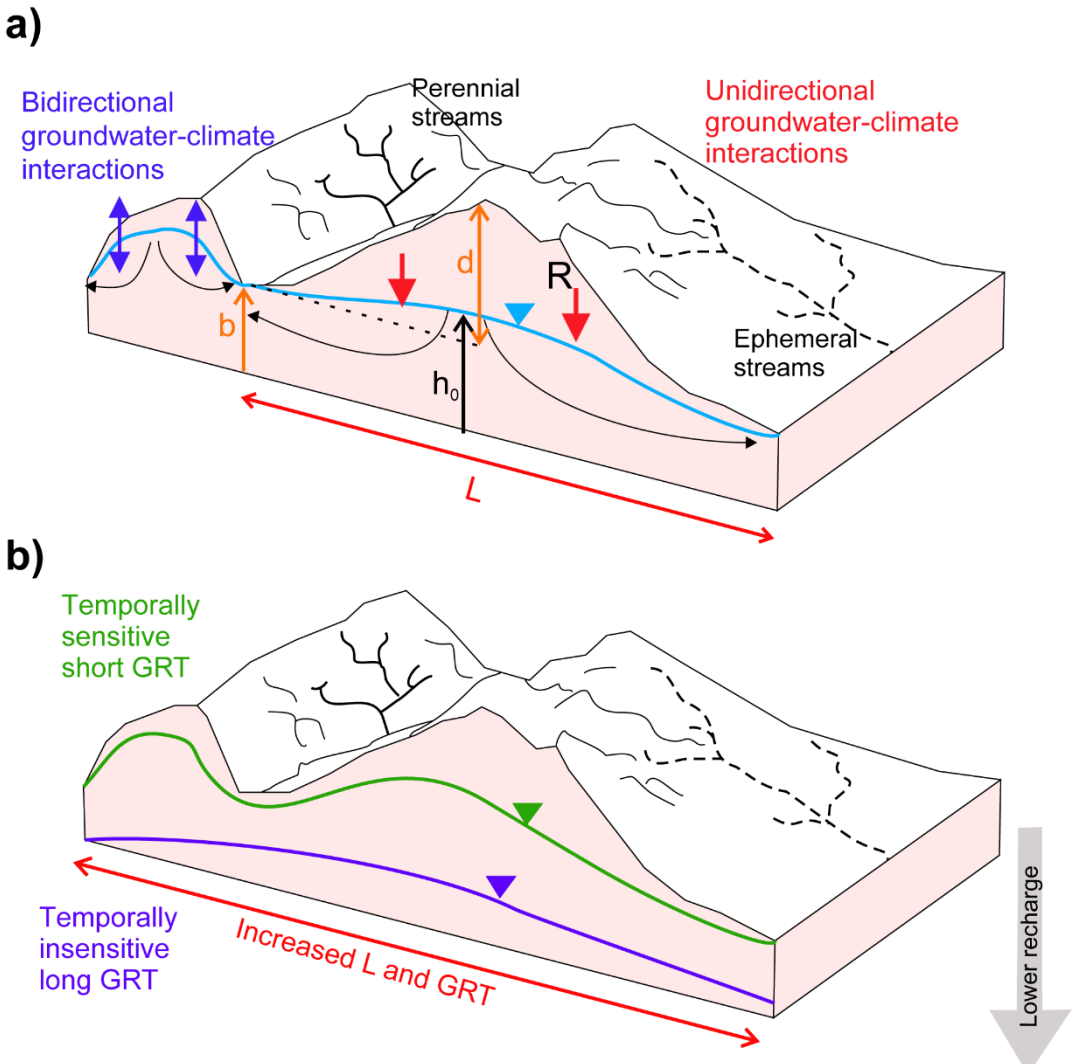

Figure Box 14-1 - Conceptual model for a) the water table ratio (WTR); and b) groundwater response time (GRT) (modified from Cuthbert et al., 2019).

Cuthbert and others (2019) modified the original linear equation for the WTR proposed by Haitjema and Mitchell-Bruker (2005) to a non-linear one, as shown in Equation Box (14-1).

$$WTR = \frac{\sqrt{b^2 + \frac{RL^2}{4K}} - b}{d} \tag{14-1}$$

where:

b and d = lengths as shown in Figure Box 14-1a (L)

R = recharge rate (LT^{-1})

L = distance between perennial streams as shown in Figure Box 14-1a (L)

K = hydraulic conductivity (LT^{-1})

The WTR is a relative measure of how full the groundwater system is (Cuthbert et al., 2019). If the WTR>1, the water-table depth is shallow (e.g., <10 m below ground level) and groundwater-climate interactions can occur bidirectionally (i.e., the climate system can give to the groundwater system in the form of recharge and receive moisture back via evapotranspiration). A WTR>1 indicates water-table conditions are *topographically controlled*, where there is a close connection between topography and water-table depth. In contrast, in a *recharge-controlled* area where WTR<1, water tables are more disconnected from the topography. While the subsurface may still receive recharge, the degree of two-way interaction between climate and groundwater is limited and interactions are predominantly unidirectional. Cuthbert and others (2019) mapped WTRs globally and found that regions with high humidity, subdued topography, and/or low permeability typically have a WTR>1, while regions with WTR<1 are more common in drier climates or more mountainous topography.

Cuthbert and others (2019) also used the concept of groundwater response time (*GRT*) to characterize sensitivity of groundwater systems to long-timescale interactions with climate (Figure Box 14-1b). *GRT* is a measure of the time it takes a groundwater system to re-equilibrate to a change in hydraulic boundary conditions. For example, if the recharge rate changes, how long it will take for a new equilibrium to be established with a stream? *GRT* is calculated as shown in Equation Box 14-2. Their results indicate a global median *GRT* of nearly 6,000 years (long memory), dominantly in areas that are arid, while only 25 percent of Earth's land surface area has a *GRT* of <100 years (short memory). The long memory of groundwater systems in drylands means that abrupt (in geological terms) changes in recharge or widely distributed groundwater abstraction will leave longer legacies.

$$GRT = \frac{L^2 S}{\beta T} \quad (14\text{-}2)$$

where:

L = distance between perennial streams as shown in Figure Box 14-1b (L)

S = storage coefficient (dimensionless)

β = constant, Cuthbert and others use π^2 to be consistent with mathematically equivalent uses of 'time constants' in other branches of science (dimensionless)

T = transmissivity (L^2T^{-1})

Return to where text linked to Box 14

Box 15 - How Plants and the Critical Zone Regulate Groundwater Recharge and Discharge in Seasonally Dry Climates

Contributed by W. J. Hahm, Department of Geography, Simon Fraser University, Burnaby, BC, Canada

Imagine that you are standing on a hillslope in northern California, USA, surrounded by the tallest trees on the planet. (Or, better still, explore virtually via Google Earth↗.) At the foot of the hillslope, a flowing stream hosts an aquatic community that includes species of threatened salmon. This ecosystem is highly dependent on water resources for survival in the summer—and yet, despite the rich life around you, the summer coincides with an approximately six-month-long period of little to no rain. Where do the trees and streams get their water in the dry season?

In rainy Mediterranean climates such as coastal California, plants and streams rely on subsurface water during the dry summer months, highlighting the importance of subsurface structure in storing wet-season water for later release. Fresh bedrock has low hydraulic conductivity and porosity, making it unsuitable for seasonal water storage. But physical and chemical weathering turn bedrock into saprolite and soil, creating interconnected porosity. The northern California Coast Ranges emerged from sea level only in the last 10 million years (Lock et al., 2006). In this rapidly uplifting and eroding environment, fresh bedrock constantly moves toward the surface. A balance must exist between the lowering of weathering fronts and surface erosion to maintain a porous, water-storing layer. This balance is maintained by processes within Earth's critical zone, from the canopy to the base of weathered bedrock.

Researchers at the Eel River Critical Zone Observatory↗ have been studying how the subsurface mediates water supply to forests and streams, including recharge and discharge processes, for over a decade. The Eel River, California's third-largest watershed, drains the rugged Northern Coast Ranges (Figure Box 15-1). Along the coast, evergreen forests with redwood, Douglas fir, live oak, and madrone cover steep hillsides, while further inland, a savanna-woodland ecosystem with deciduous oaks and annual herbaceous groundcover is common. This area receives about 2 m of rain yearly, almost all between October and April. Summers are warm and dry. Two rock types underlie much of the watershed: a slightly metamorphosed shale and sandstone unit, called the *Coastal Belt* and a highly sheared mélange unit called the *Central Belt*. These rocks record the turbulent legacy of subduction off the coast for hundreds of millions of years.

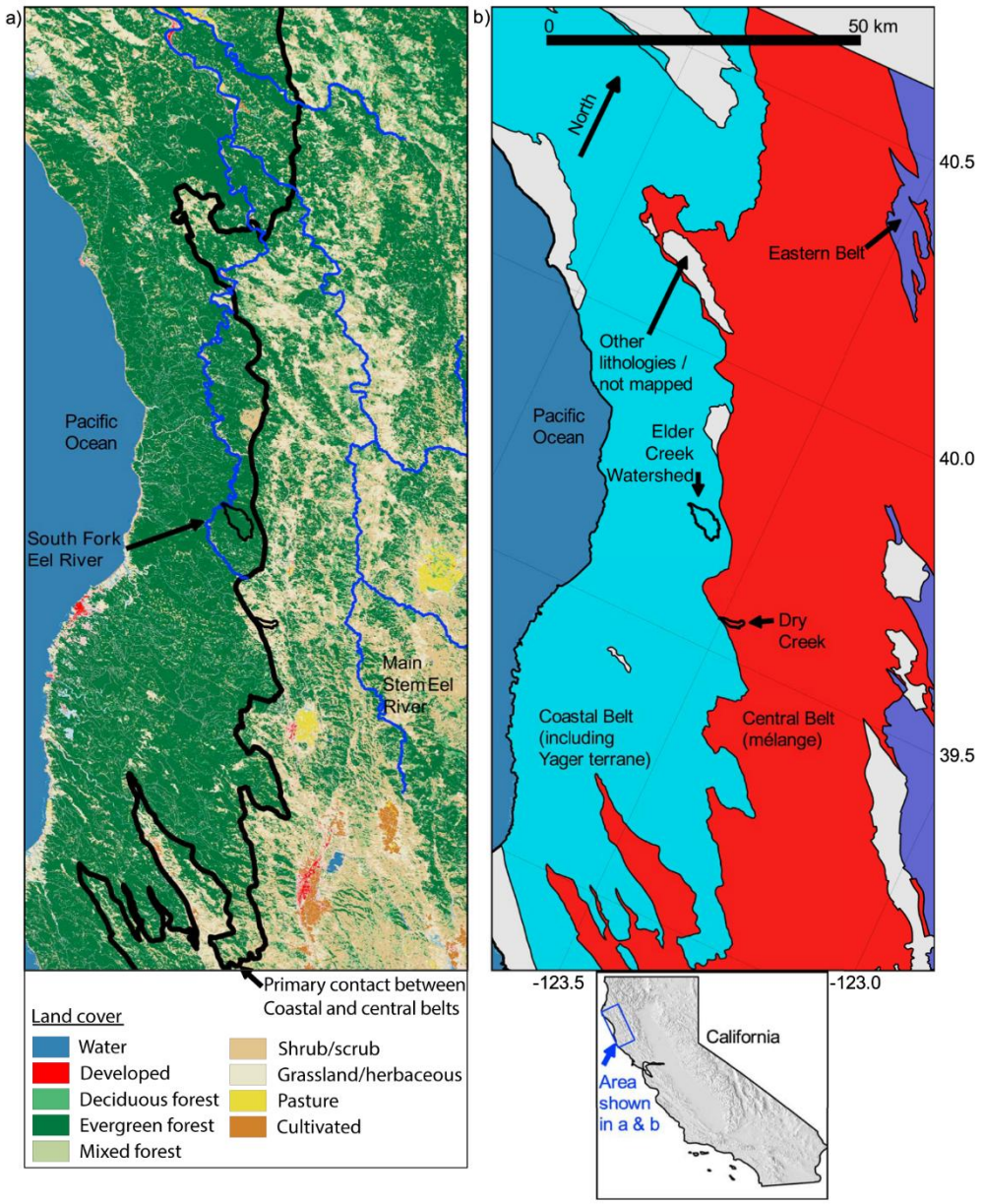

Figure Box 15-1 - Site map showing study area locations within the Eel River watershed and the correspondence between a) vegetation cover and b) lithology (reproduced from Hahm et al., 2019).

Recognizing the complexity of feedbacks in the near-surface environment calls for a holistic approach to understanding recharge and discharge. At the Eel River Critical Zone Observatory, a multidisciplinary team of hydrologists, hydrogeologists, geochemists, ecologists, geomorphologists, and soil scientists work together. LiDAR flights provide high-resolution mapping of ground surface topography and vegetation canopy. Multiple stations collect climate data. Off-grid research sites use solar panels, some high in the canopy, to recharge battery banks that power data loggers, and radios relay information in real-time to a central database. Sap flow probes track tree water use, and stream gauges record discharge. Deep borehole transects from channel to ridge allow continuous groundwater monitoring and access to hillslopes for monitoring vadose zone moisture

dynamics with neutron and nuclear magnetic resonance probes (Rempe & Dietrich, 2018). These boreholes also reveal the hillslope-scale structure of weathering front propagation into the bedrock (Figure Box 15-2). In this terrain, the repeated ridges and valleys suggest a commonality in subsurface weathering profile development. Studying ecologic and hydrologic processes in a few representative hillslope units in detail allows process-based inferences to be scaled up to understand catchment-wide and regional patterns and behavior.

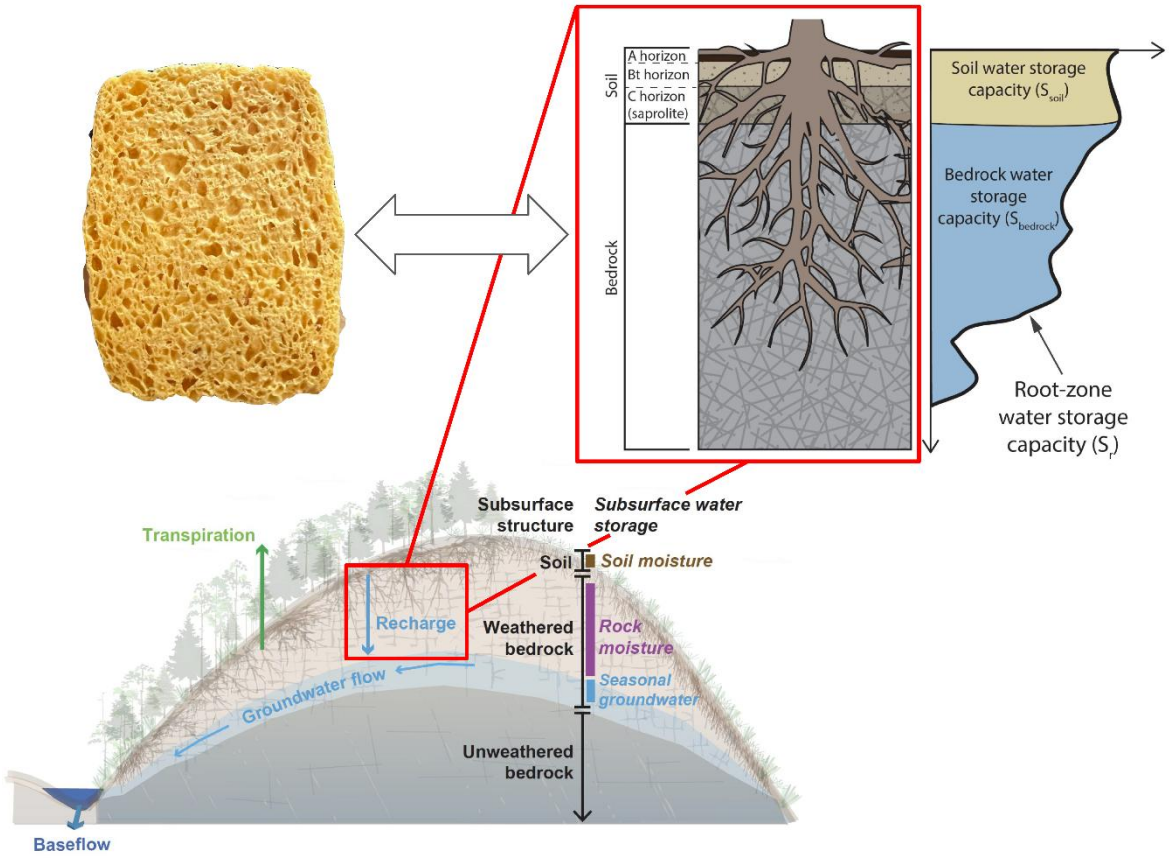

Figure Box 15-2 - The critical zone (CZ), with subsurface storage reservoirs and hydrologic fluxes within a representative 'unit' hillslope from an upland, eroding landscape (reproduced from Dralle et al., 2023, 2024).

The discoveries from these efforts can be summarized through a tour of the annual hydrologic cycle on an intensively studied hillslope bordering Elder Creek, a tributary to the South Fork Eel River in the Coastal Belt. Beginning on the hydrologic new year (October 1), the first autumn rains pass through a towering evergreen canopy of mixed broadleaf-needleleaf trees, dominated by old-growth Douglas fir, some 60 m tall. Rain that is not intercepted wets and infiltrates into the thin soils (about 0.5 m thick). The soil's hydraulic conductivity exceeds even the highest rainfall intensities, preventing infiltration-excess overland flow. Vertical moisture probe profiles show that wetting fronts can reach 1 m deep in the first large storms, while the upper soil profile continues to gain moisture (Salve et al., 2012). These first rain events, if followed by sunny days, provoke a sharp increase in tree sap flow. Although transpiration continues all summer, it reaches a

minimum just before the first rains arrive in the fall (Link et al., 2014). Although the rains have returned, the stream and groundwater show little response: negligible recharge and discharge occur at the beginning of the wet season. Some precipitation that falls directly on the channel prompts minor increases in streamflow, but streamflow conditions remain similar to end-of-summer baseflow, and groundwater tables inside hillslopes continue to recede. This is because in addition to the soil, a variably thick weathered bedrock vadose zone must also wet up before triggering recharge to the saturated zone, which then discharges at the base of hillslopes to become streamflow. The amount of rain required to replenish storage deficits throughout the unsaturated zone depends on hillslope position, local rock type, and the plant community that has depleted moisture in the unsaturated zone throughout the summer dry season (Dralle et al., 2018; Oshun et al., 2016; Rempe & Dietrich, 2018).

In general, researchers have found that the plant community has a large first-order control on when recharge and discharge begin. At sites with large forests with high evapotranspiration and interception, it can take up to 600 mm of rain for the rock moisture zone to be replenished (but not saturated) and trigger recharge, awakening the water table at the ridge from its dry season decline. However, this amount varies with hillslope position. Researchers have found that the thickness of weathered bedrock increases upslope, from channel to ridge, as does the thickness of the unsaturated zone. At the Elder Creek site in the Coastal Belt, fresh bedrock is exposed at the surface in the stream channel and coincides with the water table on the adjacent hillslope. However, at the ridgetop the depth to fresh bedrock and the water table is approximately 25 m: both the water table and the interface between fresh and weathered bedrock mimic the ground surface topography (Rempe & Dietrich, 2014). As a result, more rain is typically required to replenish vadose zone storage deficits at the ridgetop than near the channel. Once deficits are replenished, subsequent rains throughout the latter part of the wet season—sometimes thousands of mm more—do not result in large increases in rock moisture content. Instead, pressure-driven water flow through the thick vadose zone rapidly recharges the groundwater. The water table rises and falls in response to storms but remains more than 10 m below the surface at the divide. Streamflow is driven by the rising water table within the weathered bedrock: the slope and thickness of the hillslope saturated zone determine groundwater discharge. The observation that rock moisture content in the weathered bedrock vadose zone rises and then plateaus during the wet season indicates that weathered bedrock, like soil, exhibits a field-capacity-like behavior.

In the Central Belt, the weathered bedrock vadose zone in the mélange unit is much shallower, only a few meters deep at the ridgetop, resulting in lower pore space and water storage capacity. Here, just 100 mm of rain triggers a water-table response, and 200 mm completely saturates the subsurface, causing widespread saturation overland flow.

These geological differences in critical zone structure and hydrologic dynamics significantly impact ecosystems during the dry season (Figure Box 15-3). By April or May, the rains cease, and streams and groundwater recede. In the Coastal Belt, Elder Creek maintains flow, supporting year-round resident salmonids. Conversely, in the Central Belt, Dry Creek turns into stagnant, disconnected pools by early June, despite similar winter rainfall. The aquatic ecosystem in Dry Creek is fundamentally different, with a receding and expanding wetted channel network, unlike the stable network in Elder Creek (Lovill et al., 2018). These differences are due to the varying degrees of weathering front propagation into the bedrock, influencing the store versus shed behavior of subsurface critical zones.

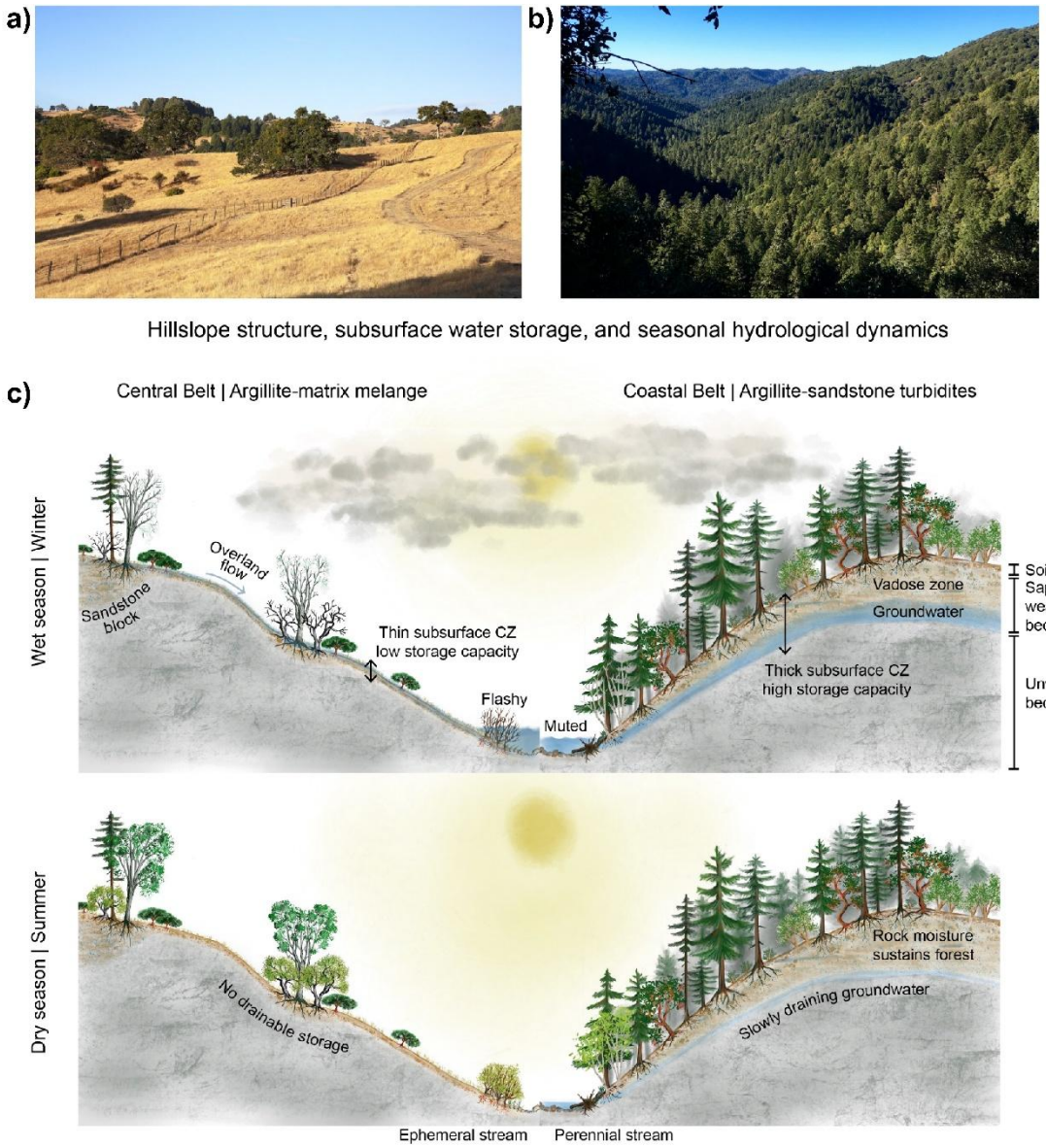

Figure Box 15-3 - Plant, subsurface, and hydrologic contrasts between the a) Central Belt and b) Coastal Belt. c) Differences between wet and dry seasons in the Central and Coastal Belts (reproduced from Dralle et al., 2023, 2024).

In the Coastal Belt, the thick subsurface critical zone stores groundwater and rock moisture, sustaining streamflow (from groundwater) and the forest (from the unsaturated zone) through the summer. Vadose zone moisture depletes throughout the dry season, with neutron probe surveys showing up to 100 mm/month of water loss from the weathered bedrock vadose zone, while only 10 mm/month leaves as streamflow (Rempe & Dietrich, 2018). This indicates that the dense forest depends on the drawdown of rock moisture for transpiration. Stream recession analysis and catchment mass balance reveal that most seasonally dynamic water occurs as unsaturated moisture, underscoring the vadose zone's role in regulating groundwater recharge and streamflow (Dralle et al., 2018).

In the Central Belt, the thin subsurface critical zone lacks the storage capacity to support a dense forest canopy. Instead, annual grasses dominate despite receiving 2 m of annual rainfall. Soil maps show soils have similar plant-available water storage capacities across the region, highlighting the importance of bedrock weathering trajectories in determining water availability for ecosystems in this seasonally dry climate (Hahm et al., 2019). Renewed interest in why bedrock weathers differently has led to theories about the roles of local and regional stress fields, chemical weathering front propagation, equilibrated pore water drainage from fresh bedrock, and frost weathering.

Considering the broader picture, we must ask where else in the world do weathered bedrock properties significantly impact groundwater recharge and discharge in upland landscapes? Despite extensive soil depth and texture mapping, comparable data for weathered bedrock is lacking. Remote sensing and geophysical approaches provide rough estimates, but we have limited methods for assessing weathered bedrock water storage properties globally (Riebe et al., 2017). Intensive hillslope-scale drilling campaigns still offer the best subsurface portraits and will be necessary to ground truth maps and parameterize models.

Recent studies show that in the continental USA, there is a strong correlation between woody vegetation and areas with thin soils (where bedrock is within 1.5 m of the surface). These areas are often eroding uplands where bedrock is actively exhumed. Remotely sensed data indicates plant water use during dry periods in these areas often exceeds soil water-holding capacities, suggesting widespread use of water from weathered bedrock by woody plants (McCormick et al., 2021). However, many questions remain: What portion of that water comes from the saturated versus unsaturated zone? How will declining snowpack in a warmer future affect the role of weathered bedrock in supplying streams and forests with water and buffering ecosystems from drought? Do some tree species preferentially use water from bedrock, and do they significantly impact dry-season streamflow? Can this information guide forest management practices toward desired outcomes? Answering these questions requires diverse scientific backgrounds and varied field sites to challenge our understanding and generate new ideas.

Return to where text linked to Box 15

10 Exercise Solutions

Solution Exercise 1

The groundwater flow system is mapped by the following.

- conceptualizing the groundwater system—where recharge and discharge might be taking place
- transcribing the hydraulic head values next to each piezometer number
- sketching equipotential lines that connect lines of equal head, remembering the conceptual system
  - *note*: the water table provides values of hydraulic head that are *equal* to the elevation at that point, so the water table provides an infinite set of values; also, equipotential lines should intersect no flow boundaries, such as groundwater divides, at 90 degrees
- after sketching the equipotential lines, sketching in flow lines perpendicular to them
  - *note*: this assumes the aquifer is homogeneous and isotropic
- identifying recharge areas where the net direction of groundwater flow is downward, and discharge areas where the net direction of groundwater flow is upward.

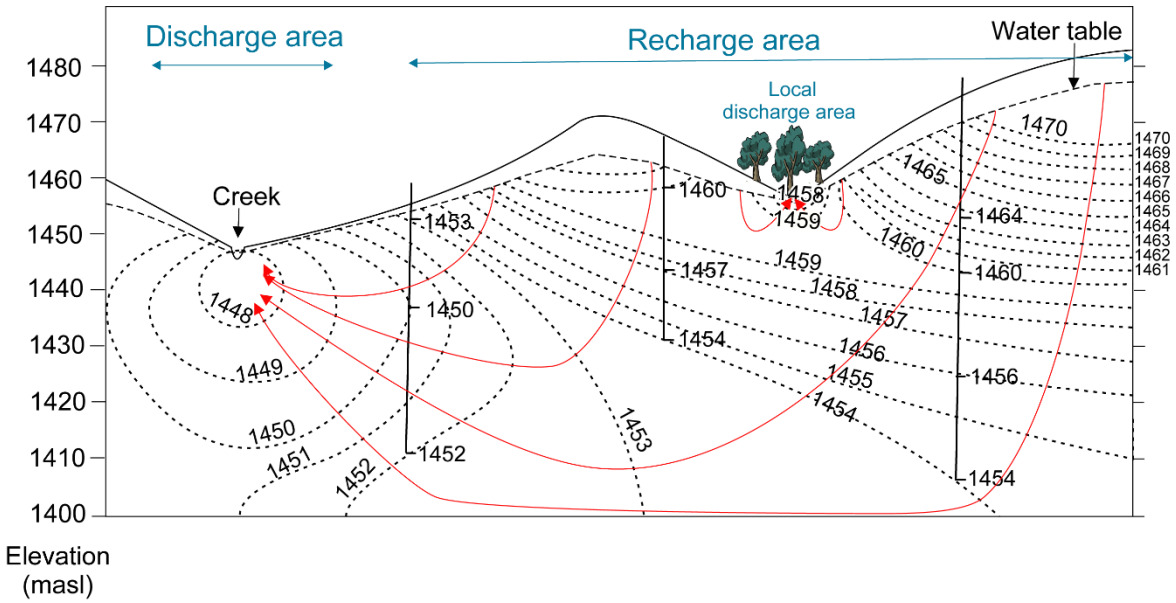

Return to Exercise 1

Return to where text linked to Exercise 1

Solution Exercise 2

a) In the simple flow system illustrated in Figure 4, the conceptual arrows representing flow indicate diffuse recharge extends from the ridge at the peak elevation nearly to the bank of the stream. The discharge area is near and to the stream along its full length.

b) The complex flow system illustrated in Figure 2 is three-dimensional within the unconfined aquifer due to the variable topography, which gives rise to local differences in vertical hydraulic gradients. Recharge areas occur where flow is downward in the high-elevation area with focused recharge from the mountain lake as well as underneath the small hills. Discharge areas occur where there is upward flow near the large lake and to a minor extent in the swales. Within the two confined aquifers, the flow is dominantly two-dimensional, along the regional sloping hydraulic gradient. Diffuse and focused recharge areas occur in the uplands and diffuse interaquifer recharge occurs from overlying aquifers. The discharge zones of the confined aquifers are not included in the diagram.

Return to Exercise 2

Return to where text linked to Exercise 2

Solution Exercise 3

a) Paving and buildings reduce the recharge area. To counter the impacts of reduced infiltration and groundwater recharge in urban areas, some municipalities are experimenting with different engineering designs (called low impact development) for capturing storm water runoff in collection ponds and creating infiltration galleries that facilitate infiltration.

b) The impact of agriculture on groundwater recharge is complex. Removal of natural vegetation for agriculture often leads to more runoff (less recharge) and soils become more vulnerable to erosion and compaction. Agricultural areas often require some form of irrigation (i.e., artificial precipitation), during the growing season to replenish soil moisture for the plants, but often too much irrigation is applied (more than the plants can use) and the excess water recharges the aquifer or is drained by agricultural drains.

c) The effect of logging on groundwater is uncertain. While the removal of trees effectively reduces evapotranspiration losses, thereby promoting groundwater recharge, the loss of the tree canopy and root systems can lead to increased runoff. Few scientific studies exist on the impact of logging on groundwater recharge.

Return to Exercise 3

Return to where text linked to Exercise 3

Solution Exercise 4

$$h_c \; for \; fine \; silt = \frac{2\,\sigma\cos(\alpha_c)}{\gamma\, r_c} = \frac{2\left(0.0742\ \frac{\mathrm{N}}{\mathrm{m}}\right)\cos(0)}{9.8x10^3\ \frac{\mathrm{N}}{\mathrm{m}^3}\,(0.000002\ \mathrm{m})} = 7.57\ \mathrm{m} = 757\ \mathrm{cm}$$

The pore radius is a rough estimate so the values should be rounded.

Soil texture	Grain diameter (cm)	Pore radius (cm)	Capillary rise (m)	Capillary rise in cm and rounded
Fine silt	0.0008	0.0002	7.5714	750
Very fine sand	0.0075	0.0015	1.0095	100
Medium sand	0.03	0.006	0.2524	25
Very coarse sand	0.2	0.1	0.0151	2

Return to Exercise 4

Return to where text linked to Exercise 4

Solution Exercise 5

Using Equation (16) and substituting values from the image provided:

$$\Psi_{soil} = \Psi_{gauge} + L$$

$\Psi 1$ = -70 cm + 35 cm = -35 cm

$\Psi 2$ = -80 cm + 50 cm = -30 cm

The matric potential is greater (i.e. more negative) for $\Psi 1$ than for $\Psi 2$ indicating the soil is dryer at the location of gauge 1. Comparatively, vegetation requires more energy to extract water from soil with a matric potential of – 35 cm ($\Psi 1$), than for a soil with a matric potential of -30 cm ($\Psi 21$).

Using Equation (17) to calculate the hydraulic head for tensiometer 1, the total distance from the bottom of the tensiometer to the elevation of the water level in the tensiometer is calculated:

$$h = \Psi + z$$

h1 = -35 cm – 30 cm = -65 cm

The hydraulic head for tensiometer 2 is calculated:

h2 = -30 cm – 45 cm = -75 cm

The difference in head between tensiometer 2 and tensiometer 1 is:

h2 - h1 = -75 cm - (-65cm) = -10 cm

The distance from the ground surface to the bottom of tensiometer 1 is:

z1 = 30 cm

The distance from the ground surface to the bottom of tensiometer 2 is:

z2 = 45 cm

The difference in this distance between the two tensiometers is:

z2 - z1 = 45 cm – 30 cm = 15 cm

The gradient is calculated as:

$$\frac{dh}{dz} = \frac{h2-h1}{dz} = \frac{-10\ cm}{15\ cm} = \text{-0.66}$$

The negative gradient indicates that water flows from location 1 to location 2. Another way to envision it is that water is flowing downward because the hydraulic head at location 1 is -65 cm, which is higher than the hydraulic head of -75 cm at location 2, which is more negative, thus lower.

Return to Exercise 5

Return to where text linked to Exercise 5

Solution Exercise 6

The average annual recharge is 275±37 mm/year. Given the small sample size, the reported standard deviation is the sample standard deviation.

The area of the aquifer is $62\ \text{km}^2\left(\frac{1\text{x}10^6\ \text{m}^2}{\text{km}^2}\right) = 6.2x10^7\ \text{m}^2$

The volumetric recharge rate is

$$275\left(\frac{\text{mm}}{\text{year}}\right)\left(\frac{1\ \text{m}}{1000\ \text{mm}}\right)6.2\times10^7\ \text{m}^2 = 1.7\times10^7\left(\frac{\text{m}^3}{\text{year}}\right)$$

Thought Question: Infiltration can continue only if room is available for water to be added at the soil surface. If the water table is already near the surface when it starts to rain, any additional rise can result in the water table intersecting the ground surface. This is groundwater flooding. In what types of hydrogeological settings might the potential for groundwater flooding be a concern?

Return to Exercise 6

Return to where text linked to Exercise 6

Solution Exercise 7

Rainy season specific discharge:

$$\text{q} = -\text{K}\frac{\text{dh}}{\text{dl}} = -5\text{x}10^{-6}\frac{\text{m}}{\text{s}}\left(\frac{215\ \text{m} - 220\ \text{m}}{50\ \text{m}}\right) = 5\text{x}10^{-7}\ \frac{\text{m}}{\text{s}}$$

Dry season specific discharge:

$$\text{q} = -\text{K}\frac{\text{dh}}{\text{dl}} = -5\text{x}10^{-6}\ \frac{\text{m}}{\text{s}}\left(\frac{214\ \text{m} - 217\ \text{m}}{50\ \text{m}}\right) = 3\text{x}10^{-7}\ \frac{\text{m}}{\text{s}}$$

The hydraulic gradient, dh/dl, in the rainy season is 5 m / 50 m (0.1 m/m). The hydraulic gradient in the dry season is 3 m / 50 m (0.06 m/m). The steeper hydraulic gradient in the wet season results in a higher specific discharge as compared to the specific discharge during the dry season.

Return to Exercise 7

Return to where text linked to Exercise 7

Solution Exercise 8

Volume of water added to the box = 0.01 m^3

Divide by the cross-sectional area to determine the height of the water if the box contained only water.

$$Height\ of\ water\ assuming\ no\ sediment = \frac{0.01\ \text{m}^3}{1\ \text{m}^2} = 0.01\ \text{m} = 1\ \text{cm}$$

But when this volume fills only pore space, we need to divide this height by the specific yield of 0.30 to determine the water-level rise.

$$Water\ table\ rise = \frac{0.01\ \text{m}}{0.30} = 0.033\ \text{m} = 3.3\ \text{cm}$$

Viewed another way, if we observe a 3.3 cm rise in the water table and the specific yield of the aquifer is 0.30, this equates to 1 cm height of water added.

Return to Exercise 8

Return to where text linked to Exercise 8

Solution Exercise 9

By extending the recession trend, the minimum water level in the well at the hydrograph peak is projected to be about 2.4 m if a precipitation event did not occur. The maximum water level in the well is about 4.0 m and occurs approximately 1.5 days after the precipitation event began. To estimate the recharge rate, the change in water level is divided by the amount of time for the change to take place multiplied by the specific yield.

$$\frac{\Delta h_1}{\Delta t_1} = 0.25\frac{4\ \text{m} - 2.4\ \text{m}}{1.5\ \text{days}} = 0.27\ \text{m/day}$$

Return to Exercise 9

Return to where text linked to Exercise 9

Solution Exercise 10

The hydraulic heads are measured at the top and bottom of the confining layer. Choosing the positive direction of z as downward, and defining the bottom of the upper aquifer as z = 0, we calculate the vertical hydraulic gradient through the confining layer is as the difference in head divided by the difference in location.

$$\frac{dh}{dz} = \frac{47\ m - 50\ m}{30\ m - 0\ m} = \frac{-3\ m}{30\ m} = -0.1$$

The negative sign indicates a negative gradient (i.e., lower head for larger values of z).

Darcy's law is used to calculate the flux. The negative sign in Darcy's law indicates that flow is opposite to the gradient, so when combined with the negative gradient produces a positive flux indicating flow in the positive z direction, which in this case is downward.

$$q = -K\frac{dh}{dz} = -1x10^{-7}\frac{m}{s}(-0.1) = 1x10^{-8}\ \frac{m}{s}\ \frac{3.16x10^{7}s}{1\ yr}\ \frac{1x10^{3}mm}{1\ m} = \frac{315\ mm}{yr}$$

Return to Exercise 10

Return to where text linked to Exercise 10

11 Notations

α = albedo (dimensionless)

$b_{average}$ = saturated thickness before and after the rise (L)

C_{leaf} = leaf conductance (LT^{-1})

C_P = concentration of Cl in the precipitation (ML^{-3})

C_R = concentration of Cl in the recharge (ML^{-3})

d_v = absolute humidity (ML^{-3})

D = hydraulic diffusivity (L^2T^{-1})

e = vapor pressure ($ML^{-1}T^{-2}$)

E = Equation 6, evaporation rate (LT^{-1})

E = Equation 23, evaporation from a stream reach (L^3T^{-1})

e_a = actual water vapor pressure ($ML^{-1}T^{-2}$)

e_s = saturation vapor pressure ($ML^{-1}T^{-2}$)

ET = evapotranspiration (L)

ET_g = daily evapotranspiration rate from the groundwater (L)

f_s = shelter factor that accounts for the fact that some leaves are sheltered from the sun and wind and thus transpire at lower rates (dimensionless)

h_c = height of the water column (L)

h = distance from the top of the capillary fringe to land surface (L)

K = hydraulic diffusivity (L^2T)

K_E = coefficient that reflects how efficiently the water vapor is transported vertically into the air by turbulent eddies in the wind (LT^2M^{-1})

K_{sat} = saturated hydraulic conductivity (LT)

L = distance between the tensiometer cup and the height at which the gauge measures (L)

LAI = leaf area index (dimensionless)

λ = weight density (specific weight) of the water ($ML^{-2}T^{-2}$) often used as 9.810^3 N/m^3

λ_v = latent heat of vaporization ($MT^{-2}\Theta^{-1}$) often in J m^{-2} ^{0}K^{-1}

L_d = downward long-wave radiation (MT^{-3}) often as W/m^2

LE = latent heat of evaporation (ML^2T^{-2}) often in J m^{-2} ^{0}K^{-1}

L_u = upward long-wave radiation (MT^{-3}) often as W/m^2

m = Equation Box 12-6, depth of wetting front penetration (L)

m = Equation 14, van Genuchten parameter derived from fitting a moisture characteristic curve, often estimated as 1-1/n (dimensionless)

v_a = wind speed (LT^{-1})

OLF = overland flow (or runoff) (L)

P = Equation 22, precipitation (L)

P = Equation 23, precipitation falling on a stream reach (L^3T^{-1})
P = Equation 25, precipitation (averaged over time) (L)
P_0 = atmospheric pressure expressed in terms of water column height (L)
Ψ = matric potential (MT^{-2}) often in J m^{-2}, and matric potential head (L)
Q_D = stream discharge at the downstream end of a reach (L^3T^{-1})
Q_{IF} = interflow into a stream reach (L^3T^{-1})
Q_{OLF} = overland flow into a stream reach (L^3T^{-1})
Q_{Seep} = groundwater inflow to a stream reach (L^3T^{-1})
Q_{Trib} = tributary flow into a stream reach (L^3T^{-1})
Q_U = stream discharge at the upstream end of a reach (L^3T^{-1})
R = recharge (L)
r = average recovery rate of the groundwater level (L)
r_c = radius of the capillary tube (L)
ρ_w = density of water (ML^{-3})
R_n = all-wave radiation (MT^{-3}) often as W/m^2
R_v = gas constant for water vapor ($ML^2\ T^{-2}\Theta^{-1}$) often as kJ m kg^{-1} $^0K^{-1}$
s = net change in the groundwater level over 24 hours (L) (positive for a rise)
ΔS = Equation 22, change in water storage in the soil column (L), positive for an increase
ΔS = Equation 23, change in storage in a stream reach (L^3T^{-1}), positive for an increase
S = storage coefficient (dimensionless)
S_d = incoming short-wave radiation at the earth surface (MT^{-3}) often as W/m^2
S_e = effective saturation (dimensionless)
σ = surface tension between the water and air (MT^{-2}) often N m^{-1}
S_s = specific storage (L^{-1})
S_Y = specific yield (dimensionless)
T = Equation 2, temperature (Θ) and in Equation 2 as ºC
T = Equation 21, transmissivity, product of thickness and hydraulic conductivity (L^2T)
T_a = air temperature (Θ)
V_T = total volume of sample (L^3)
V_w = volume of pores (L^3)
z = elevation relative to a datum (L)

12 About the Author

Diana Allen (PhD, Carleton University, 1996) is Professor Emerita of hydrogeology in the Department of Earth Sciences at Simon Fraser University in British Columbia, Canada. Her research focuses on understanding how groundwater systems respond to stressors such as climate change and extreme weather (drought and heavy rain events) and pumping. She has developed approaches for assessing risks to water security that have informed decision-makers and policies. Dr. Allen conducts field and numerical modeling-based research linking hydrological and hydrogeological processes in diverse hydroclimatological and geological settings. She was the 2013 winner of the C. J. Westerman Award by Engineers and Geoscientists BC, and the 2015 winner of the Robert N. Farvolden Award by the Canadian national chapter of the International Association of Hydrogeologists (IAH-CNC). Dr. Allen also served as co-editor of the *Canadian Water Resources Journal* for 6 years and was a member of the Groundwater Advisory Board for British Columbia. The Board made recommendations to government that ultimately led to the creation of the Groundwater Protection Regulation under the *Water Sustainability Act*. Dr. Allen is currently the past president of the IAH-CNC.

Please consider signing up for the GW-Project mailing list to stay informed about new book releases, events, and ways to participate in the GW-Project. When you sign up for our email list, it helps us build a global groundwater community. Sign up↗.